CHEMISTRY OF TETRADECACARBONYLTETRAOSMIUM

by

John Paul Canal

B.Sc., Simon Fraser University, 1998

THESIS SUBMITTED IN PARTIAL FULFILLMENT OF THE REQUIREMENTS FOR THE DEGREE OF

DOCTOR OF PHILOSOPHY

In the Department
of
Chemistry

SIMON FRASER UNIVERSITY
Fall 2004

APPROVAL

Name: John Paul Canal

Degree: Ph.D.

Title of Thesis: Chemistry of Tetradecacarbonyltetraosmium

Examining Committee

Chair: Dr. Jason Clyburne (Associate Professor)

Dr. Roland Pomeroy (Professor) Senior Supervisor

Dr. Colin Jones (Professor) Committee Member

Dr. Paul Percival (Professor) Committee Member

Dr. Ian Gay (Professor) Internal Examiner

Dr. Edward Rosenberg (Professor) External Examiner
Department of Chemistry
University of Montana

Date Approved: October 14th, 2004

SIMON FRASER UNIVERSITY

PARTIAL COPYRIGHT LICENCE

ABSTRACT

Tetradecacarbonyltetraosmium, $Os_4(CO)_{14}$ (**1**), has been employed to prepare pentanuclear rhenium-osmium carbonyl clusters. Reaction of **1** with $Re(CO)_4(L)(H)$ (L = CO, PPh_3) gave $ReOs_4(\mu\text{-}H)(CO)_{18}(L)$ (**2**) with a rare, spiked kite Re-Os_4 skeleton. Careful pyrolysis of **2** yielded $ReOs_4(\mu\text{-}H)(CO)_{17}(L)$ as the spiked tetrahedron isomer (**3a**), whereas UV irradiation of **2** gave the planar raft isomer (**3b**). The structural isomerism of **3a/3b** is believed to be the first of its kind. Further heating of $ReOs_4(\mu\text{-}H)(CO)_{18}$ provided $ReOs_4(\mu\text{-}H)(CO)_{16}$ with the expected trigonal bipyramidal $ReOs_4$ unit. The metal skeletons of **2**, **3a** and **3b** cannot be explained by polyhedral skeletal electron pair theory, the most popular theory used to rationalize cluster polyhedra. It is proposed that the shapes adopted by open clusters are those that have the maximum number of metal triangles. The study also suggests that OsOs bonds are stronger than ReOs bonds. The synthesis and structure of $Os_5(\mu\text{-}H)(H)(CO)_{18}$ is described. It has a spiked kite Os-Os_4 nucleus rather than the bow-tie Os_5 motif in $Os_5(CO)_{19}$.

Reaction of **1** with C_2Ph_2 at room temperature produced $Os_4(\mu\text{-}\eta^2\text{-}C_2Ph_2)(CO)_{14}$ (**4**) with an unusual dimetallacyclobutene (i.e., Os-C=C-Os) unit. Careful pyrolysis of **4** provided $Os_4(\mu_3\text{-}\eta^2\text{-}C_2Ph_2)(CO)_{13}$ (**5**) and subsequently $Os_4(\mu_4\text{-}\eta^2\text{-}C_2Ph_2)(CO)_{12}$ (**6**). Clusters **4**, **5** and **6** form a unique series and are models for the bonding of alkynes to various sites in heterogeneous metal catalysts. From a consideration of their structures (especially that of **4**) a new model is proposed for site-specific metal catalysis.

Hexafluorobenzene (C_6F_6) is an inert solvent for the pyrolysis of metal carbonyls. Heating **1** at 125 °C in C_6F_6 gave $Os_3(CO)_{12}$ and $Os_5(CO)_{16}$ rather than an Os_8 cluster.

More convenient and higher-yielding syntheses of $Ru_6(\mu_6\text{-}C)(\mu\text{-}CO)(CO)_{16}$ and $Os_6(CO)_{18}$ were achieved. Spectroscopic evidence for the previously unknown $Ru_xOs_{5-x}(CO)_{16}$ (x = 1, 2, 5) is presented. The structures of the unique pair $Os_4(\mu\text{-}H)(\mu\text{-}OH)(CO)_{13}.H_2O$ and $Os_4(\mu\text{-}H)(\mu\text{-}OD)(CO)_{13}$ (i.e., nonhydrated) are also described.

Carbonyl exchange in the clusters was studied by ^{13}CO labeling and variable-temperature ^{13}C NMR spectroscopy. The rate of CO exchange ranges from $<10^{-5}$ s^{-1} $[(O^{13}C)_5ReOs_4(\mu\text{-}H)(CO)_{14}]$ to $>10^{10}$ s^{-1} $[Ru_6(\mu_6\text{-}C)(\mu\text{-}CO)(CO)_{16}]$.

The investigations reported in this thesis represent a significant contribution to the field of metal carbonyl cluster chemistry.

Dedication

To my parents, Anna Maria and Rino, for their love and support.

Ai miei genitori, Anna Maria e Rino, per il loro amore ed appoggio.

Acknowledgments

I wish to express my gratitude to my senior supervisor, Dr. Roland K. Pomeroy, for his guidance, support and steady friendship. His words of encouragement were constant and his love of osmium was infectious. I am grateful to have been his student.

I would to thanks to the members of the research group (past and present), especially Valerie Hansen and Faming Jiang for initially training me.

I am thankful to all my friends in the chemistry department at SFU, especially for the candy runs with Jackie Logan, the coffee breaks "under the sun" with Laura Andronic and the daily "field trip" with Christine Wilcox.

I must thank those that assisted in the completion of this thesis. They include Diane Dickie for some figures in Chapter 1 and Sandra Aquilini for double-checking all the references. A sincere thank you to Madhvi Ramnial for proofreading this thesis and lending a hand whenever it was needed. Thanks for caring.

I also wish to thank Dr. Paul Percival for this encouragement and offers of assistance.

Thank you to the skilled technicians for their assistance in obtaining the spectroscopic data presented in this thesis. I would also like to thank those who assisted in the crystal structure determinations.

Table of Contents

Approval ii

Abstract iii

Dedication v

Acknowledgments vi

Table of Contents vii

List of Charts ix

List of Figures xi

List of Tables xv

Descriptions of Cluster Shapes xvii

Definitions xviii

1. Introduction 1

2. The $ReOs_4(\mu\text{-}H)(CO)_n$ (n = 20, 19, 18, 16) Clusters and $ReOs_3(\mu\text{-}H)(CO)_{16}$ 16

   2.1 Introduction 16

   2.2 Results and Discussion 17

   2.3 Experimental Section 52

3. The Triphenylphosphine Derivatives $ReOs_4(\mu\text{-}H)(CO)_n(PPh_3)$ (n = 18, 17), $Os_5(\mu\text{-}CO)(CO)_{17}(PPh_3)$ and $ReOs_3(\mu\text{-}H)(CO)_{15}(PPh_3)$ 60

   3.1 Introduction 60

   3.2 Results and Discussion 62

   3.3 Experimental Section 99

4. Synthesis and Characterization of $Os_5(\mu\text{-}H)(H)(CO)_{18}$ 105

   4.1 Introduction 105

   4.2 Results and Discussion 106

4.3 Experimental Section 117

5. Diphenylacetylene Derivatives of $Os_4(CO)_{14}$ 119

5.1 Introduction 119

5.2 Results and Discussion 121

5.3 Experimental Section 146

6. Pyrolysis of Binary Carbonyl Clusters of Ruthenium and Osmium 150

6.1 Introduction 150

6.2 Results and Discussion 152

6.3 Variable Temperature ^{13}C NMR Studies of the Pyrolysis Products 176

6.4 Experimental Section 194

7. $Os_4(\mu\text{-}H)(\mu\text{-}OH)(\mu\text{-}CO)(CO)_{12}$ and $Os_4(\mu\text{-}H)(\mu\text{-}OD)(\mu\text{-}CO)(CO)_{12}$ 205

7.1 Introduction 205

7.2 Results and Discussion 206

7.3 Experimental Section 223

References 226

List of Charts

Chart		Page
2.1	Puckered square and spiked triangular configurations of $Os_4(CO)_{15}(L)$	18
2.2	Proposed structure of **1**	19
2.3	Proposed mechanism for the decomposition of **1**	20
2.4	3c-2e bonds in $Os_4(CO)_{15}$	24
2.5	OsOs bond lengths in $Os_4(\mu\text{-H})(CO)_{14}(SnMe_3)$, **2**, and $Os_4(CO)_{14}(PMe_3)$	27
2.6	Merry-go-round CO exchange in **3a**	35
2.7	Metal skeletons of the $Os_5(CO)_n$ and $ReOs_4(\mu\text{-H})(CO)_n$ clusters	49
2.8	An approximate Reaction Coordinate diagram for the $ReOs_4(\mu\text{-H})(CO)_n$ (n = 19, 18 (two isomers), 16) clusters	51
3.1	3c-2e bonds proposed for $Os_4(CO)_{15}$	64
3.2	OsOs bond lengths in **2** and **6**	66
3.3	Metal-metal bond lengths and proposed bonding schemes for **7b**	74
3.4	OsOs lengths in the two independent molecules of **8**	82
3.5	Bond lengths in **7b** and **8**	83
3.6	Proposed mechanism of conversion of the two isomers of **8**	86
3.7	Metal skeletons of **7a** and **7b**	92
3.8	Some *arachno* clusters derived from, top, a pentagonal bipyramid and, bottom, a capped octahedron.	94
3.9	The centrally directed MO in triangular metal units of clusters	95
3.10	Relationship of the $ReOs_4(\mu\text{-H})(CO)_n(PPh_3)$ (n = 18, 17a, 17b) clusters	96
3.11	Metal skeletons of the $ReOs_4(\mu\text{-H})(CO)_n(L)$ clusters	98
4.1	Mode of CO exchange between the Os_2 unit and the spiked Os atom	112

4.2 Molecular structure of the $Os_5(\mu\text{-}H)_2(CO)_n$ (n = 18 - 15) series. For n = 17, 15 the predicted structures are shown 116

5.1 Rotation barriers in six and seven coordinate complexes 130

5.2 Relationship between **13**, **14** and **15** 136

5.3 Formation of **13** from $Os_4(CO)_{15}$ 138

5.4 Proposed model for site-specific surface catalysts. The corner PT site 139

5.5 Example of an edge PT site 139

5.6 (A) Mutual CO exchange on the $Os(CO)_3$ units involved in the alkyne bridge of **16**. (B) Rotation of the alkyne ligand on the Os triangle 144

6.1 Axial-equatorial merry-go-round exchange of carbonyl ligands across an M-M bond (M = Fe, Ru, Os) 176

6.2 (A) Structure of $Ru_6(\mu_6\text{-}C)(CO)_{17}$ (**18**). (B) Mode of CO exchange for carbonyls attached to the equatorial Ru atoms in **18** 179

6.3 Structure of $Os_5(CO)_{16}$ and proposed carbonyl exchanges in the molecule 187

6.4 Mode of carbonyl exchange in $Ru_2Os(CO)_{12}$ at -90 °C 190

6.5 Mode of carbonyl exchange in $RuOs_2(CO)_{12}$ at -55 °C 192

7.1 Labelling in the ^{13}C NMR spectrum of $Os_4(\mu\text{-}H)(\mu\text{-}OH)(\mu\text{-}CO)(CO)_{12}$. (A) Carbonyl exchange at Os(3). (B) Merry-go-round CO exchange about the Os(2)Os(3)Os(4) triangle of $Os_4(\mu\text{-}H)(\mu\text{-}OH)(\mu\text{-}CO)(CO)_{12}$ 214

List of Figures

Figure		Page
1.1	Structure of $Os_4(CO)_{14}$	1
1.2	(A) Structure of $Os_6(CO)_{18}$. (B) Structure of $Os_7(CO)_{21}$	3
1.3	(A) Structure of $Os_4(CO)_{15}$. (B) Structure of $Os_4(CO)_{16}$	8
1.4	Structure of $Os_4(\mu\text{-H})(CO)_{14}(SnMe_3)$	9
1.5	Structure of $Os_3(CO)_{11}[Os(CO)_4(CNBu^t)]$	10
1.6	Structure of $Os_5(CO)_{18}(CNBu^t)$	11
1.7	Structure of $Os_5(\mu\text{-CO})(CO)_{16}(PMe_3)$	12
1.8	Structure of $Os_5(CO)_{15}(eq\text{-}PMe_3)$	12
2.1	^{13}C NMR spectrum of $ReOs_4(\mu\text{-H})(CO)_{20}$ (**1**) in CH_2Cl_2/CD_2Cl_2	18
2.2	Molecular structure of $ReOs_4(\mu\text{-H})(CO)_{19}$ (**2**)	21
2.3	$^{13}C\{^1H\}$ NMR spectra of **2**: (A) Sample prepared from ^{13}CO enriched $Os_4(CO)_{14}$. (B) Sample prepared from ^{13}CO enriched $Re(CO)_5(H)$after 5 days (C) Sample prepared from ^{13}CO enriched $Re(CO)_5(H)$	28
2.4	Molecular structure of $ReOs_4(\mu\text{-H})(\mu\text{-CO})(CO)_{17}$ (**3a**)	32
2.5	$^{13}C\{^1H\}$ NMR spectra of **3a**	34
2.6	IR (KBr) spectrum (ν(CO) region) of $ReOs_4(\mu\text{-H})(CO)_{18}$ (**3b**)	37
2.7	Proposed structure for $ReOs_4(\mu\text{-H})(CO)_{18}$ (**3b**)	38
2.8	IR (hexane) spectra (ν(CO) region) of **1**, **2**, **3a**, and **4**	39
2.9	Molecular structure of $ReOs_4(\mu\text{-H})(CO)_{16}$ (**4**)	40
2.10	The $^{13}C\{^1H\}$ NMR spectra of **4**	42
2.11	IR (hexane) spectrum (ν(CO) region) of $ReOs_3(\mu\text{-H})(CO)_{16}$ (**5**)	44
2.12	Molecular structure of $ReOs_3(\mu\text{-H})(CO)_{16}$ (**5**)	45

2.13 (A) The ^{13}C NMR spectra of $(O^{13}C)_5ReOs_3(\mu\text{-}H)(CO)_{11}$ (**5**) at 21 °C and -30 °C (B) The ^{13}C NMR spectrum of $(OC)_5ReOs_3(\mu\text{-}H)(^{13}CO)_{11}$ (**5**) at 21 °C 47

3.1 Molecular structure of $Os_4Re(\mu\text{-}H)(CO)_{18}(PPh_3)$ (**6**) 62

3.2 The $^{13}C\{^1H\}$NMR spectrum of $Os_4Re(\mu\text{-}H)(CO)_{18}(PPh_3)$ (**6**) 67

3.3 IR (CH_2Cl_2) spectra (ν(CO) region) of (A) **9** and (B) **10** 70

3.4 IR spectra (ν(CO) region) of $ReOs_4(\mu\text{-}H)(CO)_n(PPh_3)$ (n = 18, **6**; n = 17, **7a**, **7b**) clusters in hexane 72

3.5 Molecular structure of $ReOs_4(\mu\text{-}H)(CO)_{17}(PPh_3)$ (**7b**) 73

3.6 The ^{13}C NMR spectrum of $ReOs_4(\mu\text{-}H)(CO)_{17}(PPh_3)$ (**7b**) 77

3.7 IR (hexane) spectrum (ν(CO) region) of **8**. 78

3.8 Molecular structures of the two independent molecules of $Os_5(\mu\text{-}CO)(CO)_{16}(PPh_3)$ (**8**) 79

3.9 Mass spectra of **7a** and **8** 81

3.10 Spin saturation transfer experiment on **8**. Irradiation of the highest field ^{31}P NMR resonance resulted in transfer to the signal of the second isomer 85

3.11 The ^{13}C NMR spectrum of **8** in CH_2Cl_2 87

3.12 IR spectrum (ν(CO) region; hexane solution) of **11** 88

3.13 Molecular structure of $ReOs_3(\mu\text{-}H)(CO)_{15}(PPh_3)$ (**11**) 89

4.1 IR (hexane) spectrum (ν(CO) region) of $Os_5(\mu\text{-}H)(H)(CO)_{18}$ (**12**) 107

4.2 Molecular structure of $Os_5(\mu\text{-}H)(H)(CO)_{18}.CH_2Cl_2$ (**12.CH_2Cl_2**) 108

4.3 The ^{13}C NMR spectrum of $Os_5(\mu\text{-}H)(H)(CO)_{18}$ (**12**) in CD_2Cl_2 at 0 °C 111

5.1 Common bonding modes of alkyne ligands in cluster complexes 120

5.2 Molecular structure of $Os_4(\mu\text{-}\eta^2\text{-}C_2Ph_2)(CO)_{14}$ (**13**) 122

5.3 The ^{13}C NMR spectrum of CO-enriched $Os_4(\mu\text{-}\eta^2\text{-}C_2Ph_2)(CO)_{14}$ (**13**) 124

5.4 Molecular structures of the two independent molecules of $Os_4(\mu_3\text{-}\eta^2\text{-}C_2Ph_2)(CO)_{13}$ (**14**) 126

5.5 VT ^{13}C NMR spectra of CO-enriched $Os_4(\mu_3\text{-}\eta^2\text{-}C_2Ph_2)(CO)_{13}$ (**14**) 128

5.6 IR (hexane) spectra (ν(CO) region) of **13 – 15** 132

5.7 Molecular structure of $Os_4(\mu_4\text{-}\eta^2\text{-}C_2Ph_2)(CO)_{12}$ (**15**) 133

5.8 VT ^{13}C NMR spectra of CO-enriched $Os_4(\mu_4\text{-}\eta^2\text{-}C_2Ph_2)(CO)_{12}$ (**15**) 135

5.9 VT ^{13}C NMR spectra of $Os_3(\mu_3\text{-}\eta^2\text{-}C_2Ph_2)(CO)_{10}$ (**16**) in CD_2Cl_2/CH_2Cl_2 142

5.10 (A) Structure of **16**. (B) General structure of $Os_3(alkyne)(CO)_{10}$ clusters 142

5.11 The ^{13}C NMR spectrum of $Os_3(\mu\text{-}\eta^4\text{-}C_4Ph_4)(CO)_9$ (**17**) 145

5.12 Solid-state structure of $Os_3(\mu\text{-}\eta^4\text{-}C_4Ph_4)(CO)_9$ (**17**) 145

6.1 IR (KBr) spectrum of **19** 154

6.2 XRD spectrum of **19** 155

6.3 SEM of **19**. (A) Bulk material. (B). Granular composition of **19** and the spheres of SiO_2. (C) Carbon rich rectangular compound on surface of **19** 156

6.4 IR spectrum of $Ru_5(CO)_{16}$ 159

6.5 Molecular structure of $Os_3(CO)_9(\mu_3\text{:}\eta^2\text{:}\eta^2\text{-}C_6H_6)$ 162

6.6 IR (KBr) spectrum of **22** 163

6.7 SEM of **22**. (A) Bulk material. (B) SiO_2 on the bulk material 163

6.8 Part of the chain structure of the $[Ru(CO)_4]_n$ 166

6.9 Mass spectrum of **26/27** 167

6.10 IR spectrum (ν(CO) region) of the mixture of **26/27** (in hexane) 168

6.11 Mass spectrum of **31** 173

6.12 IR spectrum (hexane; ν(CO) region) of **31** 174

6.13 Structures of $M_4(\mu_4\text{-}Bi)_2(CO)_{12}$ (M = Ru, Os) 175

6.14 Possible structures for $Os_4(\mu_4\text{-}C)_2(CO)_{12}$ 175

6.15 VT ^{13}C NMR spectra of $Ru_6(\mu_6\text{-}C)(CO)_{17}$ 178

6.16 IR (hexane) spectra (ν(CO) region) of (A) $Fe_3(CO)_{12}$, (B) $Os_4(CO)_{14}$, (C) $Ru_6(\mu_6\text{-}C)(CO)_{17}$ 181

6.17 (A) Proposed structure of $Ru_5(CO)_{16}$. (B) The ^{13}C NMR spectrum of products from eq 6.6 184

6.18 (A) Structure of $Os_6(CO)_{18}$ (**21**). (B) The ^{13}C NMR spectrum of **21** 185

6.19 VT ^{13}C NMR spectra of $Os_5(CO)_{16}$ 187

6.20 The ^{13}C NMR spectra of $Ru_2Os(CO)_{12}$ at 0 °C and -90 °C 188

6.21 The ^{13}C NMR spectrum of $RuOs_2(CO)_{12}$ at 21 °C and -50 °C 191

6.22 Overlap of the d orbital on M (M= Fe, Ru, Os) with the in-phase and out-of-phase combinations of the π^* orbital of CO 194

7.1 (A) IR spectrum (KBr disk) of $Os_4(\mu\text{-}H)(\mu\text{-}OH)(\mu\text{-}CO)(CO)_{12}$ (**28**). (B) IR spectrum (hexane; ν(CO) region) of **28** 207

7.2 The molecular structure of $Os_4(\mu\text{-}H)(\mu\text{-}OH)(\mu\text{-}CO)(CO)_{12}.H_2O$ (**28.H_2O**) 208

7.3 Hydrogen bonding interactions in **28** 211

7.4 ^1H NMR spectrum of (A) $Os_4(\mu\text{-}H)(\mu\text{-}OD)(\mu\text{-}CO)(CO)_{12}$ (**32**) and (B) $Os_4(\mu\text{-}H)(\mu\text{-}OH)(\mu\text{-}CO)(CO)_{12}$ (**28**) 212

7.5 Variable temperature $^{13}C\{^1H\}$ NMR spectra of $Os_4(\mu\text{-}H)(\mu\text{-}OH)(\mu\text{-}CO)(CO)_{12}$.. 213

7.6 The molecular structure of $Os_4(\mu\text{-}H)(\mu\text{-}OD)(\mu\text{-}CO)(CO)_{12}$ (**32**) 216

7.7 IR (KBr) spectra of $Os_4(\mu\text{-}H)(\mu\text{-}OH)(\mu\text{-}CO)(CO)_{12}.H_2O$ (**28.H_2O**) and $Os_4(\mu\text{-}H)(\mu\text{-}OD)(\mu\text{-}CO)(CO)_{12}$ (**32**). (A) The ν(OH) region. (B) The ν(CO) region 219

List of Tables

Table		Page
2.1	Selected bond lengths (Å) and angles (°) for $ReOs_4(\mu\text{-}H)(CO)_{19}$ (**2**)	22
2.2	Unbridged ReRe, ReOs and OsOs bond lengths (Å)	23
2.3	Site energy values (kcal mol^{-1}) for the terminal and bridging hydride positions in $ReOs_4(\mu\text{-}H)(CO)_{19}$	26
2.4	Selected bond lengths (Å) and angles (°) for $ReOs_4(\mu\text{-}H)(\mu\text{-}CO)(CO)_{17}$ (**3a**)	32
2.5	Site energy values (kcal mol^{-1}) for the terminal and bridging hydride positions in $ReOs_4(\mu\text{-}H)(\mu\text{-}CO)(CO)_{17}$	33
2.6	Selected bond lengths (Å) and angles (°) for $ReOs_4(\mu\text{-}H)(CO)_{16}$ (**4**)	40
2.7	Site energy values (kcal mol^{-1}) for the terminal and bridging hydride position in $ReOs_4(\mu\text{-}H)(CO)_{16}$ (**4**)	41
2.8	Selected bond lengths (Å) and angles (°) for $ReOs_3(\mu\text{-}H)(CO)_{16}$ (**5**)	45
2.9	Site energy values (kcal mol^{-1}) for the terminal and bridging hydride positions in $ReOs_3(\mu\text{-}H)(CO)_{16}$ (**5**)	46
3.1	Selected bond lengths (Å) and angles (°) for $ReOs_4(\mu\text{-}H)(CO)_{18}(PPh_3)$ (**6**)	63
3.2	Site energy values (kcal mol^{-1}) for the terminal and bridging hydride positions in $ReOs_4(\mu\text{-}H)(CO)_{18}(PPh_3)$ (**6**)	66
3.3	Selected bond lengths (Å) and angles (°) for $ReOs_4(\mu\text{-}H)(CO)_{17}PPh_3$ (**7b**)	73
3.4	Site energy values (kcal mol^{-1}) for the terminal and bridging hydride positions in $ReOs_4(\mu\text{-}H)(CO)_{17}(PPh_3)$ (**7b**)	75
3.5	Selected bond lengths (Å) and angles (°) for $Os_5(\mu\text{-}CO)(CO)_{16}(PPh_3)$ (**8**)	80
3.6	Selected bond lengths (Å) and angles (°) for $ReOs_3(\mu\text{-}H)(CO)_{15}(PPh_3)$ (**11**)	90
3.7	Site energy values (kcal mol^{-1}) for the terminal and bridging hydride positions in $ReOs_3(\mu\text{-}H)(CO)_{15}(PPh_3)$ (**11**)	91

4.1 Selected bond lengths (Å) and angles (°) for $Os_5(\mu\text{-}H)(H)(CO)_{18}.CH_2Cl_2$ (**12.CH_2Cl_2**) 108

4.2 Site energy (kcal mol^{-1}) for the terminal and bridging hydride positions in $Os_5(\mu\text{-}H)(H)(CO)_{18}.CH_2Cl_2$ (**12.CH_2Cl_2**) 109

5.1 Selected bond lengths (Å) and angles (°) for $Os_4(\mu\text{-}\eta^2\text{-}C_2Ph_2)(CO)_{14}$ (**13**) 122

5.2 Selected bond lengths (Å) and angles (°) for $Os_4(\mu_3\text{-}\eta^2\text{-}C_2Ph_2)(CO)_{13}$ (**14**) 127

5.3 Summary of the reaction conditions and percent yields for **13** - **17** 132

5.4 Selected bond lengths (Å) and angles (°) for $Os_4(\mu_4\text{-}\eta^2\text{-}C_2Ph_2)(CO)_{12}$ (**15**) 134

5.5 The CC and OsC bond lengths of the alkyne-Os unit in **13** - **15** 137

6.1 X-ray powder diffraction (XRD) pattern of **19** and Ru metal 155

6.2 Summary of EDX data for minor materials of **19**. (A) spheres; (B) rectangular... 157

6.3 Summary of EDX data for bulk **19** 158

6.4 Carbonyl stretching frequencies (cm^{-1}) for (A) $Ru_xOs_{3-x}(CO)_{12}$ (x = 0-3) and (B) $Ru_xOs_{5-x}(CO)_{16}$ (x = 0 - 2, 5) 160

6.5 The CO-stretching frequencies (cm^{-1}) for $Ru_5(CO)_{16}$ and **18** in hexane..... 160

6.6 Summary of C/O/Os values from the EDX analysis of **22** 164

6.7 Comparison of the IR spectrum (ν(CO) region; in hexane) of **31** with those of some $M_4(\mu_4\text{-}X)_2(CO)_{12}$ clusters 175

7.1 Bond lengths (Å) and angles (°) for $Os_4(\mu\text{-}H)(\mu\text{-}OH)(\mu\text{-}CO)(CO)_{12}.H_2O$ (**28.H_2O**) and $Os_4(\mu\text{-}H)(\mu\text{-}OD)(\mu\text{-}CO)(CO)_{12}$ (**32**) 208

7.2 Site energies (kcal mol^{-1}) for the terminal and bridging hydride positions in $Os_4(\mu\text{-}H)(\mu\text{-}OH)(\mu\text{-}CO)(CO)_{12}.H_2O$ (**28.H_2O**) and $Os_4(\mu\text{-}H)(\mu\text{-}OD)(\mu\text{-}CO)(CO)_{12}$ (**32**) 210

Description of Cluster Shapes

kite
(planar)

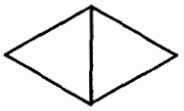

rhomboidal
(planar)

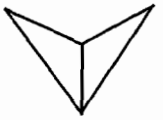

butterfly
(non-planar)

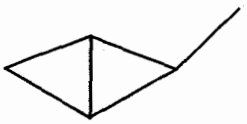

spiked kite

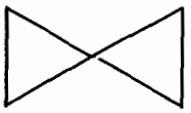

bow-tie

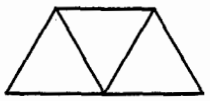

raft

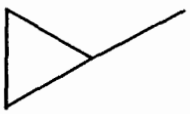

spiked triangle

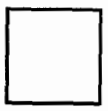

puckered square

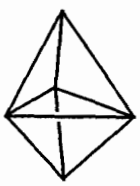

trigonal bipyramidal

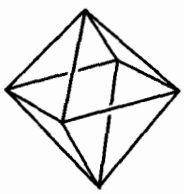

octahedron

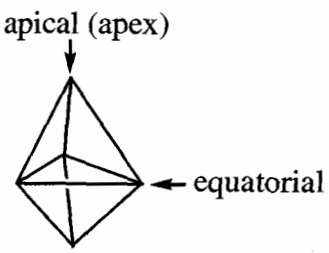

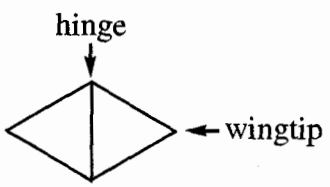

Definitions

a. **Polyhedral skeletal electron pair theory** (PSEPT): A set a rules used to predict the shape of the metal skeleton adopted by a cluster based on the number of skeletal electron pairs. Also referred to as Wade's rules. (see ref 1)

b. **PR_3**: Designation for any tertiary P donor ligand. (e.g. triphenylphosphine, PPh_3)

c. **Pyrolysis**: As it applies to the production of clusters, it involves the use of temperatures in the range of ~45 - 260 °C to break metal-ligand bonds and produce new metal-metal bonds. Pyrolysis may also lead to complete decomposition.

d. **Site energy**: The potential energy of a hydride ligand in a transitional metal cluster, as calculated by the XHYDEX program. (see below)

e. **Transitional metal cluster**: As defined by Shriver and Atkins, they are "molecular complexes with metal-metal bonds that form triangular or larger closed structures. This definition excludes M-M-M compounds." [1]

f. **VT**: Variable temperature.

g. **XHYDEX program**: A program developed by A. G. Orpen (University of Bristol) to calculate the potential energy for a hydride ligand in the different coordination sites on a transition metal cluster. (Discussed further in the Experimental section of Chapter 2)

h. **σ-donor, π-acceptor**: A σ-donor is a unit that donates electron density to another unit through a filled σ-orbital. A π-acceptor is a unit that accepts electron density from another until through an empty π orbital.

i. **μ_n**: Represents a ligand bridging two or more metal atoms. The subscript indicates the number of metal atoms bridged. It is omitted when equal to two.

j. **η^n**: Indicates the connectivity of a ligand (usually carbon) to a transition metal. The superscript (n) indicates the number of ligating atoms in the ligand that bind to the metal. If all the possible ligating atoms are bound to the metal the superscript is dropped.

   For example: $(\eta^5\text{-}C_5Me_5)Ir(CO)_2$ and $(\eta\text{-}C_5H_5)Ir(CO)_2$
   (The H atoms of C_5H_5 do not bind the metal)

k. **3c-2e**: Three center, two electron.

Chapter 1. Introduction

This thesis is concerned with aspects of the chemistry of tetradecacarbonyltetraosmium, hereafter referred to as $Os_4(CO)_{14}$. Pomeroy and coworkers first reported this tetrahedral compound in 1988 and a view of the molecule, as determined by X-ray crystallography, is shown in Figure 1.1. This compound belongs to

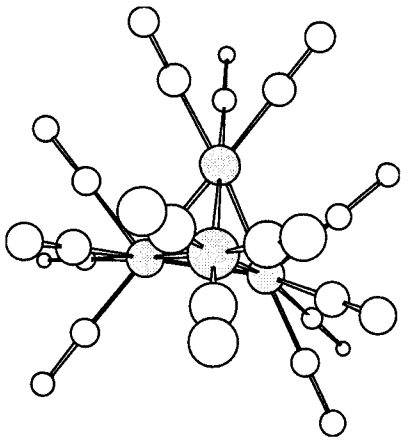

Figure 1.1. Structure of $Os_4(CO)_{14}$.

a class of molecules called condensed transition metal carbonyl clusters. In this thesis the term "condensed" cluster is reserved for clusters that share at least one face and those fused by one atom or an edge as an "open" cluster. (The term cluster and the formula indicate that all metals are bound by at least one metal-metal bond to the central unit.) Most cluster chemists define a cluster according to the Shriver and Aktins description that is "metal clusters [are] molecular complexes with metal-metal bonds that form triangular or larger closed structures. This definition excludes M-M-M compounds." (Here we refer to these compounds as chain complexes.) Closed structures held together by non-transition elements and without metal-metal interactions are called cage compounds.[1]

Although the first metal carbonyl cluster, $Fe_3(CO)_{12}$, was reported in 1907 by Dewar and Jones,[2] progress in this area of organometallic chemistry was limited until the late 1960's. Interest in these compounds grew due to improvements to X-ray crystallography that allowed their structures to be unambiguously determined. Without this technique the detailed study of clusters would be impossible and, unless otherwise stated, the structures shown in this study were determined by X-ray crystallography.

The energy crisis of the 1970's produced a flurry of activity into the relationship between clusters and catalytic activity on metal surfaces, as well as the potential uses of clusters as heterogeneous or homogenous catalysts.[3] Because of these and other studies various aspects of cluster chemistry have been investigated to an extent that this field has become an important and separate area of inorganic chemistry. The number of textbooks dealing with the chemistry of metal clusters illustrates the importance of this subject.[4]

For reasons that are not fully understood, osmium forms more carbonyl clusters than any other element and, consequently, the chemistry of Os carbonyl clusters has played a key role in advancing the field.[5] Since the initial developments in this area in the late 1960's, a major challenge for cluster chemists has been the development of systematic synthetic routes to clusters. In the 1980's a prominent researcher in this field wrote that "the preparation of clusters remains almost entirely an accidental affair and few systematic routes have been devised."[4e] Since that time there has been an increase in the number of systematic routes available to produce new metal carbonyl clusters.[3,4f,6] A thorough review of the main methods employed to increase the nuclearity of metal carbonyl clusters is found in reference 3. Presented here are some of the procedures that

are important to this thesis, as well as some recent developments in the area of synthesis of transition metal clusters.

The most common method employed to obtain higher nuclearity metal carbonyl clusters from compounds with a lower nuclearity is by pyrolysis.[7] In 1975, Eady, Johnson and Lewis opened up the area of high nuclearity osmium carbonyl clusters with their description of the pyrolysis of $Os_3(CO)_{12}$. (Any cluster with more than three metal atoms is referred to as a higher nuclearity cluster.) This reaction produced clusters containing five to eight osmium atoms (eq 1.1).[5,8] The structure of $Os_6(CO)_{18}$ (a capped

$$Os_3(CO)_{12} \xrightarrow{210 - 250\ ^\circ C} Os_5(CO)_{16} + Os_5(\mu_5\text{-}C)(CO)_{15} + Os_6(CO)_{18} + Os_7(CO)_{21} + Os_8(CO)_{23} + Os_8(\mu_6\text{-}C)(CO)_{21} \quad (1.1)$$

trigonal bipyramid) and $Os_7(CO)_{21}$ (a capped octahedron) are shown in Figures 1.2.

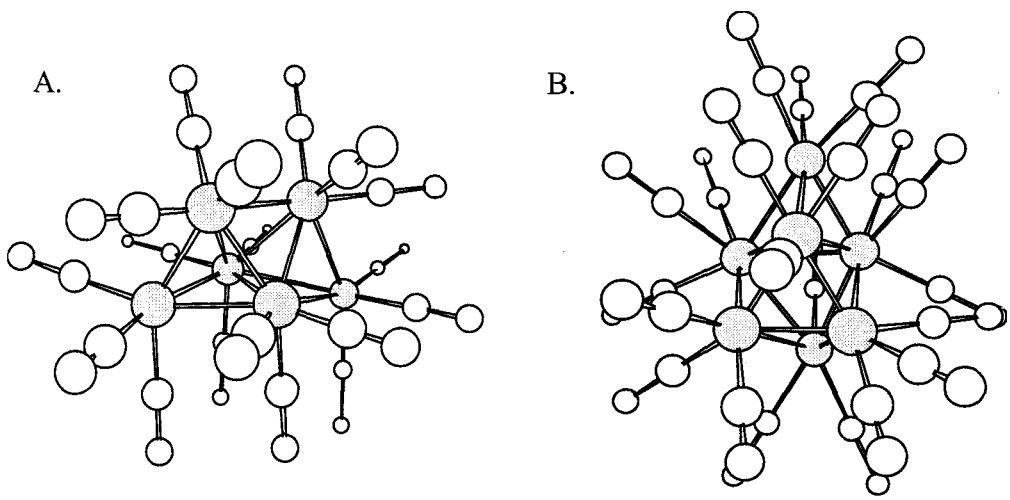

$Os_6(CO)_{18}$ $Os_7(CO)_{21}$

Figure 1.2. (A) Structure of $Os_6(CO)_{18}$. (B) Structure of $Os_7(CO)_{21}$.

Pyrolysis is still an important method for the synthesis of new clusters as illustrated by the work in this thesis. Indeed, many metal carbonyl clusters can only be

produced by this method.[9] Recently a new binary carbonyl of osmium ($Os_{12}(CO)_{30}$) was produced from the pyrolysis of $Os_6(CO)_{16}(\mu\text{-}O)(\mu\text{-}OH)_2(\mu\text{-}CO)_2$ (eq 1.2).[10]

$$Os_6(CO)_{16}(\mu\text{-}O)(\mu\text{-}OH)_2(\mu\text{-}CO)_2 \xrightarrow{200\ ^\circ C} Os_{12}(CO)_{30} \qquad (1.2)$$

Whereas other transition metals form at most three neutral binary carbonyls that are stable at room temperature, 14 are known for osmium although, as discussed in Chapter 6, the existence of $Os_8(CO)_{23}$ has not been independently confirmed. (Osmium forms innumerable trinuclear carbonyl clusters that contain other noncarbonyl ligands.)[11]

Another recent example of a cluster prepared by pyrolysis is the Ru_4 compound derived from a trinuclear Ru precursor (eq 1.3).[12]

$$Ru_3(CO)_{10}(dppe) \xrightarrow{110\ ^\circ C} Ru_4(CO)_9\{\mu_4\text{-}\eta^2\text{-}PCH_2CH_2P(C_6H_5)_2\}(\mu_4\text{-}\eta^4\text{-}C_6H_4) \qquad (1.3)$$

dppe = $(C_6H_5)_2PCH_2CH_2P(C_6H_5)_2$

Photolysis can also be used to obtain clusters of increased nuclearity, but the method is uncommon. Photolysis of $(Me_3P)(OC)_4OsCr(CO)_5$ gives $(OC)_5Cr[Os(CO)_3(PMe_3)]_2$,[13] while the formation of $Cp_2Rh_2(CO)_3$ and $Cp_3Rh_3(CO)_3$ occurs when $CpRh(CO)_2$ is irradiated with UV light (eq 1.4/1.5).[14]

$$(Me_3P)(OC)_4OsCr(CO)_5 \xrightarrow{h\nu} (OC)_5Cr[Os(CO)_3(PMe_3)]_2 \qquad (1.4)$$

$$CpRh(CO)_2 \xrightarrow{h\nu} Cp_2Rh_2(CO)_3 + Cp_3Rh_3(CO)_3 \qquad (1.5)$$

Photolysis has also been employed to prepare mixed metal clusters through the exchange of metal centers. A series of mixed metal clusters have been produced by the exchange of an M (M = Fe, Ru, Os) atom with a W atom in trinuclear clusters, as shown in eq 1.6.[15]

$$M_3(\mu_3\text{-}S)(\mu_3\text{-}CO)(CO)_9 + W(CO)_6 \xrightarrow{h\nu} M_2W(\mu_3\text{-}S)(CO)_{11} \qquad (1.6)$$

M = Fe, Ru, Os

Photolysis is, however, a common method to bring about decarbonylation of transition metal carbonyl clusters. This method was employed to produce some of the compounds presented in this thesis. The reaction shown in eq 1.7 is a recent illustration of this technique (Hapy = 2-amino-6-phenylpyridine).[16]

$$Os_3(\mu\text{-H})(\mu\text{-}\eta^2\text{-HapyPh-N-N'})(CO)_{10} \xrightarrow{h\nu} Os_3(\mu\text{-H})(\mu_3\text{-}\eta^2\text{-HapyPh-N-N'})(CO)_9 \quad (1.7)$$

Some other recent examples of homonuclear transition metal clusters are presented below. The hexanuclear rhodium cluster, $Rh_6(CO)_{14}[P(Mepy)Ph_2]$ was isolated in 57% yield by refluxing $Rh_4(CO)_{12}$ in CH_2Cl_2 in the presence of the bidentate ligand 3-methyl-2-pyridyl)diphenylphosphane ($P(Mepy)Ph_2$) (eq 1.8).[17]

$$Rh_4(CO)_{12} + P(Mepy)Ph_2 \xrightarrow{40\ ^\circ C} Rh_6(CO)_{14}[P(Mepy)Ph_2] \quad (1.8)$$

A procedure that gives the dianion $[Ru_{10}(\mu_6\text{-C})(CO)_{24}]^{2-}$ in high yield from the reaction of CaC_2 with $Ru_3(CO)_{12}$ has recently been described (eq 1.9).[18] This anionic

$$CaC_2 + Ru_3(CO)_{12} \xrightarrow{66\ ^\circ C} Ca[Ru_{10}(\mu_6\text{-C})_2(CO)_{24}] \quad (1.9)$$

cluster is particularly interesting in that it contains two $Ru_6(\mu_6\text{-C})$ units (i.e., a bare C atom in an octahedron of Ru atoms). This unit is also found in $Ru_6(\mu_6\text{-C})(CO)_{17}$ a cluster discussed in Chapter 6.

The rational syntheses of high nuclearity heteronuclear metal clusters are more difficult than the preparation of homonuclear analogues; it still remains a challenge for cluster chemists.[3,4] Several syntheses have however been recently reported. Here we mention a few examples. (Another example was presented in eq 1.6.)

A new strategy to synthesize mixed metal clusters has been developed by Adams and coworkers. It involves the addition of highly nucleophilic unsaturated metal

complexes (e.g., $M(PBu^t_3)_2$; M = Pt, Pd) across RuRu, RuPt or RhRh bonds of smaller clusters. An example is shown in eq 1.10.[19]

$$Rh_4(CO)_{12} + nPd(PBu^t_3)_2 \longrightarrow Rh_4(CO)_{16}[Pd(PBu^t_3)]_n \quad (1.10)$$
$$n = 3, 4$$

Stepwise metal exchange reactions do not increase the nuclearity of a cluster, but provide another route to produce mixed metal clusters. For example, clusters of the type $Co_2M(\mu_3\text{-}CR)(\eta^5\text{-}Ind)(CO)_8$ (M = Mo, W; R = H, CH_3, C_6H_5, $COOC_2H_5$; Ind = C_9H_7) have been prepared by the reaction shown below (eq 1.11).[20]

$$Co_3(\mu_3\text{-}CR)(CO)_9 + K(Ind)M(CO)_3 \longrightarrow Co_2M(\mu_3\text{-}CR)(CO)_8(\eta^5\text{-}Ind) \quad (1.11)$$

M = Mo, W; R = H, CH_3, C_6H_5, $COOC_2H_5$; Ind = C_9H_7

In another reaction a high nuclearity cluster containing Co and niobium resulted from the reaction of $(\eta^5\text{-}Bu^tC_5H_4)NbTe_2H$ with $Co_2(CO)_8$ (eq 1.12).[21]

$$(\eta^5\text{-}Bu^tC_5H_4)NbTe_2(H) + Co_2(CO)_8 \longrightarrow [(\eta^5\text{-}Bu^tC_5H_4)(OC)Nb]_2[Co_9Te_6(CO)_8] \quad (1.12)$$

The synthesis of clusters by redox condensation was first reported by Hieber in 1965. This method was recently utilised to produce the mixed metal tetranuclear clusters $M_2M'_2(\mu\text{-}CC_6H_5)(\mu_3\text{-}CC_6H_5)(\mu\text{-}CO)_3(CO)_3(\eta^5\text{-}C_5H_5)_2$ (M = Mn, Re; M′ = Rh, Ir) (eq 1.13).[22]

$$[\eta^5\text{-}(C_5H_5)(CO)_2M(CC_6H_5)]^+ + [M'(CO)_4]^- \xrightarrow{< -50\ ^\circ C} M_2M'_2(\mu\text{-}CC_6H_5)(\mu_3\text{-}CC_6H_5)(\mu\text{-}CO)_3(CO)_3(\eta^5\text{-}C_5H_5)_2 \quad (1.13)$$

M = Mn, Re; M′ = Rh, Ir

Another recent example is the reaction of $[Co(CO)_4]^-$ with $PCl_2(TMP)$ to give $Co_3[\mu_3\text{-}P(TMP)][\mu\text{-}P(Cl)(TMP)](CO)_7$ (eq 1.14).[23] The same anion reacts with Ln (Ln =

$$K[Co(CO)_4] + PCl_2(TMP) \longrightarrow Co_3[\mu_3\text{-}P(TMP)][\mu\text{-}P(Cl)TMP](CO)_7 \quad (1.14)$$

TMP =2,2,6,6,tertamethypiperidyl

Yb, Eu) in Et_2O to produce anionic tetranuclear Co clusters that coordinate with Ln through the O atoms of two or three carbonyl ligands to form a polymeric array (eq 1.15).[24]

$$Hg[Co(CO)_4]_2 + Ln \longrightarrow \{(Et_2O)_3Ln[Co_4(CO)_{11}]\}_\infty \quad (1.15)$$

Ln = Yb, Eu

The displacement by donor ligands of weakly coordinated substituents such as acetonitrile or cyclooctene (COE) bound to triosmium clusters (i.e., $Os_3(CO)_{12-n}(MeCN)_n$; n = 1, 2;[25,26] and $Os_3(CO)_{10}(COE)_2$) is widely used in the preparation of substituted trinuclear osmium clusters.[27] Pomeroy and coworkers have exploited this protocol for the systematic synthesis of higher nuclearity clusters of osmium. The most recent example is the first rational synthesis of the heptaosmium cluster $Os_7(CO)_{20}(CNBu^t)$ by the addition of $Os(CO)_4(CNBu^t)$ to $Os_6(CO)_{18}$ in the presence of MeCN and Me_3NO (eq 1.16).[28] Although $Os_6(CO)_{16}(MeCN)_2$ was not isolated, it is believed to be the

$$Os_6(CO)_{18} + Os(CO)_4(CNBu^t) \xrightarrow[MeCN]{Me_3NO} Os_7(CO)_{20}(CNBu^t) \quad (1.16)$$

intermediate that facilitates the addition of $Os(CO)_4(CNBu^t)$. The $Os_7(CO)_{20}(CNBu^t)$ cluster has a capped octahedral skeleton like the parent $Os_7(CO)_{21}$.

Of importance to this thesis is the reaction of $Os_3(CO)_{10}(COE)_2$ with $Os(CO)_5$ to give $Os_4(CO)_{15}$, the first reported example of a tetranuclear binary carbonyl of Osmium (eq 1.17).[29] A more convenient synthesis of $Os_4(CO)_{15}$ is presented in this thesis.

$$Os_3(CO)_{10}(COE)_2 + Os(CO)_5 \longrightarrow Os_4(CO)_{15} \quad (1.17)$$

Addition of carbon monoxide at or below room temperature to $Os_4(CO)_{15}$ (Figure 1.3A) yields the elusive $Os_4(CO)_{16}$ with a puckered square arrangement of Os atoms (Figure 1.3B).[30] Unlike $Os_3(CO)_{12}$ that is stable in C_6F_6 solution to ~150 °C (Chapter 6),

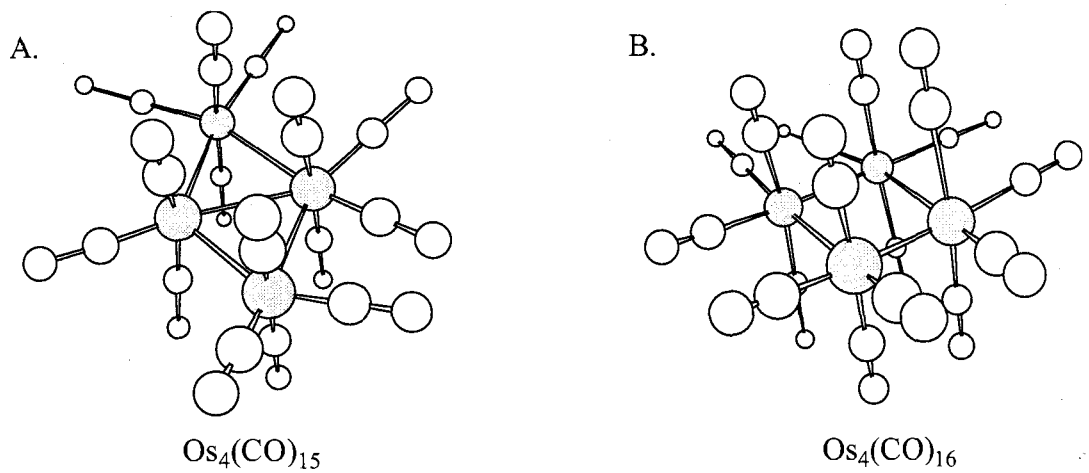

Figure 1.3. (A) Structure of $Os_4(CO)_{15}$. (B) Structure of $Os_4(CO)_{16}$.

$Os_4(CO)_{16}$ decomposes in hexane at room temperature. Heating or UV irradiation of $Os_4(CO)_{15}$ causes decarbonylation to afford $Os_4(CO)_{14}$, the central cluster of this thesis.[31] It is of interest that tetrahedral clusters with 14 carbonyl ligands had been predicted to be unstable from both MO and steric arguments.[32,33] These tetranuclear Os carbonyl clusters (i.e., $Os_4(CO)_n$; n = 14 - 16) were not reported until 1987-88 and consequently the investigation into the chemistry of tetranuclear Os clusters has trailed that of the penta- and hexa- nuclear carbonyl clusters of Os.[4c]

The structure of $Os_4(CO)_{15}$ revealed an unusual planar kite configuration with adjacent short (~2.77 Å) and long (~3.00 Å) peripheral Os-Os bonds. A similar pattern of metal-metal bond lengths is also found in related compounds such as $Os_4(CO)_{14}(PMe_3)$ and $Cp^*IrOs_3(CO)_{12}$ ($Cp^* = \eta^5$-C_5Me_5).[29,34] The unusual OsOs lengths were rationalized in terms of 3c-2e OsOs bonds such that the long bonds had an order of 0.5 and the short bonds an order 1.5. In this way, each Os atom achieves an 18 electron configuration.

(The vast majority of osmium carbonyl compounds obey the rule.) In contrast, the previously determined structure of $ReOs_3(\mu\text{-}H)(CO)_{15}$ consists of a planar kite arrangement of metal atoms with roughly equal metal-metal bond lengths.[35]

The most common carbonyl of Os, $Os_3(CO)_{12}$, is inert to substitution at moderate temperatures and must be chemically activated (e.g., as $Os_3(CO)_{11}(MeCN)$) in order to provide $Os_3(CO)_{11}(L)$ derivatives (L = PR_3, $CNBu^t$, etc). On the other hand, $Os_4(CO)_{14}$ readily adds L under mild conditions to yield $Os_4(CO)_{14}(L)$ (e.g., $Os_4(CO)_{14}(CNBu^t)$).[36] Furthermore, addition of $HSnMe_3$ to $Os_4(CO)_{14}$ gives $Os_4(\mu\text{-}H)(CO)_{14}(SnMe_3)$, with the same valence electron count as $Os_4(CO)_{15}$. The structure (Figure 1.4) of the tin cluster

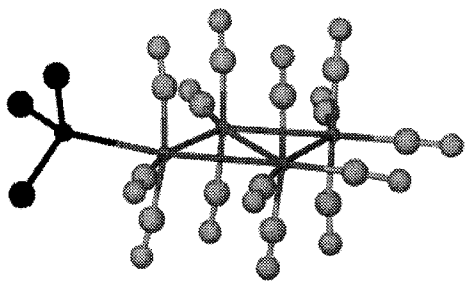

Figure 1.4. Structure of $Os_4(\mu\text{-}H)(CO)_{14}(SnMe_3)$.

contains one long and three short peripheral OsOs bonds a variation on the pattern seen in $Os_4(CO)_{15}$.[37] The hydride ligand was confidently placed across one of the short OsOs bonds. This is contrary to what is often found for bridging hydride ligands in trinuclear clusters. In the latter clusters a single hydride ligand usually bridges the longest MM bond.[7b,38,39]

Pomeroy and coworkers have shown that 18-electron complexes of formula $Os(CO)_4(L)$ (L = CO, PR_3, $CNBu^t$) can act as 2-electron donor ligands in much the same way as a PR_3 ligand. Some examples of complexes that possess these ligands are

$(OC)_5OsOs(CO)_3(GeCl_3)(Cl)$,[40] $(Me_3P)(OC)_4OsW(CO)_5$[41] and $Os_3(CO)_{11}$-$[Os(CO)_4(CNBu^t]$.[42] The metal-metal bonds in these complexes are dative (donor-acceptor) bonds with the Os atom acting as the donor. Most metal-metal bonds in organometallic complexes are nondative covalent bonds. The analogous $Ru(CO)_4(L)$ complexes are only weak donors, and the Fe compounds do not form these complexes.[43]

Note that $Os_3(CO)_{11}[Os(CO)_4(CNBu^t)]$ represents a cluster synthesis reaction and takes place under mild conditions (eq 1.18; L = Bu^tNC). A view of the molecule is

$$Os_3(CO)_{12} + Me_3NO \xrightarrow[25°C]{CH_3CN} Os_3(CO)_{11}(CH_3CN)$$

$$Os_3(CO)_{11}(CH_3CN) + Os(CO)_4(L) \xrightarrow{25°C} Os_3(CO)_{11}[Os(CO)_4(L)] \qquad (1.18)$$

$L = CNBu^t, PMe_3$

given in Figure 1.5. Note that the rod-like $CNBu^t$ substituent occupies the electronically preferred site cis to the OsOs bond and trans to a CO ligand.

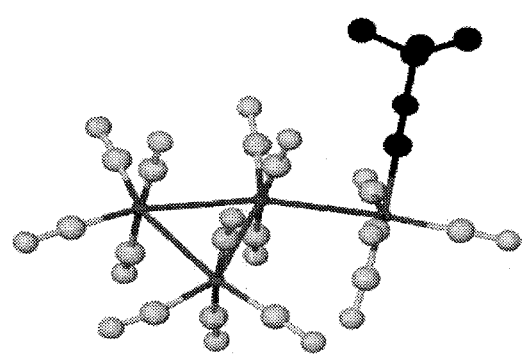

Figure 1.5. Structure of $Os_3(CO)_{11}[Os(CO)_4(CNBu^t)]$.

A natural extension of the investigations described above is the addition of $Os(CO)_4(L)$ (L = CO, PR_3, $CNBu^t$) to $Os_4(CO)_{14}$ to provide pentaosmium clusters. Reaction of $Os_4(CO)_{14}$ with $Os(CO)_4(L)$ in CH_2Cl_2 at room temperature gives $Os_5(CO)_{18}(L)$ in good yield (eq 1.19).[44,45,46] These clusters have a bow-tie metal Os_5

$$Os_4(CO)_{14} + Os(CO)_4(L) \xrightarrow{25°C} Os_5(CO)_{18}(L) \qquad (1.19)$$

$L = CO, CNBu^t, PMe_3$

arrangement as shown for $CNBu^t$ derivative in Figure 1.6. Once again the sterically-

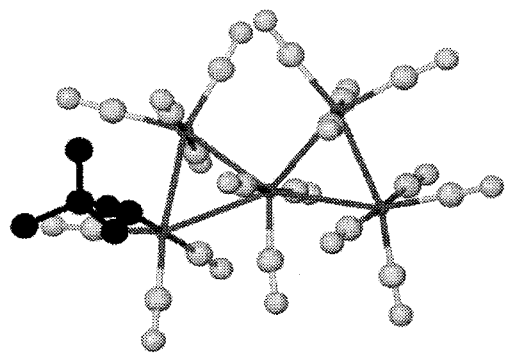

Figure 1.6. Structure of $Os_5(CO)_{18}(CNBu^t)$.

undemanding isocyanide ligand occupies an axial rather than an equatorial position. (The phosphine ligand in $Os_5(CO)_{18}(PMe_3)$ is in the corresponding equatorial site.)

Careful heating of $Os_5(CO)_{18}(L)$ in solution affords $Os_5(\mu\text{-}CO)(CO)_{16}(L)$ (eq 1.20). These clusters have a planar raft configuration as depicted for the PMe_3 complex in Figure 1.7. Note that the bulky P ligand is in a less hindered equatorial site of the

$$Os_5(CO)_{18}(L) \xrightarrow[-CO]{\sim 45°C} Os_5(\mu\text{-}CO)(CO)_{16}(L) \qquad (1.20)$$

$L = CO, CNBu^t, PMe_3$

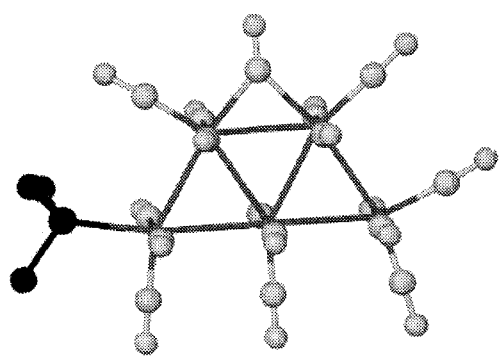

Figure 1.7. Structure of $Os_5(\mu\text{-}CO)(CO)_{16}(PMe_3)$.

molecule and there is a bridging carbonyl. We shall return to this structure later.

Continued mild pyrolysis of $Os_5(\mu\text{-}CO)(CO)_{16}(L)$ yielded $Os_5(CO)_{15}(L)$ with no evidence for $Os_5(CO)_{16}(L)$ (eq 1.21). The $Os_5(CO)_{15}(L)$ clusters have a trigonal

$$Os_5(\mu\text{-}CO)(CO)_{16}(L) \xrightarrow[-2CO]{>65^\circ C} Os_5(CO)_{15}(L) \qquad (1.21)$$

$L = CO, CNBu^t, PMe_3$

bipyramidal Os_5 skeleton.[45,46] This is the structure predicted by polyhedral skeletal electron pair theory (PSEPT), the most popular theory used to rationalize cluster polyhedra. A view of the equatorial isomer of $Os_5(CO)_{15}(eq\text{-}PMe_3)$ is displayed in Figure 1.8. In this molecule the PMe_3 is in arguably the most hindered site, that is, bound to the

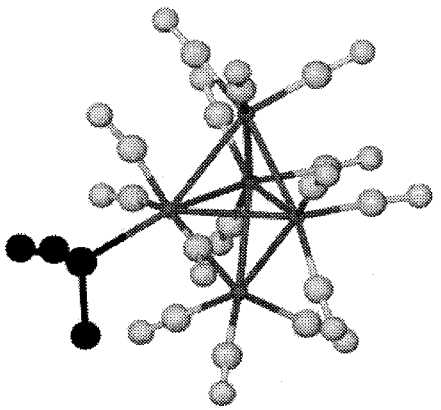

Figure 1.8. Structure of $Os_5(CO)_{15}(eq\text{-}PMe_3)$.

the unique Os atom that has four terminal ligands. This isomer is thermodynamically more preferred to the $Os_5(CO)_{15}(ax\text{-}PMe_3)$ isomer where the PMe_3 is in the least restricted site (i.e., attached to an Os atom in axial position). Obviously, electronic reasons override steric considerations in determining the site preference of the non-carbonyl ligand L in $Os_5(CO)_{15}(L)$ clusters.[45,46]

The binary carbonyls, $Os_5(CO)_{19}$ and $Os_5(CO)_{16}$, had been previously synthesized (e.g., eq 1.1) and their structures determined by Johnson, Lewis and coworkers. The

cluster $Os_5(\mu\text{-}CO)(CO)_{17}$ however was unknown until a study by Pomeroy and coworkers. This cluster would never be observed in a reaction carried out above 65 °C (e.g., a typical pyrolysis reaction). It had been assumed that $Os_5(\mu\text{-}CO)(CO)_{17}$ would have an edge-bridged tetrahedron as a metal skeleton, and not a planar structure. A similar planar raft structure is also observed in $Os_6(CO)_{17}[P(OMe)_3]_4$.[47] As will be explained in this thesis, these planar structures can not be rationalized by PSEPT.

It is apparent that from the examples given immediately above that much of cluster chemistry is poorly understood. The structures, the nonexistence of some clusters, the site preference of ligands in clusters, etc. cannot be adequately explained by using current knowledge. As we shall also see in this thesis, the barriers to the CO exchange processes that occur in the clusters are also not understood. Some of these exchange rates are phenomenally fast. In $Os_4(CO)_{14}$ it has been estimated that CO exchange occurs at a rate $>10^6$ s^{-1} at -130 °C.

A major aspect of Dr Pomeroy's research program has been the systematic synthesis of osmium carbonyl clusters in which minor changes such as the number of carbonyl, hydride and noncarbonyl ligands are investigated. (Recall that the systematic synthesis of clusters is in itself a difficult task.) It is hoped that in this manner dramatic changes in the properties of clusters accompanying a minor change in composition will provide a better understanding to the chemistry of metal clusters.

A major theme of this thesis (Chapters 2 and 3) was to extend the methodology described above to the synthesis of heteronuclear clusters that have $ReOs_4(\mu\text{-}H)$ cores and compare them with the analogous Os_5 clusters, that is, what is the effect of replacing an Os atom in a pentaosmium cluster with a Re(H) unit. In this respect the project has

been singularly successful. Many of the $ReOs_4(\mu\text{-}H)$ clusters have completely different structures to the Os_5 compounds. For example, $ReOs_4(\mu\text{-}H)(CO)_{19}$ does not have the bow-tie arrangement of metal atoms as in $Os_5(CO)_{19}$. The Re derivative has a "spiked kite" configuration that has only been observed once before. In Chapter 4 the synthesis and structure of $Os_5(\mu\text{-}H)(H)(CO)_{18}$ is described (i.e., a change of two H ligands for a CO ligand). It also has a spiked kite Os-Os_4 nucleus rather than the bow-tie motif. From the results a preliminary explanation of the structures based on the number of metal triangles is presented.

Chapter 5 is concerned with the products formed by the addition of diphenylacetylene (C_2Ph_2) to $Os_4(CO)_{14}$. This is the first time the addition of an organic ligand to $Os_4(CO)_{14}$ has been studied and it was therefore hoped the investigation would be of potential interest to catalysis. In this respect, the project was also successful. In particular, the isolation under mild conditions of $Os_4(\mu\text{-}\eta^2\text{-}C_2Ph_2)(CO)_{14}$ (along with $Os_4(\mu_3\text{-}\eta^2\text{-}C_2Ph_2)(CO)_{13}$ and $Os_4(\mu_4\text{-}\eta^2\text{-}C_2Ph_2)(CO)_{12}$) has suggested a new model for surface catalysis.

In Chapter 6 is reported the unsuccessful attempt to convert $Os_4(CO)_{14}$ into an Os_8 cluster by pyrolysis; compare, the conversion $Os_3(CO)_{12}$ to $Os_6(CO)_{18}$ (eq 1.1). Although the experiment was unsuccessful it was found that C_6F_6 was a suitable solvent for pyrolysis reactions. This in turn led to improved syntheses of $Ru_6(\mu_6\text{-}C)(\mu\text{-}CO)(CO)_{16}$ and $Os_6(CO)_{18}$ (Figure 1.2). The latter synthesis is employed in the Pomeroy laboratory for the preparation of Os_7 clusters (e.g., eq 1.16). Spectroscopic evidence for the unknown $Ru_xOs_{5-x}(CO)_{16}$ (x = 5, 2, 1) is also given in Chapter 6.

In the pyrolysis of $Os_4(CO)_{14}$ trace amounts of $Os_4(\mu\text{-}H)(\mu\text{-}OH)(CO)_{13}$ were isolated. In Chapter 7 a rational synthesis of the by-product and its partially deuterated analogue, $Os_4(\mu\text{-}H)(\mu\text{-}OD)(CO)_{13}$ are reported. The structures form a unique pair $Os_4(\mu\text{-}H)(\mu\text{-}OH)(CO)_{13}.H_2O$ and $Os_4(\mu\text{-}H)(\mu\text{-}OD)(CO)_{13}$ (i.e., nonhydrated). A tentative explanation why the deuterated derivative is not hydrated in the crystalline state is offered.

Carbonyl exchange in most of the clusters presented in this thesis was studied by ^{13}CO labelling and variable temperature ^{13}C NMR spectroscopy. The rate of CO exchange ranges from $<10^{-5}$ s^{-1} $[(O^{13}C)_5Re\text{-}Os_4(\mu\text{-}H)(CO)_{14}]$ to $>10^{10}$ s^{-1} $[Ru_6(\mu_6\text{-}C)(\mu\text{-}CO)(CO)_{16}]$. The latter rate is close to the infrared time scale and the IR spectrum of this cluster is abnormal in having a simple spectrum with broad peaks.

Chapter 2.* The $ReOs_4(\mu\text{-}H)(CO)_n$ (n = 20, 19, 18, 16) clusters and $ReOs_3(\mu\text{-}H)(CO)_{16}$

2.1 Introduction

Unlike $Os_3(CO)_{12}$, $Os_4(CO)_{14}$ readily reacts in solution at room temperature with donor molecules. Of particular relevance to this study is the addition of $Os(CO)_4(L)$ (L = CO, PMe_3, Bu^tNC) to $Os_4(CO)_{14}$ in solution at or below room temperature to give $Os_5(CO)_{18}(L)$.[44-46] Upon mild pyrolysis the pentanuclear derivatives undergo stepwise decarbonylation to give the corresponding $Os_5(CO)_{17}(L)$ and $Os_5(CO)_{15}(L)$ clusters. (There was no evidence for $Os_5(CO)_{16}(L)$.)[44-46]

This chapter reports the reactions of $Os_4(CO)_{14/15}$ with $Re(CO)_5(H)$ to give the $ReOs_4(\mu\text{-}H)(CO)_n$ (n = 20, 19, 18 (two isomers), 16) clusters, as well as $ReOs_3(\mu\text{-}H)(CO)_{16}$. There were two reasons for undertaking this study. As discussed in the introductory chapter, the rational synthesis of metal clusters, particularly heteronuclear clusters, remains a challenge in metal carbonyl cluster chemistry although several syntheses have been reported recently.[3,4a,16-24] Furthermore, it has been previously observed that the replacement of a carbonyl ligand with two H ligands in a metal carbonyl cluster often causes a rearrangement of the metal skeleton. For example, $Os_4(CO)_{14}(PMe_3)$ has a planar kite Os_4 unit whereas in $Os_4(\mu\text{-}H)_2(CO)_{13}(PMe_3)$ the osmium atoms have a nonplanar butterfly geometry.[34,48,49] The binary carbonyl $Os_7(CO)_{21}$ has a capped octahedral Os_7 nucleus whereas the metal unit in $Os_7(\mu\text{-}$

---

* Parts of this chapter were reproduced with permission. Canal, J. P.; Yap, G. P. A.; Pomeroy, R. K. *Organometallics* **2003**, *22*, 3439. (Reference 86) Copyright 2003 American Chemical Society.

$H)_2(CO)_{20}$ consists of a capped trigonal bipyramidal Os_6 polyhedron with the seventh Os atom bridging the OsOs edge directly opposite the capping Os atom.[50,51] It was therefore of interest to compare structures of the $ReOs_4(\mu\text{-}H)(CO)_n$ clusters with the known structures of the $Os_5(CO)_n$ analogues.[44,52,53,54] Significant changes to the metal skeletal geometry upon minor changes in ligand and metal composition provide insight to metal cluster bonding.

2.2 Results and Discussion

$ReOs_4(\mu\text{-}H)(CO)_{20}$ (1) The reaction of $Re(CO)_5(H)$ with $Os_4(CO)_{15}$ in toluene at 0 °C gave a yellow/orange precipitate; the mass, IR and NMR spectroscopic evidence indicated it was $ReOs_4(\mu\text{-}H)(CO)_{20}$ (**1**) (eq 2.1). It decomposed in solution at room

$$Os_4(CO)_{15} + Re(CO)_5(H) \xrightarrow{0\ ^\circ C} \underset{\mathbf{1}}{ReOs_4(\mu\text{-}H)(CO)_{20}} \qquad (2.1)$$

temperature over a period of 3 h; one of the decomposition products was identified as the poorly characterized $ReOs_3(\mu\text{-}H)(CO)_{16}$.[55] (The binary carbonyl $Os_4(CO)_{16}$ readily decomposes in solution at room temperature to give $Os_3(CO)_{12}$[30,56]) Although the instability of $ReOs_4(\mu\text{-}H)(CO)_{20}$ prevented its complete characterization, it was examined by IR spectroscopy, mass spectrum (parent ion) and ^1H and ^{13}C NMR spectroscopy.

Clusters of the type $Os_4(CO)_{15}(L)$ are found to adopt either a puckered square (L = CO, PF_3) or a spiked triangular (L = $P(OCH_2)_3CMe$, PMe_3) configuration of metal atoms as shown diagrammatically in Chart 2.1.[30,56] The $^{13}C/^{13}C\{^1H\}$ NMR spectrum of ^{13}CO-enriched **1** (both $Re(CO)_5(H)$ and $Os_4(CO)_{15}$ ^{13}CO-enriched) was complicated by signals due to a small amount of $ReOs_3(\mu\text{-}H)(CO)_{16}$. Nevertheless, the NMR data (Figure 2.1) is consistent with a spiked triangular structure for **1** (Chart 2.2). In

particular, a signal of intensity 4 at δ 191.2 is in the region expected for the resonance of an $Os(CO)_4$ unit.

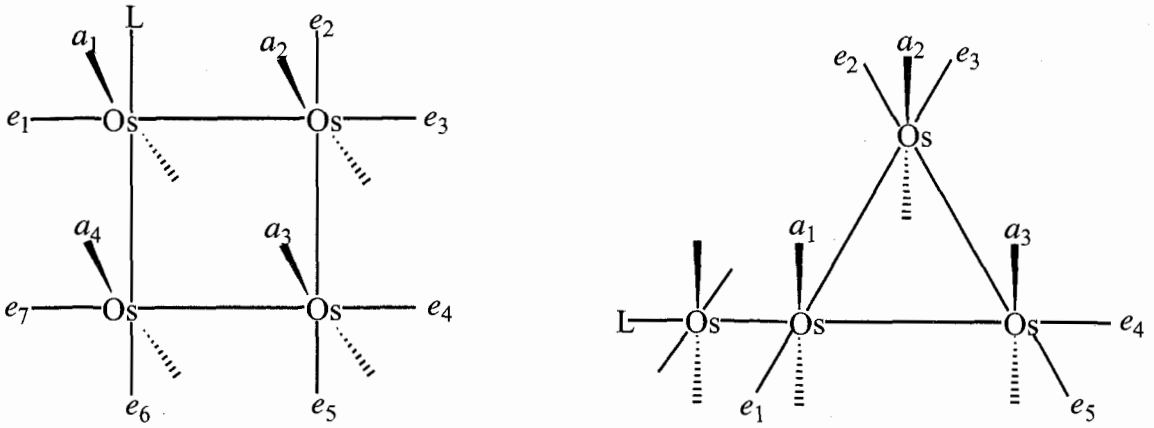

Chart 2.1. Puckered square and spiked triangular configuration of $Os_4(CO)_{15}(L)$.

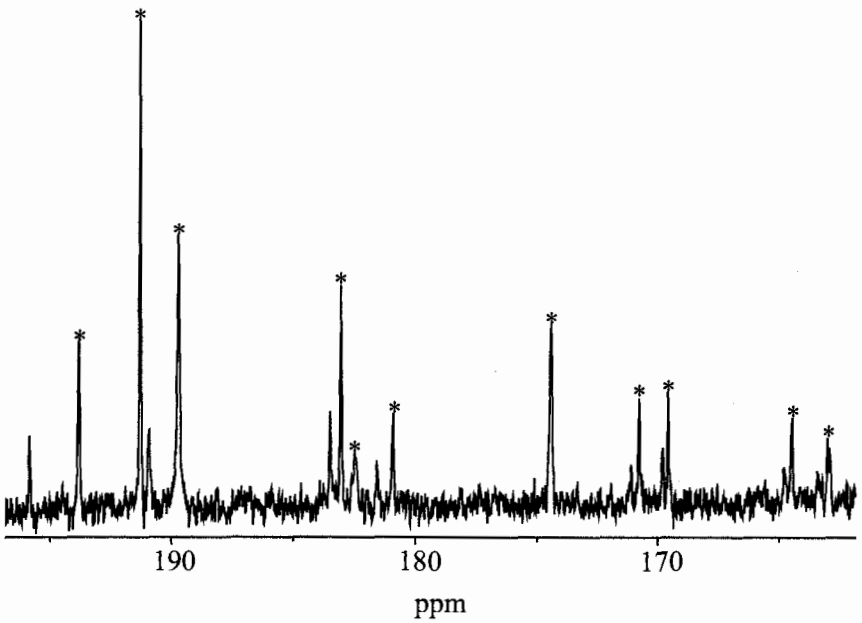

Figure 2.1. ^{13}C NMR spectrum of **1** in CH_2Cl_2/CD_2Cl_2 (* due to **1**).

Furthermore, there are only five signals of intensity 1 in the shift range for signals due to equatorial carbonyls attached to osmium.[57] In the ^1H-coupled ^{13}C NMR spectrum only the signal at δ 162.9, (due to an equatorial carbonyl on Os) was split into a doublet (J_{HC} = 9.2 Hz). This suggests that the H ligand bridges the OsOs bond trans to the spike

Os atom. (Trans couplings are typically an order of magnitude greater than cis couplings.) The structures of $(OC)_5ReOs_3(\mu\text{-}H)(CO)_{10}$-$(CH_3CN)$ and $[(OC)_5Re]_2Os_3(\mu\text{-}H)_2(CO)_{10}$, however, indicate the hydride ligands bridge OsOs bonds cis to the $Re(CO)_5$ substituents.[58,59] It is believed that the H ligand in $ReOs_4(\mu\text{-}H)(CO)_{20}$ similarly bridges the OsOs cis to the spike Os atom (i.e., as shown in Chart 2.2) and one of the CH couplings is small because the HOsC angle to this C atom is not near 180°. This is also observed for $ReOs_4(\mu\text{-}H)(CO)_{19}$ discussed below.

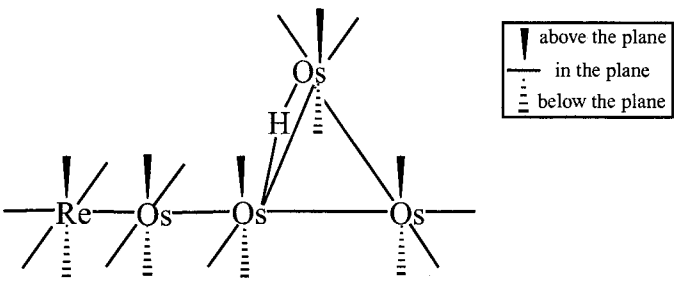

Chart 2.2. Proposed structure of **1**.

Decomposition of 1 As mentioned above, clusters of the type $Os_4(CO)_{15}(L)$ adopt two different structures (puckered square or spiked triangle) depending on the electronic properties of L. Of the known examples (L = CO, PMe_3, PF_3, $CNBu^t$, $P(OCH_2)_3CMe$) the spiked triangle arrangement of metal atoms is the more stable; the square clusters readily decompose in solution at room temperature.[56,30] Although **1** has a spiked triangle arrangement, it also is unstable at ambient conditions which is contrary to previous observations. The decomposition of **1** produces $ReOs_3(\mu\text{-}H)(CO)_{16}$ and some $Os(CO)_5$, which would seem likely to result from the square form of **1** and not the spiked triangular form. It may be that the spiked triangular isomer of **1** is in equilibrium with a small amount of the square isomer of **1**, and that decomposition proceeds through the

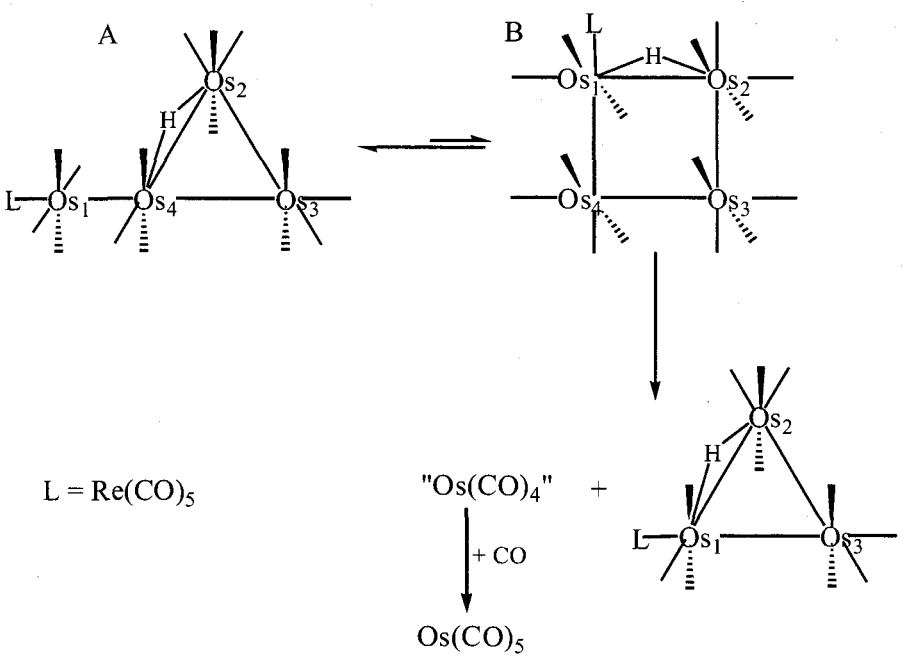

Chart 2.3. Proposed mechanism for the decomposition of **1**.

latter isomer. This is shown in Chart 2.3 and accounts for the observed products. The decomposition of square $Os_4(CO)_{16}$ to give $Os_3(CO)_{12}$ supports the idea that $ReOs_3(\mu\text{-}H)(CO)_{16}$ and $Os(CO)_5$ are produced through the unstable square arrangement.

$ReOs_4(\mu\text{-}H)(CO)_{19}$ (2) Compound **2** was prepared by the addition of $Re(CO)_5(H)$ to $Os_4(CO)_{14}$ in CH_2Cl_2 at room temperature (eq 2.2). The complex was isolated in

$$Os_4(CO)_{14} + Re(CO)_5(H) \xrightarrow{21\ ^\circ C} \underset{\mathbf{2}}{ReOs_4(\mu\text{-}H)(CO)_{19}} \qquad (2.2)$$

almost quantitative yield as deep red, air-stable crystals that were characterized by C/H/N analysis, mass (parent ion), IR, ^1H and ^{13}C NMR spectroscopy, and by X-ray crystallography.

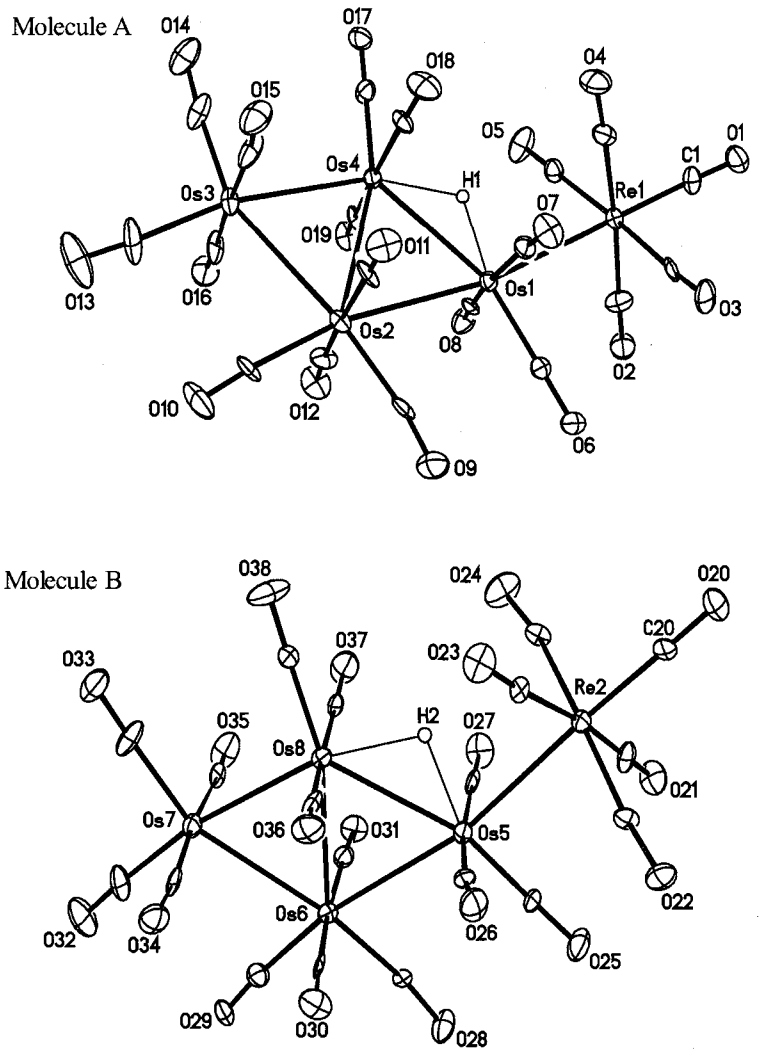

Figure 2.2. Molecular structure of $ReOs_4(\mu\text{-}H)(CO)_{19}$ (**2**).

The structure of **2**[a] has two crystallographically independent molecules in the unit cell; views of the molecules are given in Figure 2.2. Selected bond lengths and angles for **2** are given in Table 2.1. Rhenium and osmium atoms cannot be distinguished reliably by X-ray crystallography because their X-ray scattering is so similar. The site of the Re

[a] The structures described in this chapter were determined by Dr. G. P. A. Yap at the University of Ottawa.

Table 2.1. Selected bond lengths (Å) and angles (°) for $ReOs_4(\mu\text{-}H)(CO)_{19}$ (**2**).

Bond Lengths

Molecule **A**		Molecule **B**	
Re(1)-Os(1)	2.953(1)	Re(2)-Os(5)	2.947(1)
Os(1)-Os(2)	3.038(1)	Os(5)-Os(6)	3.014(1)
Os(1)-Os(4)	2.892(1)	Os(5)-Os(8)	2.904(1)
Os(2)-Os(3)	2.961(1)	Os(6)-Os(7)	2.960(1)
Os(2)-Os(4)	2.945(1)	Os(6)-Os(8)	2.928(1)
Os(3)-Os(4)	2.802(1)	Os(7)-Os(8)	2.813(1)
Re(1)-C(1)	1.88(2)	Re(2)-C(20)	1.94(2)
Re-C(*rad.*) range	1.95(2) - 2.03(2)	Re-C(*rad.*) range	1.97(2) - 2.01(2)
Os-C range	1.87(2) - 1.99(2)	Os-C range	1.83(2) - 1.98(2)
Os(1)-H(1)	2.0(1)	Os(5)-H(2)	2.0(1)
Os(2)-H(1)	2.0(1)	Os(8)-H(2)	2.0(1)
Os(2)·· C(2)[a]	2.69(1)	Os(4)·· C(4)[a]	2.84(1)
Os(3)·· C(3)[a]	2.82(1)		

[a] Weak interaction.

Bond Angles

Molecule **A**		Molecule **B**	
Re(1)-Os(1)-Os(4)	111.50(3)	Re(2)-Os(5)-Os(8)	109.57(3)
Re(1)-Os(1)-Os(2)	169.82(3)	Re(2)-Os(5)-Os(6)	168.69(3)
Os(2)-Os(1)-Os(4)	59.49(2)	Os(6)-Os(5)-Os(8)	59.27(2)
Os(3)-Os(2)-Os(4)	56.65(3)	Os(5)-Os(6)-Os(7)	115.55(3)
Os(1)-Os(2)-Os(3)	114.43(3)	Os(5)-Os(6)-Os(8)	58.49(2)
Os(1)-Os(2)-Os(4)	57.78(2)	Os(7)-Os(6)-Os(8)	57.09(2)
Os(2)-Os(3)-Os(4)	61.39(2)	Os(6)-Os(7)-Os(8)	60.88(3)
Os(1)-Os(4)-Os(2)	62.74(3)	Os(5)-Os(8)-Os(6)	62.25(2)
Os(1)-Os(4)-Os(3)	124.70(3)	Os(5)-Os(8)-Os(7)	124.24(3)
Os(2)-Os(4)-Os(3)	61.96(3)	Os(6)-Os(8)-Os(7)	62.03(2)

atom is however confidently assigned on the basis of the metal-metal bond lengths, mode of synthesis and the ^{13}C NMR data described below.

Unbridged ReOs bonds reported in the literature range in length from 2.931 to 3.006 Å whereas unbridged OsOs bonds in chain complexes are typically in the range 2.871 to 2.918 Å.[60] A summary of the ReOs bond lengths found in the literature is shown in Table 2.2 (The data in this table was originally presented in reference 60). The

Table 2.2. Unbridged ReRe, ReOs and OsOs bond lengths (Å).[a]

Compound	ReRe Length	Compound	OsOs Length
$Re_2(CO)_{10}$	3.041	$(OC)_3(Cl)(L)Os[Os(CO)_4]_3$-$Os(L)(Cl)(CO)_3$	2.871, 2.891
$Re_2(CO)_8(CNC_6H_3Me_2)_2$	3.047	$(OC)_3(L)_2ReOs(CO)_4$-$Os(CO)_3(L)Re(L)(CO)_4$	2.875
$Re_2(CO)_9(L)$	3.048	$(OC)_4(L)ReOs(CO)_3(L)$-$Os(CO)_3(L)Re(L)(CO)_4$	2.876
$Re_2(CO)_7(CNMe)_3$	3.049	$(Cl)[Os(CO)_3(L)]_2$-$Mn(CO)_5$	2.881
$Re_2(CO)_6(CNC_6H_3Me_2)_4$	3.081	$(OC)_2(Br)(L)_2OsOs(CO)_4$-$Mn(CO)_5$	2.889
		$(OC)_3(I)(L)Os[Os(CO)_3(L)]_2$-$Mn(CO)_5$	2.889, 2.893
Compound	ReOs Length	$(OC)_3(L)_2OsOs(CO)_4$-$Os_3(\mu\text{-}Cl)_2(CO)_9$	2.900,[b] 2.905[b]
$(OC)_4(L)ReOs(CO)_3(L'$-$Os(CO)_3(L)Re(L)(CO)_4$	2.933, 2.931	$(OC)_4(L)OsOs(CO)_3(L)$-$W(CO)_5$	2.907[b]
$[(OC)_5Re]_2Os_3(H)_2(CO)_{10}$	2.952, 2.983	$(OC)_4(L)OsOs_3(CO)_{11}$	2.918[b]
$(Me_3P)(OC)_3(Br)OsRe(CO)_5$	2.977	$(OC)_3(L)_2OsOs(CO)_4$-$W(CO)_5$	2.940[b]
$(OC)_3(L)_2OsRe(CO)_4(Cl)$[c]	2.982[b]		
$(OC)_3(L)_2ReOs(CO)_4$-$Os(CO)_3(L)Re(L)(CO)_4$	2.943, 2.952		
$(Me_3P)(OC)_4OsRe(CO)_4(Br)$	3.006[b]		
$(OC)_3(L)_2OsRe(CO)_4(Br)$[c]	3.007[b]		

[a] See ref. 60 for the original references for the structures. [b] Dative bond. [c] Unpublished work from the Pomeroy laboratory.

ReOslengths in the independent molecules of **2** of 2.947(1) and 2.953(1) Å are therefore within the range reported for unbridged ReOs bonds.

The metal framework in **2** consists of a planar Os_4 rhomboid that is also found in $Os_4(CO)_{15}$, with the $Re(CO)_5$ unit bound in an equatorial site to one of the wingtip Os atoms. The Os_4 arrangement in $Os_4(CO)_{15}$ and some of its derivatives have been dubbed a kite configuration.[29,36] The metal skeleton in **2** may therefore be described as a "spiked

kite." There are several reports in the literature of metal carbonyl cluster complexes with a spiked butterfly arrangement, that is, where the M_4 rhomboid is nonplanar. Two recent examples are $Ru_5(\mu_5\text{-}C_2Ph_2)(\mu\text{-}PPh_2)(dppm)(CO)_{12}$ and $(\eta^5\text{-}C_5Me_5)RhRu_4(\mu\text{-}H)[\mu_5\text{-}B(\mu\text{-}H)_2](\mu\text{-}CO)_2(CO)_{11}$.[61,62] There is however only one previous report of a pentanuclear cluster in which the rhomboid is flat and that is $Os_5(\mu\text{-}H)(\eta^2\text{-}C_6F_5NNNC_6F_5)(CO)_{17}$.[63] Besides **2,** two more examples of a spiked kite cluster, $(ReOs_4(\mu\text{-}H)(CO)_{18}(PPh_3)$ and $Os_5(H)(\mu\text{-}H)(CO)_{18})$, will be presented in Chapter 3 and Chapter 4.

The OsOs lengths in $Os_4(CO)_{15}$ are unusual in that the peripheral bonds consist of two long (about 3.00 Å) bonds between $Os(CO)_4$ units and two short bonds (about 2.77 Å) that involve the hinge $Os(CO)_3$ fragment.[29,36] The hinged OsOs bond is 2.948(1) Å. Bonds between osmium atoms in open Os cluster compounds are usually within 0.05 Å of 2.877 Å the average OsOs distance in $Os_3(CO)_{12}$.[64] The OsOs lengths in $Os_4(CO)_{15}$ have been rationalized in terms of 3c-2e bonds to give OsOs bonds of order 1.5 and 0.5 (Chart 2.4).[29,36] In this way each Os atom achieves an 18 electron configuration.

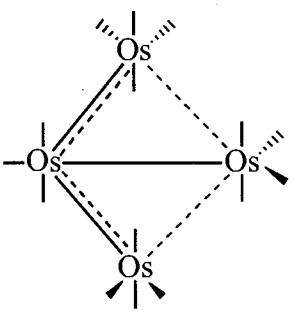

Chart 2.4. 3c-2e bonds in $Os_4(CO)_{15}$.

(Semi-emperical MO calculations, however, give an alternative view.[65]) In **2** the peripheral OsOs bonds that involve the Os atom of the hinge $Os(CO)_4$ unit are likewise long at 3.038(1) and 2.961(1) Å (molecule **A**), and 3.014(1) and 2.960(1) Å (molecule

B). The OsOs bonds that include the Os atom of the $Os(CO)_3$ grouping are 2.802(1) and 2.892(1) Å (molecule **A**) and 2.813(1) and 2.904(1) Å (molecule **B**). The longer bond in each pair is believed to be bridged by the hydride ligand rather than one of the long OsOs bonds (see below). The presence of a single bridging hydride ligand invariably causes an elongation of about 0.12 Å to an OsOs bond in hydrido Os_3 cluster compounds of which there are numerous examples.[66] The lengthening of the Os(1)Os(4) bond in **2** compared to that in $Os_4(CO)_{15}$ caused by the presence of the bridging hydride ligand is therefore slightly less than this value. The hinge OsOs bond (2.945(1), 2.928(1) Å) although somewhat long is more typical of a single OsOs bond.

Hydride ligands cannot be located in hydrido metal carbonyl clusters especially when they are bound to third row transition metal atoms as those in this thesis. The scattering of X-rays by atoms is proportional to Z^2 where Z is the atomic number of the atom. An Os atom therefore scatters X-rays over five thousand times more effectively than a hydrogen atom. The scattering of the latter is consequently lost in the background noise. The hydride ligand in **2** and the other hydrido clusters described in this thesis are placed by the use of Orpen's XHYDEX program.[67] Details of the XHYDEX program are given in the Experimental Section. This program has been used by the Pomeroy group for some 20 years and has never failed in the correct prediction for the placement of a hydride ligand in a hydrido-osmium cluster.

Placement of the H ligand across the Os(1)Os(4) bond gave a "site energy" of 1.2 by the program (Table 2.3). This is in the range of 0.2 - 10.6 previously found for bridging hydride ligands. Support for this placement also comes from the Os(2)Os(4)-C(17) angle that is 163.7(6)°. The corresponding angle in $Os_4(CO)_{15}$ (Chart 2.4) is 180°

by crystallography. The next lowest site energy was for the hydride ligand in a terminal position on Os(4) at 10.5 which is outside the range (2.2 - 7.5) previously determined for terminal metal hydride site energies.

Table 2.3. Site energy values (kcal mol^{-1}) for the terminal and bridging hydride positions in $ReOs_4(\mu\text{-}H)(CO)_{19}$.

Bridging Positions

Molecule **A**		Molecule **B**	
Os(1)-Re(1)	17.1	Os(5)-Re(2)	14.1
Os(1)-Os(2)	33.5	Os(5)-Os(6)	33.2
Os(1)-Os(4)	**1.2**	Os(5)-Os(8)	**1.6**
Os(2)-Os(3)	42.8	Os(6)-Os(7)	47.9
Os(2)-Os(4)	40.2	Os(6)-Os(8)	45.0
Os(3)-Os(4)	28.0	Os(7)-Os(8)	26.9

Terminal Positions

Molecule **A**		Molecule **B**	
Re(1)	71.3	Re(2)	50.0
Os(1)	14.4	Os(5)	15.3
Os(2)	79.6	Os(6)	56.4
Os(3)	57.2	Os(7)	52.9
Os(4)	10.5	Os(8)	10.6

As implied above, it might have been expected that the H ligand bridges one of the long OsOs bonds in the molecule. However, the site energies determined for these positions (33.5 and 42.8 for bridging Os(1)Os(2) and Os(2)Os(4), respectively) clearly indicate the H ligand is not located across either of these bonds (Table 2.3).

Cluster **2** is similar to $Os_4(\mu\text{-}H)(CO)_{14}(SnMe_3)$ that was prepared by the addition of $HSnMe_3$ to $Os_4(CO)_{14}$.[37] The tin derivative has the same configuration as **2**, but with the $SnMe_3$ unit replacing the $Re(CO)_5$ grouping. Persuasive structural and spectroscopic evidence indicates that, like **2**, in $Os_4(\mu\text{-}H)(CO)_{14}(SnMe_3)$ the H ligand bridges the OsOs bond cis to the noncarbonyl ligand that is unusually short for a Os(μ-H)Os grouping. As shown in Chart 2.5 the OsOs distances in the tin compound show interesting differences

to the corresponding distances in **2**. (The distances for **2** are the mean of the distances found in the independent molecules in the unit cell.) Also shown in Chart 2.5 are the OsOs lengths in $Os_4(CO)_{14}(PMe_3)$ that has the same electron count as **2** and $Os_4(\mu\text{-}H)(CO)_{14}(SnMe_3)$, but lacks a bridging hydride.[34,48]

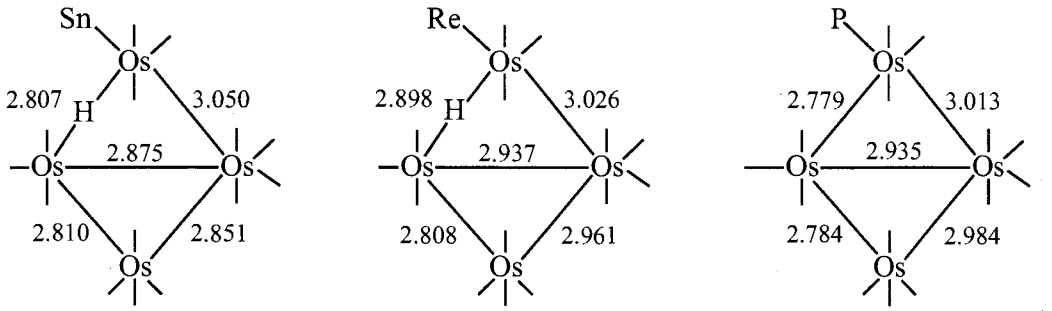

$Os_4(\mu\text{-}H)(CO)_{14}(SnMe_3)$ $Os_4(\mu\text{-}H)(CO)_{14}[Re(CO)_5]$ (**2**) $Os_4(CO)_{14}(PMe_3)$

Chart 2.5. OsOs bond lengths in $Os_4(\mu\text{-}H)(CO)_{14}(SnMe_3)$, **2**, and $Os_4(CO)_{14}(PMe_3)$.

It is our view that the OsOs bond lengths in these clusters cannot be readily explained by using simple bonding arguments. It is well known, however, that metal-metal bonds, especially those that involve third row transition metals, are often soft and sensitive to crystal packing forces.[68] The differences in analogous OsOs lengths of the molecules shown in Chart 2.5 might therefore simply be the result of different packing forces within the crystals. This would be especially true if the OsOs bonds had a bond order of less than 1 as proposed for $Os_4(CO)_{15}$ (Chart 2.4). On the other hand, in a study from the Pomeroy laboratory an analysis of 18 crystal structures of the type $Os_3(CO)_{11}(PR_3)$ indicated that crystal packing forces were small, and rarely accounted for more than a difference of 0.02 Å in the OsOs lengths.[69]

The $^{13}C\{^1H\}$ NMR spectrum of **2** prepared from ^{13}C-enriched (~30%) $Os_4(CO)_{14}$ and unenriched $Re(CO)_5(H)$ displayed signals (Figure 2.3A) consistent with the solid state structure of **2** with the exception that the signals due to the carbonyls attached to the

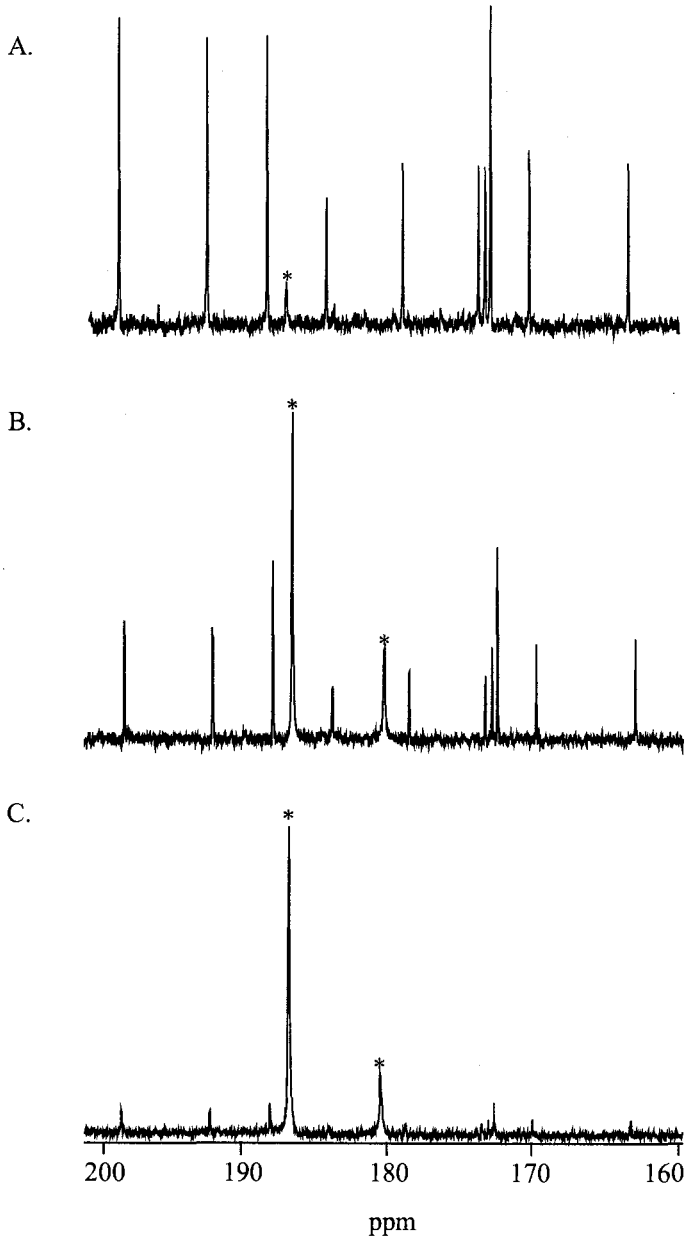

Figure 2.3. $^{13}C\{^{1}H\}$ NMR spectra of **2** (in CH_2Cl_2/CD_2Cl_2): (A) Sample prepared from ^{13}CO enriched $Os_4(CO)_{14}$. (B) Sample prepared from ^{13}CO enriched $Re(CO)_5(H)$ after 5 days. (C) Sample prepared from ^{13}CO enriched $Re(CO)_5(H)$. Peaks marked with an asterisk (*) are due to CO ligands attached to the Re atom.

Re atom are very weak. This could be due to the absence of CO exchange between the Re and Os carbonyls in **2**, or to quadrupolar broadening of these signals due to the rhenium atom (both naturally occurring isotopes of Re have spin 5/2). In order to

distinguish between the two possibilities, **2** was prepared from unenriched $Os_4(CO)_{14}$ and ^{13}CO-enriched $Re(CO)_5(H)$. The $^{13}C\{^1H\}$ NMR spectrum of this sample is given in Figure 2.3C and clearly shows strong signals due to the Re carbonyls, but weak resonances due to the Os carbonyls. The spectrum was also recorded after the sample had been allowed to stand at room temperature for 5 days (Figure 2.3B). The signals due to the Os carbonyls had significantly increased in intensity, but were still not of the expected intensity for complete scrambling of the ^{13}CO ligands over all the available carbonyl sites. Carbonyl exchange between the $Re(CO)_5$ grouping and the rest of the cluster is thus slow on the synthetic time scale at room temperature. In this respect it resembles the CO exchange in $(OC)_5MnRe(^{13}CO)_5$.[70]

The ^{13}C NMR resonances for the Os carbonyls of **2** consist of four signals of intensity 2 due to axial carbonyls and five attributed to equatorial CO ligands with intensity 1 which is as predicted from the solid state structure (Figure 2.2). One of the axial signals (at δ 172.6) is shifted to high field such that it is in the region where peaks due the equatorial carbonyls normally occur. This was also observed in the $^{13}C\{^1H\}$ NMR spectra of $Os_4(CO)_{14}(PMe_3)$ and $Os_4(\mu\text{-}H)(CO)_{14}(SnMe_3)$ and probably reflects the usual bonding in these derivatives. This resonance can be assigned to the axial carbonyls on Os(2).[34,37,48] By analogy, the high field resonances with intensity of 1 at δ 169.9 and 163.2 are assigned to the equatorial carbonyls of this atom.

The H-coupled ^{13}C NMR spectrum of **2** showed coupling to two resonances due to axial carbonyls (δ 198.1 and 192.2) and three resonances attributed to equatorial carbonyls (δ 184.0, 178.7 and 173.4). The couplings were in the range 2.6 - 3.4 Hz except that to the signal at δ 184.0, which was 6.7 Hz. The resonance at δ 184.0 can be

confidently assigned as due to C(6) (Figure 2.2) as it is directly trans to the H atom. The coupling pattern might be considered more consistent with placement of the H ligand across the long Os(1)Os(2) or Os(2)Os(3) bond. It is believed the H ligand does indeed bridge the Os(1)Os(4) bond and that one of the small couplings to a signal attributed to an equatorial carbonyl is the all-trans, three-bond coupling to C(13) (Figure 2.2) and is larger than normal because of the delocalized bonding in the molecule. The resonance that exhibits the other small coupling is assigned to the equatorial carbonyl cis to the H bond (i.e., C(18) Figure 2.2A). The C-H couplings observed in the spectrum of **2** are similar to the corresponding couplings in $Os_4(\mu\text{-}H)(CO)_{14}(SnMe_3)$ where the evidence for the positioning of the H ligand is stronger.[37]

The two hydrogen coupled resonances (δ 198.1, J_{CH} = 2.6 Hz and 192.2, J_{CH} = 3.4 Hz) both with an intensity of 2 can be assigned to the pair of axial carbonyls on Os(1) and Os(4) (Figure 2.3A). In the ^{13}C NMR spectra of $Os_4(CO)_{14}(PMe_3)$ and $Os_4(\mu\text{-}H)(CO)_{14}(SnMe_3)$ the resonance of the carbonyls attached to $Os(CO)_3$ unit of the hinged OsOs bond experience a large down field shift, suggesting that the signal δ 198.1 results from the axial CO's on Os(1).[34,37,48] The remaining two resonances of the carbonyls bound to Os atoms at δ 188.0 (intensity 2) and δ 173.0 (intensity 1) are assigned to the axial carbonyls on Os(3) and the equatorial CO numbered 14 on Os(3) (Figure 2.2). The signals due to the carbonyls bound to Re are confidently assigned on the basis of their intensity. The resonance at δ 186.7 with intensity 4 is assigned to the four carbonyls cis to the ReOs bond and that at δ 180.4 with intensity 1 is assigned to the CO trans to the ReOs bond (Figure 2.3C). Note that these signals are somewhat broadened compared to

the resonances of the Os carbonyls. This broadening is attributed to quadrupolar broadening mentioned above.

$ReOs_4(\mu\text{-}H)(\mu\text{-}CO)(CO)_{17}$ (3a) "Spiked Tetrahedron" Careful heating of **2** in hexane at 85 °C for 24 h produced as a precipitate compound **3a** (eq 2.3). The complex

$$ReOs_4(\mu\text{-}H)(CO)_{19} \xrightarrow{85°C} \underset{\textbf{3a}}{ReOs_4(\mu\text{-}H)(\mu\text{-}CO)(CO)_{17}} \qquad (2.3)$$

was isolated as orange air stable crystals upon recrystallization from CH_2Cl_2. It was characterized by C/H/N analysis, IR, mass (parent ion), ^1H and ^{13}C NMR spectroscopy, and X-ray crystallography. The structure of **3a** consists of a spiked tetrahedral arrangement of metal atoms (Figure 2.4). (Selected bond lengths and angles for **3a** are given in Table 2.4). There is a bridging carbonyl present in the molecule which is rare for Os carbonyl cluster complexes, although a bridging carbonyl is present in $Os_5(\mu\text{-}CO)(CO)_{17}$ a cluster with the same 76-electron count as **3a**.[44,53,71] As before, the spike metal atom is confidently assigned as the Re atom based on the metal-metal lengths. The spike metal-metal length of 2.970(1) Å is typical of an unsupported ReOs bond. The XHYDEX program indicated that the hydride ligand bridges Os(1)Os(2) (Table 2.5) and consistent with this view is that the OsOs vector is long at 2.963(1) Å. The other OsOs lengths are significantly shorter and are in the range 2.733(1) to 2.873(1) Å. The shortest OsOs distance is associated with the bridging carbonyl group; the other two short metal-metal distances involve the Os atom of the $Os(CO)_3$ grouping. The shorter OsOs lengths

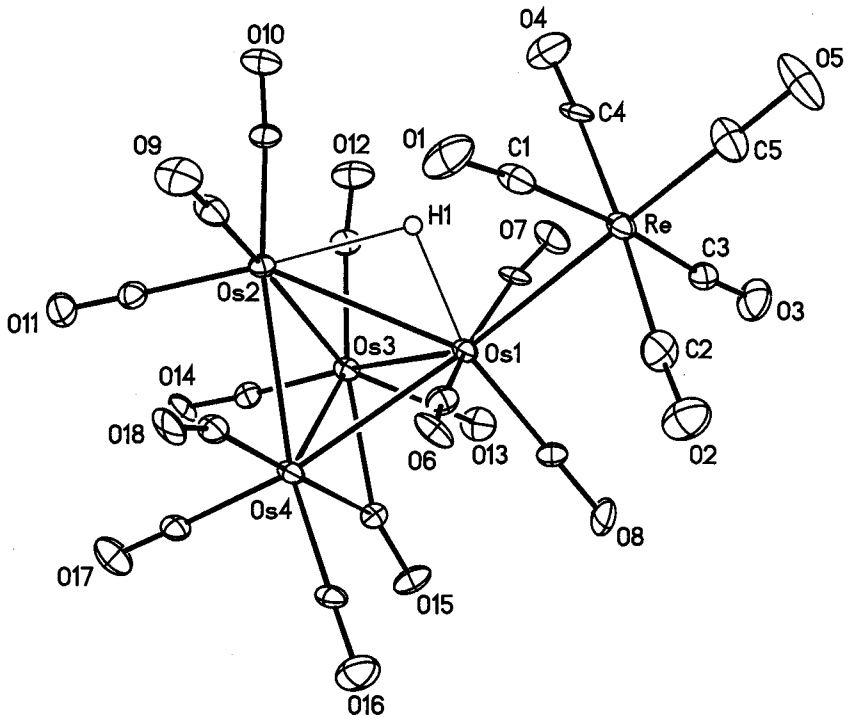

Figure 2.4. Molecular structure of $ReOs_4(\mu\text{-}H)(\mu\text{-}CO)(CO)_{17}$ (**3a**).

Table 2.4. Selected bond lengths (Å) and angles (°) for $ReOs_4(\mu\text{-}H)(\mu\text{-}CO)(CO)_{17}$ (**3a**).

Bond Lengths			
Re-Os(1)	2.970(1)	Os(2)-Os(3)	2.837(1)
Os(1)-Os(2)	2.963(1)	Os(2)-Os(4)	2.804(1)
Os(1)-Os(3)	2.873(1)	Os(3)-Os(4)	2.733(1)
Os(1)-Os(4)	2.860(1)		
Re-C(5)	1.89(2)	Os(3)-C(15)	2.19(2)
Re-C(*rad.*) range	1.99(2) - 2.02(2)	Os(4)-C(15)	2.10(2)
Os(4)-C(*term.*) range	1.84(2) – 1.96(2)		
Os(1)-H	1.83		
Os(2)-H	2.14		

Bond Angles			
Re-Os(1)-Os(2)	115.82(3)	Os(3)-Os(2)-Os(4)	57.96(2)
Re-Os(1)-Os(3)	148.32(3)	Os(1)-Os(3)-Os(2)	62.51(2)
Re-Os(1)-Os(4)	150.65(3)	Os(1)-Os(3)-Os(4)	61.27(2)
Os(2)-Os(1)-Os(3)	58.15(2)	Os(2)-Os(3)-Os(4)	60.41(2)
Os(2)-Os(1)-Os(4)	57.55(3)	Os(1)-Os(4)-Os(2)	63.08(3)
Os(3)-Os(1)-Os(4)	56.95(2)	Os(1)-Os(4)-Os(3)	61.78(2)
Os(1)-Os(2)-Os(3)	59.34(2)	Os(2)-Os(4)-Os(3)	61.63(2)

Table 2.5. Site energy values (kcal mol^{-1}) for the terminal and bridging hydride positions in $ReOs_4(\mu\text{-}H)(\mu\text{-}CO)(CO)_{17}$.

Bridging Positions			
Os(1)-Re(1)	14.9	Os(2)-Os(3)	41.2
Os(1)-Os(2)	**0.6**	Os(2)-Os(4)	52.9
Os(1)-Os(3)	40.7	Os(3)-Os(4)	35.8
Os(1)-Os(4)	41.0		

Terminal Positions			
Re(1)	62.3	Os(3)	73.0
Os(1)	9.9	Os(4)	72.2
Os(2)	14.5		

(compared to say those in $Os_3(CO)_{12}$) are typical of OsOs lengths found in more condensed Os carbonyl clusters such as $Os_5(CO)_{16}$, $Os_6(CO)_{18}$ and $Os_7(CO)_{21}$.[50,54,71,72]

The spiked tetrahedral arrangement of metal atoms is extremely rare in metal carbonyl cluster chemistry. It is found in $Os_6(\mu\text{-}H)(\eta^2\text{-}C_6F_5NNNC_6F_5)(\mu\text{-}CO)(CO)_{19}$ that has the same $Os_4(\mu\text{-}H)(\mu\text{-}CO)(CO)_{12}$ unit as **3a**.[73] The arrangement is also present in $RuOs_4(\mu\text{-}H)_3(\mu_3\text{-}\eta^6\text{-}C_6H_5)(CO)_{12}[P(OMe)_3]$ and $Ru_2Os_3(\mu\text{-}H)(\mu_3\text{-}\eta^5\text{-}C_5H_4)(\eta^5\text{-}C_5H_5)(CO)_{11}[P(OMe)_3]$; in each case the spike metal-metal bond is bridged by ligands.[74,75] In the dianion $[Ir_8(CO)_{22}]^{2-}$ two Ir_4 tetrahedra are fused by an unbridged IrIr bond.[76]

Cluster **3a** is much less soluble than the other pentanuclear clusters reported here and those mentioned in the Introduction.[44-46] The calculated densities for the $ReOs_4(\mu\text{-}H)(CO)_n$ clusters (3.484, 3.697, 3.879 Mg m^{-3} for n = 19, 18, 16) do not suggest any unusually strong intramolecular forces present in **3a** (n = 18). The shortest intermolecular separations are five O···O contacts around 2.9 Å.

The insolubility of **3a** prevented its study by $^{13}C\{^1H\}$ NMR spectroscopy below room temperature. The spectrum (Figure 2.5) at ambient temperature in CH_2Cl_2/CD_2Cl_2

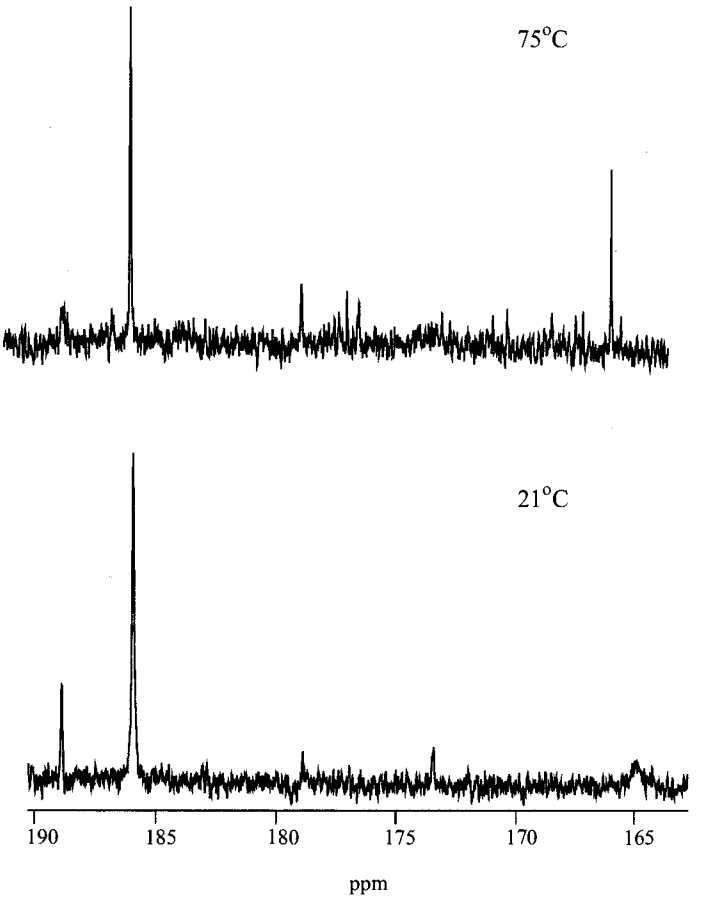

Figure 2.5. $^{13}C\{^1H\}$ NMR spectra of **3a**. The solvent for the room temperature spectrum was CH_2Cl_2/CD_2Cl_2; for the spectrum at 75 °C it was $C_2H_2Cl_4/C_2D_2Cl_4$.

was obtained with difficulty (~30% ^{13}CO enriched in all sites; 37,000 scans). As such the spectrum consisted of two intense signals (at δ 188.9 and 185.1) in an approximate 1:4 ratio that are confidently assigned as due to the carbonyls of the $Re(CO)_5$ unit. Of much weaker intensity were two resonances at δ 178.9 and 173.4 in a 1:2 ratio and a broad signal centered at δ 165. (The same spectrum was obtained on samples from two different preparations.) In the spectrum at 75 °C ($C_2H_2Cl_4/C_2D_2Cl_4$, 31,623 scans; Figure 2.5) the signal originally at δ 188.1 had broadened (at δ 188.9). Because the peak width

of the signal originally at δ 185.9 appeared unchanged, the broadening is attributed to quadrupolar coupling to Re rather than the result of CO exchange. (Quadrupolar broadening increases with temperature.) In the Os-CO region there was a relatively strong signal at δ 165.3 plus several other signals that were hardly discernible above the background (Figure 2.5). The most intense of the weak signals was at δ 178.9; this signal was attributed to $ReOs_4(\mu\text{-}H)(CO)_{16}$ the thermal decomposition product of **3a** (see below). The presence of this product was confirmed by a $^{13}C\{^1H\}$ NMR spectrum (in CH_2Cl_2/CD_2Cl_2, RT) of the sample recovered after the spectrum at 75 °C had been determined.

The NMR results are interpreted as follows. The carbonyls attached to the Re atom are rigid on the NMR scale. The carbonyls bound to the Os atom of the $Os(CO)_3[Re(CO)_5]$ grouping (i.e., carbonyls *a* and *b* in Chart 2.6) are also rigid at room temperature but undergo mutual exchange at 75 °C such that the ^{13}C signals are broadened into the baseline or that the coalesced signal is not sufficiently above background to be confidently assigned. The carbonyls in the Os_3 plane that contain the bridging carbonyl (i.e., the carbonyls labeled *c* in Chart 2.6) undergo exchange to give

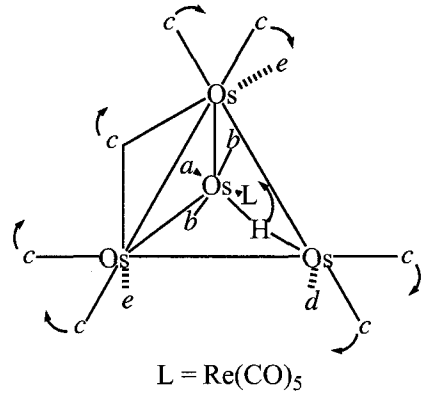

L = $Re(CO)_5$

Chart 2.6. Merry-go-round CO exchange in **3a**.

the broad signal at δ 165 that sharpens in the spectrum at 75 °C. Cluster compounds with a single bridging CO ligand typically undergo rapid merry-go-round CO exchange in the plane containing the M(μ-CO)M grouping.[77] (In order to maintain equivalent electronic configurations between the different states requires the hydride ligand to move counter to the motion of the CO exchange as shown in Chart 2.6.) The ^{13}C NMR chemical shifts of bridging carbonyls are typically 30 ppm to low field of the shifts of terminal carbonyls.[78] To cause coalescence of two signals due to the two different types of carbonyls would require a rate of exchange of approximately 7×10^3 s^{-1}.

It is unclear why the signals due to the carbonyls on the Os atoms were of low intensity. It is tentatively attributed to partial saturation due to long T_1 relaxation times of the C atoms of these ligands. The intensity of these signals, however, did not change when the spectrum was recorded with the relaxation agent $Cr(acac)_3$ added to the solution.[79]

$ReOs_4(\mu\text{-}H)(CO)_{18}$ (3b) "Raft" When a solution of **2** (or **3a**) was subjected to ultraviolet radiation for 8 hours a purple, air-stable precipitate formed that was collected on the centrifuge (eq 2.4). Due to its insolubility in common organic solvents complete

$$ReOs_4(\mu\text{-}H)(CO)_{19} \xrightarrow{h\nu} \underset{\textbf{3b}}{ReOs_4(\mu\text{-}H)(CO)_{18}} \qquad (2.4)$$

characterization was not possible. A C/H/N analysis of the compound was obtained along with a solid-state IR (Figure 2.6), mass (parent ion), and ^1H NMR spectroscopy (over 2000 scans were required to obtain an observable signal). From this data the purple precipitate is assigned the formula $ReOs_4(\mu\text{-}H)(CO)_{18}$ (**3b**), that is, it is an isomer of **3a**.

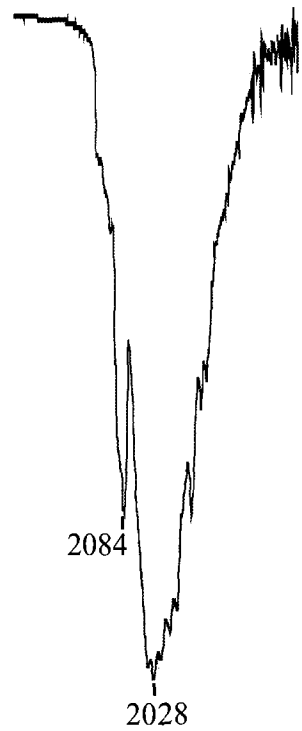

Figure 2.6. IR (KBr) spectrum (ν(CO) region) of $ReOs_4(\mu\text{-}H)(CO)_{18}$ (**3b**).

Crystals of **3b** suitable for X-ray diffraction study could not be obtained because of its insolubility. In Chapter 3 the PPh_3 derivatives of **3a** and **3b** are described (i.e. $ReOs_4(\mu\text{-}H)(\mu\text{-}CO)(CO)_{16}[P(C_6H_5)_3]$ **a** and **b** forms). In this case the purple isomer (i.e., analogous to **3b**) was shown by X-ray crystallography to contain a planar raft arrangement of metal atoms. When a carbonyl is replaced by a phosphine ligand there is usually retention of the metal skeleton. For example this is seen in $Os_5(CO)_nL$ (n = 18, 17, 15; L = CO, PMe_3) and $Os_3(CO)_{11}L$ (L = CO, PR_3).[45,69] Compound **3b** is therefore assigned the raft structure as shown in Figure 2.7.

The ^1H NMR spectrum of **3b** contained a single resonance at δ -13.9, which is consistent with a bridging H ligand in the molecule. The IR spectrum of **3b** does not

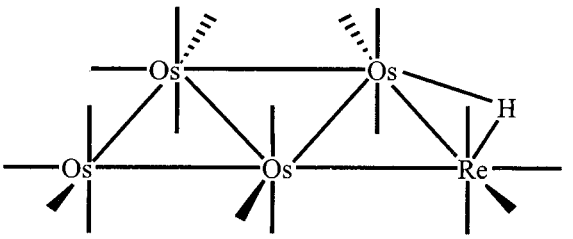

Figure 2.7. Proposed structure for $ReOs_4(\mu\text{-}H)(CO)_{18}$ (**3b**).

contain a band in the bridging CO region, indicating that all the carbonyls are terminal as found for the raft form of $ReOs_4(\mu\text{-}H)(CO)_{17}[P(C_6H_5)_3]$. However, the isoelectronic $Os_5(\mu\text{-}CO)(CO)_{17}$ does contain a bridging CO.[44] Although $Os_5(\mu\text{-}CO)(CO)_{17}$ is soluble in CH_2Cl_2, $Os_6(CO)_{21}$ that is also believed to have a raft arrangement of Os atoms is highly insoluble and has not been characterized crystallographically.

$ReOs_4(\mu\text{-}H)(CO)_{16}$ (4) Heating of **2** (or a suspension of **3**) in hexane at 95 °C for 4 d gave **4** (48% yield) after work up. Alternatively, **4** can be made in a greater yield (78%) by the pyrolysis of **3b** in hexane at 80 °C for 3 hours (eq 2.5). No evidence for the

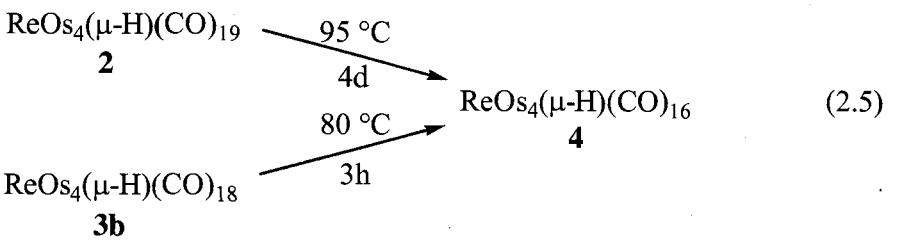

(2.5)

production of **3a** during the pyrolysis of **3b** was observed. In both cases the complex was isolated by recrystallization from CH_2Cl_2 to give dark red, almost black, air-stable crystals which were characterized by C/H/N analysis, IR (Figure 2.8), mass (parent ion), ^1H and ^{13}C NMR spectroscopy, and X-ray crystallography.

The structure of **4** as determined by X-ray crystallography is shown in Figure 2.9; selected bond lengths and angles are collected in Table 2.6. The Re atom once again is

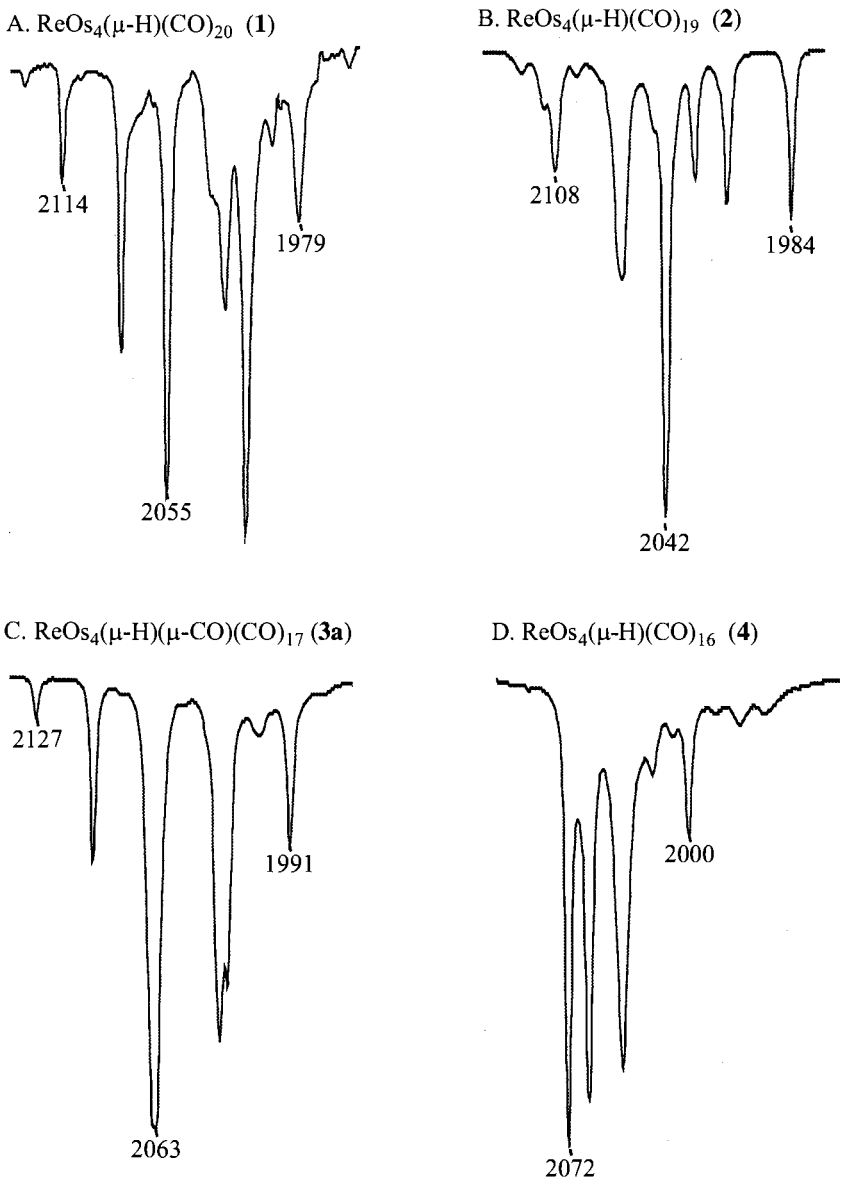

Figure 2.8. IR (hexane) spectra (ν(CO) region) of **1**, **2**, **3a**, and **4**.

placed in the site shown on the basis of the metal-metal bond lengths: the (unbridged) lengths involving this metal atom are significantly longer than those between the other metal atoms (2.8911(6) - 2.9978(6) Å versus 2.7468(6) - 2.8209(6) Å). As indicated by the XHYDEX program the H ligand bridges the longest metal-metal vector (3.0840(6) Å) (Table 2.7). The trigonal bipyramidal arrangement of metal atoms in **4** is the structure

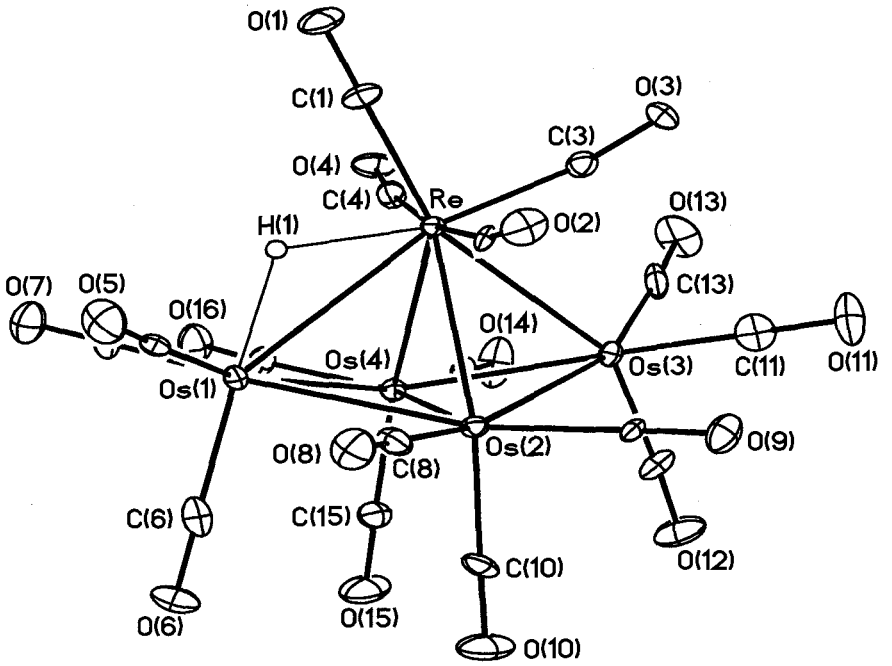

Figure 2.9. Molecular structure of $ReOs_4(\mu\text{-}H)(CO)_{16}$ (**4**).

Table 2.6. Selected bond lengths (Å) and angles (°) for $ReOs_4(\mu\text{-}H)(CO)_{16}$ (**4**).

Bond Lengths			
Re-Os(1)	3.0840(6)	Os(1)-Os(2)	2.8209(6)
Re-Os(2)	2.8911(6)	Os(1)-Os(4)	2.7978(6)
Re-Os(3)	2.9978(6)	Os(2)-Os(3)	2.7776(6)
Re-Os(4)	2.9170(6)	Os(2)-Os(4)	2.7995(6)
		Os(3)-Os(4)	2.7468(6)
Re-C (range)	1.96(1) - 2.01(1)	Os(3) - C (range)	1.88(1) - 1.94(1)
Re-H	1.83	Os(1)-H	1.82

Bond Angles			
Os(1)-Re-Os(2)	56.23(1)	Os(1)-Os(2)-Os(3)	112.95(2)
Os(1)-Re-Os(3)	100.24(2)	Os(1)-Os(2)-Os(4)	59.71(1)
Os(1)-Re-Os(4)	55.50(1)	Os(3)-Os(2)-Os(4)	59.01(1)
Os(2)-Re-Os(3)	56.25(2)	Re-Os(3)-Os(2)	59.93(1)
Os(2)-Re-Os(4)	57.63(1)	Re-Os(3)Os(4)	60.85(1)
Os(3)-Re-Os(4)	55.32(1)	Os(2)-Os(3)-Os(4)	60.89(2)
Re-Os(1)-Os(2)	58.43(1)	Re-Os(4)-Os(1)	65.28(2)

table cont'd

Re-Os(1)-Os(4)	59.23(2)	Re-Os(4)-Os(2)	60.72(1)
Os(2)-Os(1)-Os(4)	59.77(2)	Re-Os(4)-Os(3)	63.83(2)
Re-Os(2)-Os(1)	65.34(2)	Os(1)-Os(4)-Os(2)	60.53(1)
Re-Os(2)-Os(3)	63.82(2)	Os(1)-Os(4)-Os(3)	114.65(2)
Re-Os(2)-Os(4)	61.65(2)	Os(2)-Os(4)-Os(3)	60.10(1)

Table 2.7. Site energy values (kcal mol^{-1}) for the terminal and bridging hydride positions in $ReOs_4(\mu\text{-}H)(CO)_{16}$ (**4**).

Bridging Positions

Os(1)-Re(1)	**2.7**	Os(2)-Re(4)	41.4
Os(1)-Os(2)	46.4	Os(2)-Os(5)	67.4
Os(1)-Os(4)	34.3	Os(3)-Os(4)	37.5
Os(2)-Os(3)	35.8	Os(3)-Os(5)	45.0
		Os(4)-Os(5)	47.2

Terminal Positions

Re(1)	25.3	Os(3)	46.7
Os(1)	14.9	Os(4)	62.7
Os(2)	75.2		

expected for a 72 electron cluster and is the skeleton found for the isoelectronic $Os_5(CO)_{16}$.[4f,54,71] The Re-bound CO ligands that are not cis to the H atom (i.e., CO(2), CO(3) and CO(4)) show weak bridging interactions with the neighboring osmium atom. (The shortest of these interactions is Os(2)...C(2) at 2.69(1) Å.) Furthermore, whereas the ReCO(1) angle is 179.5(10)°, the other ReCO angles are in the range 167.7(9) - 169.8(10)°. In other words, the CO ligands other than CO(1) are showing incipient bridging character, which is consistent with the CO exchange described below.

The $^{13}C\{^1H\}$ NMR spectrum of **4** (^{13}CO enriched) in CH_2Cl_2/CD_2Cl_2 at room temperature consisted of a somewhat broadened singlet at δ 181.4 (Figure 2.10). This is indicative of rapid carbonyl exchange over the entire $ReOs_4$ unit. As reported in Chapter 6, the ^{13}C NMR spectrum of $Os_5(CO)_{16}$ at room temperature is also a singlet. The spectrum of **4** at -90 °C has five sharp signals in a 2:1:2:1:1 ratio plus some barely

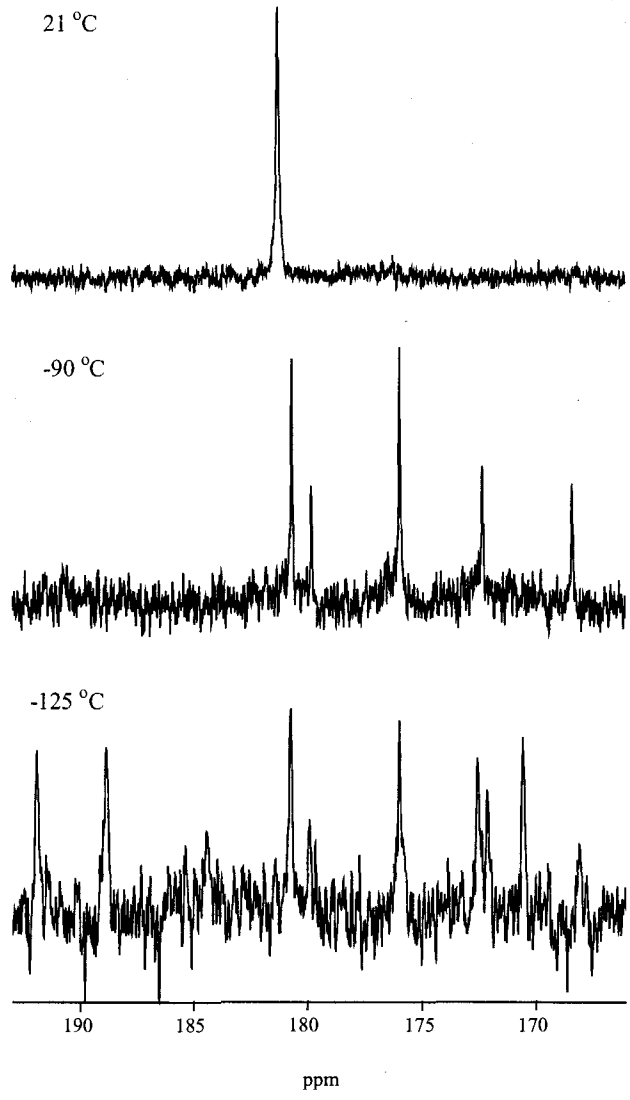

Figure 2.10. The $^{13}C\{^{1}H\}$ NMR Spectra of **4**. The solvent for the room temperature spectrum and that at -90 °C was CD_2Cl_2; for the spectrum at -125 °C it was $CHFCl_2/CD_2Cl_2$.

discernible broad peaks (Figure 2.10). Only the resonance at highest field (i.e., that at δ167.9) exhibited hydrogen coupling (of 6.9 Hz). This indicates the hydride ligand is rigid at this temperature and that the signal can be confidently assigned to the CO trans to the H atom (i.e., C(6) in Figure 2.9). That this carbonyl is rigid implies that the other two (chemically equivalent) carbonyls on Os(1) are also rigid and accounts for a signal of intensity 2. The remaining sharp signals in a 2:1:1 intensity ratio are readily assigned to

the carbonyls of the $Re(CO)_4$ grouping because a rigid $Os(CO)_3$ unit would not give resonances with this intensity pattern. It is believed that the carbonyls of each of the $Os(CO)_3$ units that are not involved with the bridging H ligands are undergoing mutual exchange within the particular $Os(CO)_3$ unit. (There is probably no exchange between carbonyls on different Os atoms at this temperature, but this cannot be ruled out.)[80,81] This causes broadening of the signals of these $Os(CO)_3$ groups into the baseline. Exchange of carbonyls within individual $Os(CO)_3$ units is a feature of hexanuclear Os carbonyl clusters.[80,81]

The ^{13}C NMR spectrum at -125 °C (in $CHFCl_2/CD_2Cl_2$) although not of high quality (Figure 2.10) is consistent with the solid state structure (i.e., all carbonyls rigid on the NMR time scale). The spectra contain 10 resonances in a 2:2:1:2:1:2:2:1:2:1 ratio, with the equivalent CO pairs of CO(5)CO(7), CO(8)CO(16), CO(9)CO(14), CO(10)CO(15) and CO(11)CO(13) accounting for the five signals of intensity 2 (Figure 2.9). Only the signals at δ 168.1 can be confidently assigned to as due to C(6) while the other three resonances with intensity 1 are due to C(1), C(3) or (C12).

Improved Preparation of $ReOs_3(\mu\text{-}H)(CO)_{16}$ (5) As previously discussed, the reaction of $Os_4(CO)_{15}$ and $Re(CO)_5(H)$ in CH_2Cl_2 at room temperature for 3 hours initially produced $ReOs_4(\mu\text{-}H)(CO)_{20}$ (**1**) which decomposed into $ReOs_3(\mu\text{-}H)(CO)_{16}$ (**5**) and $Os(CO)_5$ (eq 2.6). Because **5** has only been partly characterized in previous studies it

$$Os_4(CO)_{15} + Re(CO)_5(H) \longrightarrow \underset{\mathbf{5}}{ReOs_3(\mu\text{-}H)(CO)_{16}} + Os(CO)_5 \qquad (2.6)$$

was decided to fully characterize it here. The solid products from the decomposition of **1** were subjected to chromatography. The yellow band yielded a yellow solid that was recrystallized from CH_2Cl_2 to give air-stable, bright yellow crystals in an almost

quantitative yield. This yield is similar to the previous preparations.[82] The compound was initially identified by its reported ^{1}H NMR spectrum, mass spectrum and the similarity of its IR spectrum (Figure 2.11) to that of $MnOs_3(\mu\text{-}H)(CO)_{16}$.[55,82] Additional characterizations by ^{13}C NMR spectroscopy and X-ray crystallography were performed.

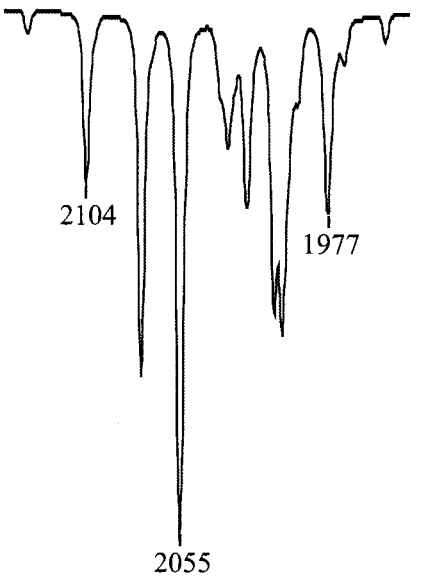

Figure 2.11. IR (hexane) spectrum (ν(CO) region) of $ReOs_3(\mu\text{-}H)(CO)_{16}$ (**5**).

The molecular structure of **5** (Figure 2.12) contains a spiked triangle arrangement of metal atoms, with the Re atom assigned to the "spike" position, which is similar to the structure of $ReOs_3(\mu\text{-}H)(CO)_{15}(NCCH_3)$ and that proposed for of $MnOs_3(\mu\text{-}H)(CO)_{16}$.[55,59a] It is also the structure predicted by Shapley *et al.* As before, the Re atom was confidently assigned based on the method of synthesis, the metal-metal bond lengths and spectroscopic data. A bond length of 2.9695(9) Å for the spiked ReOs bond in **5** (Table 2.8) is within the range of unsupported ReOs bonds and very similar to the unbridged ReOs bond lengths found in Table 2.2 and the $ReOs_4(\mu\text{-}H)(CO)_n$ (n = 19, 18) compounds discussed above.

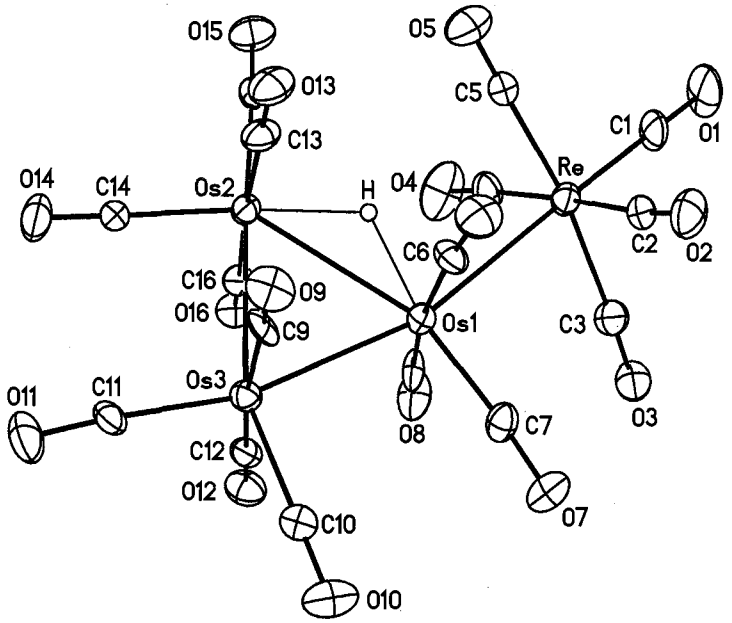

Figure 2.12. Molecular structure of $ReOs_3(\mu\text{-}H)(CO)_{16}$ (**5**).

Table 2.8. Selected bond lengths (Å) and angles (°) for $ReOs_3(\mu\text{-}H)(CO)_{16}$ (**5**).

Bond Lengths			
Re-Os(1)	2.9695(9)	Re-C(1)	1.93(2)
Os(1)-Os(2)	3.0291(8)	Re-C(*rad.*) range	1.95(2) - 2.207(17)
Os(1)-Os(3)	2.8624(8)	Os-C range	1.877(16) - 2.037(16)
Os(2)-Os(3)	2.9090(9)	Os(1)-H	1.83
		Os(2)-H	1.83

Bond Angles			
Re-Os(1)-Os(2)	106.85(3)	Os(2)-Os(1)-Os(3)	59.10(2)
Re-Os(1)-Os(3)	165.46(3)	Os(1)-Os(2)-Os(3)	57.59(2)
		Os(1)-Os(3)-Os(2)	63.31(2)

The two shortest metal-metal bonds, 2.8624(9) Å for Os(1)Os(3) bond and 2.9090(9) Å for the Os(2)Os(3) bond, are close to 2.877 Å the average Os-Os bond length in $Os_3(CO)_{12}$. At 3.0291(8) Å the Os(1)Os(2) bond is the longest OsOs bond in the cluster and indicates it is bridged by the H ligand. The bond cis to the $Re(CO)_5$ unit

is not a π-acceptor like the carbonyl ligand. The metal-metal bond cis to a ligand with poor π-acceptor properties are often long because of the increased electron density found in the bond.[69,83] The OsOs bond lengths in **5** are similar to those found in $ReOs_3(\mu\text{-}H)(CO)_{15}(NCCH_3)$ and $[(OC)_3(Me_3P)_2Re(\mu\text{-}H)]_2Os_3(CO)_{10}$ with the hydride ligand across the longest OsOs bond as is typical for hydrido-osmium-carbonyl clusters.[59a,82,83] The XHYDEX program gave a site energy of 1.0 for this location (Table 2.9). The next lowest value was a terminal position that had a site energy of 14.2. This is above the previously determined acceptable limits for terminal hydride ligands

Table 2.9. Site energy values (kcal mol^{-1}) for the terminal and bridging hydride positions in $ReOs_3(\mu\text{-}H)(CO)_{16}$ (**5**).

Bridging Positions			
Os(1)-Os(2)	**1.0**	Os(1)-Re	20.0
Os(1)-Os(3)	24.2	Os(2)-Os(3)	31.1

Terminal Positions			
Re(1)	74.7	Os(2)	14.8
Os(1)	14.2	Os(3)	49.4

The ^1H NMR spectrum of **5** consists of a singlet at δ -19.0, which is in the region for bridging hydride ligands. The $^{13}C\{^1H\}$ NMR spectrum of **5** prepared from ^{13}CO-enriched (~30%) $Os_4(CO)_{15}$ and unenriched $Re(CO)_5H$ contained resonances which are consistent with the solid state molecular structure of **5** except that, once again, the signals due to the carbonyl attached to the Re atom are not seen (Figure 2.13B). As with **2**, **5** was prepared from unenriched $Os_4(CO)_{15}$ and ^{13}CO-enriched $Re(CO)_5(H)$. The $^{13}C\{^1H\}$ NMR spectrum of this sample at room temperature contains two broad resonances

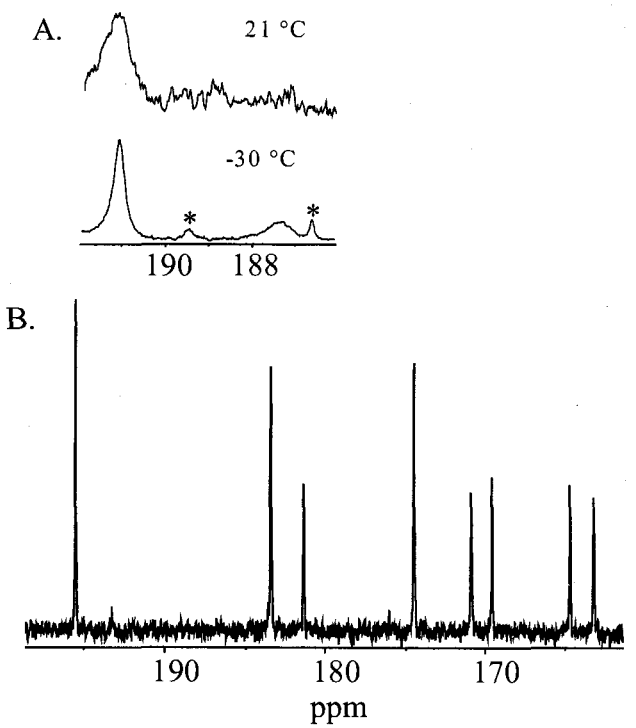

Figure 2.13. (A) The ^{13}C NMR spectra of $(O^{13}C)_5ReOs_3(\mu\text{-}H)(CO)_{11}$ (**5**) at 21 °C and -30 °C. (B) The ^{13}C NMR spectrum of $(OC)_5ReOs_3(\mu\text{-}H)(^{13}CO)_{11}$ (**5**) at 21 °C. (* = impurities)

at δ 190.7 and 189.5. At –30 °C the resonances became sharper and had an approximate intensity ratio of 4 to 1 (Figure 2.13A). It is known that NMR signals subject to the quadrupolar broadening sharpen at lower temperatures because self-decoupling of the quadrupolar nucleus increases.[84] The two spectra in Figure 2.13A were obtained on samples from different preparations. The sample used for the spectrum at -30 °C evidently has impurities not present in the other sample. When the sample was left overnight at room temperature, weak signals due to OsCO groups did appear that indicates CO exchange is slow on the synthetic time scale in **5** at room temperature. Since **5** is the product of the decomposition of **1**, this result indicates that there is also slow exchange of carbonyls across the ReOs bond in **1**. Slow exchange of carbonyls across a ReOs bond is seen in other clusters such as **2** and $Re_2Os_3(\mu\text{-}H)_2(CO)_{20}$. The

resonance at δ 190.7 with an intensity of 4 is assigned to the carbonyls on Re cis to the ReOs bond (CO(2-5)), while the signal with an intensity of one is assigned to the CO on Re which is trans to the ReOs bond (CO(1) in Figure 2.13A).

The ^{13}C NMR spectrum of **5** prepared from ^{13}CO enriched $Os_4(CO)_{15}$ (i.e., $(OC)_5ReHOs_3(^{13}CO)_{11}$) showed five resonances with an intensity of 1 that are assigned to the equatorial carbonyls on the Os atoms and three signals with an intensity of 2 that are assigned to the corresponding axial carbonyls. This pattern is consistent with the solid state structure (Figure 2.13B) and numerous clusters of the type $Os_3(CO)_{11}(PR_3)$. The H-coupled ^{13}C NMR spectrum of **5** showed coupling (9.9 Hz) to just one resonance namely the signal to highest field at δ 163.2. This high field signal (intensity 1) can be confidently assigned as due to C(14) since it is directly trans to the H atom (Figure 2.13B). Coupling to C(7) does not occur since it is not directly trans to the H atom.

Careful pyrolysis of **5** at 60 - 90 °C in C_6F_6 produced $Os_3(CO)_{12}$ and unidentified decomposition products. In other words, the known $Re(\mu\text{-}H)Os_3(CO)_{15}$ was not produced in the reaction as might have been expected.

Comparison of $ReOs_4(\mu\text{-}H)(CO)_n$ (n = 19, 18, 16) with $Os_5(CO)_n$ Compound **2** can be considered as a cluster of the type $Os_4(CO)_{14}(L)$ where L is $Re(CO)_5$ and with a H ligand associated with the Os_4 nucleus. As such the Os_4 skeleton resembles the Os framework in $Os_4(CO)_{14}(L)$ (L = CO, $CNBu^t$,[29,36] PMe_3[34,48]) allowing for a slight expansion of the skeleton due to the presence of the hydride ligand. Likewise, compound **3a** has a similar Os_4 unit to that found in $Os_4(CO)_{13}(L)$ (L = CO,[31] PMe_3[34,48]). In other words, the presence of a single bridging hydride ligand does not cause a major change in the geometry in these clusters.

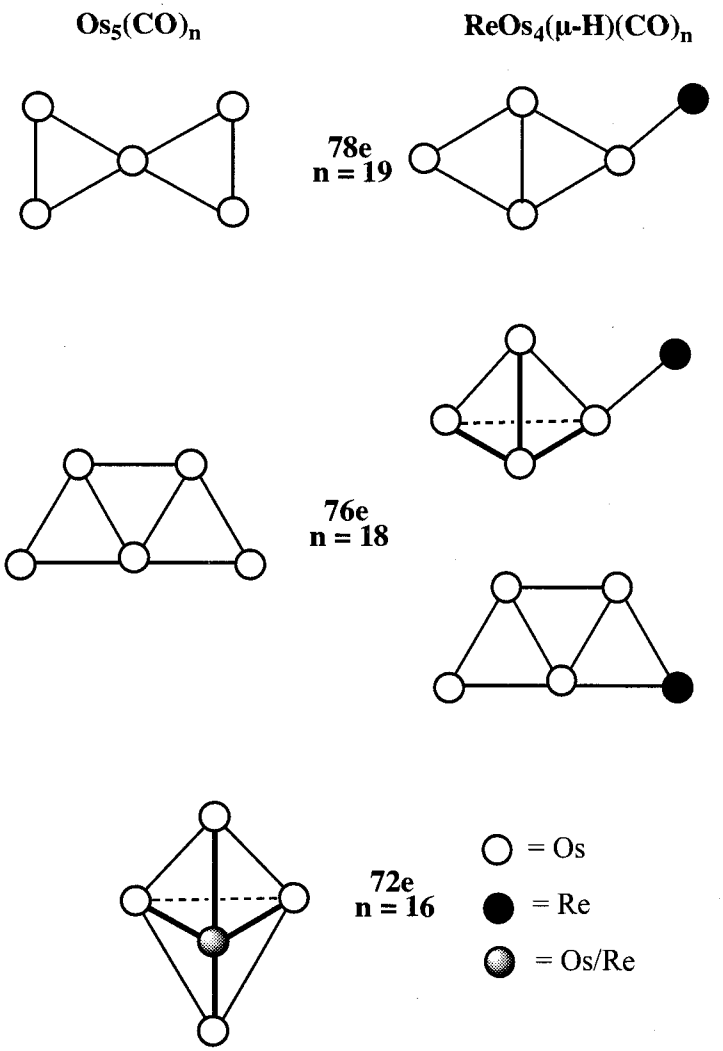

Chart 2.7. Metal skeletons of the $Os_5(CO)_n$ and $ReOs_4(\mu\text{-}H)(CO)_n$ clusters.

In Chart 2.7 are shown the metal skeletons found for the $Os_5(CO)_n$ clusters [44,52-54] along with the corresponding skeletons reported here for the $ReOs_4(\mu\text{-}H)(CO)_n$ molecules. As can be seen, the metal skeleton found for $Os_5(CO)_{19}$ differs from that in **2** although both have six metal-metal bonds expected from electron counting rules. The same situation is observed for the structures of $Os_5(\mu\text{-}CO)(CO)_{17}$ and **3a** in that both compounds have seven metal-metal bonds but the connectivity is different. The proposed metal skeleton of **3b** is, however, the same as that in $Os_5(\mu\text{-}CO)(CO)_{17}$. Both $Os_5(CO)_{16}$

and **4** have a trigonal bipyramidal metal skeletal as expected from electron counting rules.[3,4a]

It has not been established that **2** is the thermodynamically stable form for this cluster. It may be that the $Re(CO)_5$ unit is kinetically inert under the preparative conditions employed and prevents the conversion of **2** to the isomeric form of its $Os_5(CO)_{19}$ analogue with its bow-tie configuration of metal atoms. (There was no infrared evidence in the conversion of **2** to **3a** or **3b** for compounds other than those isolated.) It is noted that the metal framework found for **2** maximizes the number of OsOs bonds in the cluster. There is only one ReOs bond in the structures of **2** whereas if **2** assumed the skeleton in the $Os_5(CO)_{19}$ there would be a minimum of two ReOs bonds (Chart 2.7). The differences in the structures might therefore be rationalized if an OsOs bond is stronger than a similar ReOs bond. As discussed above OsOs bonds are significantly shorter than comparable ReOs bonds, which is consistent with this view.[85] Evidence is presented below to show that **3a** (spiked tetrahedron with one ReOs bond) is indeed more stable than **3b** the raft form with two ReOs bonds. On the other hand, in **4** the $Re(CO)_4$ grouping occupies an equatorial rather than axial position in the trigonal bipyramidal metal skeleton that maximizes the number of ReOs bonds.

The thermodynamic stability of **3** was investigated. As illustrated in Chart 2.8 the pyrolysis of **3a** and **3b** both result in the formation of **4** though milder conditions are required for **3b**, suggesting that **3b** is destabilized relative to **3a**. That the conversion of the spike tetrahedron to the raft structure requires the absorption of UV light supports the notion that the raft configuration is thermodynamically less stable than the spiked

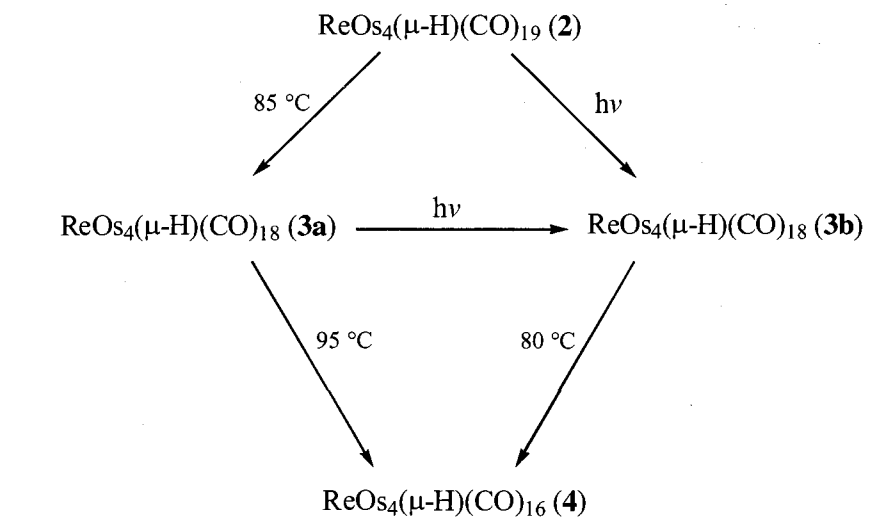

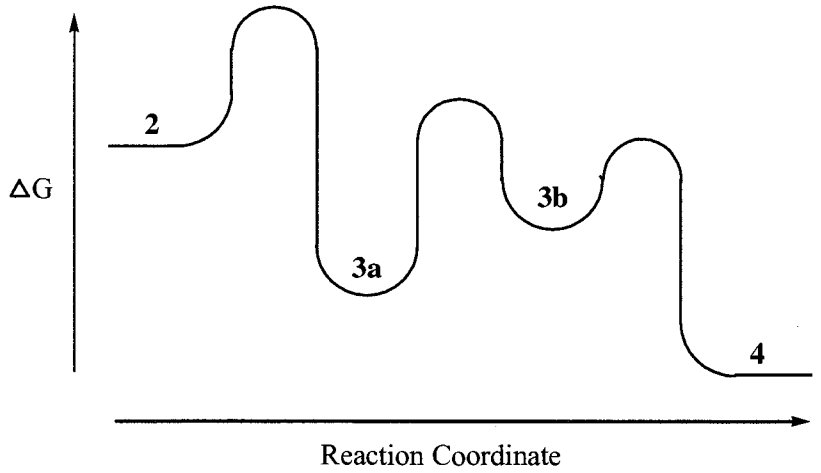

Chart 2.8. An approximate Reaction Coordinate diagram for the $ReOs_4(\mu\text{-}H)(CO)_n$ (n = 19, 18 (two isomers), 16) clusters.

tetrahedral form. Though no evidence for the production of **3a** was observed during the pyrolysis of **3b**, the conversion of the raft structure back to the spiked tetrahedron is observed for the PPh_3 derivatives of **3a/3b** (reported in Chapter 3). This evidence indicates that the raft metal skeleton arrangement is thermodynamically unstable relative to the spiked tetrahedral form for these ReOs clusters. The stability of the **3a/3b** isomers supports the idea that the cluster with the most OsOs bonds (and fewer ReOs bonds) is

the most stable for **3** and probably **2**.

The formation of **4** from **3a** must involve breaking of an OsOs bond in the Os_4 tetrahedron of **3a** and the formation of three ReOs bonds, but the formation of **4** from **3b** requires only the formation of two ReOs bonds. In $Os_5(CO)_{16}$ the Os atom with four carbonyl ligands (shaded circle Chart 2.7) has a formal 20 electron count. A referee of a manuscript resulting from this work pointed out that with the Re atom in this site in **4** the electron density in the cluster is more evenly distributed because rhenium has one less electron than osmium.[86]

An approximate reaction coordinate diagram for the conversions described here is given in Chart 2.8. This study provides further evidence for skeletal variability in open metal carbonyl clusters that is not readily predicted by current bonding theories (see, however, Chapter 3).[87]

2.3 Experimental Section

The following general procedures were applied to all the experimental work reported in this thesis unless otherwise stated. Manipulations of starting materials and products were carried out under a nitrogen atmosphere with the use of standard Schlenk techniques. Hydrocarbon solvents were refluxed over potassium, distilled and stored over molecular sieves before use. Dichloromethane was dried in a similar manner except that CaH_2 was employed as the drying agent. The hexane solvent used throughout these studies was a mixture of isomers of hexanes.

NMR spectra were recorded on a Bruker AMX400 spectrometer at the appropriate operating frequencies for ^1H and ^{13}C NMR spectra (400.0 and 100.6 MHz, respectively). Infrared spectra were recorded on a Bomen MB 100 spectrometer. Mass

spectra were obtained by Dr. D. McGillvary at the University of Victoria on a Kratos Concept double focusing mass spectrometer with a LSIMS source. Dr. D. McGillvary may have obtained the mass spectrum of some of the initial compounds examined in this study on the same Kratos Concept spectrometer but with a FAB source. M. K. Yang of the Microanalytical Laboratory at Simon Fraser University carried out the C/H/N microanalyses. The ultraviolet irradiations were performed with a Hanovia 200 W lamp inside a water-cooled quartz jacket. The reactants were contained in quartz Carius tube (12 cm x 3 cm) fitted with a Teflon valve. There was approximately 3 cm between the edge of the solution and the UV lamp. The other Carius tubes employed in this study were made of thick-walled Pyrex glass and are fitted with a Teflon valve. Typical dimensions were 12 x 3 cm.

The XHYDEX program of A. G. Orpen (University of Bristol) was used to predict the location of H ligand in the hydrido transitional-metal clusters. Based on the X-ray diffraction data, the *x,y,z* coordinates of the non-hydrogen atoms of the cluster are used to determine the potential energy of each of the postulated hydride sites. The potential energy is optimized by a minimization of the intramolecular interactions that involve the hydride ligand. This results in site energy values (kcal mol^{-1}) that can be used to make quantitative comparison between the possible sites. For each hydride bonding mode acceptable site energy ranges have been determined: terminal: 2.2 - 7.5; edge bridging: 0.2 - 10.6; face capped (μ_3): -0.07 - 2.24.

An improved preparation for $Os_4(CO)_{15}$ and $Os_4(CO)_{14}$ is given in Chapter 6. Samples used for $^{13}C\{^1H\}$ NMR spectra were enriched to ~25-30% with ^{13}CO and were prepared from ^{13}CO-enriched $Os_4(CO)_{14}$ and/or ^{13}CO-enriched $Re(CO)_5(H)$ (see text).

The ^{13}CO-enriched $Os_4(CO)_{14}$ was made from ^{13}CO-enriched $Os_3(CO)_{12}$; The ^{13}CO-enriched $Re(CO)_5(H)$ was synthesized from ^{13}CO-enriched $Re(CO)_5(Br)$.[88] The following precursory compounds were prepared by literature procedures: $Re(CO)_5(H)$, $Os(CO)_5$, $Os_3(CO)_{10}(CH_3CN)_2$.[89,90,91]

Preparation of $ReOs_4(\mu\text{-}H)(CO)_{20}$ (1) To a solution of $Os_4(CO)_{15}$ (20 mg, 0.017 mmol) in toluene (20 mL) was added an excess of $Re(CO)_5(H)$ in hexane. The reaction was stirred for 15 min during which time the green solution turned bright yellow. An infrared spectrum of this solution indicated the presence of $ReOs_4(\mu\text{-}H)(CO)_{20}$ and $ReOs_3(\mu\text{-}H)(CO)_{16}$ in an approximate 1:1 ratio. The solution was reduced to approximately half its initial volume and stored overnight at -29 °C, to yield orange crystals of **1** (4 mg, 16%). (The crystals were not suitable for X-ray crystallography.) In a second preparation the solution after the reaction period was evaporated to dryness and the solid subjected to chromatography on a silica gel column (1 x 10 cm). Elution with hexane/CH_2Cl_2 (99/1 by volume) gave a yellow band of $ReOs_3(\mu\text{-}H)(CO)_{16}$ immediately followed by an orange band of the desired product. Collection of the orange band gave a sample of **1** that was almost pure by IR spectroscopy. The compound decomposes in solution at room temperature; one of the decomposition products was identified by IR, ^1H and ^{13}C NMR spectroscopy as the known $ReOs_3(\mu\text{-}H)(CO)_{16}$.[55,82] $ReOs_4(\mu\text{-}H)(CO)_{20}$: IR (hexane) $\nu(CO)$ 2135 (w), 2114 (m), 2081 (s), 2055 (vs), 2029 (sh), 2022 (s), 2009 (vs), 1995 (w), 1979 (s), 1968 (sh), 1950 (w), 1932 (w) cm^{-1}; even in the spectra of the best samples there were weak bands due to $ReOs_3(\mu\text{-}H)(CO)_{16}$: ($\nu(CO)$ 2136 (w), 2104 (m), 2075 (s), 2055 (vs), 2029 (m), 2020 (m), 2005 (s), 2001 (s), 1994 (w), 1977 (m), 1969 (w), 1948 (w) cm^{-1}); ^1H NMR (benzene-d_6) δ -18.9 (s); $^{13}C/^{13}C\{^1H\}$ NMR (CD_2Cl_2, -50

°C) δ 193.8 (2C, *ax*-Os-*C*), 191.2 (4C, $Os(CO)_4$), 189.6 (br, 4C, Re-*C*), 183.0 (2C, *ax*-Os-*C*), 182.5 (br, 1C Re-*C*), 180.9 (1C, *eq*-Os-*C*), 174.4 (br, >2C, *ax*-Os-*C*, degenerate with signal of $ReOs_3(\mu\text{-H})(CO)_{16}$), 170.8 (1C, *eq*-Os-*C*), 169.6 (1C, *eq*-Os-*C*), 164.4 (1C, *eq*-Os-*C*), 162.9 (1C, J_{HC} = 9.2 Hz, *eq*-Os-*C*); weak signals at δ 195.8, 190.9, 183.5, 181.6, 171.1, 169.8, 164.8, 163.4 were attributed to $ReOs_3(\mu\text{-H})(CO)_{16}$ by comparison with a spectrum of a pure sample; MS (LSIMS) *m/z* 1507.6 (M^+) (Calcd for M^+ = 1510 (100%), 1508 (98.2%)).

Preparation of $ReOs_4(\mu\text{-H})(CO)_{19}$ (2) To a stirred solution of $Os_4(CO)_{14}$ (25 mg, 0.022 mmol) in CH_2Cl_2 (25 mL) at room temperature was added an excess amount of $Re(CO)_5(H)$ in hexane. The colour of the solution immediately changed from brown/red to deep red. The solution was evaporated to dryness and the resulting solid recrystallized from CH_2Cl_2. The analytical sample of **2** was obtained in a greater than 95% yield as air-stable, deep red crystals: IR (hexane) ν(CO) 2108 (m), 2075 (m), 2058 (m), 2042 (vs), 2036 (sh), 2019 (s, br), 1995 (w), 1984 (m), 1978 (sh), 1966 (w) cm^{-1}; ^1H NMR (CD_2Cl_2) δ -14.5 (s); $^{13}C/^{13}C\{^1H\}$ NMR (CD_2Cl_2, RT, see text) δ 198.1 (2C, *ax*-Os-*C* J_{CH} = 2.6 Hz), 192.2 (2C, *ax*-Os-*C* J_{CH} = 3.4 Hz), 188.0 (2C, *ax*-Os-*C*), 186.7 (4C, Re-*C*), 184.0 (1C, *eq*-Os-*C*, J_{CH} = 6.9 Hz), 180.4 (1C, Re-*C*) 178.7 (1C, *eq*-Os-*C* d, J_{CH} = 2.7 Hz), 173.4 (1C, *eq*-Os-*C* J_{CH} = 2.7 Hz), 173.0 (1C, *eq*-Os-*C*), 172.6 (2C, *ax*-Os-*C*), 169.9 (1C *eq*-Os-*C*), 163.2 (1C *eq*-Os-*C*); MS (LSIMS) *m/z* 1481.6 (M^+) (Calcd for M^+ = 1482 (100%), 1480 (98.3%)). Anal. Calcd for $C_{19}HO_{19}Os_4Re$: C, 15.42; H, 0.07. Found: C, 15.54; H, 0.08.

Preparation of $ReOs_4(\mu\text{-H})(\mu\text{-CO})(CO)_{17}$ (3a) To a flame dried Carius tube was added $ReOs_4(\mu\text{-H})(CO)_{19}$ (16 mg, 0.011 mmol) and hexane (25 mL). The tube was

cooled to -196 °C and the solution degassed with three freeze-pump-thaw cycles and the vessel sealed under vacuum. The reaction mixture was then heated at 85 °C for 24 h during which time a yellow-orange precipitate formed. The mixture was cooled to room temperature and the mother solution decanted from the precipitate. The precipitate was washed with hexane (2 x 10 mL) and dried on the vacuum line to give **3** (13 mg, 83%). The analytical sample of **3** was obtained as air-stable, orange crystals by recrystallization from CH_2Cl_2: IR (hexane) ν(CO) 2127 (w), 2096 (m), 2063 (vs), 2029 (s), 2025 (sh), 2007 (w), 1991 (m) cm^{-1}; ^1H NMR (CD_2Cl_2) δ -18.8 (s); $^{13}C\{^1H\}$ NMR (CD_2Cl_2, RT) δ 188.9 (m, Re-*C*), 185.9 (vs, Re-*C*), 178.9 (w), 173.4 (w), 164.8 (w/broad); MS (LSIMS) *m/z* 1451.7 (M^+) (Calcd for M^+ = 1454 (100%), 1452 (98.2%)). Anal. Calcd for $C_{18}HO_{18}Os_4Re$: C, 14.88; H, 0.07. Found: C, 15.01; H, 0.09.

Preparation of $ReOs_4(\mu\text{-}H)(CO)_{18}$ (3b) To a flame dried Carius tube was added $ReOs_4(\mu\text{-}H)(CO)_{19}$ (25 mg, 0.017 mmol) and toluene (25 mL). The tube was cooled to -196 °C and the solution degassed with three freeze-pump-thaw cycles and the vessel sealed under vacuum. The reaction mixture was exposed to ultraviolet radiation for 8 h, during which time the original red solution changed to orange/brown and a very fine purple precipitate had formed. (The same product results with $ReOs_4(\mu\text{-}H)(CO)_{18}$ as the starting material although it is less suitable method because of the insolubility of the starting compound.) Attempts to decant the solvent from the precipitate resulted in loss of the product and therefore the mixture was centrifuged before the solution was decanted off. The precipitate was washed three times with CH_2Cl_2 in the centrifuge tube and allowed to air dry. The solid was transferred to a Schlenk tube and dried on the vacuum line to give an analytically pure sample of **3b** (13.2 mg, 54%), as a purple precipitate.

The insolubility of **3b** in all common solvents prevented its complete characterization: IR (KBr) ν(CO) 2133 (w, sh), 2111 (w, sh), 2084 (s), 2040 (w, sh), 2028 (vs, broad), 2016 (w, sh), 1999 (w, sh), 1985 (w, sh), 1975 (w, sh), 1958 (m, sh), 1941 (m, sh), 1931 (m, sh) cm^{-1}; ^1H NMR (CD_2Cl_2) δ -13.9 (s) (small peak even after 2141 scans); MS (LSIMS) *m/z* 1453 (M^+) (Calcd for M^+ = 1454 (100%), 1452 (98.2%)). Anal. Calcd for $C_{18}HO_{18}Os_4Re$: C, 14.88; H, 0.07. Found: C, 14.83; H, 0.04.

Preparation of $ReOs_4(\mu\text{-}H)(CO)_{16}$ (4) A flame dried Carius tube was charged with $ReOs_4(\mu\text{-}H)(CO)_{19}$ (20 mg, 0.013 mmol) and hexane (20 mL). The vessel was cooled to -196 °C and the solution degassed with three freeze-pump-thaw cycles and the tube sealed under vacuum. This vessel was then heated at 95 °C for 4 d; the solution was degassed as described above and the vessel resealed under vacuum every 24 h. Over this period the red solution turned orange (due to formation of **3**) and then red/brown at the completion of the reaction, which resulted in a 48 % yield (9 mg) of **4** after work up (given below).

In an alternative reaction, $ReOs_4(\mu\text{-}H)(CO)_{18}$ (**3b**) (20 mg, 0.014 mmol) was added to a flame dried Carius tube, which was charged with hexane (20 mL). The vessel was cooled to -196 °C and the solution degassed with three freeze-pump-thaw cycles and the tube sealed under vacuum. After 3 h at 80 °C the initially clear solution containing the insoluble **3b** became red/brown. After work up (given below) **4** was collected in a 78% yield (15 mg).

For both methods, after completion of the reaction the solvent was removed on the vacuum line and the remaining solid recrystallized from CH_2Cl_2 to give **4** as analytically-pure, air-stable, dark red (almost black) crystals. IR (hexane) ν(CO) 2106

(w), 2096 (w), 2072 (vs), 2060 (vs), 2040 (vs), 2022 (w), 2010 (w), 2000 (m), 1984 (w), 1970 (w), 1955 (w) cm^{-1}; ^1H NMR (CD_2Cl_2) δ -20.4 (s); ^{13}C NMR (CD_2Cl_2, RT) δ 181.4 (s, br); $^{13}C/^{13}C\{^1H\}$ NMR (CD_2Cl_2, -90 °C) δ 180.4 (2C), 179.6 (1C), 175.6 (2C), 172.0 (1C), 167.9 (1C, d, J_{CH} = 6.9 Hz); ^{13}C NMR ($CD_2Cl_2/CHFCl_2$, -125 °C) δ 191.9 (2C), 188.8 (2C), 184.4 (~1C), 180.7 (2C), 179.9 (1C), 176.0 (2C), 172.6 (2C), 172.1 (1C), 170.6 (2C), 168.1 (~1C); MS (LSIMS) *m/z* 1397.8 (M^+) (Calcd for M^+ = 1398 (100%), 1396 (98.6%)). Anal. Calcd for $C_{16}HO_{16}Os_4Re$: C, 13.75; H, 0.07. Found: C, 13.83; H, 0.09.

Preparation of $ReOs_3(\mu\text{-}H)(CO)_{16}$ (5) To a solution of $Os_4(CO)_{15}$ (20 mg, 0.017 mmol) in toluene (20 mL) was added an excess of $Re(CO)_5(H)$ in hexane and the reaction stirred. After 15 min the initially green solution turned bright yellow. An IR spectrum of the solution at this state indicated it contained $ReOs_4(\mu\text{-}H)(CO)_{20}$ and $ReOs_3(\mu\text{-}H)(CO)_{16}$ in an approximate 1:1 ratio. Allowing the solution to stir for 4 hours caused complete conversion of $ReOs_4(\mu\text{-}H)(CO)_{20}$ into $ReOs_3(\mu\text{-}H)(CO)_{16}$ and some $Os(CO)_5$ (identified by IR spectroscopy). The solution after the reaction period was evaporated to dryness (**Caution:** $Os(CO)_5$ is volatile and is removed with the solvent). The remaining solid was subjected to chromatography on a silica gel column (1 x 10 cm). Elution with hexane/CH_2Cl_2 (99/1 by volume) gave a yellow band of $ReOs_3(\mu\text{-}H)(CO)_{16}$ (**5**). Compound **5** was identified by its reported ^1H NMR (δ = -18.8) and mass spectrum (M^+ = 1212). An analytically pure sample of $ReOs_3(\mu\text{-}H)(CO)_{16}$ was obtained by crystallization from CH_2Cl_2 as air-stable, yellow crystals in a ~ 95% yield. IR (hexane) 2136 (w), 2104 (m), 2075 (s), 2055 (vs), 2029 (m), 2020 (m), 2005 (s), 2001 (s), 1994 (w), 1977 (m), 1969 (w), 1948 (w) cm^{-1}; ^1H NMR (CD_2Cl_2) δ -19.0 (s); $^{13}C/^{13}C\{^1H\}$

NMR (CD_2Cl_2) of $(OC)_5Re(\mu\text{-}H)Os(^{13}CO)_{11}$ δ 195.5 (2C), 183.4 (2C), 181.3 (1C), 174.5 (2C), 170.9 (1C), 169.6 (1C), 164.7 (1C), 163.2 (1C, d, J_{CH} = 9.9 Hz); ^{13}C NMR of $(O^{13}C)_5Re(\mu\text{-}H)Os(CO)_{11}$ (CD_2Cl_2, RT) δ 190.7 (broad), 189.5 (v. broad); (CD_2Cl_2, -30 °C) δ 190.6 (4C), 188.8 (1C, broad); MS (LSIMS) *m/z* 1205.7 (M^+) (Calcd for M^+ = 1206 (100%), 1208 (99.4%)).

Chapter 3. The Triphenylphosphine Derivatives $ReOs_4(\mu\text{-}H)(CO)_n(PPh_3)$ (n = 18, 17), $Os_5(\mu\text{-}CO)(CO)_{16}(PPh_3)$ and $ReOs_3(\mu\text{-}H)(CO)_{15}(PPh_3)$

3.1 Introduction

The investigation into the structures adopted by metal carbonyl clusters of the same nuclearity and electron count is an important aspect of cluster chemistry.[3,4(e,f)] Also of importance are the isomer(s) produced when carbonyl ligands are replaced by other two electron donor species, such as P-donor ligands.[92]

The use of phosphine or phosphite ligands (PR_3) is widespread in cluster chemistry since a vast array of "R" groups are available to allow for easy manipulation of the electronic and steric properties of the ligands and hence at the metal it is coordinated to in the cluster. P-donor ligands are better σ donors and poorer π acceptors than carbonyls. This results in a site preference for the noncarbonyl ligand.[93] The competing influences of the steric and electronic effects of the phosphine ligands determine their position normally either trans to a metal-metal bond or to a carbonyl ligand. This results in different possible locations for the phosphine ligand and therefore the possibility of isomers for clusters substituted by one or more PR_3 ligands. Because of their better π acceptor properties, a CO ligand tends to favour a location that is trans to a poor π-acceptor ligand, such as a phosphine ligand, because this reduces the competition for π electrons. Often steric effects of this arrangement override the favourable electronic interactions and the phosphine ligand is located in a position trans to a metal-metal bond where there are fewer steric interactions. This is the case for trinuclear metal carbonyl clusters (e.g, $Os_3(CO)_{11}(PR_3)$) in which the phosphine invariably occupies a site trans to the metal-metal bond.[69] In binuclear compounds the phosphine is generally located in the

less steric site trans to the metal-metal bond, although compounds where the PR_3 substituent is cis to the metal-metal bond are known. An example is $(OC)_3(Me_3P)_2OsW(CO)_5$.[41,94]

In higher nuclearity clusters there are more chemically different coordination sites for the phosphine ligand than the two possible sites found in the bi and trinuclear metal carbonyl clusters. It was therefore of interest to investigate the isomers obtained by replacing a carbonyl with a PR_3 ligand in $ReOs_3(\mu\text{-}H)(CO)_{16}$ and the $ReOs_4(\mu\text{-}H)(CO)_n$ (n = 19, 18, 16) clusters reported in Chapter 2.

In this chapter the systematic synthesis of mixed metal clusters of rhenium and osmium with a PPh_3 ligand, namely $ReOs_4(\mu\text{-}H)(CO)_n(PPh_3)$ (n = 18, 17(a), 17(b)) and $ReOs_3(\mu\text{-}H)(CO)_{15}(PPh_3)$ are reported. (Additional products isolated from the preparation of these compounds will also be briefly described.) The characterization of these products is discussed along with a discussion of their structures. The two isomers of $ReOs_4(\mu\text{-}H)(CO)_{17}(PPh_3)$ constitute an extremely rare case of two clusters with the same molecular formula, but with differing metal skeletons. Consideration of this pair of clusters has led to a new proposal concerning the structures of metal clusters. As discussed in Chapter 2 it was not established that the spiked tetrahedral unit in $ReOs_4(\mu\text{-}H)(CO)_{18}$ was thermodynamically more stable than the planar raft unit. The isolation of both structural isomers of $ReOs_4(\mu\text{-}H)(CO)_{17}(PPh_3)$ provides the answer to this question.

3.2 Results and Discussion

$ReOs_4(\mu\text{-}H)(CO)_{18}(PPh_3)$ (6) Addition of $Re(CO)_4(PPh_3)(H)$ to $Os_4(CO)_{14}$ in CH_2Cl_2 at room temperature afforded $Os_4Re(\mu\text{-}H)(CO)_{18}(PPh_3)$ (**6**) in almost quantitative yield after 18 hours (eq 3.1). The product was isolated as air-stable, deep red crystals that

$$Os_4(CO)_{14} + Re(CO)_4(PPh_3)(H) \xrightarrow{25\ ^\circ C} \underset{\mathbf{6}}{ReOs_4(\mu\text{-}H)(CO)_{18}(PPh_3)} \qquad (3.1)$$

were characterized by C/H/N analysis, IR, mass (parent ion), ^1H and ^{13}C NMR spectroscopy and X-ray crystallography.

The molecular structure of **6** has a spiked kite arrangement of metal atoms with the Re atom in the spike position (Figure 3.1)[b]. Selected bond lengths and angles for **6** are displayed in Table 3.1. The location of the Re atom was confidently assigned based

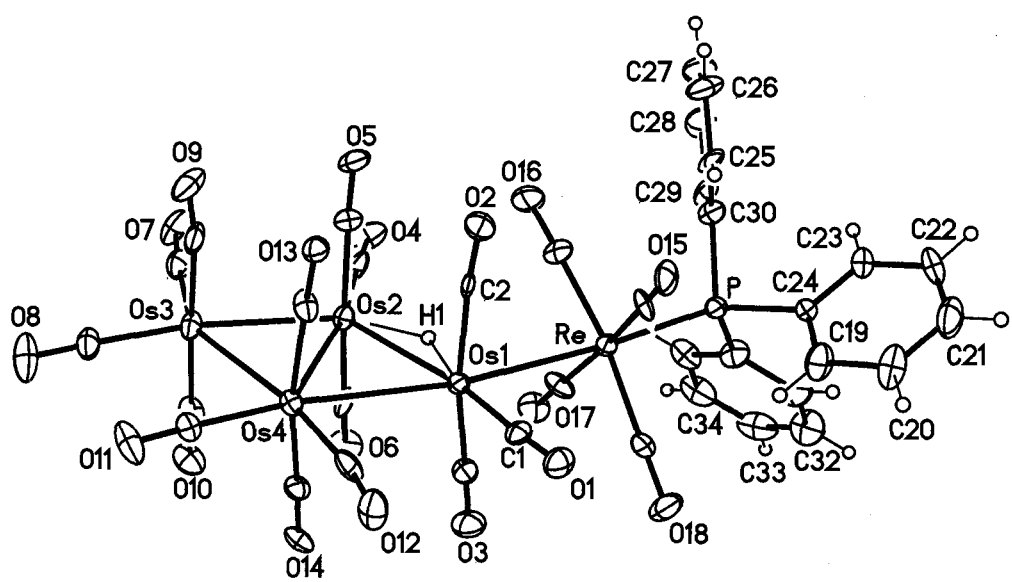

Figure 3.1. Molecular structure of $Os_4Re(\mu\text{-}H)(CO)_{18}(PPh_3)$ (**6**).

---

[b] The structures **6** and **11** were determined by Dr. G. P.A. Yap (University of Ottawa).

Table 3.1. Selected bond lengths (Å) and angles (°) for $ReOs_4(\mu\text{-}H)(CO)_{18}(PPh_3)$ (**6**).

Bond Lengths

Re-Os(1)	2.962(1)	Re-P	2.370(6)
Os(1)-Os(2)	2.899(1)	P-C range	1.83(1)-1.86(1)
Os(1)-Os(4)	3.002(1)	Re-C(*rad.*) range	1.94(2)-2.02(2)
Os(2)-Os(3)	2.811(1)	Os(4)-C(*term.*)	1.84(2)-1.97(2)
Os(2)-Os(4)	2.944(1)	Os(1)-H	1.63(8)
Os(3)-Os(4)	2.956(1)	Os(2)-H	1.63(8)

Bond Angles

Os(1)-Re-P	176.1(1)	Os(3)-Os(2)-Os(4)	61.77(3)
Re-Os(1)-Os(2)	109.08(4)	Os(2)-Os(3)-Os(4)	61.32(3)
Re-Os(1)-Os(4)	168.78(4)	Os(1)-Os(4)-Os(2)	58.36(3)
Os(2)-Os(1)-Os(4)	59.81(3)	Os(1)-Os(4)-Os(3)	115.24(4)
Os(1)-Os(2)-Os(3)	123.58(4)	Os(2)-Os(4)-Os(3)	56.90(3)
Os(1)-Os(2)-Os(4)	61.83(3)		

on the method of synthesis of **6**, the metal-metal bond lengths and spectroscopic data. The triphenylphosphine substituent is also attached to this metal atom as might be expected. As reported below, migration of a PPh_3 ligand from one metal atom to another can however occur.

As discussed in Chapter 2, unbridged ReOs bonds reported in the literature range in length from 2.931 to 3.006 Å whereas unbridged OsOs bonds in chain complexes are typically in the range 2.871 to 2.918 Å.[60] The ReOs length in **6** of 2.962(1) Å is therefore within the range reported for unbridged ReOs bonds.

As for **2**, the metal framework in **6** consists of a planar Os_4 rhomboid with the $Re(CO)_4(PPh_3)$ unit bound in an equatorial site on one wingtip Os atom. The metal

skeleton in **6** has the spiked kite metal atom geometry found for **2**. As discussed in Chapter 2, this is an extremely rare geometry for metal clusters. A further example of a cluster with this metal skeleton, $Os_5(H)(\mu\text{-}H)(CO)_{18}$, is reported in Chapter 4.

The OsOs lengths in $Os_4(CO)_{15}$ are unusual in that the peripheral bonds consist of two long (about 3.00 Å) bonds between $Os(CO)_4$ units and two short bonds (about 2.77 Å) that involve the $Os(CO)_3$ fragment.[29,36] Bonds between osmium atoms in open cluster compounds are usually within 0.05 Å of 2.877 Å the average OsOs distance in $Os_3(CO)_{12}$.[64] The lengths of $Os_4(CO)_{15}$ have been rationalized in terms of 3c-2e bonds as shown Chart 3.1.[29,36] In **6** the peripheral OsOs bonds that involve the Os atom of hinge

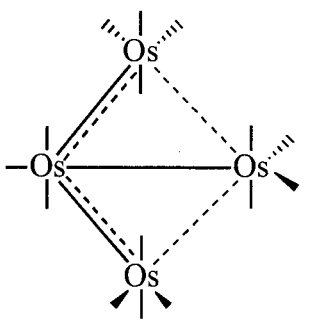

Chart 3.1. 3c-2e bonds proposed for $Os_4(CO)_{15}$.

$Os(CO)_4$ unit (Os(1)Os(4), Os(3)Os(4)) are likewise long at 3.002(1) and 2.956(1) Å (Table 3.1.). The OsOs bonds that include the Os atom of the $Os(CO)_3$ grouping (Os(1)Os(2), Os(2)Os(3)) are 2.899(1) and 2.811(1) Å. The longer bond of the later pair (Os(1)Os(2)) is believed bridged by the hydride ligand rather than one of the other longer OsOs bonds (see below). The presence of a single bridging hydride ligand usually causes an elongation of about 0.12 Å to an OsOs bond in Os cluster compounds.[66] The lengthened Os(1)Os(2) bond in **6** caused by the presence of the bridging hydride ligand is

therefore slightly less than this value. The hinge OsOs bond (2.944(1) Å) although somewhat long is more typical of a single OsOs bond.

Placement of the H ligand across the Os(1)Os(2) bond in **6** produced the lowest site energy of 1.8 (Table 3.2) with the XHYDEX program.[67] This is in the range of 0.2 - 10.6 previously found for bridging hydride ligands. Support for this placement also comes from the Os(4)Os(2)C(4) angle that is 170.5(6)°. The corresponding angle in $Os_4(CO)_{15}$ is 180° by crystallography. The lowest site energy for the hydride ligand in a terminal position is 6.6 on Os(2) which is in the range (2.2 - 7.5) previously determined for terminal metal hydride site energies.[67] The ^{13}C NMR spectrum of **6**, however, does not support the placement of the hydride on Os(2). As implied above, it might have been expected that the H ligand bridges one of the long OsOs bonds in the molecule. However, the site energies determined for these positions (17.4 and 15.7 for bridging Os(1)Os(4) and Os(3)Os(4), respectively) clearly indicate the H ligand is not located across either of these bonds (Table 3.2).

The OsOs bond lengths in **6** are similar to the corresponding lengths in **2** (Chart 3.2). The OsOs lengths are discussed in Chapter 2 and the arguments used there apply to the lengths in **6**. The location of PPh_3 ligand trans to a ReOs bond rather than the electronically preferred cis site can be attributed to steric effects.

The ^{13}C NMR spectrum of **6** prepared from ^{13}CO-enriched (~30%) $Os_4(CO)_{14}$ displayed eleven signals with the approximate intensity ratio of 2:3:2:2:1:1:1:1:2:1:1, as would be expected for the solid state molecular structure (Figure 3.1). The signal at δ

Table 3.2. Site energy values (kcal mol^{-1}) for the terminal and bridging hydride positions in $ReOs_4(\mu\text{-}H)(CO)_{18}(PPh_3)$ (**6**).

Bridging Positions

Os(1)-Re	27.3	Os(2)-Os(3)	4.1
Os(1)-Os(2)	**1.8**	Os(2)-Os(4)	11.2
Os(1)-Os(4)	17.4	Os(3)-Os(4)	15.7

Terminal Positions

Re	58.3	Os(3)	27.2
Os(1)	19.9	Os(4)	6.6
Os(2)	14.7		

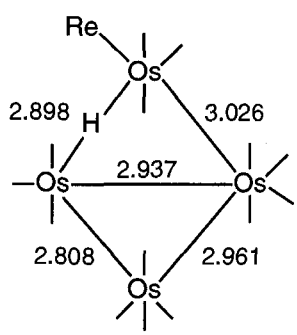

$Os_4(\mu\text{-}H)(CO)_{14}[Re(CO)_5]$ (**2**)

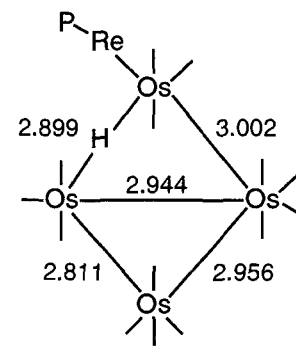

$Os_4(\mu\text{-}H)(CO)_{14}[Re(CO)_4(PPh_3)]$ (**6**)

Chart 3.2. OsOs bond lengths in **2** and **6**.

194.2 (intensity 3) showed coupling to ^{31}P (J_{CP} = 5.3 Hz), which allows for its assignment to the four radial carbonyls on Re (C(15-18)) (Figure 3.2).[95] As mentioned in Chapter 2, CO exchange across the ReOs bond in **2** and **5** is slow. The signal at δ 173.1 (intensity 2) is shifted to high field such that it is in the region where peaks due to equatorial carbonyls occur. As seen in the ^{13}C NMR spectrum of **2** the resonances due to the carbonyls of the

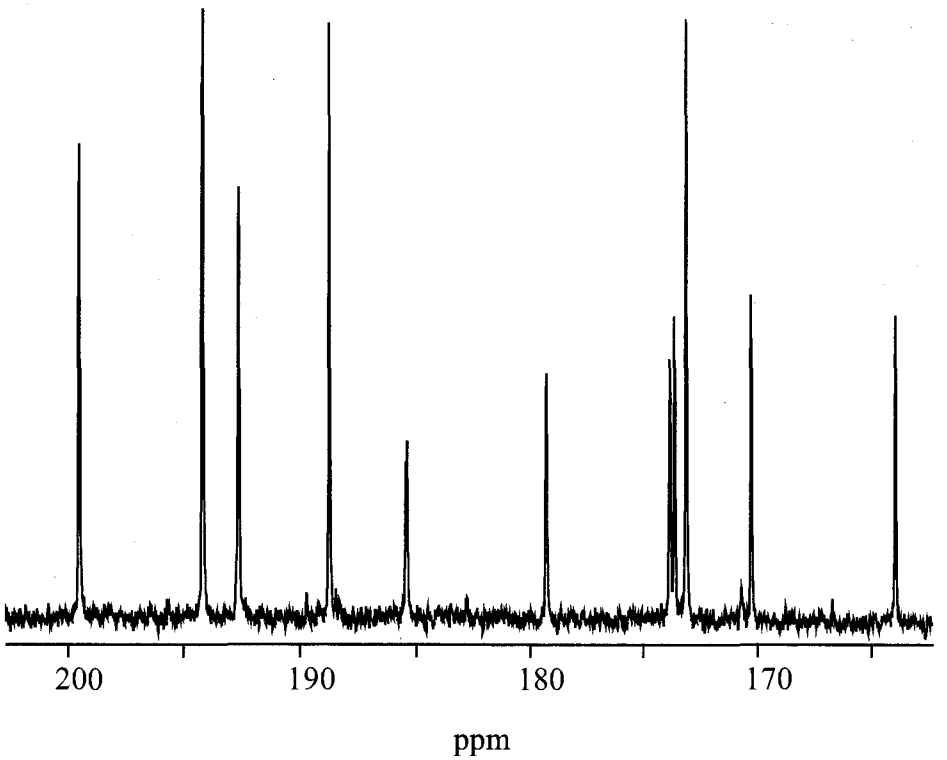

Figure 3.2. The $^{13}C\{^{1}H\}$NMR spectrum of $Os_4Re(\mu\text{-}H)(CO)_{18}(PPh_3)$ (**6**) in CH_2Cl_2/CD_2Cl_2.

$Os(CO)_4$ unit of the hinge OsOs bond experience a large high field shift, presumably due to the unusual bonding in the cluster. As such, this resonance can be confidently assigned to the axial carbonyls on Os(4). By analogy, the two highest field signals with intensity 1 (δ 170.3 and 163.9) can be assigned to the two equatorial carbonyls on Os(4) (Figure 3.1). The remaining three resonances with intensity of 2 (δ 199.5, 192.6 and 188.7) can be assigned to the axial carbonyls on Os(1), Os(2) and Os(3). A comparison of the ^{13}C NMR spectrum of **6** with that of **2** suggests that the signal at δ 199.5 be assigned to the axial carbonyls of Os(2), the signal at δ 192.6 be assigned to the axial carbonyls on Os(1) with the axial carbonyls on Os(3) assigned to the resonance at δ 188.7.

The $^{13}C\{^1H\}$ NMR spectrum of **6** showed coupling to two resonances with intensity one. The signal at δ 179.3, which showed the largest coupling, is confidently assigned to the CO(1), which is trans to the hydrogen atom. The signal at δ 185.4 with the smaller coupling is assigned to CO(4), which is cis to the hydrogen ligand. In clusters the trans CH coupling is greater than the cis coupling. The remaining two singlets both with intensity 1 correspond to the two equatorial carbonyls on Os(3).

$ReOs_4(\mu\text{-}H)(CO)_{17}(PPh_3)$ (7a) "Spiked Tetrahedron Isomer" Careful heating of **6** in toluene at 85 °C for 6 hours produced a mixture of compounds (eq 3.2).

$$\underset{\mathbf{6}}{ReOs_4(\mu\text{-}H)(CO)_{18}(PPh_3)} \xrightarrow{85\ ^\circ C} \underset{\mathbf{7a}}{ReOs_4(\mu\text{-}H)(CO)_{17}(PPh_3)} + \mathbf{8} + \mathbf{9} + \mathbf{10} + Os_4(\mu\text{-}H)_2(CO)_{13} + Os_3(CO)_{12} \qquad (3.2)$$

Separation by column chromatography produced new compounds that are believed to be $ReOs_4(\mu\text{-}H)(CO)_{17}(PPh_3)$ (**7a**) and $Os_5(\mu\text{-}CO)(CO)_{16}(PPh_3)$ (**8**) as well as the orange (**9**) and blue (**10**) bands of minor products along with the bands due to the known $Os_4(\mu\text{-}H)_2(CO)_{13}$[96] and $Os_3(CO)_{12}$. Complete characterization of **7a** proved problematic due to variable yields and the difficulty encountered in obtaining a pure sample. Performing the reaction under apparently the same conditions did not produce similar results. The reaction as written often produced **7a** as a mixture with **6**. The separation of **7a** from **6** proved difficult. An extension of the reaction time or elevation of the temperature also failed to drive the reaction to completion. A small amount of a pure sample of **7a** was obtained by re-heating the isolated mixture of **7a/6** at 85 °C in toluene with careful monitoring of the reaction by IR spectroscopy to determine when or if complete conversion to **7a** had occurred. The time to accomplish this result was variable. It is now

realized that this was probably due to the fact that **7a** is in equilibrium with **6**. Heating of the mixture of **7a/6** did not produce **8**. The mixture decomposed to $Os_4(\mu\text{-}H)_2(CO)_{13}$ and $Os_3(CO)_{12}$. All attempts to crystallize **7a** were unsuccessful. A pure sample of ^{13}CO-enriched **7a** for ^{13}C NMR spectroscopy could not be obtained because the purification step could not be monitored by IR spectroscopy. All ^{13}C NMR spectra of samples of **7a** contained resonances due to a mixture of products such that the spectra could not be confidently interpreted. A small amount of pure **7a** was obtained in one preparation that allowed its characterization by IR, mass (parent ion) and ^1H NMR spectroscopy. (The ^1H NMR spectrum indicated the presence of a bridging hydride ligand.) There was insufficient material for a C/H/N analysis.

Pyrolysis of the raft isomer **7b** (discussed below) at 70 °C for 7 hours also produced **7a** along with $Os_3(CO)_{11}(PPh_3)$[69] and $Os_4(\mu\text{-}H)_2(CO)_{13}$ (eq 3.3). Like the

$$\underset{\textbf{7b}}{ReOs_4(\mu\text{-}H)(CO)_{17}(PPh_3)} \xrightarrow{70\ ^\circ C} \underset{\textbf{7a}}{ReOs_4(\mu\text{-}H)(CO)_{17}(PPh_3)} + Os_4(\mu\text{-}H)_2(CO)_{13} + Os_3(CO)_{11}(PPh_3) \qquad (3.3)$$

reaction shown in eq 3.2, this reaction also proved erratic with similar difficulties in obtaining a pure sample of **7a**.

The molecular formula of **7a** as $ReOs_4(\mu\text{-}H)(CO)_{17}(PPh_3)$ is based on its mass spectrum. It is presumed to have a spiked tetrahedron arrangement with Re in the spike position like $ReOs_4(\mu\text{-}H)(\mu\text{-}CO)(CO)_{17}$ (**3a**) that was discussed in Chapter 2. Both compounds result from the pyrolysis of $ReOs_4(\mu\text{-}H)(CO)_{18}(L)$ (L = CO, PPh_3) and the ultraviolet irradiation of **7a** or **3a** both produce the raft isomer (discussed in the next section).

It was hoped that the pyrolysis of **6** or **7a** would yield $ReOs_4(\mu\text{-}H)(CO)_{15}(PPh_3)$ in order to determine the site preference of the P ligand. (Two positional isomers of $Os_5(CO)_{15}(PMe_3)$ have been structurally characterized.[45]) The pyrolysis of **6** at various temperatures (up to 120 °C) and for different times failed to produce any other products than those shown in eq 3.2. It may be that the PPh_3 ligand is too bulky to be accommodated in the trigonal bipyramidal $ReOs_4$ cluster. Compound **8** will be discussed in the next section. Compounds **9** and **10** were both examined by mass and IR spectroscopy (Figure 3.3). The result of the mass spectra clearly indicated that compounds**9** or **10** were not the desired $ReOs_4(\mu\text{-}H)(CO)_{15}(PPh_3)$. These compounds were not examined further.

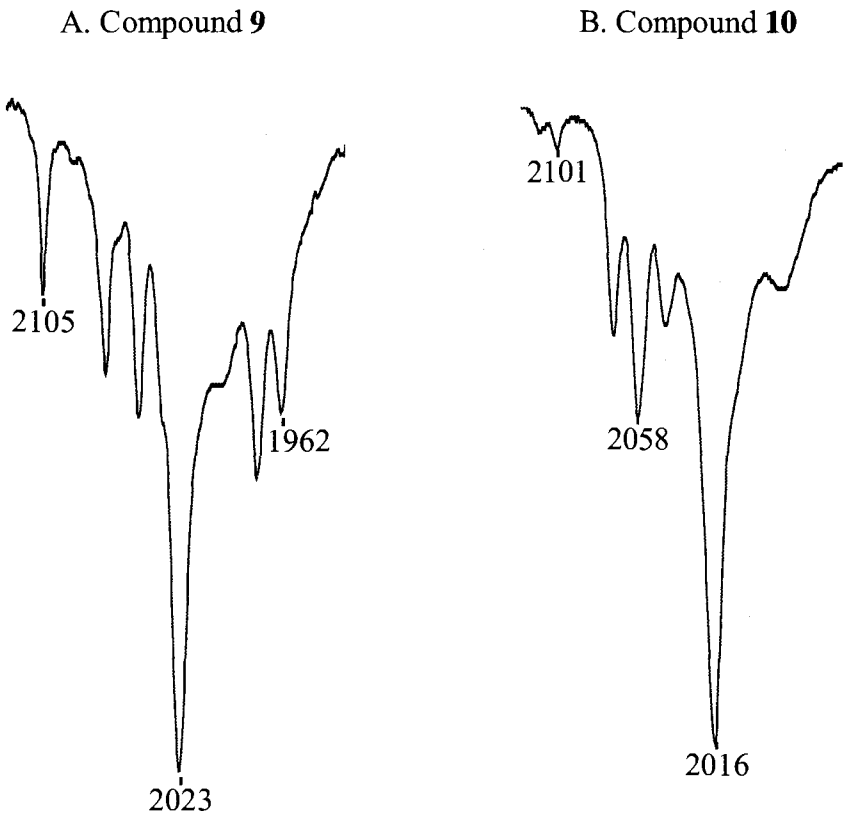

Figure 3.3. IR (CH_2Cl_2) spectra (ν(CO) region) of (A) **9** and (B) **10**.

$ReOs_4(\mu\text{-}H)(CO)_{17}(PPh_3)$ (7b) "Raft Isomer" A solution of $ReOs_4(\mu\text{-}H)(CO)_{18}(PPh_3)$ (**6**) was irradiated with ultraviolet light for 6 hours. A mixture of compounds resulted that were separated by column chromatography. Two new compounds, $ReOs_4(\mu\text{-}H)(CO)_{17}(PPh_3)$ (**7b**) and $Os_5(\mu\text{-}CO)(CO)_{17}(PPh_3)$ (**8**), were isolated along with $Os_4(\mu\text{-}H)_2(CO)_{13}$ (eq 3.4). Compound **7b** was also formed when **7a**

$$\underset{\mathbf{6}}{ReOs_4(\mu\text{-}H)(CO)_{18}(PPh_3)} \xrightarrow{h\nu} \underset{\mathbf{7b}}{ReOs_4(\mu\text{-}H)(CO)_{17}(PPh_3)} + \mathbf{8} + Os_4(\mu\text{-}H)_2(CO)_{13} \quad (3.4)$$

in toluene was subjected to ultraviolet irradiation for 2 hours (eq 3.5).

$$\underset{\mathbf{7a}}{ReOs_4(\mu\text{-}H)(CO)_{17}(PPh_3)} \xrightarrow{h\nu} \underset{\mathbf{7b}}{ReOs_4(\mu\text{-}H)(CO)_{17}(PPh_3)} + Os_4(\mu\text{-}H)_2(CO)_{13} \quad (3.5)$$

The new compound, $ReOs_4(\mu\text{-}H)(CO)_{17}(PPh_3)$ (**7b**) was crystallized from CH_2Cl_2 as air-stable brown crystals that were characterized by C/H/N analysis, IR (Figure 3.4), mass (parent ion), ^1H and ^{13}C NMR spectroscopy, and by X-ray crystallography. Compound **7b** is dichroic: as a crystalline solid it is brown, but when allowed to dry as a thin film it is purple. As the thickness of the film increases it turns brown. The structure of **7b** (Figure 3.5)[c] consists of a planar raft arrangement of metal atoms with the Re atom in a corner site and the phosphorus ligand in an equatorial position attached to the Re atom. Selected bond length and angle data are given in Table 3.3. The location of the Re atom is consistent with the compounds described in Chapter 2 where the Re atoms adopt

[c] The structures **7b** and **8** were determined by Dr. M. J. Jennings (University of Western Ontario).

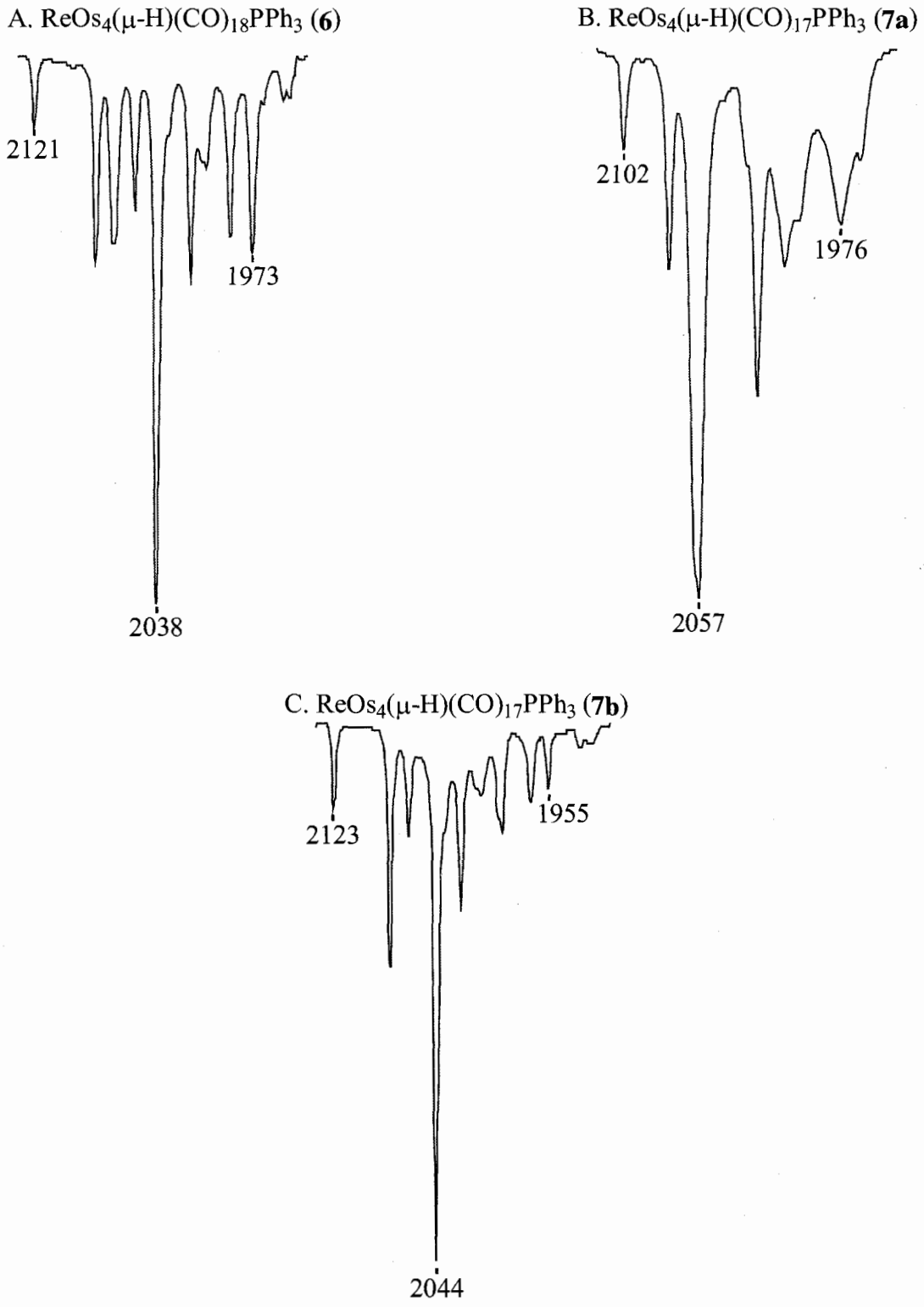

Figure 3.4. IR spectra (ν(CO) region) of $ReOs_4(\mu\text{-}H)(CO)_n(PPh_3)$ (n = 18, **6**; n = 17, **7a**, **7b**) clusters in hexane.

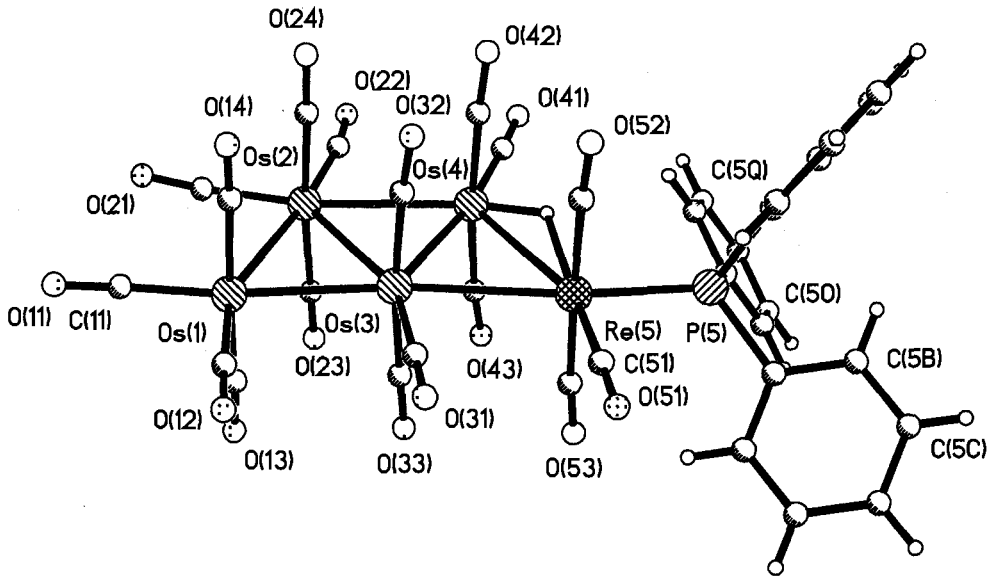

Figure 3.5. Molecular structure of $ReOs_4(\mu\text{-}H)(CO)_{17}(PPh_3)$ (**7b**).

Table 3.3. Selected bond lengths (Å) and angles (°) for $ReOs_4(\mu\text{-}H)(CO)_{17}PPh_3$ (**7b**).

Bond Lengths

Re(5)-Os(3)	3.0282(8)	Re(5)-P(5)	2.3604(4)
Re(5)-Os(4)	3.0308(7)	P(5)-C range	1.836(6)-1.855(7)
Os(1)-Os(2)	2.9667(7)	Re-C(*ax.*) range	1.97(1)-1.97(1)
Os(1)-Os(3)	2.8030(8)	Re-C(*eq.*)	1.89(1)
Os(2)-Os(3)	2.9095(7)	Os(4)-C(*term.*) range	1.88(1)-1.96(1)
Os(2)-Os(4)	2.9678(8)	Os(4)-H[a]	1.80
Os(3)-Os(4)	2.8157(7)	Re(5)-H	1.91

Bond Angles

Os(4)-Re(5)-P(5)	115.01(8)	Os(2)-Os(1)-Os(3)	60.49(2)
Os(3)-Re(5)-P(5)	170.32(8)	Os(1)-Os(2)-Os(3)	56.97(2)
Os(3)-Re(5)-Os(4)	55.38(2)	Os(1)-Os(2)-Os(4)	114.21(2)
Re(5)-Os(3)-Os(1)	172.67(2)	Os(3)-Os(2)-Os(4)	57.24(2)
Re(5)-Os(3)-Os(2)	124.77(2)	Os(1)-Os(3)-Os(2)	62.54(2)
Re(5)-Os(3)-Os(4)	62.36(2)	Os(1)-Os(3)-Os(4)	124.96(2)
Re(5)-Os(4)-Os(2)	122.59(2)	Os(2)-Os(3)-Os(4)	62.42(2)
Re(5)-Os(4)-Os(3)	62.26(2)	Os(2)-Os(4)-Os(3)	60.33(2)

[a] M-H distances from the XHYDEX program.

the site that minimizes the number of ReOs bonds. (Exchanging the Re in **7b** with one of the inner Os atoms would increase the number of ReOs bonds from two to three or four.)

The ReOs bonds lengths in **7b** of 3.0282(8) Å (Re(5)Os(3)) and 3.0308(7) Å (Re(5)Os(4)) (Table 3.3; Chart 3.3) are both significantly longer than the range of unbridged ReOs lengths reported in the literature (see Table 2.2, page 23).[60] The lengths

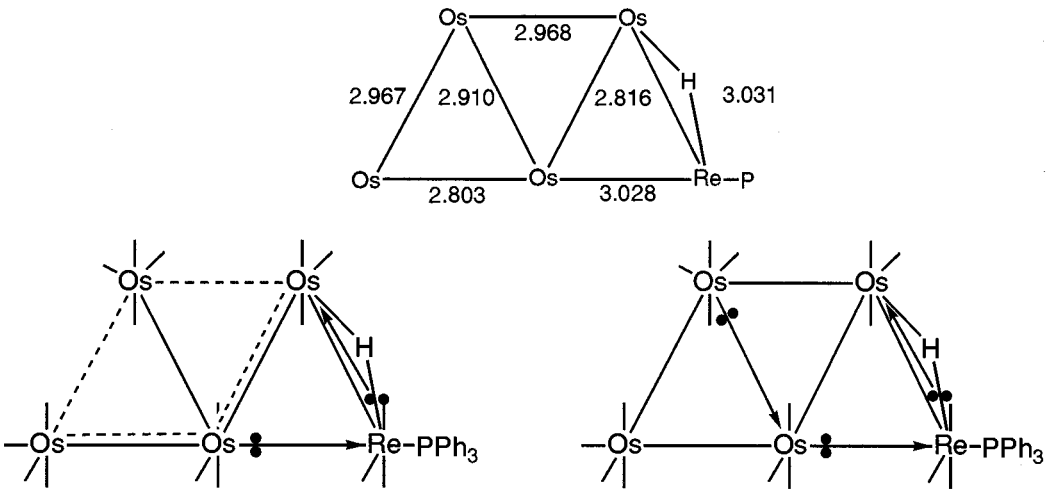

Chart 3.3 Metal-metal bond lengths and proposed bonding schemes for **7b** (CO groups have been omitted).

of the ReOs bonds suggest that they are both bridged by a H atom, but the ^{1}H NMR spectrum of the compound consists of only one signal coupled to the phosphorus atom (J_{PH} = 10.4 Hz). Furthermore, the presence of two H atoms would require that **7b** be a radical and paramagnetic. This is also inconsistent with the NMR spectrum that consisted of sharp signals typical of a diamagnetic compound. The XHYDEX program gave a site energy of 0.6 for the hydride ligand bridging Re(5)Os(4) whereas across the other ReOs bond gave a site energy of 9.0 (Table 3.4).[67] In other words, the hydride ligand bridges the slightly longer ReOs bond. The P-H coupling in the ^{1}H NMR

Table 3.4. Site energy values (kcal mol^{-1}) for the terminal and bridging hydride positions in $ReOs_4(\mu\text{-}H)(CO)_{17}(PPh_3)$ (**7b**).

Bridging Positions

Os(1)-Os(2)	16.5	Os(3)-Os(4)	9.6
Os(1)-Os(3)	11.3	Os(3)-Re(5)	9.0
Os(2)-Os(3)	12.9	Os(4)-Re(5)	**0.6**
Os(2)-Os(4)	12.4		

Terminal Positions

Os(1)	55.1	Os(4)	11.1
Os(2)	92.2	Re(5)	10.8
Os(3)	72.3		

spectrum of **7b** is consistent with the hydride ligand in a cis position to the triphenylphosphine group.[97] It is generally observed for metal carbonyl clusters with a phosphine and a bridging hydride ligand that the hydride bridges the metal-metal bond that is cis to the phosphorus atom.

The question then arises as to why the other ReOs bond is so long. (The lengthening is too large to be attributed to the trans influence of the PPh_3 unit; see structure **8** below.) Two views of the bonding in **7b** based on the 18-electron rule are given in Chart 3.3 (above). In the first view the Os_4 unit has similar bonding as that proposed for $Os_4(CO)_{15}$ (see Chart 3.1) with OsOs bonds of order 0.5 and 1.5. In the second view the hinge bond of the Os_4 unit (i.e., Os(2)Os(3)) is considered a dative bond and the other OsOs bonds nondative 2c-2e bonds. As with $Os_4(CO)_{15}$ we prefer the first view because it is more consistent with the OsOs bond lengths. The OsOs bonds of proposed order 0.5 have lengths 2.9667(7) and 2.9678(8) Å whereas the bonds of order 1.5 have lengths 2.8030(8) and 2.8157(7). As mentioned previously, in most open clusters of Os the OsOs lengths are within 0.05 Å of 2.877 Å, the average OsOs distance in $Os_3(CO)_{12}$. This is the case for $Os_5(\mu\text{-}CO)(CO)_{16}(PPh_3)$ described below.

In each view of the bonding, to obey the 18 electron rule both the electrons from the ReH bond must be donated to the Os(2) atom (i.e., a 3c-2e bond). This in turn requires that Os(3)Re be a dative bond as shown. Because the Os(3)Re bond is a dative bond it need not be in the range of lengths for nondative ReOs bonds. Obviously, an explanation of the different metal-metal bond lengths in **7b** based on a molecular orbital approach that involves centrally directed MOs (see below) would be preferable.

It is evident that the $ReOs_4(\mu\text{-}H)(CO)_{17}(L)$ (L = CO, **3a**, **3b**; L = PPh_3, **7a**, **7b**) compounds can exist with a spiked tetrahedral (isomer **a**) or a planar raft (isomer **b**) metal skeleton. These isomers are believed to be the first case of two clusters with the same molecular formula but with different metal skeletons. The structures of the clusters described here and other open clusters are discussed in detail in the last section of this chapter.

The ^{13}C $\{^1H\}$ NMR spectrum of **7b** prepared from ^{13}CO-enriched **6** displayed signals (Figure 3.6) consistent with the solid-state structure. In the carbonyl region of the spectrum, the signals centred at δ 203.1 and δ 194.1 with an intensity ratio of 2:1 both exhibited P-C coupling. The resonance at δ 203.1 can therefore be confidently assigned to the axial carbonyls on Re(5) with the assignment of the doublet at δ 194.1 due to the equatorial CO on Re(5) (Figure 3.5). These two resonances are broader than those due to

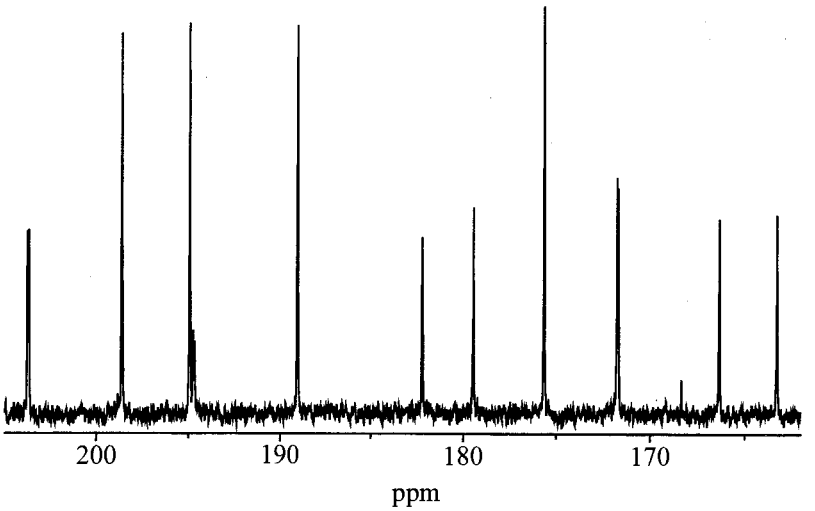

Figure 3.6. The ^{13}C NMR spectrum of $ReOs_4(\mu\text{-}H)(CO)_{17}(PPh_3)$ (**7b**).

the carbonyls on the Os atoms. Because the two naturally occurring isotopes of Re both have spin 5/2, it is common for the resonances of carbonyls bound to a Re atom to be broader. The remaining resonances have an intensity ratio of 2:2:2:1:1:2:1:1:1:1, which is expected from the four remaining pairs of axial carbonyls and six different equatorial carbonyls bound to Os atoms. The ^{13}C NMR spectrum showed H coupling to two resonances. This allowed for assignment of the resonance at δ 194.4 (J_{CH} = 3.8 Hz) to the axial CO on Os(4) and that at δ 178.9 (J_{CH} = 22.7 Hz) to the equatorial CO on Os(4) (Figure 3.5).

$Os_5(\mu\text{-}CO)(CO)_{16}(PPh_3)$ (8) As shown in eq 3.2 (above), $Os_5(\mu\text{-}CO)(CO)_{16}(PPh_3)$ (**8**) is produced in the pyrolysis of **6**. When **6** was heated at 95 °C for 4 hours in a reaction otherwise similar to eq 3.2, the same products were produced except the yield of **8** increased to 20%. As illustrated in eq 3.4 above, **8** also results in low yield (~3%) from the ultraviolet radiation of **6** in toluene for 6 hours (eq 3.6). Crystallization of **8** from

$$\underset{\mathbf{6}}{ReOs_4(\mu\text{-}H)(CO)_{18}(PPh_3)} \xrightarrow[h\nu]{95\ ^\circ C\ or} \underset{\mathbf{8}}{Os_5(\mu\text{-}CO)(CO)_{16}(PPh_3)} + \text{other products} \quad (3.6)$$

C_6F_6 produced air-stable, purple crystals. The compound was analyzed by IR (Figure 3.7), mass (parent ion), ^1H, ^{13}C and $^{31}P\{^1H\}$ NMR spectroscopy, and X-ray crystallography. The NMR data indicated the presence of two isomers (see below).

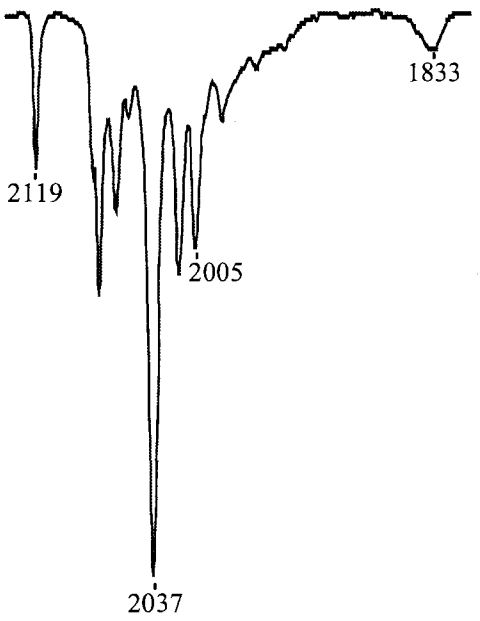

Figure 3.7. IR (hexane) spectrum (ν(CO) region) of **8**.

After much effort, crystals of X-ray quality were obtained by slow evaporation of the solvent from a solution of **8** in C_6F_6 at room temperature. This method is similar to that employed to obtain crystals of the related compound $Os_5(\mu\text{-}CO)(CO)_{16}(PMe_3)$, a cluster that was also difficult to crystallize.[98] The molecular structure of **8** as determined by X-ray crystallography consists of two independent molecules in the unit cell that are chemically identical and differ only in the orientation of the phenyl rings (Figure 3.8, next page). Selected bond lengths and angles for **8** are given in Table 3.5.

It was initially thought that Os(5) was a Re atom because a PPh_3 ligand was attached to this atom. This would make **8** another isomer of the **7a/b** clusters, provided it also possessed a hydride ligand. (Lack of a hydride ligand would make the cluster a 75

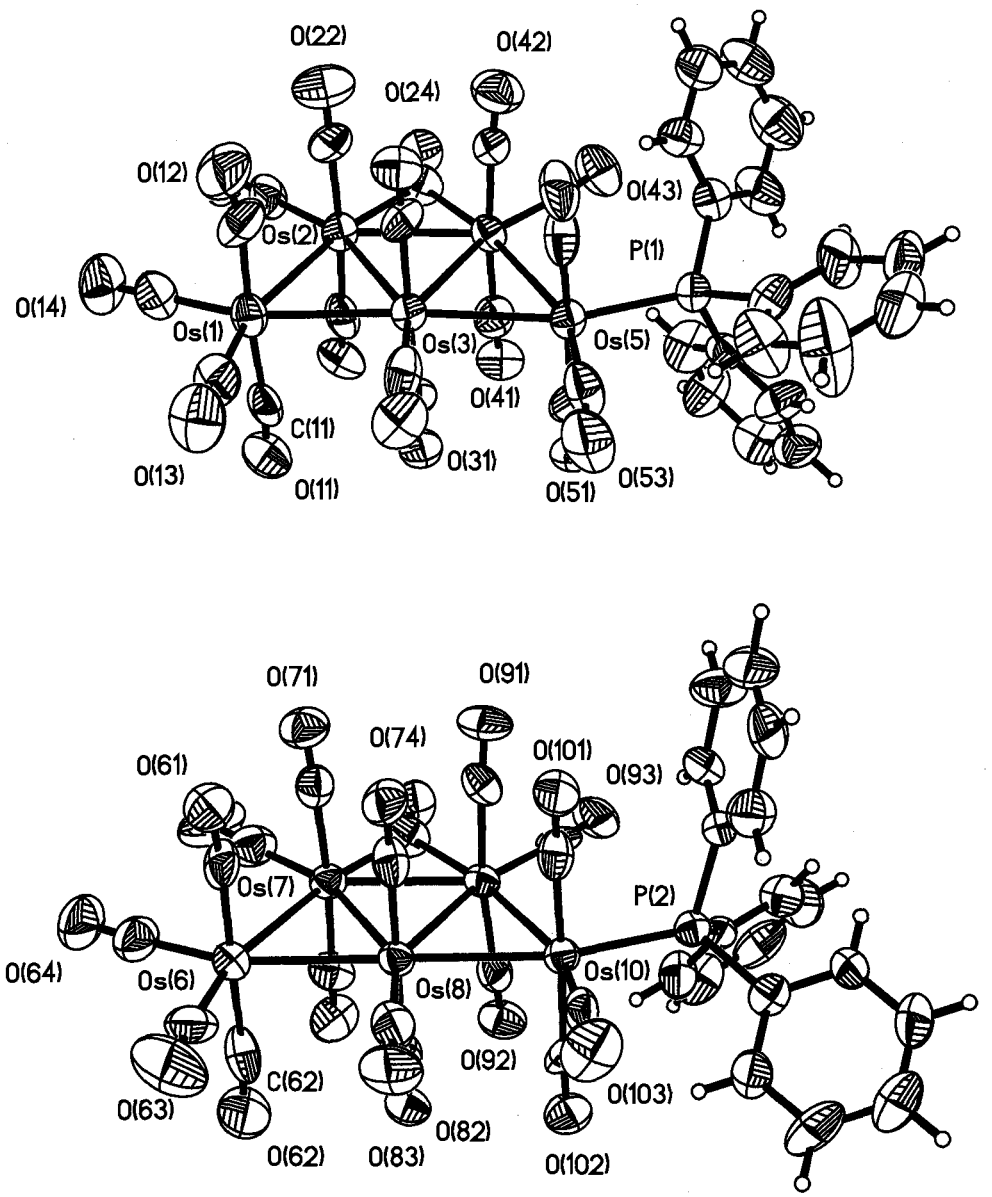

Figure 3.8. Molecular structures of the two independent molecules of $Os_5(\mu\text{-}CO)(CO)_{16}(PPh_3)$ (**8**).

Table 3.5. Selected bond lengths (Å) and angles (°) for $Os_5(\mu\text{-}CO)(CO)_{16}(PPh_3)$ (**8**).

Bond Lengths

Molecule **A**		Molecule **B**	
Os(1)-Os(2)	2.8794(9)	Os(6)-Os(7)	2.8879(9)
Os(1)-Os(3)	2.8550(8)	Os(6)-Os(8)	2.8486(8)
Os(2)-Os(3)	2.8666(8)	Os(7)-Os(8)	2.8730(8)
Os(2)-Os(4)	2.8395(8)	Os(7)-Os(9)	2.8414(8)
Os(3)-Os(4)	2.8533(8)	Os(8)-Os(9)	2.8528(8)
Os(3)-Os(5)	2.9040(8)	Os(8)-Os(10)	2.9077(8)
Os(4)-Os(5)	2.9129(8)	Os(9)-Os(10)	2.9017(8)
Os-C(term.)	1.88(2)-1.97(2)	Os-C(term.) range	1.88(2)-1.96(2)
Os-C (bridging)	2.12(2)/2.12(2)	Os-C (bridging)	2.09(2)/2.22(2)
Os(5)-P(1)	2.365(4)	Os(5)-P(1)	2.355(4)

Bond Angles

Os(2)-Os(1)-Os(3)	59.99(2)	Os(7)-Os(6)-Os(8)	60.11(2)
Os(1)-Os(2)-Os(3)	59.58(2)	Os(6)-Os(7)-Os(8)	59.27(2)
Os(1)-Os(2)-Os(4)	119.57(3)	Os(6)-Os(7)-Os(9)	119.16(3)
Os(3)-Os(2)-Os(4)	60.00(2)	Os(8)-Os(7)-Os(9)	59.58(2)
Os(1)-Os(3)-Os(2)	60.43(2)	Os(6)-Os(8)-Os(7)	60.63(2)
Os(1)-Os(3)-Os(4)	119.94(3)	Os(6)-Os(8)-Os(9)	120.13(3)
Os(1)-Os(3)-Os(5)	176.71(3)	Os(6)-Os(8)-Os(10)	179.02(3)
Os(2)-Os(3)-Os(4)	59.53(2)	Os(7)-Os(8)-Os(9)	59.50(2)
Os(2)-Os(3)-Os(5)	120.28(3)	Os(7)-Os(8)-Os(10)	119.98(3)
Os(4)-Os(3)-Os(5)	60.78(2)	Os(9)-Os(8)-Os(10)	60.49(2)
Os(2)-Os(4)-Os(3)	60.47(2)	Os(7)-Os(9)-Os(8)	60.60(2)
Os(2)-Os(4)-Os(5)	120.91(3)	Os(7)-Os(9)-Os(10)	121.29(3)
Os(3)-Os(4)-Os(5)	60.47(2)	Os(8)-Os(9)-Os(10)	60.69(2)
Os(3)-Os(5)-Os(4)	58.75(2)	Os(8)-Os(10)-Os(9)	58.82(2)
Os(2)-C(24)-Os(4)	84.1(6)	Os(7)-C(74)-Os(9)	82.3(6)
O(24)-C(24)-Os(2)	136.7(2)	O(74)-C(74)-Os(7)	143.7(2)
O(24)-C(24)-Os(4)	139.2(2)	O(74)-C(74)-Os(9)	133.9(12)
P(1)-Os(5)-C(53)	98.3(5)	P(2)-Os(10)-C(103)	94.6(4)

electron species, that is, a radical.) A careful examination of the ^1H NMR spectrum, however, revealed no signals in the high field region expected for a bridging hydride ligand. An examination of the metal-metal bond lengths of **8** showed (Table 3.5) that the longest of the bonds had a length of 2.9129(8) Å, too short for a ReOs bond, but entirely consistent with an OsOs bond. A re-examination of the mass spectrum of **8** indicated that

it was more consistent with an Os_5 cluster than a $ReOs_4(H)$ cluster (see Figure 3.9). Because of the five isotopes of osmium and weak signals of the parent ion, the exact mass (i.e., to 1 amu) of these clusters is difficult to determine. On the basis of this evidence, **8** is formulated as $Os_5(\mu\text{-}CO)(CO)_{16}(PPh_3)$. It is apparent that under the more vigorous conditions used to prepare **8** that the PPh_3 unit has migrated from a Re to an Os atom. Although rare, migration of a P donor ligand has been observed previously.[41]

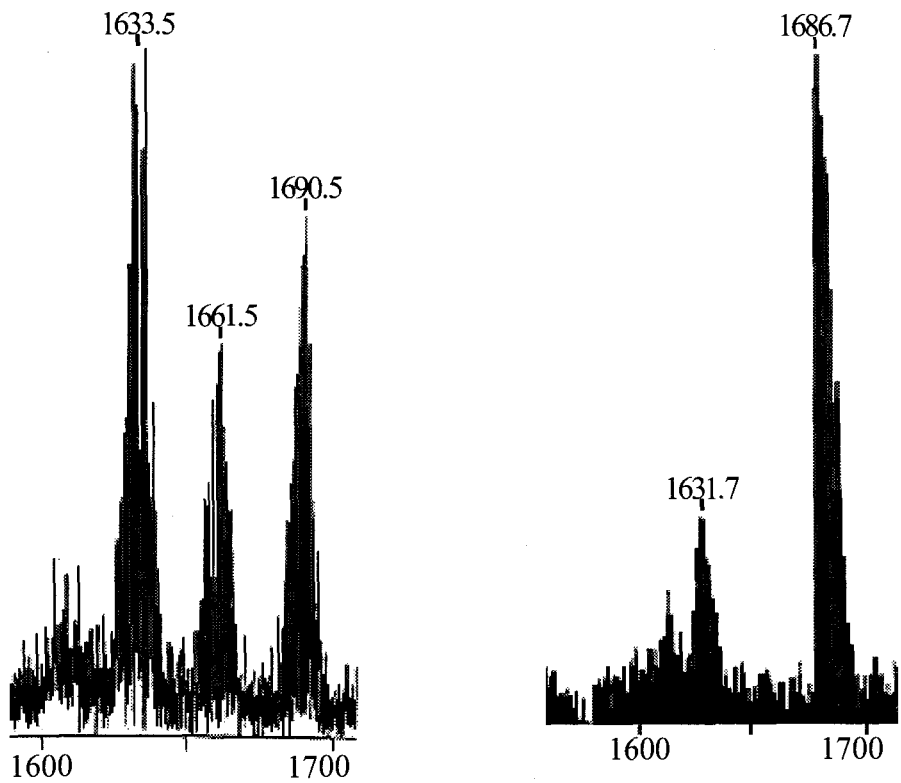

A. $Os_5(\mu\text{-}CO)(CO)_{16}(PPh_3)$ B. $ReOs_4(\mu\text{-}H)(CO)_{17}(PPh_3)$

Figure 3.9. Mass spectra of **7a** and **8**.

As can be seen from Figure 3.8, **8** has a planar Os_5 arrangement of metal atoms. Besides **2** and **7b** described in this thesis, this geometry is also found in $Os_5(CO)_{17}(L)$ (L

= CO,[44] PMe_3[45]). The OsOs lengths in the two independent molecules are shown in Chart 3.4. In molecule **A** a phenyl group makes a closer approach to the neighbouring

$Os_5(\mu\text{-}CO)(CO)_{16}(PPh_3)$ (**8**)

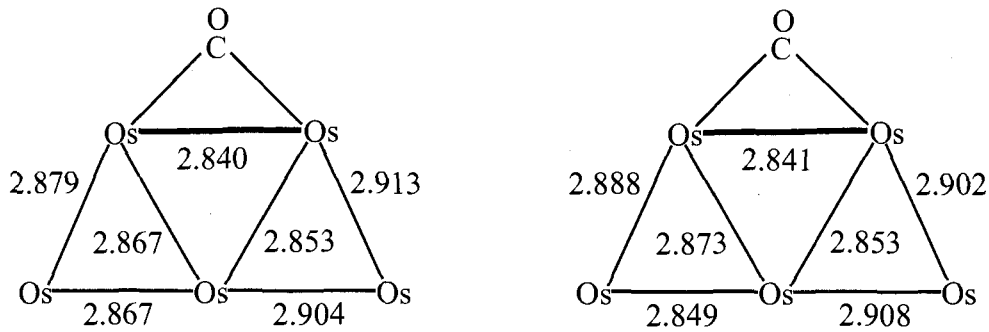

molecule A molecule B

Chart 3.4. OsOs lengths in the two independent molecules of **8**.

Os atom than in molecule **B** and may account for the lengthening (of 0.011 Å) of the OsOs cis to the phosphine ligand in **A** compared to the corresponding length **B**. Of interest is that there is a corresponding compression (of 0.01 Å) of the OsOs bond in **A** that is diametrically opposite to the long bond (in bold, Chart 3.4). The OsOs length trans to the phosphine ligand (Os(3)Os(5): 2.9040(8) Å molecule **A**; Os(8)Os(10): 2.9077(8) Å molecule **B**) are somewhat longer than the bond trans to a CO ligand (Os(1)Os(3): 2.8550(8) Å molecule **A**; Os(6)Os(8): 2.8486(8) Å molecule **B**) and may be attributed to the trans influence of PPh_3 that is a better σ donor than CO. The shortest OsOs bond is that bridged by the CO ligand (2.8395(8) Å molecule **A;** 2.8414(8) Å molecule **B**). The average OsOs bond length in **8** is 2.873 Å (for lengths in **A** and **B** combined) that is close to 2.877 Å, the average OsOs length in $Os_3(CO)_{12}$. All the OsOs distances are within 0.04 Å of this distance. The OsOs bond lengths in **8** are also within 0.012 Å (for both molecules) of the corresponding bond lengths in $Os_5(CO)_{17}(PMe_3)$.[45]

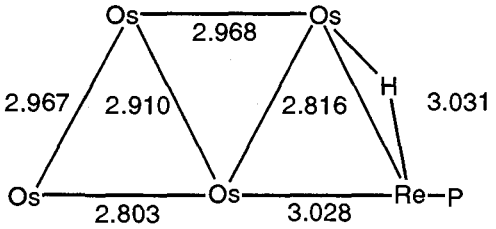

$ReOs_4(\mu\text{-}H)(CO)_{17}(PPh_3)$ (**7b**)

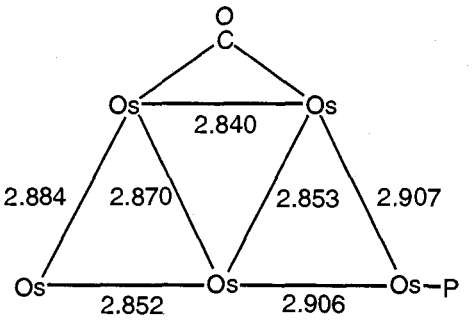

$Os_5(\mu\text{-}CO)(CO)_{16}(PPh_3)$ (**8**)

Chart 3.5. Bond lengths in **7b** and **8** (the lengths in **8** are the mean of the two lengths of the two independent molecules in the unit cell).

In Chart 3.5 the OsOs lengths in **7b** are compared to those in **8**. Although the difference in the two molecules is a change from a ReH unit in **7b** to an Os atom in **8** there is a remarkable difference in the metal-metal bond lengths in the two molecules that reflects the unusual bonding in the Re derivative. If the OsOs bonds in **8** are each considered as conventional (i.e., nondative) 2c-2e bonds then each Os atom obeys the 18 electron rule. In other words there are no unusual dative OsOs bonds or bonds of half order in **8**.

An unusual feature of **8**, which is also found in $Os_5(CO)_{17}(L)$ (L = CO,[44] PMe_3[45]), is the bridging carbonyl ligand. Such ligands are not common in osmium carbonyl cluster chemistry.[7,99] Unlike $Os_5(\mu\text{-}CO)(CO)_{17}$ that has an asymmetric-bridging CO, the bridging CO in **8** is symmetric like that found in $Os_5(\mu\text{-}CO)(CO)_{16}(PMe_3)$.[44,45] Because a bridging CO is more electron withdrawing than a terminal carbonyl it has been proposed that a bridging carbonyl offers the cluster added means to delocalize electron density onto the ligand, with a semi-bridging (asymmetric) ligand at an intermediate stage.[100] Because

phosphine ligands are poorer π-acceptors than carbonyl, the replacement of a CO with PPh_3 leaves more electron density on the metal center. To aid in the delocalization of the electrons the asymmetric bridging CO (of $Os_5(CO)_{18}$) shifts into a symmetric bridging position in **8**.

The infrared spectrum of **8** in hexane (Figure 3.7) contains a broad, weak absorption at 1833 cm^{-1}, which is a characteristic of a bridging carbonyl. This indicates that the bridging carbonyl is present in solution as well as in the solid state. The pattern of the CO-stretching bands of **8** is the same as seen in the IR spectrum of $Os_5(CO)_{17}(PMe_3)$.[45]

The $^{31}P\{^1H\}$ NMR spectrum of **8** indicated that the compound was a mixture of two isomers in a 0.3:1 ratio. These were shown to be in rapid equilibrium by a spin saturation transfer experiment (Figure 3.10, next page). Saturation of the largest signal at δ 3.0 caused a transfer to the other singlet at δ 5.9. This technique has been used by the Pomeroy group to show that the isomers of $(Me_3P)(OC)_4OsW(CO)_5$ are in dynamic equilibrium.[41] The rate of exchange necessary for the spin saturation transfer experiment to be successful depends on the T_1 of the nuclei, but is usually in the range of 1 to 1 x 10^{-2} s^{-1}. These rates are not sufficient to cause NMR line broadening (>10 s^{-1}) but sufficiently fast such that the isomers cannot be physically separated. For separation the rate of exchange needs to be < 10^{-3} s.

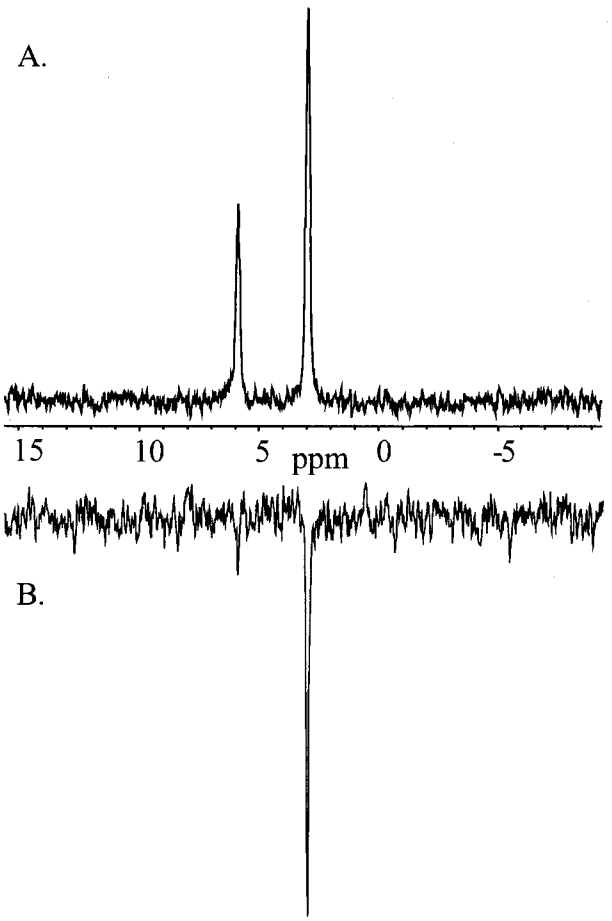

Figure 3.10. Spin saturation transfer experiment on **8**. Irradiation of the highest field ^{31}P NMR resonance resulted in transfer to the signal of the second isomer. (A) ^{31}P NMR spectrum of **8**. (B) Difference spectrum.

The second isomer is believed to have the phosphine ligand located at the other equatorial position of Os(5) (i.e., CO(53)) (**8b** Chart 3.6, next page). Similar isomers were postulated for $Os_5(CO)_{17}(PMe_3)$. In both molecules the phosphine is trans to the OsOsOs chain in the solid state. This is also observed in the molecular structure of **7b**. The placement of the phosphine ligand trans to the OsOsOs chain (**8a** Chart 3.6) is therefore believed to be the more stable form, that is, the preferred form in solution. Conversion between the two isomers can be achieved by an equatorial merry-go-round

exchange of ligands, as shown in Chart 3.6. (This is mechanism is discussed in Chapter 7 for the CO exchange in $Ru_6(\mu_6\text{-}C)(CO)_{17}$.) Since the PPh_3 ligand does not bridge an

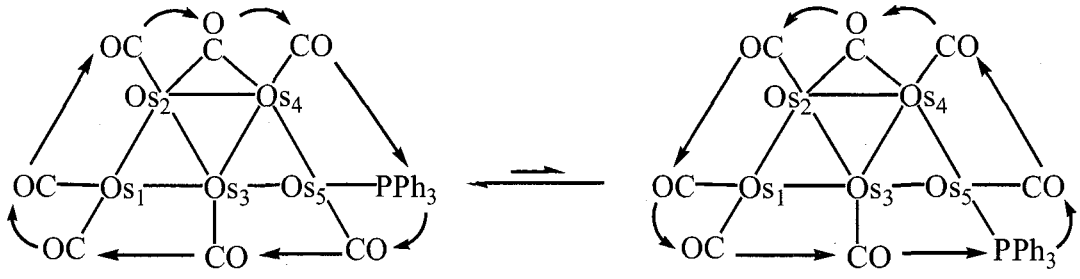

8a **8b**

Chart 3.6. Proposed mechanism of conversion of the two isomers of **8**.

OsOs bond, the exchange is limited to the clicking motion back and forth between the two equatorial positions of PPh_3. This equatorial clicking motion has been observed in the isomers of $(OC)_5M[Os(CO)_3(PR_3)]_2$ (M = Cr, W).[41]

The $^{13}C\{^1H\}$ NMR spectrum of **8** is also consistent with two isomers in solution. The $^{13}C\{^1H\}$ NMR spectrum of **8** (Figure 3.11) contains two low field doublets centred at δ 201.8 and 200.3. The ratio of the two doublets of 0.3:1 is the same as the ratio of the signals in the ^{31}P NMR spectrum, indicating that the doublets are from the different isomers with one set of signals 0.3 the intensity of the other.

The $^{13}C\{^1H\}$ NMR spectrum of each isomer should have 5 resonances of intensity 2 due to the axial carbonyls and 7 resonances of intensity 1 due to the equatorial carbonyls. The overlap of the two spectra will result in 24 signals with one set of resonances 0.3 the intensity of the other set. The $^{13}C\{^1H\}$ NMR spectrum of **8** does indeed have this pattern. The spectrum contains 5 resonances of intensity 2 at δ 200.3 (center of the doublet), 197.0, 193.7, 191.9 and 184.5 as well as 7 signals of intensity 1 at δ 186.4, 184.5, 184.2, 178.0, 175.2, 168.2, 168.0 which are due to one of the isomers (**8a**)

(Figure 3.11). At a third of the intensity of these signals are the resonances due to the other isomer (**8b,** Chart 3.6). This set of signals also contain 5 resonances of equal intensity with an integration value of 2 at δ 201.8 (center of the doublet), 196.1, 193.4, 190.5 and 188.6 as well as 6 signals of intensity 1 at δ 185.8, 182.7, 182.2, 171.8, 170.5,

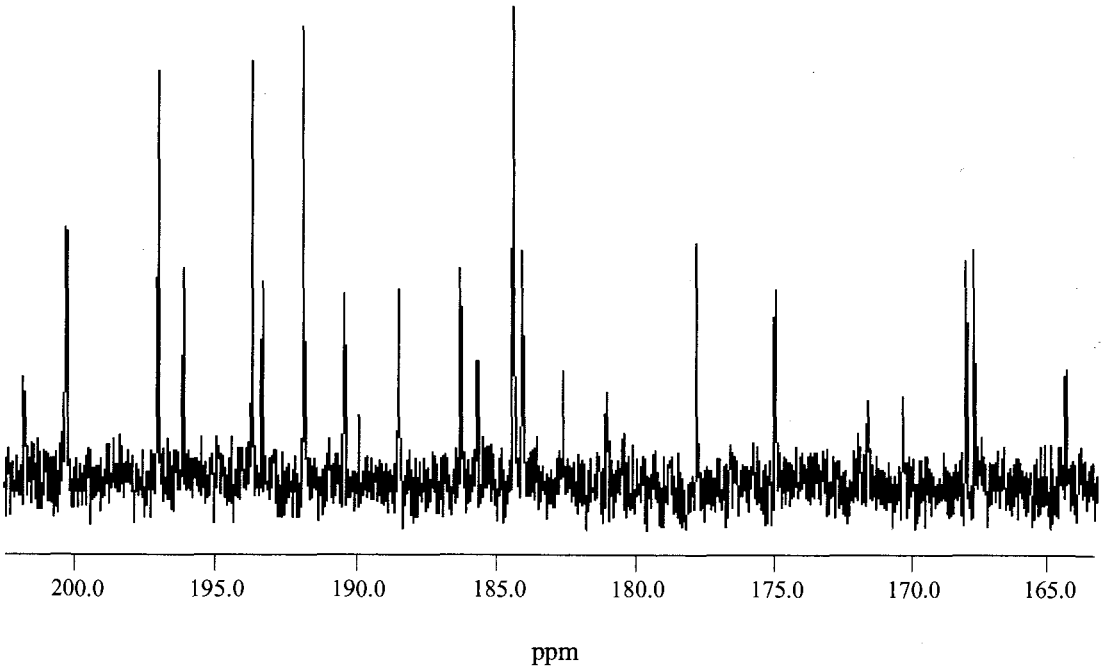

Figure 3.11. The ^{13}C NMR spectrum of **8** in CH_2Cl_2.

and 164.6. The remaining resonance of intensity one is either overlapped by another signal or is weak and cannot be discerned from the baseline noise. Even after a long term acquisition time (42 hours) and high ^{13}CO enrichment of the starting material (~ 60% enrichment of $Os_3(CO)_{12}$) the background noise is significant enough to mask a weak signal.

In the $^{13}C\{^1H\}$ NMR spectrum of **8** the resonance due to the equatorial carbonyl on Os(5), which is cis to the PPh3, did not show P-C coupling as in the corresponding spectrum in of **7b**. This was not unexpected since the P-C coupling of a resonance due to a C atom cis to a phosphine depends greatly on the angle between them, and goes to zero

at ~100° as found in many compounds.[101] In **8** the $POs(CO)_{eq}$ angles are 98.3(5)° (molecule **A**) and 94.6(4)° while the corresponding angle in **7b** is 88.2(4)°.

$ReOs_3(\mu\text{-}H)(CO)_{15}(PPh_3)$ (11) The reaction of $Os_4(CO)_{15}$ with $Re(CO)_4(PPh_3)(H)$ at 40 °C afforded the previously unknown $ReOs_3(\mu\text{-}H)(CO)_{15}(PPh_3)$ (**11**) after chromatography (eq 3.7). The compound was isolated as red, air-stable crystals

$$Os_4(CO)_{15} + Re(CO)_4(PPh_3)(H) \xrightarrow{40\ °C} \underset{\mathbf{11}}{ReOs_3(\mu\text{-}H)(CO)_{15}(PPh_3)} + \mathbf{6} \qquad (3.7)$$

that were characterized by IR (Figure 3.12), mass (parent ion) spectroscopy and X-ray crystallography. The reaction of $Os_4(CO)_{15}$ with $Re(CO)_5(H)$ produced $ReOs_4(\mu\text{-}H)(CO)_{20}$, but there was no evidence for the $ReOs_4(\mu\text{-}H)(CO)_{19}(PPh_3)$ analogue, even

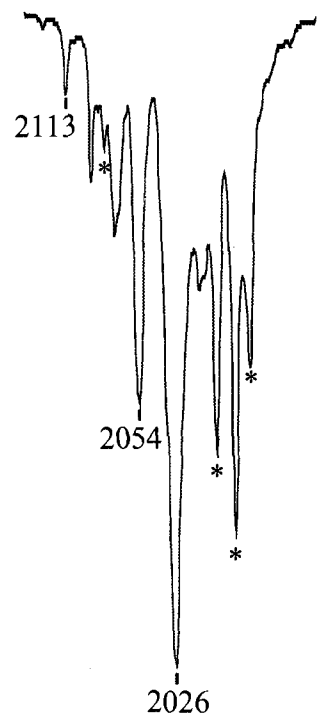

Figure 3.12. IR spectrum (ν(CO) region; hexane solution) of **11** (* Overlap with bands due to $Re(CO)_4(PPh_3)(H)$).

when the reaction was carried out at lower temperatures. Complete characterization of **11** was difficult because although stable in the solid state it was unstable in solution. Several attempts to isolate pure **11** were unsuccessful. Synthesis of **11** by the method used to prepare $ReOs_3(\mu\text{-}H)(CO)_{16}$ (**5**) met with the same problem. Although the IR spectrum of the reaction mixture indicated the formation of **11**, decomposition to $ReOs_3(\mu\text{-}H)(CO)_{14}(PPh_3)$, $Os_3(CO)_{11}(PPh_3)$[69] and $Os_3(CO)_{12}$ took place during attempts to isolate **11**.

In one preparation crystals of X-ray quality were however obtained and a structure determination was carried out. The molecular structure of **11** consists of a spiked triangle with Re in the spiked position and the phosphine ligand located on the Re atom cis to the ReOs bond (Figure 3.13). Location of the PPh_3 ligand trans to the ReOs

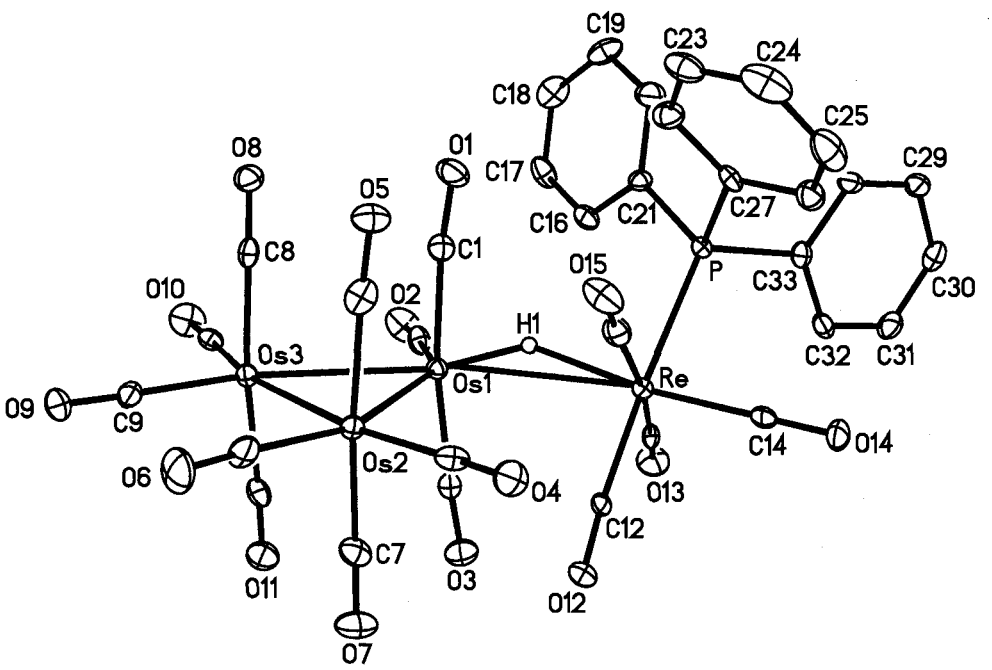

Figure 3.13. Molecular structure of $ReOs_3(\mu\text{-}H)(CO)_{15}(PPh_3)$ (**11**).

Table 3.6. Selected bond lengths (Å) and angles (°) for $ReOs_3(\mu\text{-}H)(CO)_{15}(PPh_3)$ (**11**).

Bond Lengths			
Re-Os(1)	3.2398(4)	Re-C range	1.930(7)-2.201(7)
Os(1)-Os(2)	2.9243(4)	Os-C range	1.859(7)-1.955(8)
Os(1)-Os(3)	2.8665(5)	P-C range	1.827(7)-1.843(6)
Os(2)-Os(3)	2.8912(4)	Re-P	2.493(2)
Re-H	1.99(5)	Os(1)-H	1.48(5)

Bond Angles			
C(12)-Re-P	174.2(2)	Os(2)-Os(1)-Os(3)	59.895(8)
C(14)-Re-P	85.0(2)	Os(1)-Os(2)-Os(3)	59.061(9)
Re-H(1)-Os(1)	138(4)	Os(1)-Os(3)-Os(2)	61.04(1)

bond would be expected because it reduces the steric interactions experienced by PPh_3. It is usually found that P donor ligands, especially the bulky PPh_3 ligand, adopt sites trans to the metal-metal bond in bimetallic and cluster molecules. Some examples are $(R_3P)(OC)_4MM'(CO)_5$ (M = M' = Mn; M = Os, M' = Cr, Mo, W)[41,94] and the spiked triangular $(R_3P)(OC)_3OsOs_3(CO)_{11}$ clusters.[34] Note the last class of clusters are similar to **11**. Furthermore, all other PPh_3 derivatives described in this thesis have the P substituent trans to a metal-metal bond. That **11** is unusual with the bulky PPh_3 ligand in a cis position to the ReOs bond can be attributed to the long length of the metal-metal bond as discussed below. This reduces the steric interactions of the PPh_3 with the neighbouring carbonyls such that it can adopt the electronically preferred cis site (i.e., trans to the strong π-acceptor CO group). Except for small ligands such as $P(OCH_2)_3CCH_3$, phosphine ligands are generally located trans to a metal-metal (M-M) bond.[69,83]

The location of the Re atom was confidently assigned based on the metal-metal bond lengths, the mode of synthesis and its similarity to **5**. The ReOs bond in **11** at 3.2398(4) Å is unusually long, but similar to the values found for the hydrogen bridged

ReOs bonds in $[(OC)_3(Me_3P)_2Re(\mu\text{-}H)]_2Os_3(CO)_{10}$.[83] These lengths are however amongst the longest reported for ReOs lengths and are 0.27 Å longer than the unbridged ReOs bond found in **6** (Table 3.6). The bond length obviously indicates that the hydride ligand is located across the ReOs bond. This is in agreement with the XHYDEX program that gave the lowest site energy (2.6) for this location (Table 3.7).[67] The next lowest site energy (5.6) was for the H ligand across the Os(1)-Os(2) bond that is also in the range for bridging hydrides. All calculated site energies for the terminal positions in **11** were

Table 3.7. Site energy values (kcal mol^{-1}) for the terminal and bridging hydride positions in $ReOs_3(\mu\text{-}H)(CO)_{15}(PPh_3)$ (**11**).

Bridging Positions

Os(1)-Re	**2.6**	Os(1)-Os(3)	35.6
Os(1)-Os(2)	5.6	Os(2)-Os(3)	12.2

Terminal Positions

Re(1)	11.3	Os(2)	32.2
Os(1)	13.9	Os(3)	11.5

outside the accepted range (2.2-7.5) for terminal metal hydrides.[67] The placement of the hydride ligand across the ReOs bond was also expected because it is cis to the PPh_3 substituent. Because PPh_3 is a poorer π-acceptor than a CO ligand there will be less delocalization of electron density of Re onto the ligands, resulting in a more electron rich ReOs bond, which attracts the H ligand. The increase in electron density also increases the $d\pi$ - $d\pi$ repulsive interaction between the two metal centers that increases the bond length.[83] This explains why the ReOs bond in **11** is much longer than in **6**. The lengthening of the M-M bond cis to a phosphine ligand is consistently observed in cluster chemistry though it is not clear why there is little effect on the trans M-M bond.[83]

The OsOs lengths in **11** at 2.8912(4) Å for the Os(2)Os(3) bond, 2.8665(4) Å for the bond trans to the ReOs bond and 2.9243(4) Å for the bond cis to the ReOs bond are within the range expected for unbridged OsOs bonds. As observed for $Os_3(CO)_{11}(PR_3)$[69] clusters and **6**, the OsOs bond cis to the non-carbonyl ligand in **11** is also longer than the other OsOs bonds of the Os_3 triangle.

Structures of Open Clusters Let us consider the two structural isomers of formula $ReOs_4(\mu\text{-}H)(CO)_{17}(PPh_3)$ (**7a** = spiked tetrahedron; **7b** = planar raft; Chart 3.7).

$ReOs_4(\mu\text{-}H)(CO)_{17}(PPh_3)$

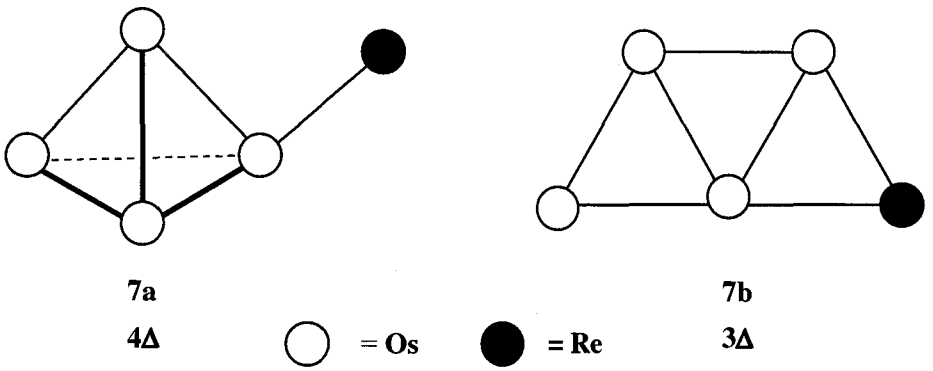

Chart 3.7. Metal skeletons of **7a** and **7b**.

Certainly, **7a** has more OsOs bonds and may account for why it is more stable than **7b** that has one fewer OsOs bond. The Re atom contributes 7, the four Os atoms 32, the H atom 1, the CO ligands 34, and the PPh_3 ligand 2 electrons to the cluster for a total of 76 electrons. In order for each transition metal to obey the 18 electron rule (i.e., 90 electrons) each metal must share some of its valence electrons to form metal-metal bonds. The number of metal-metal bonds required to make the cluster "electron precise" is (90 - 76)/2 or seven metal-metal bonds. Both **7a** and **7b** have seven metal-metal bonds in agreement with the rule. The 18 electron rule however makes no prediction as to the arrangement of the M-M bonds.

For the polyhedral skeletal electron pair theory (PSEPT) each transition metal atom requires 12 electrons to bind the external ligands with the remaining electrons used for cluster bonding. For $ReOs_4(\mu\text{-}H)(CO)_{17}(PPh_3)$ the number of cluster bonding pairs is therefore (76 - 60)/2 or 8 cluster bonding pairs. Because there are five metal atom vertices (n) in the cluster it is an (n + 3) cluster system. PSEPT theory would predict that **7** should be based on a regular polyhedron with seven vertices (that requires n + 1 cluster bond pairs) with two of the vertices missing (an *arachno* cluster). The regular polyhedra found for clusters with seven vertices are the pentagonal bipyramid (PBP) found in $[B_7H_7]^{2-}$ and $B_5C_2H_7$, and the capped octahedron (COC) as in $Os_7(CO)_{21}$.[102] Another regular geometry found for seven-coordinate coordination complexes is the capped trigonal prism. This geometry will not be considered here as it gives similar results to those for the capped octahedron.

In Chart 3.8 are given some *arachno* clusters based on the PBP and COC polyhedra (not all possibilities are shown). The only planar cluster amongst the structures predicted by PSEPT is the pentagon and this structure has never been observed in metal carbonyl clusters. It is apparent that planar raft structures cannot be accommodated by PSEPT. Planar raft structures are also found in the derivatives of $Os_6(CO)_{21}$, $Os_6(CO)_{17}[P(OMe)_3]_4$ (that also has n + 3 cluster bond pairs).[47] It is also apparent from Chart 3.8 that the spiked tetrahedron is also not predicted by PSEPT. It is a general observation of open clusters that they do not obey PSEPT.

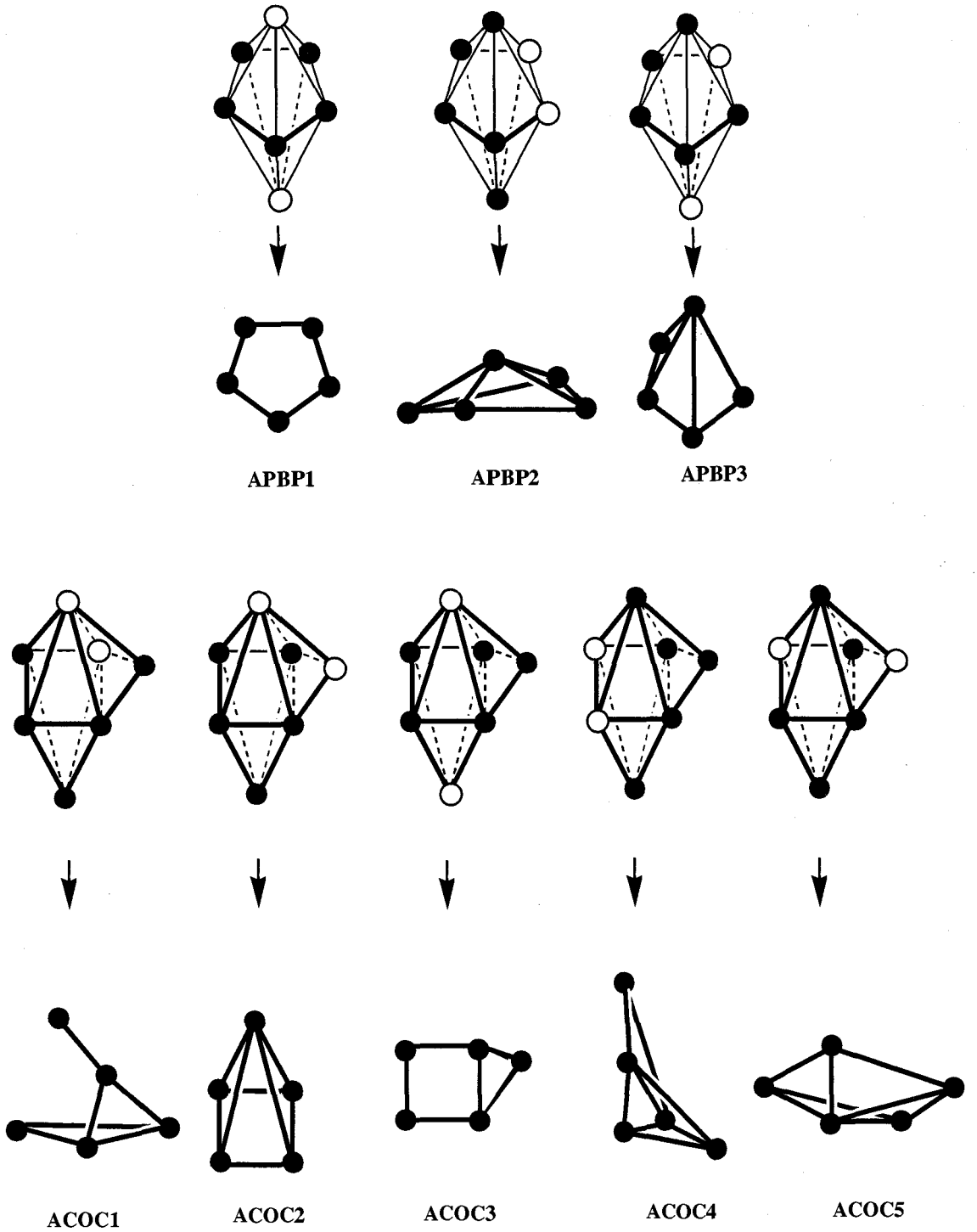

Chart 3.8. Some *arachno* clusters derived from, top, a pentagonal bipyramid and, bottom, a capped octahedron. (Not all possibilities are shown.)

Theoretical treatments of the metal-metal bonding in the triangular $Os_3(CO)_{12}$ and related clusters is framed in terms of a centrally directed MO, as shown in Chart 3.9, and

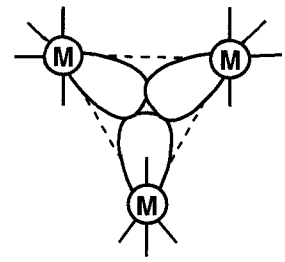

Chart 3.9. The centrally directed MO in triangular metal units of clusters.

two edge-bridging MO's. Experimental support for this view is the observation that $Os_4(CO)_{16}$ (with a puckered square Os_4 skeleton) decomposes in solution at room temperature to give $Os_3(CO)_{12}$.[30] This would not be expected if the OsOs bonds in these molecules were conventional 2c-2e metal-metal bonds. Indeed, the idea that metal atoms in clusters bind via a centrally directed AO and two tangential AO's is the fundamental assumption of PSEPT.[3]

Given this, it is tentatively proposed that the structure adopted by an open cluster is the one *that maximizes the number of triangular M_3 units for the number of nondative metal-metal bonds predicted by the 18 electron rule.* It is proposed to call the "rule" the maximum number of triangle rule ("MNTR"). This rule rationalizes why **7b** (three M_3 units) is less stable than **7a** (four M_3 units) and why these geometries are not predicted by PSEPT. The only structure with seven MM bonds predicted by the PSEPT with $(n + 3)$ cluster bond pairs is APBP3 that has three M_3 units. At the moment the MNTR idea is in its initial stages of development, but it successfully predicts that the spiked triangle (as found in **11** and most $Os_4(CO)_{15}(L)$ clusters) should be more stable than a square M_4 unit,[83,56] and why the bow-tie (as in $Os_5(CO)_{19}$ [52]) and the spiked kite (e.g., cluster **2** and

6) each with six MM bonds and with two M_3 triangles is preferred over a square with one edge part of a triangle. The MNRT also is successful in predicting the structures of condensed clusters such as $Os_5(CO)_{16}$ (trigonal bipyramidal Os_5)[54] and $Os_6(CO)_{18}$ (capped trigonal bipyramidal). It is not successful in predicting octahedral structures such as $Ru_6(\mu_6\text{-}C)(\mu\text{-}CO)(CO)_{16}$ [103] and $[Os_6(CO)_{18}]^{2-}$ [104] unless the arbitrary assumption is made that in these clusters the square M_4 unit is made up of two triangles with peripheral bonds of order 0.5.

Conclusion The mono triphenylphosphine derivatives of $Os_4Re(\mu\text{-}H)(CO)_n$ (n = 19, 18) and $ReOs_3(\mu\text{-}H)(CO)_{15}(PPh_3)$ have the same configurations as the parent carbonyl compounds. These clusters are in agreement with the idea presented in Chapter 2 that the difference in structure between the mixed metal compounds and the $Os_5(CO)_n$ (n= 19, 18, 16) clusters (Chart 2.6) can be attributed to the greater strength of an OsOs bond compared to a comparable ReOs bond. The relationship of compounds **6**, **7a** and **7b** helped to complete Chart 2.7, by showing that the raft structure of **7b** can be converted into the a spiked tetrahedron by pyrolysis. As for the **3a** and **3b** clusters, the ultraviolet irradiation of the spiked tetrahedron produced the raft structure (Chart 3.10).

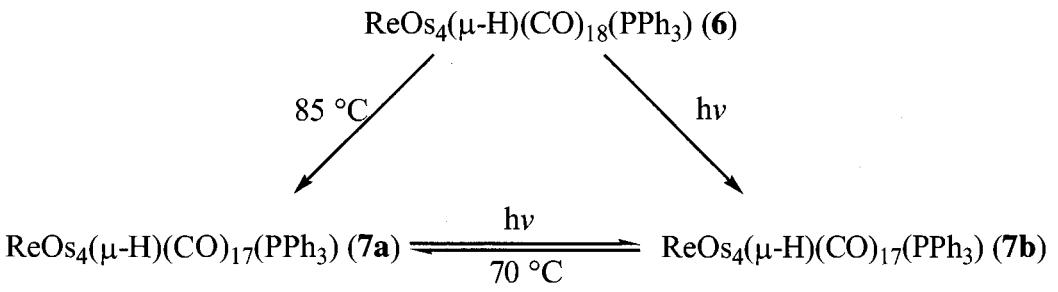

Chart 3.10. Relationship of the $ReOs_4(\mu\text{-}H)(CO)_n(PPh_3)$ (n = 18, 17a, 17b) clusters.

This indicates that in both cases the raft form is thermodynamically less stable than the spiked tetrahedral isomer. This has led to a tentative proposal concerning the structures adopted by open clusters

The addition of the PPh_3 in these compounds provided an illustration of the opposing electronic and steric effects that govern the site adopted by this ligand. Although the environment around the Re in **6** and **11** appear similar, in **6** the PPh_3 is located in the sterically-favoured position while in **11** it is located in the electronically-preferred site, namely, cis to the ReOs bond. In **7b**, the PPh_3 ligand is located in an equatorial position that minimizes steric repulsion.

The set of clusters $ReOs_4(\mu\text{-}H)(L)(CO)_n$ (L= CO, n = 20, 19, 18(a), 18(b), 16; L = PPh_3, n = 18, 17(a), 17(b)) provide a systematic investigation of the structure, therefore bonding, which occurs in a series of clusters which differ by a stepwise loss of a 2 electron donor. This series contains what is believed to be the first example of interconverting isomers that differ by the arrangement of the metal atoms (Chart 3.11).[11b]

$ReOs_4(\mu\text{-}H)(CO)_n(L)$

80e
L = CO, n = 20

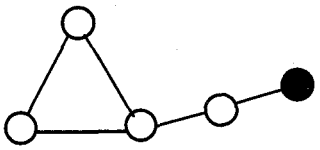

78e
L = CO, n = 19
L = PPh_3, n = 18

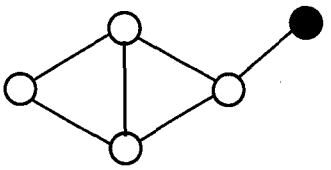

76e
L = CO, n = 18
L = PPh_3, n = 17

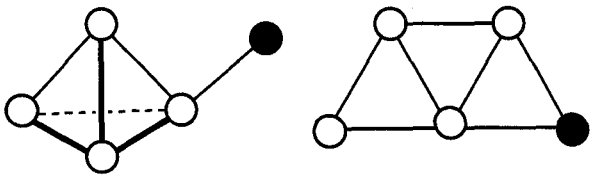

72e
L = CO, n = 16

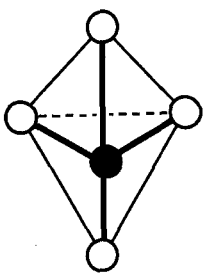

○ = Os

● = Re

Chart 3.11. Metal skeletons of the $ReOs_4(\mu\text{-}H)(CO)_n(L)$ clusters.

3.3 Experimental

The general procedures used for the syntheses and analyses are described in the Experimental Section of Chapter 2. The preparation of $Re(CO)_4(PPh_3)(H)$[105] was carried out by the literature procedure. The $^{31}P\{^1H\}$ NMR spectra were recorded on a Bruker AMX 600 spectrometer. The spin saturation transfer experiment was performed on a Bruker AMX 600 spectrometer with a 3.33 ms mixing time. The carbonyl region of the $^{13}C\{^1H\}$ NMR spectrum of **8** was recorded on a Varian AS 500 spectrometer (operating frequency 125.8 Hz).

Preparation of $ReOs_4(\mu\text{-}H)(CO)_{18}(PPh_3)$ (6) To a solution of $Os_4(CO)_{14}$ (25 mg, 0.022 mmol) in CH_2Cl_2 (20 mL) at room temperature was added $Re(CO)_4(PPh_3)(H)$ (12 mg, 0.021 mmol). This solution was allowed to stir overnight at room temperature, during which time the colour of the solution changed from brown/red to deep red. The solution was evaporated to dryness and the resulting solid recrystallized from CH_2Cl_2. The analytical sample of **6** was obtained in a greater than 95% yield as air-stable, deep red crystals: IR (hexane) ν(CO) 2121 (m), 2080 (m), 2068 (m), 2053 (m), 2038 (vs), 2030 (w, sh), 2015 (m), 2005 (w), 1988 (m), 1973 (m), 1965 (w, sh), 1951 (w), 1948 (w) cm^{-1}; ^1H NMR (C_6D_6) δ -13.7 (s); $^{13}C/^{13}C\{^1H\}$ NMR (CD_2Cl_2, RT) δ 199.5 (2C), 194.2 (d, 2C, J_{CP} = 5.3 Hz), 192.6 (2C), 188.7 (4C), 185.4 (1C, J_{CH} = 6.1 Hz), 179.3 (1C, J_{CH} = 2.3 Hz), 173.8 (1C), 173.6 (1C), 173.1 (2C), 170.3 (1C), 163.9 (1C); 133.6-133.5, 132.1-131.8, 128.1-127.9 (weak signals due to the phenyl atoms.); MS (LSIMS) *m/z* 1715.9 (M^+) (Calcd for M^+ = 1716 (100%), 1715 (91.9%)). Anal. Calcd for $C_{19}HO_{19}Os_4Re$: C, 25.22; H, 0.94. Found: C, 25.16; H, 0.92.

Preparation of $ReOs_4(\mu\text{-}H)(CO)_{17}(PPh_3)$ (7a) To a flame-dried Carius tube was added $ReOs_4(\mu\text{-}H)(CO)_{18}(PPh_3)$ (**6**) (25 mg, 0.015 mmol) and toluene (15 mL). The tube was cooled to -196 °C and the solution degassed with three freeze-pump-thaw cycles and the vessel sealed under vacuum. The reaction mixture was then heated at 85 °C for 6 h; more two freeze-pump-thaw cycles of the reaction mixture were performed during this period. The resulting solution was evaporated and the remaining solid subjected to chromatography on a silica gel column (1.5 x 20 cm). Elution with hexane/CH_2Cl_2 (90/10 by volume) gave six bands. The first small yellow band contained the known $Os_3(CO)_{12}$ (~2 mg). This was followed by a larger yellow band that consisted of the known cluster $Os_4(\mu\text{-}H)_2(CO)_{13}$ (~4 mg, 24%). The orange band that came next contained a mixture of (**6**) and the desired product $ReOs_4(\mu\text{-}H)(CO)_{18}(PPh_3)$ (**7a**) (8 mg, 33%). Succeeding the orange band was a purple band of the new compound (**8**) (3mg, 12%) described below. This band was followed by another orange band (**9**) (<1mg, <5%) and then a blue band (**10**) (<1mg, <5%). The compounds giving rise to the last two bands were not identified.

A slight variation in the temperature, reaction time, or the number of freeze-thaw-degas cycles performed during the reaction significantly altered the ratio of products. The separation of **7a** from **6** proved exceedingly difficult. The band containing the mixture of **7a** and **6** was collected from the column and transferred to a Carius tube to which was added toluene (5 mL). The tube was cooled to -196 °C and the solution degassed with three freeze-pump-thaw cycles and the vessel sealed under vacuum. The solution was heated at 85 °C and the reaction carefully monitored by IR to determine the end point. (Again, the reaction did not behave in a predictable manner and often

conversion of **6** to **7a** did not occur.) Once the reaction was completed as determined by IR spectroscopy the sample was subjected to chromatography on a silica gel column as described above, yielding **7a** (2mg, 8%).

Preliminary results showed that the pyrolysis of $ReOs_4(\mu\text{-}H)(CO)_{18}(PPh_3)$ (**7b**) (an isomer of **7a** discussed in the next section) (25 mg, 0.015 mmol) in toluene (20 mL) at 70 °C for 7 hours produced $Os_3(CO)_{11}(PPh_3)$,[69] $Os_4(\mu\text{-}H)_2(CO)_{13}$ as well as a small amount of **7a**. (This reaction also appeared to be sensitive to minor changes in the conditions.) **7a**: IR (hexane) ν(CO) 2102 (m), 2075 (m), 2057 (vs), 2023 (s), 2007 (m), 1999 (w, sh), 1976 (m), 1964 (w, sh) cm^{-1}; ^1H NMR (CD_2Cl_2) δ -22.2 (s); MS (LSIMS) *m/z* 1686.7 (M^+) (Calcd for M^+ = 1688 (100%), 1686 (97.0%)). A C/H/N analysis was not carried out because of insufficient amounts of a pure sample. **9**: IR (CH_2Cl_2) ν(CO) 2105 (m), 2087 (w), 2068 (m), 2048 (m), 2032 (w, sh), 2023 (vs), 1997 (w, sh), 1977 (s), 1962 (m) cm^{-1}; MS (LSIMS) *m/z* 1389.9 (M^+). **10**: IR (CH_2Cl_2) ν(CO) 2111 (w), 2101 (w), 2071 (m), 2058 (s), 2043 (m), 2016 (vs), 1981 (w) cm^{-1}; MS (LSIMS) *m/z* 1308.0 (M^+).

Preparation of $ReOs_4(\mu\text{-}H)(CO)_{17}PPh_3$ (7b) To a flame dried Carius tube (quartz, fitted with a Teflon valve) was added $ReOs_4(\mu\text{-}H)(CO)_{18}PPh_3$ (35 mg, 0.020 mmol) and toluene (25 mL). The tube was cooled to -196 °C and the solution degassed with three freeze-pump-thaw cycles and the vessel sealed under vacuum. The reaction mixture was exposed to ultraviolet radiation for 6 h, during which time the original red solution changed to purple/brown. The resulting solution was evaporated and the solid subjected to chromatography on a silica gel column (2 x 16 cm). Elution with hexane/CH_2Cl_2 (9:1) gave a trace amount of $Os_4(\mu\text{-}H)_2(CO)_{13}$ followed by an orange

band that contained $Os_3(CO)_{12}$ and $Re(CO)_4(PPh_3)(H)$ (< 1% yield). Next off the column was the red/orange band of unreacted $ReOs_4(\mu\text{-}H)(CO)_{18}(PPh_3)$, followed by the purple band of compound **8** (~1 mg; ~3%) (see next section), then the brown band of **7b**. The analytical sample of **7b** was obtained as air-stable dark brown crystals by recrystallization from CH_2Cl_2 (13 mg, 38 %). As a thin film **7b** appears purple.

Repeating the above reaction but with a reaction time of 4 h and with $ReOs_4(\mu\text{-}H)(CO)_{17}(PPh_3)$ (**7a**) instead of $ReOs_4(\mu\text{-}H)(CO)_{18}(PPh_3)$ also results in $ReOs(\mu\text{-}H)(CO)_{17}(PPh_3)$ (**7b**) along with $Os_4(\mu\text{-}H)_2(CO)_{13}$. The difficulty in obtaining pure **7a** makes this a less convenient preparation of **7b** than the first method. **7b**: IR (hexane) ν(CO) 2123 (m), 2080 (s), 2065 (m), 2044 (vs), 2035 (w, sh), 2024 (s), 2012 (w), 2008 (w), 1994 (m), 1991 (m), 1969 (m), 1955 (m), 1929 (w), 1921 (w) cm^{-1}; ^1H NMR (CD_2Cl_2) δ -13.76 (d, J_{PH} = 10.4 Hz); $^{13}C/^{13}C\{^1H\}$ NMR (CD_2Cl_2, RT) δ 203.1 (2C, J_{PC} = 7.6 Hz), 198.0 (2C), 194.4 (2C, J_{CH} = 3.8 Hz), 194.1 (1C, J_{CP} = 8.3 Hz), 188.5 (2C), 181.6 (1C), 178.9 (1C, J_{CH} = 22.7 Hz), 175.1 (2C), 171.2 (1C), 171.1 (1C), 165.8 (1C), 162.8 (1C); 133.1 (d, J_{CP} = 10.6 Hz), 132.7, 131.1, 130.7 (d, J_{CP} = 1.5 Hz), 128.9, 128.8, 128.7; (The signals due to the phenyl atoms (128.7-133.1) appeared to be genuine but we were unable to interpret the extra peaks in this region of the spectrum. The ratio of these resonances is 2:0.15:1:1:1:1:1.) MS (LSIMS) *m/z* 1688.7 (M^+) (Calcd. for M^+= 1688 (100%), 1686 (97.0%).). Anal. Calcd for $C_{35}H_{16}O_{17}Os_4PRe$: C, 24.92; H, 0.96. Found: C, 24.66; H, 1.14.

Preparation of $Os_5(\mu\text{-}CO)(CO)_{16}(PPh_3)$ (8) As mentioned in the preparation of **7a** above, the pyrolysis of **6** also produces **8**. A slight modification of the procedure is described here that yields the same products but improved the yield of **8**. To a flame

dried Carius tube was added $ReOs_4(\mu\text{-}H)(CO)_{18}(PPh_3)$ (**6**) (50 mg, 0.030 mmol) and toluene (15 mL). The tube was cooled to -196 °C and the solution degassed with three freeze-pump-thaw cycles and the vessel sealed under vacuum. The reaction mixture was then heated at 95 °C for 4 h with no additional freeze-pump-thaw cycles during the reaction. Isolation of by column chromatography, as described above, gave **8** (10 mg, 20%) as well as the other products. The analytical sample of **8** was obtained as air-stable, purple crystals (not suitable for X-ray crystallography) by recrystallization in CH_2Cl_2. Crystals suitable for X-ray crystallography were obtained by the slow evaporation of a solution of **8** in C_6F_6 at room temperature. **8**: IR (hexane) ν(CO) 2119 (m), 2095 (w), 2091 (w), 2079 (w, sh), 2074 (s), 2063 (m), 2052 (w), 2046 (w, sh), 2037 (vs), 2018 (s), 2005 (s) 1986 (w), 1961 (w), 1941 (w), 1833 (w, broad) cm^{-1}; In solution **8** is an equilibrium of two isomers; NMR resonances written in regular text are assigned to the major isomeric **8a**, those in *italics* are assigned to isomer **8b** (By ^{31}P NMR ratio of isomers 0.3:1). ^{31}P NMR (CD_2Cl_2) δ *5.9*, 3.0; $^{13}C\{^1H\}$ NMR (CD_2Cl_2) δ *201.8* (d, 2C, J_{CP} = 5.1 Hz), 200.3 (d, 2C, J_{CP} = 5.8 Hz), 197.0 (2C), *196.1* (2C), 193.7 (2C), *193.4* (2C), 191.9 (2C), *190.5* (2C), *188.6* (2C), 186.4 (1C), *185.8* (1C), 184.5 (1C), 184.5 (2C), 184.2 (1C), *182.7* (1C), *181.2* (1C), 178.0 (1C), 175.2 (1C), *171.8* (1C), *170.5* (1C), 168.2 (1C), 168.0 (1C), *164.6* (1C); 133.1 (J_{PC} = 10.6 Hz), 131.5 131.1, 129.1, 129.0, 128.9 (weak signals due to the phenyl C atoms.); MS (LSIMS) *m/z* 1689.3 (M^+) (Calcd for M^+ = 1690 (100%), 1689 (91.9%)).

Preparation of $ReOs_3(\mu\text{-}H)(CO)_{15}(PPh_3)$ (11) To a round-bottom flask containing toluene (20 mL) was added $Os_4(CO)_{15}$ (30 mg, 0.025 mmol) and $Re(CO)_4(PPh_3)(H)$ (22 mg, 0.025 mmol). The green solution was stirred at room

temperature for 3 h and then at 40 °C for 2 h. The resulting red solution was evaporated to dryness on the vacuum line and the resulting solid chromatographed on a silica column (1.5 x 16 cm). Elution with hexane/CH_2Cl_2 (90:10, by volume) produced bands of $Os_3(CO)_{12}$ and **6**, followed by the red band of **11**. This band was evaporated to dryness and the solid crystallized from CH_2Cl_2 at -29 °C. After a week, air-stable, red crystals of **11** were isolated (<1 mg, <3%) that were used for the characterization of **11**: IR (hexane) ν(CO) 2131 (w), 2113 (m), 2092 (m), 2086 (w), 2081 (w), 2072 (m), 2069 (w), 2054 (s, broad), 2026 (vs, broad), 2004 (vw, sh), 2001 (vw, sh), 1990 (s), 1976 (s), 1968 (s), 1955 (w), 1948 (w) (Sample may contain $Re(CO)_4(PPh_3)(H)$, *ν*(CO) (hexane): 2081 (m), 1992 (s), 1977 (vs), 1964 (s)); MS (LSIMS) *m/z* 1439.8 (M^+) (Calcd. for M^+ = 1442 (100%), 1440 (99.6%)). (Successful isolation of **11** occurred only once. Not enough material was isolated to fully characterize **11**.)

Chapter 4. Synthesis and characterization of $Os_5(\mu\text{-}H)(H)(CO)_{18}$

4.1 Introduction

As mentioned in Chapter 2, addition of $Os(CO)_4(L)$ (L = CO, PMe_3, Bu^tNC) to $Os_4(CO)_{14}$ provides $Os_5(CO)_{18}(L)$ clusters that undergo decarbonylation to give the corresponding $Os_5(CO)_n(L)$ (n = 17, 15) clusters.[44-46] This protocol represents an important development in the rational synthesis of metal clusters that as mentioned previously remains a challenge in cluster chemistry.[3,4a]

Replacement of a CO with two H ligands in a metal carbonyl cluster often causes a different arrangement of the metal atoms in the resulting hydrido cluster. For example, a planar kite configuration is adopted by $Os_4(CO)_{13}(PMe_3)$ whereas the Os atoms in $Os_4(\mu\text{-}H)_2(CO)_{12}(PMe_3)$ are in a nonplanar butterfly arrangement.[34,48,49] Both, however, have the same number of Os_3 triangles. The compound $Os_7(CO)_{21}$ has a capped octahedral metal skeleton, but the Os core of $Os_7(\mu\text{-}H)_2(CO)_{20}$ is a capped trigonal bipyramid.[50,51] In Chapter 2 it was argued that the differences in the structures of $ReOs_4(\mu\text{-}H)(CO)_n$ (n = 19, 18) compared to $Os_5(CO)_n$ was due to the change in transition metals and not due to the presence of the bridging H ligand in the former clusters. It was therefore of interest to compare the structure of the $Os_5(\mu\text{-}H)_2(CO)_{n-1}$ clusters with those of the $Os_5(CO)_n$ analogues.[44,52-54] Furthermore, there are cases where an $M_x(\mu\text{-}H)_2(CO)_n$ (x > 3) cluster is known, but the isoelectronic $M_x(CO)_{n+1}$ is unknown. For example, only two binary carbonyl clusters with six Os atoms have been isolated, namely, the 84 electron $Os_6(CO)_{18}$ (Chapter 6) and the 90 electron $Os_6(CO)_{21}$.[106] On the other hand the 86 and 88 electron hydrido clusters $Os_6(\mu\text{-}H)_2(CO)_n$ (n = 18, 19) have been prepared and

their structures determined. [27a,107] Likewise, $Os_5(\mu\text{-}H)_2(CO)_{16}$ is known but $Os_5(CO)_{17}$ has not been isolated.[108]

In this chapter the isolation and characterization of $Os_5(\mu\text{-}H)(H)(CO)_{18}$ is described along with attempts to make $Os_5(\mu\text{-}H)_2(CO)_{17}$ to link up with the known $Os_5(\mu\text{-}H)_2(CO)_n$ (n = 16, 15) clusters, thereby completing the series.

4.2 Results and Discussion

$Os_5(\mu\text{-}H)(H)(CO)_{18}$ (12) Addition of $Os(CO)_4(H)_2$ to $Os_4(CO)_{14}$ in toluene at room temperature afforded $Os_5(\mu\text{-}H)(H)(CO)_{18}$ (**12**) in almost quantitative yield after about five minutes (eq 4.1).[d] The product was isolated as pink/orange flakes upon

$$Os_4(CO)_{14} + Os(CO)_4(H)_2 \longrightarrow Os_5(\mu\text{-}H)(H)(CO)_{18} \quad (4.1)$$

recrystallization from hexane. Considerable difficulty was experienced in the preparation of crystals of **12** suitable for X-ray crystallography. Crystals as the CH_2Cl_2 solvate (i.e., **12.CH_2Cl_2**) were finally obtained by a careful layering of a solution containing $Os(CO)_4(H)_2$ over a cold (-25 °C) solution of $Os_4(CO)_{14}$ in CH_2Cl_2. After two days at -29 °C, thin red rhomboidal crystals were obtained. In air at room temperature the quality of the crystals rapidly decreased presumably due to loss of solvent of crystallization (see below). The compound reacts with CH_2Cl_2 at room temperature. It is well known that the complexes with terminal hydride ligands react with chlorinated solvents to give the corresponding chloride derivative. Compound **12** was characterized by C/H/N analysis,

---

[d] The reaction of $Os(CO)_4(H)_2$ with $Os_4(CO)_{14}$ was first studied by Ms. Xuiyin Sun and Dr. Pomeroy.

IR (Figure 4.1), mass (parent ion), ^{1}H and ^{13}C NMR spectroscopy, and X-ray crystallography.

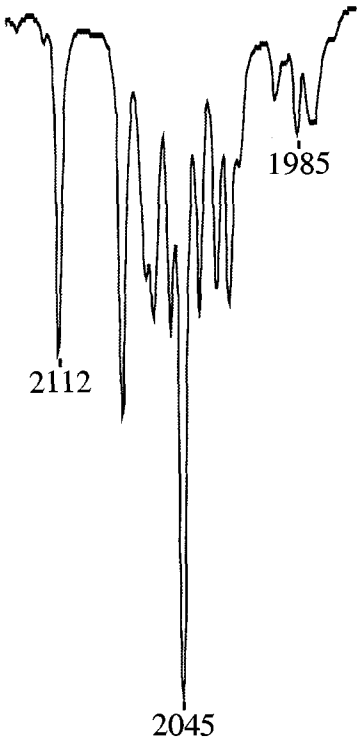

Figure 4.1. IR (hexane) spectrum (ν(CO) region) of $Os_5(\mu\text{-}H)(H)(CO)_{18}$ (**12**).

The molecular structure of **12.CH_2Cl_2** was determined at -100 °C by Dr. B. Patrick of the University of British Columbia. The structure consists of a planar Os_4 rhomboid (like that in $Os_4(CO)_{15}$) with an $Os(CO)_4(H)$ unit in the equatorial site of a wingtip Os atom, that is, a spiked kite arrangement (Figure 4.2). This configuration is the same as that adopted by **2** and **6** as described in Chapter 2 and 3. As mentioned there, prior to this work there was only one previously reported example of a pentanuclear cluster in which the Os_4 rhomboid is flat (i.e., $Os_5(\mu\text{-}H)(\eta^2\text{-}C_6F_5NNNC_6F_5)(CO)_{17}$).[63]

The OsOs lengths of the peripheral bonds in **12.CH_2Cl_2** have the same pattern as those in $Os_4(CO)_{15}$ (see Chapter 2). The OsOs bonds that involve the $Os(CO)_4$ unit

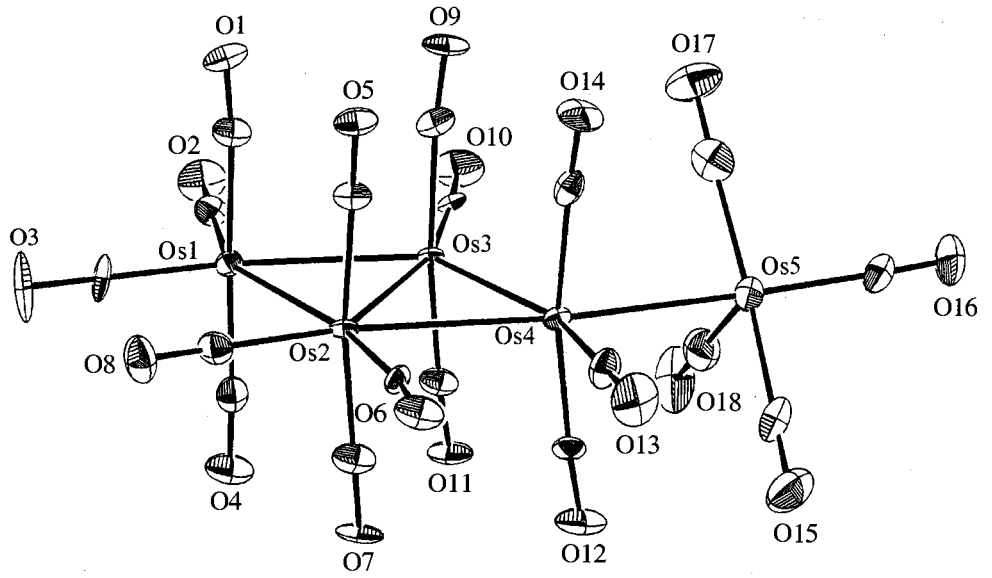

Figure 4.2. Molecular structure of $Os_5(\mu\text{-}H)(H)(CO)_{18}.CH_2Cl_2$ (**12.CH_2Cl_2**).

Table 4.1. Selected bond lengths (Å) and angles (°) for $Os_5(\mu\text{-}H)(H)(CO)_{18}.CH_2Cl_2$ (**12.CH_2Cl_2**).

Bond Lengths

Os(1)-Os(2)	2.9569(6)	Os(3)-Os(4)	2.9079(6)
Os(1)-Os(3)	2.8068(7)	Os(4)-Os(5)	2.8993(7)
Os(2)-Os(3)	2.9321(6)		
Os(2)-Os(4)	3.0290(7)	Os-C(*term.*) range	1.86(1) - 2.00(2)

Bond Angles

Os(2)-Os(1)-Os(3)	61.09(2)	Os(2)-Os(4)-Os(3)	59.15(1)
Os(1)-Os(2)-Os(3)	56.93(1)	Os(2)-Os(4)-Os(5)	167.29(2)
Os(1)-Os(2)-Os(4)	115.29(2)	Os(3)-Os(4)-Os(5)	108.17(2)
Os(3)-Os(2)-Os(4)	58.37(1)	Os(4)-Os(5)-CO(15)	86.3(4)
Os(1)-Os(3)-Os(2)	61.98(2)	Os(4)-Os(5)-CO(16)	175.7(4)
Os(1)-Os(3)-Os(4)	124.46(2)	Os(4)-Os(5)-CO(17)	86.0(4)
Os(2)-Os(3)-Os(4)	62.49(2)	Os(4)-Os(5)-CO(18)	85.2(4)

(Os(1)Os(2) = 2.9569(6); Os(2)Os(4) = 3.0290(7) Å) are considerably longer than the other peripheral bonds (Os(1)Os(3) = 2.8068(7); Os(3)Os(4) = 2.9079(6) Å; Table 4.1). The hinge OsOs length is 2.9321(6) Å. These lengths are typical for clusters that contain the unusual bonding seen in $Os_4(CO)_{15}$ and can be compared to the lengths of similar clusters given in Chart 3.2 (Chapter 3). The spike OsOs length at 2.8993(7) Å is shorter

than the corresponding length (2.925 Å) found in $Os_6(\mu\text{-}H)(H)(CO)_{19}$ that has a similar spike $Os(CO)_4(H)$ unit as **12.CH_2Cl_2**.[27a] The OsOs lengths in **12.CH_2Cl_2** may be compared with 2.877 Å the average OsOs length in $Os_3(CO)_{12}$.[64]

The terminal hydride ligand was placed at the "vacant" equatorial site on Os(5) by use of the XHYDEX program; this position gave a site energy of 2.2 (Table 4.2). This is in the range previously determined for the site energies of terminal metal hydrides.[67] The next lowest values are outside the range. The XHYDEX program placed the bridging hydride across the Os(3)Os(4) bond. The hydride ligand in this location gave by far the lowest site energy at 1.4 and again is in the range for bridging hydride ligands (Table 4.2).[67] Further support for this placement comes from the Os(2)Os(3)C(10) angle which

Table 4.2. Site energy (kcal mol^{-1}) for the terminal and bridging hydride positions in $Os_5(\mu\text{-}H)(H)(CO)_{18}.CH_2Cl_2$ (**12.CH_2Cl_2**).

Bridging Positions

Os(1)-Os(2)	15.6	Os(2)-Os(4)	9.2
Os(1)-Os(3)	9.3	Os(3)-Os(4)	**1.4**
Os(2)-Os(3)	10.5	Os(4)-Os(5)	9.1

Terminal Positions

Os(1)	58.6	Os(4)	17.9
Os(2)	83.6	Os(5)	**2.2**
Os(3)	10.7		

is 164.9(4)°. The corresponding angle in $Os_4(CO)_{15}$ is 180° (imposed by crystal symmetry). As in **2** and **6**, the bridging hydride ligand in **12.CH_2Cl_2** is not placed across the longest bond as is usual in Os carbonyl clusters with bridging H ligands. As mentioned in Chapter 2, in clusters with the unusual Os_4 bonding arrangement as in $Os_4(CO)_{15}$ the hydride ligand is placed across one of the shorter OsOs bonds, namely, Os(3)Os(4). Nevertheless, this bond at 2.9079(6) Å is considerably lengthened compared to the corresponding bond in $Os_4(CO)_{15}$ (2.774(1) Å).[29,36]

Excluding the longest OsC bond, the average OsC length in **12** is 1.93 Å. The Os(5)C(18) length is long at 2.00(2) Å and reflects the known strong trans influence of H ligands.[102]

The ^{1}H NMR spectrum of **12** exhibits a singlet in the terminal hydride region at δ -9.0, and a second singlet at δ -14.4 in the bridging region consistent with the view that **12** has a terminal and a bridging hydrogen ligand. The resonances do not have H-H coupling that can be taken that they are three or more bonds from each other consistent with the XHYDEX predictions.

The $^{13}C\{^{1}H\}$ NMR spectrum of **12** prepared from ^{13}CO-enriched $Os_4(CO)_{14}$ displayed signals consistent with the solid state structure of **12** with the exception that the signals due to the carbonyls attached to the spike Os atom are weak (Figure 4.3, next page). The spectrum is of low quality because solubility problems necessitated CH_2Cl_2/CD_2Cl_2 as the solvent, but **12** slowly reacts with the CH_2Cl_2 and therefore an extended acquisition time to improve the signal to noise ratio of the spectrum was not possible. The 2:2:2:1:1:1:0.7:1:2:0.5:1:1 ratio of signals contains the same pattern of resonances observed for the carbonyls attached to the Os_4 kite unit in **2** and **6** plus two weak signals due to the carbonyls on the spike Os atom. The four resonances with intensity 2 can be assigned to the four axial carbonyls on the Os_4 kite unit. The resonance at δ 172.7 is shifted to high field such that it is in the region where peaks due to equatorial carbonyls normally occur. This is observed in the spectra of **2** and **6** and is attributed to the unusual bonding in the compounds. As such this resonance can be

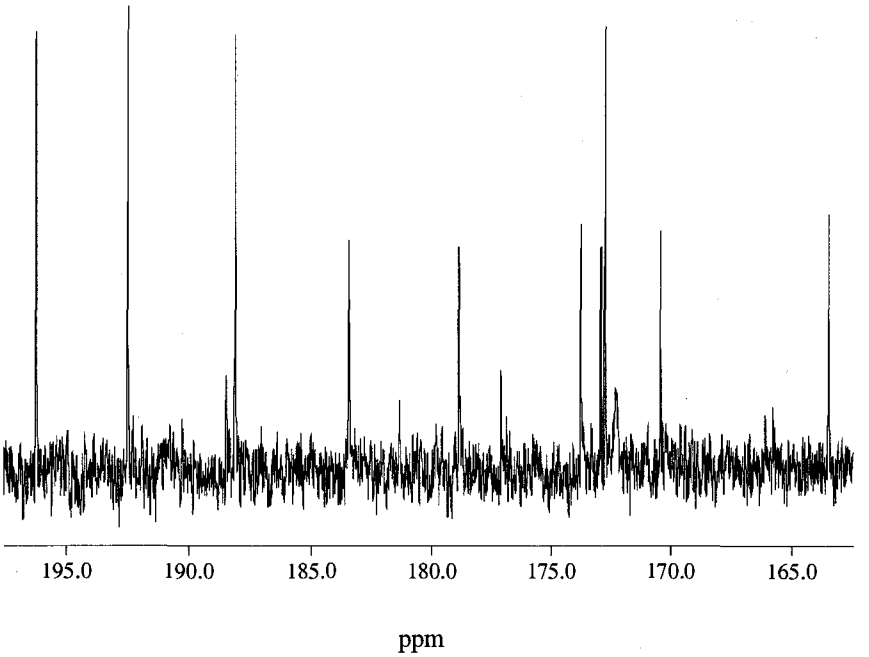

Figure 4.3. The ^{13}C NMR spectrum of $Os_5(\mu\text{-}H)(H)(CO)_{18}$ (**12**) in CD_2Cl_2 at 0 °C.

assigned to the axial carbonyls on Os(2). Similarly the high field resonances with intensity 1 at δ 170.4 and 163.5 are assigned to the equatorial carbonyls of Os(2). The signals at δ 196.3 and 192.5 with intensity 2 showed small H couplings that allows for their assignment to the axial carbonyls on Os(3) or Os(4), a more precise assignment is not possible at this time. The remaining signal of intensity 2 at δ 188.1 is therefore assigned to the axial carbonyls on Os(1) (Figure 4.3).

Of the remaining signals in the spectrum with intensity 1 only one resonance (at δ 172.7) does not show H coupling and is therefore attributed to C(2). The signal at δ 183.4 has the largest H coupling and is assigned to C(13) since it is directly trans to the bridging H ligand. (As previously noted, trans H couplings are much larger than cis H couplings.[78]) The two H-coupled signals at δ 178.9 and 173.7 can be assigned to C(10), with the coupling due to the cis H ligand, and C(3) which experiences an all-trans, three bond coupling to the bridging H. As discussed previously in Chapter 2, it is believed this

coupling is larger than normal due to the delocalized bonding in the molecule. The chemical shifts of these resonances and the C-H couplings mirror those in the ^{13}C NMR spectrum of **2**.

Two weak signals at δ 177.1 and 172.3 are believed due to the carbonyls cis to the hydride ligand on Os(5), the spike Os atom (Figure 4.3). That these signals are less intense than expected is attributed to slow exchange of the ^{13}C label from the ^{13}CO-enriched $Os_4(CO)_{14}$ unit with the unenriched spike $Os(CO)_4(H)$ moiety. The resonance due to the carbonyl trans to the terminal hydride C(18) is not observed. This can be rationalized on the basis of the mode of CO exchange across the spiked OsOs bond. The exchange of carbonyls on the Os_4 unit and those on the spike Os atom is believed to occur through a three-centred, axial-equatorial merry-go-round mechanism across the Os(2)Os(4)Os(5) bonds of **12** as shown in Chart 4.1. For electronic reasons the H never bridges the spike OsOs bond and also does not occupy the axial site on the spike Os atom. For this reason CO(18) (i.e., the CO trans to the H ligand) is unable to participate in the exchange and therefore does not become ^{13}C-enriched, and consequently its ^{13}C

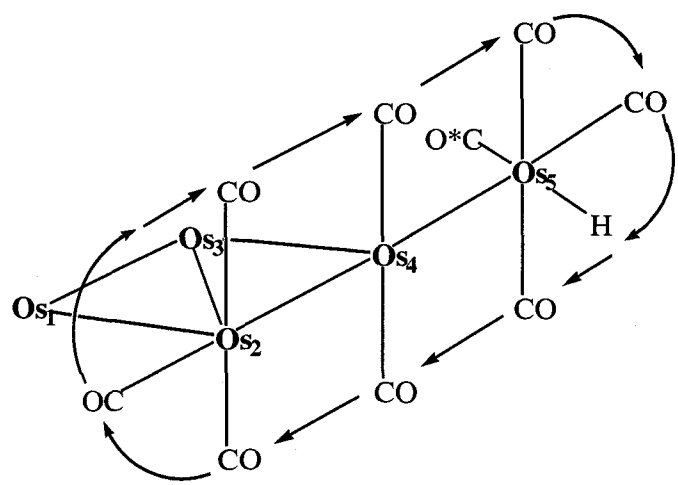

Chart 4.1. Mode of CO exchange between the Os_2 unit and the spiked Os atom. The CO(*) does not participate in the exchange (The other carbonyls omitted for clarity).

NMR resonance is too weak to observe. A similar situation was observed in the $^{13}C\{^{1}H\}$ NMR spectrum of $Os_4(CO)_{15}(CNBu^t)$ that contains a spiked $Os(CO)_4L$ unit as in **12** except that the H atom is replaced by $CNBu^t$.[42] Also, it has been found in the other spiked clusters reported in this thesis that the CO exchange over the spiked Os-M (M = Re, Os) bond can be extremely slow, which results in poor ^{13}CO enrichment for these carbonyls and therefore weak NMR signals.

The signals at δ 177.1 (J_{CH} = 9.9 Hz) and 172.3 (J_{CH} = 3.6 Hz) have an approximate 2:1 intensity. The ratio is only approximate because of the small signal to noise ratio mentioned above. The former resonance is therefore assigned to the two carbonyls cis to the OsOs bond and cis to the terminal H ligand, and the latter signal to the axial CO on the spike Os atom (i.e., trans to the spike OsOs bond). These carbonyl resonances exhibited significant H-^{13}C coupling even though the signals are cis to a H atom. The Os-CO angles about the spike Os atom (86.0 - 85.2°) deviate from 90°. That may result in increased *s* character in the molecular orbitals shared by the C and H atoms. This in turn would increase the coupling between the atoms.

Pyrolysis of $Os_5(\mu\text{-}H)(H)(CO)_{18}$ In an attempt to prepare $Os_5(\mu\text{-}H)_2(CO)_{17}$ and thus complete the $Os_5(\mu\text{-}H)_2(CO)_n$ (n = 18-15) series, **12** was carefully heated in toluene at 65 °C overnight. The reaction produced a mixture of compounds (eq 4.2) that after

$$Os_5(\mu\text{-}H)(H)(CO)_{18} \xrightarrow{65\ ^\circ C} Os_3(CO)_{12} + Os_4(\mu\text{-}H)_2(CO)_{13} + Os_5(CO)_{19} + Os_5(\mu\text{-}H)_2(CO)_{16} \qquad (4.2)$$

separation by chromatography were identified by IR spectroscopy as $Os_3(CO)_{12}$, $Os_4(\mu\text{-}H)_2(CO)_{13}$, $Os_5(CO)_{19}$ and $Os_5(\mu\text{-}H)_2(CO)_{16}$. Alteration of the reaction time or temperature (45 - 85 °C) failed to produce the desired $Os_5(\mu\text{-}H)_2(CO)_{17}$. The identity of

$Os_5(\mu\text{-}H)_2(CO)_{16}$ was also confirmed by mass spectroscopy.[27c] The yield of $Os_5(\mu\text{-}H)_2(CO)_{16}$ (~ 10%) produced by the method depicted in eq 4.2 could not be compared to literature syntheses since the yield is either not reported, or it is referred to as a minor product.[27c,96,109,110] The yield of $Os_5(CO)_{19}$ in this reaction (~10%) is much lower than the 78% previously reported,[44] although eq 4.2 does suggest that the reaction of **12** with CO might provide another high yield route, but this was not investigated.

Photolysis of **12** with UV light in toluene for 2 hours also did not give $Os_5(\mu\text{-}H)_2(CO)_{17}$, but rather $Os_5(CO)_{19}$, $Os_4(\mu\text{-}H)_2(CO)_{13}$, $Os_3(CO)_{12}$ and unreacted **12**. The production of $Os_5(\mu\text{-}H)_2(CO)_{19}$ from the reaction of $Os(CO)_4(H)_2$ and $Os_4(CO)_{15}$ in toluene at room temperature (as well as at 0 °C and -29 °C) was also not successful. The reaction produced $Os_3(CO)_{12}$, $Os_3(\mu\text{-}H)_2(CO)_{10}$ and $Os_4(\mu\text{-}H)_2(CO)_{13}$ after isolation by column chromatography and identified by IR spectroscopy.

The $Os_5(\mu\text{-}H)_2(CO)_n$ Series When compound **12** is added to the known $Os_5(\mu\text{-}H)_2(CO)_{16}$ and $Os_5(\mu\text{-}H)_2(CO)_{15}$ complexes they form another cluster series with the three members differing only by the number of carbonyls. Such series are exceedingly rare.[6a,27c,96,109,111] Once again it allows for an examination of cluster shapes and bonding as small changes to cluster composition, a major objective of this thesis. The $Os_5(\mu\text{-}H)_2(CO)_n$ (n = 18, 16, 15) series can be used to examine the effect of the replacement of a CO ligand by two hydrogen atoms (Chart 4.2, page 116).[44] Compound **12**, like **2** discussed in Chapter 2, can be considered a cluster of the type $Os_4(CO)_{14}(L)$ where L = $Os(CO)_4(H)$ and the hydride ligand is associated with the Os_4 nucleus. The skeletal arrangement of the Os_4 unit in **12.CH_2Cl_2** resembles the configuration of the Os atoms in

$Os_4(CO)_{14}(L)$ (L = CO, $CNBu^t$,[29,36] PMe_3[34,48]) with the allowance of slight expansion due to the hydride ligand.

The previously reported molecular structures of $Os_5(\mu\text{-}H)_2(CO)_{16}$ (Chart 4.2) consist of a bridging $Os(CO)_4$ across an OsOs bond of a Os_4 tetrahedron. (The two crystal forms differ in their packing arrangements.) The metal skeleton is the same as that proposed for $Os_5(CO)_{17}$ the unknown intermediate in the conversion of $Os_5(CO)_{18}$ to $Os_5(CO)_{16}$.[53] Although $Os_5(\mu\text{-}H)_2(CO)_{15}$ has been characterized by IR spectroscopy, mass spectrum and ^1H NMR spectroscopy its molecular structure has not been determined.[27c,96,109] It has been proposed that the compound has a trigonal bipyramidal structure, the same structure adopted by $Os_5(CO)_{16}$ and as predicted by PSEPT.[27c,54] (It would be worthwhile to confirm the structure $Os_5(\mu\text{-}H)_2(CO)_{15}$ by X-ray crystallography.)

In order to convert the spiked kite of **12.CH_2Cl_2** into the bridged tetrahedron of $Os_5(\mu\text{-}H)_2(CO)_{16}$ two possible structures for the $Os_5(\mu\text{-}H)_2(CO)_{17}$ intermediate can be postulated. These are a spiked tetrahedron structure analogous to that in **3** or the raft arrangement of metals that is adopted by **7b** (Chart 4.2). Note that the metal skeleton in $Os_5(\mu\text{-}H)_2(CO)_{16}$ has a structure consistent with the maximum number of M_3 triangles for a cluster with eight MM bonds proposed in Chapter 3.

Although more work needs to be done to fill in the missing structures, based on the available information the presence of the two hydride ligands in these pentanuclear Os clusters does not cause a major change in the geometry of the clusters.

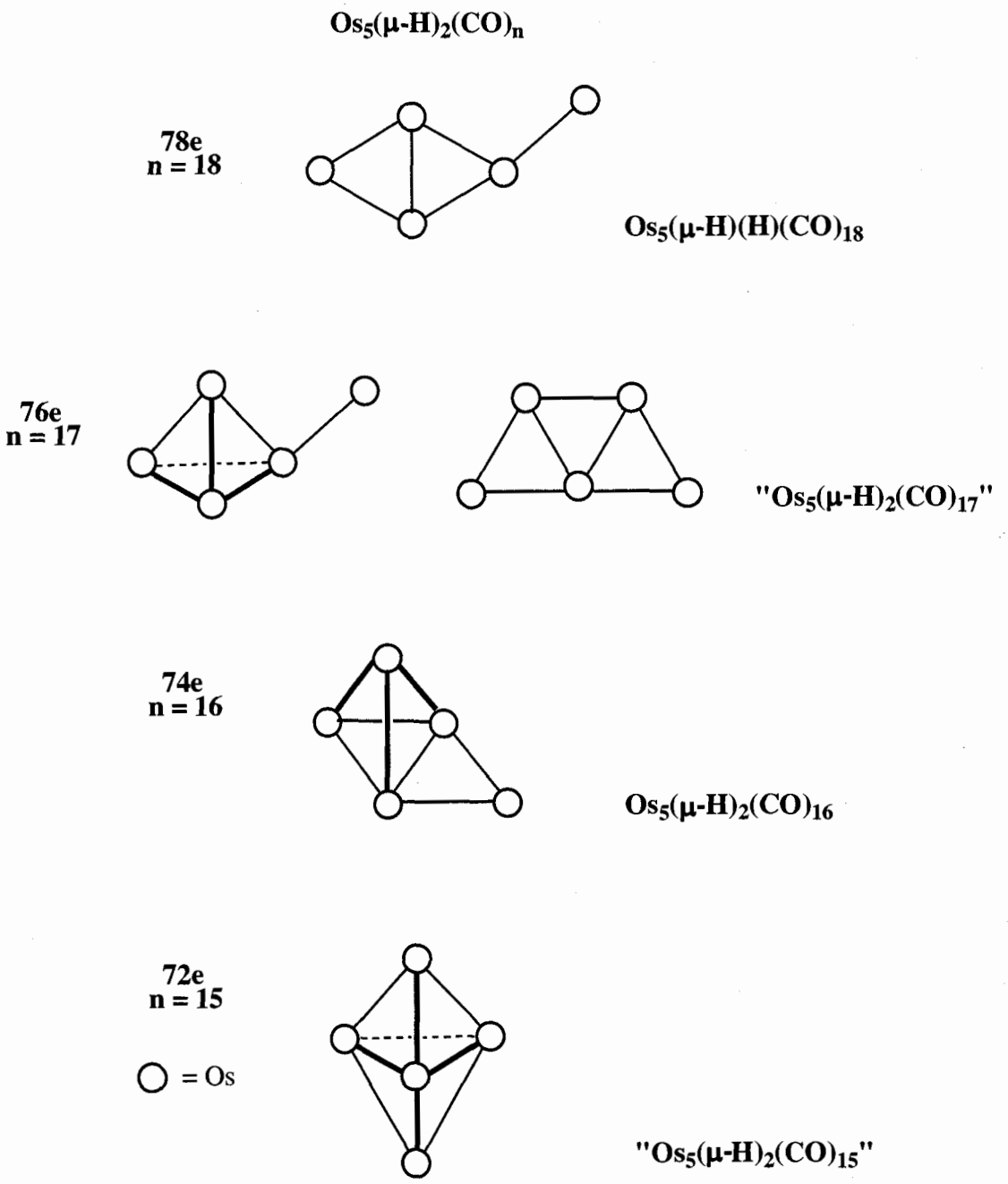

Chart 4.2. Molecular structure of the $Os_5(\mu\text{-}H)_2(CO)_n$ (n = 18 – 15) series. For n = 17, 15 the predicted structures are shown.

4.3 Experimental

The general procedure used for the synthesis and analysis has been described in the Experimental Section of Chapter 2. The preparation of $Os(CO)_4(H)_2$ was carried out by the literature procedure.[112] The $^{13}C/^{13}C\{^1H\}$ NMR spectra were recorded on a Varian AS 500 spectrometer.

Preparation of $Os_5(\mu\text{-}H)(H)(CO)_{18}$ (12) To a stirred solution of $Os_4(CO)_{14}$ (25 mg, 0.022 mmol) in hexane (25 mL) at room temperature was added an excess amount of $Os(CO)_4(H)_2$ in hexane. The colour of the solution immediately changed from brown/red to red/orange. The solution was evaporated to dryness and the resulting solid was dissolved in a minimum amount of hexane and placed in the freezer (at -29 °C) which produced an analytically-pure sample of **12** as air-stable, non-transparent, glistening pink/orange flakes in a greater than 95% yield. (The flakes were not suitable for X-ray crystallography.) Crystals suitable for X-ray crystallography were prepared in the following manner. To a Schlenk tube which had been placed in an acetone-dry ice bath at -25 °C was added $Os_4(CO)_{14}$ (10 mg, 0.0087 mmol) and CH_2Cl_2 (5 mL). The solution was stirred until the $Os_4(CO)_{14}$ dissolved and the stir bar was removed. An excess (~ 5 mL) of $Os(CO)_4(H)_2$ in hexane was carefully layered over the $Os_4(CO)_{14}$ solution. The Schlenk tube was carefully (so as not to mix the layers) placed in the freezer (at -29 °C). After 2 d, **$12.CH_2Cl_2$** was produced as unstable, red/orange crystals that were collected and stored in liquid N_2. At room temperature the crystals lost their form rendering them unsuitable for X-ray crystallography. The crystals cannot be stored in a coating of CH_2Cl_2 at room temperature since CH_2Cl_2 reacts with **12.** Compound **12**: IR (hexane) ν(CO) 2134 (vw), 2120 (vw), 2112 (s), 2077 (s), 2064 (w, sh), 2060 (m), 2051 (m), 2045

(vs), 2036 (m), 2027 (m), 2020 (m), 2015 (w), 1996 (w), 1985 (w), 1978 (w), 1976 (w), 1966 (vw) cm^{-1}; ^1H NMR (benzene-d_6) δ –9.0 (s), -14.4 (s); $^{13}C/^{13}C\{^1H\}$ NMR (CD_2Cl_2, 0 °C) δ 196.3 (2C, J_{CH} = 1.2 Hz), 192.5 (2C, J_{CH} = 2.6 Hz), 188.1 (2C), 183.4 (1C, J_{CH} = 5.7 Hz), 178.9 (1C, J_{CH} = 1.9 Hz), 177.1 (2C, J_{CH} = 9.9 Hz) 173.7 (1C, J_{CH} = 1.9 Hz), 172.9 (1C), 172.7 (2C), 172.3 (1C, J_{CH} = 3.6 Hz), 170.4 (1C), 163.5 (1C); MS (LSIMS) *m/z* 1456.6 (M^+) (Calcd for M^+ = 1458 (100%), 1457 (91.4%)). Anal. Calcd for $C_{19}H_4Cl_2O_{18}Os_4$: C, 14.79; H, 0.26. Found: C, 14.97; H (below detection limit)[e]

Pyrolysis of 12 To a flame-dried Carius tube was added **12** (10 mg, 0.0069 mmol) and toluene (5 mL). The tube was degassed with three freeze-pump-thaw cycles, and the vessel sealed under vacuum and heated at 65 °C overnight. The solution was transferred to a Schlenk tube and the solvent removed on the vacuum line. The solid was then subjected to chromatography on a silica gel column (1 x 12 cm). Elution with hexane/toluene (95:5) gave in order of elution, a yellow band of $Os_4(\mu\text{-}H)_2(CO)_{13}$ (~2 mg, ~25 %), an orange/red band of $Os_5(CO)_{19}$ (~1 mg, ~10%), an orange/brown band of $Os_5(\mu\text{-}H)_2(CO)_{16}$ (~1 mg, ~10 %) followed by a yellow band that consisted of a trace amount of $Os_3(CO)_{12}$. The IR spectrum of $Os_5(\mu\text{-}H)_2(CO)_{16}$ was in agreement with the reported values: IR(hexane) ν(CO) 2122 (w), 2083 (s), 2060 (s), 2049 (s), 2045 (m,sh), 2038 (w), 2010(m) cm^{-1}.[27c] MS (LSIMS) *m/z* 1401.0 (M^+) (Calcd for M^+ = 1402 (100%), 1401 (91.3%)).

---

[e] Sample was prepared by Ms. Xuiyin Sun.

Chapter 5. Diphenylacetylene derivatives of $Os_4(CO)_{14}$

5.1 Introduction

Alkynes react with metal carbonyl compounds to form complexes with remarkable structural diversity.[113] For example, 20 different types of complexes have been isolated from the reaction of alkynes with $Fe_3(CO)_{12}$. The number of iron atoms in these compounds ranges from one to four and often includes more than one alkyne ligand.[113(b-d)] Although investigations of complexes with alkyne units date back to the late 1950s these complexes continue to attract attention.[114] The studies often deal with the unique bonding present in these systems, as well as their ability to act as catalysts for reactions such as the hydrogenation of alkynes.[115] The bonding adopted by the alkyne ligand on metal clusters is believed to mimic the bonding of alkyne groups on the surface of metal catalysts. As such, metal-alkyne clusters have been used as models to help understand the behaviour of the reactants during catalytic reactions on metal surfaces.[116]

For clusters of a given nuclearity different bonding modes are found for the alkyne ligand. Thorough reviews discussing the bonding modes adopted by alkyne ligands with coordination numbers of 2 to 5 is presented in reference 113. Introduced below are the bonding modes that are present in the compounds discussed in this chapter.

Several modes of bonding are found when an alkyne ligand bridges two metal atoms. As shown in Figure 5.1A, one mode involves the side-on addition of the alkyne group parallel to the MM bond. In this arrangement the alkyne ligand forms a σ bond to each metal and acts as a 2 electron donor. When an alkyne ligand binds a M_3 unit, the most common bonding geometry is with two σ bonds between the alkyne ligand and two metal centers and a π bond to the third (Figure 5.1B).[113(a-e),117,118] The most common

bonding mode for an alkyne ligand coordinated to four metal atoms is the alignment of the CC vector of the alkyne group parallel to the hinge bond of a butterfly metal skeleton, with two σ bonds to the hinge M atoms and π bonds to the wingtip M atoms. This produces a distorted M_4C_2 octahedron (Figure 5.1C).[18,111(f,i),113(a-e),119]

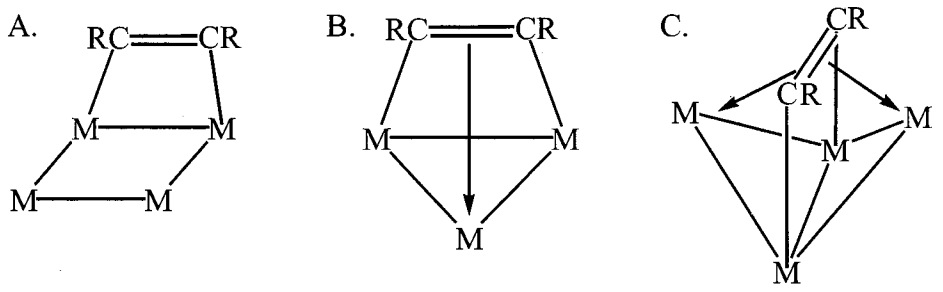

Figure 5.1. Selected bonding modes of alkyne ligands in cluster complexes.

Examinations of the change in the alkyne bonding mode that occurs as a carbonyl cluster loses or gains a CO ligand in a stepwise fashion have been limited. A few one-step conversions are known in which the coordination number of the alkyne converts from three to four, but these reactions are often accompanied by the addition of other ligands.[111f,i] Beside the derivatives reported in this chapter, there exists only one series, $Os_3(C_2Ph_2)(CO)_n$ (n = 11, 10, 9), in which there is a stepwise loss of two CO ligands without the addition of other ligands.[113b,120,121] Of these trinuclear compounds only the structure of $Os_3(\mu_3\text{-}\eta^2\text{-}C_2Ph_2)(CO)_{10}$ has been determined by X-ray crystallography, with the other two species poorly characterized.

In this chapter the reaction of diphenylacetylene (PhCCPh) with $Os_4(CO)_{14}$ is described. The series of compounds, $Os_4(\mu_x\text{-}\eta^2\text{-}C_2Ph_2)(CO)_n$ (n = 14, x = 2; n = 13, x = 3; n = 12, x = 4), thus isolated represent the stepwise loss of two carbonyl ligands from an alkyne-containing metal carbonyl cluster. The structures of the three clusters have

been determined and they provide important insights into the bonding of an alkyne on a metal surface. With these insights a new model for the mechanism of surface catalysis is proposed. Two known trinuclear Os compounds containing alkyne ligands were also isolated and their previously unreported ^{13}C NMR spectroscopic data is discussed.

5.2 Results and discussion

$Os_4(\mu\text{-}\eta^2\text{-}C_2Ph_2)(CO)_{14}$ (13) Compound **13** was isolated as dark red needles in about 70% yield from the reaction of $Os_4(CO)_{14}$ in CH_2Cl_2 at room temperature with an excess of C_2Ph_2 (eq 5.1). An excess of diphenylacetylene ensured that **13** formed quickly

$$Os_4(CO)_{14} + C_2Ph_2 \xrightarrow{25\ ^\circ C} \underset{\mathbf{13}}{Os_4(\mu\text{-}\eta^2\text{-}C_2Ph_2)(CO)_{14}} + \text{other products} \qquad (5.1)$$

as it slowly loses CO at room temperature to give $Os_4(\mu_3\text{-}\eta^2\text{-}C_2Ph_2)(CO)_{13}$ (**14**) (see the next section). Besides **14,** other products isolated from the reaction shown in eq. 5.1 were the known clusters $Os_3(\mu_3\text{-}\eta^2\text{-}C_2Ph_2)(CO)_{10}$ (**16**)[7b,120,135] and $Os_3(\mu\text{-}\eta^4\text{-}C_4Ph_4)(CO)_9$ (**17**).[7b,122] The VT $^{13}C\{^1H\}$ NMR spectra of **16** and **17** are also discussed below. The products **13-17** are brightly coloured, air-stable and readily separated by column chromatography. Compound **13** was characterized by C/H/N analysis, IR, mass (parent ion), ^1H and ^{13}C NMR spectroscopy and X-ray crystallography.

The structure of **13** (as the CH_2Cl_2 solvate)[f] reveals an approximately planar Os_4C_2 unit (Figure 5.2); selected bond lengths and angles for **13** are given in Table 5.1. The Os_4 unit adopts a flat butterfly or kite arrangement with five OsOs bonds that range in length from 2.859(2) to 2.916(2) Å. These lengths are typical for open Os clusters.

[f] Determined by Dr. M. J. Jennings at the University of Western Ontario.

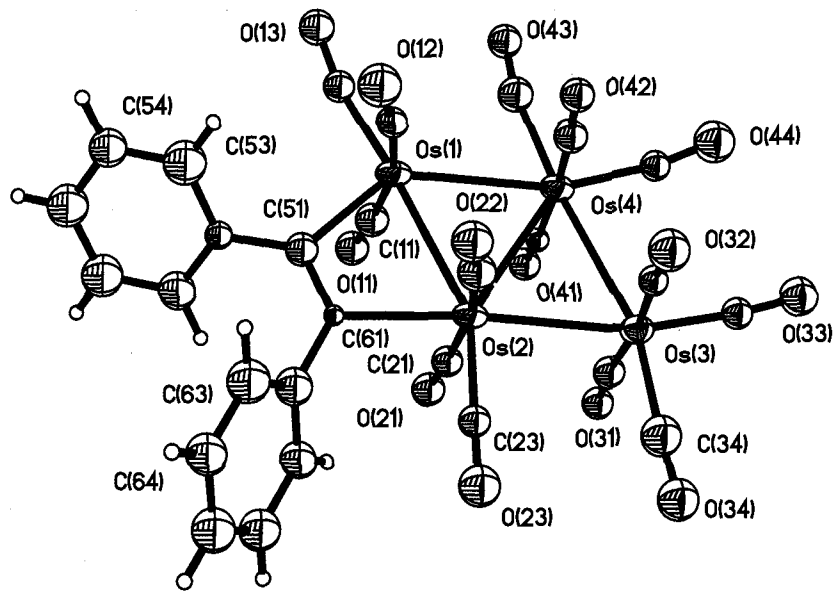

Figure 5.2. Molecular structure of $Os_4(\mu\text{-}\eta^2\text{-}C_2Ph_2)(CO)_{14}$ (**13**).

Table 5.1. Selected bond lengths (Å) and angles (°) for $Os_4(\mu\text{-}\eta^2\text{-}C_2Ph_2)(CO)_{14}$ (**13**).

Bond Lengths

Os(1)-Os(2)	2.866(2)	Os(1)-C(51)	2.13(3)
Os(1)-Os(4)	2.859(2)	Os(2)-C(61)	2.28(3)
Os(2)-Os(3)	2.880(2)	C(51)-C(61)	1.32(4)
Os(2)-Os(4)	2.916(2)	Os-CO range	1.84 (4)-1.96 (3)
Os(3)-Os(4)	2.907(2)		

Bond Angles

Os(2)-Os(1)-Os(4)	61.25(5)	Os(2)-Os(1)-C(51)	73.5(8)
Os(1)-Os(2)-Os(3)	119.44(6)	Os(1)-Os(2)-C(61)	65.5(6)
Os(1)-Os(2)-Os(4)	59.25(5)	Os(1)-C(51)-C(52)	126(2)
Os(3)-Os(2)-Os(4)	60.20(4)	Os(1)-C(51)-C(61)	108(2)
Os(2)-Os(3)-Os(4)	60.52(4)	Os(2)-C(61)-C(51)	113(2)
Os(1)-Os(4)-Os(3)	118.77(6)	Os(2)-C(61)-C(62)	119(2)
Os(1)-Os(4)-Os(2)	59.51(4)		
Os(2)-Os(4)-Os(3)	59.28(4)		

The average OsOs bond distance in $Os_3(CO)_{12}$ is 2.877 Å.[64] If it is assumed that the OsOs bonds are single nondative covalent bonds then Os(1) has a 17 and Os(4) a 19 electron count. In order for each Os atom to obey the 18 electron rule therefore requires the Os(1)Os(4) bond be a dative metal-metal bond with the Os(4) atom donating two electrons to Os(1).

The Os_2C_2 unit is a dimetallacyclobutene derivative. The geometry about each C atom of the unit is approximately trigonal planar although the internal OsCC angles (108(2) and 113(2)°) are somewhat compressed from the ideal value of 120° (Table 5.1). The CC bond length of the unit of 1.32(4) Å is consistent with an uncoordinated CC double bond. The OsC bond lengths of 2.13(3) and 2.28(3) Å indicate the bonds are single bonds. These bonds lengths and angles are comparable with those found in $Os_2(\mu\text{-}\eta^2\text{-}C_2(CO_2CH_3)_2)(CO)_8$ (CC bond: 1.33(1) Å; OsC bond: 2.138(5); OsCC angle: 111.2(2)).[123] This compound contains a similar Os-C=C-Os unit to **13**. The CC bond length (1.53(3) Å) found in the Os-C-C-Os unit of $Os_2(\mu\text{-}\eta^2\text{-}C_2H_4)(CO)_8$ is longer than the CC length in **13** and typical of a single CC bond.[124] This single CC length (1.53(3) Å) is similar to that found in **15** discussed below. The OsC lengths of the Os-C=C-Os unit in **13** may also be compared with the OsC lengths in **13** that involve carbonyl ligands; these lengths are significantly shorter and are in the range 1.84(4) to 1.96(3) Å. Metal-carbonyl bonds, of course, have significant π bonding character.

Dimetallacyclobutene compounds are comparatively rare and a search of this term in the literature by SciFinder Scholar yielded only 12 publications containing compounds with this bonding motif.[113,125,126] Of these examples only one compound, $Ir_4[(\mu\text{-}\eta^2\text{-}C_2(MeCO_2)_2]_2[(\mu_4\text{-}\eta^2\text{-}C_2(MeCO_2)_2]_2(CO)_8$, contains more than two metal atoms. Some

other recent examples are $Ir_2(\mu\text{-}\eta^2\text{-}C_2R_2)(\eta^5\text{-}C_9H_7)_2(CO)_2$ (R = Ph, Tol), $Re_2Cp^*_2(\mu\text{-}\eta^2\text{-}C_2(CO_2CH_3)_2(CO)_4$.

The $^{13}C\{^1H\}$ NMR spectrum of **13** (^{13}CO enriched) in CD_2Cl_2/CH_2Cl_2 at ambient temperature exhibits four signals of intensity 2 (δ 192.13, 192.08, 184.6, 175.4) and six signals of intensity 1 in the carbonyl region (Figure 5.3). This observation is in agreement with the view that **13** has the same structure in solution as in the solid-state, and that the carbonyls are rigid in solution at this temperature. Typically resonances due to axial carbonyl ligands come to lower field than those due to equatorial carbonyls.[78] As can be seen from Figure 5.3, one of the signals of intensity 2 is to higher field than expected and one signal of intensity 1 is at lower field. These anomalous signals may be due to the carbonyls attached to Os(1) and reflect the unusual OsOs bonding at this atom.

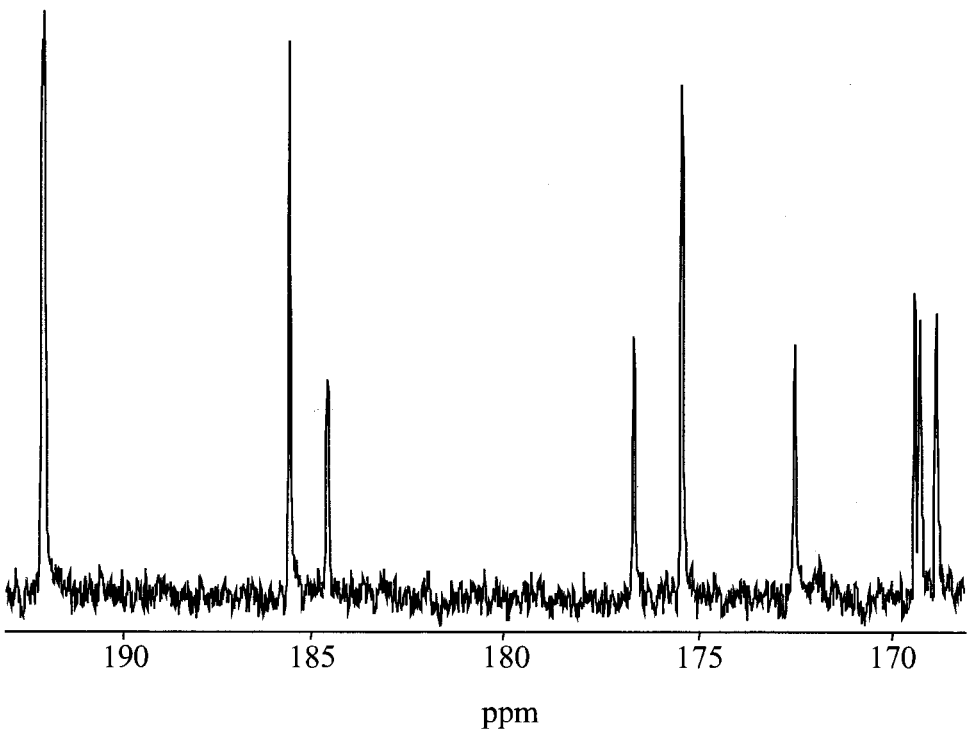

Figure 5.3. The ^{13}C NMR spectrum of ^{13}CO-enriched $Os_4(\mu\text{-}\eta^2\text{-}C_2Ph_2)(CO)_{14}$ (**13**).

Preliminary results indicated that the reaction of acetylene with $Os_4(CO)_{14}$ produced a compound similar to **13**. The reaction produced a purple compound whose mass spectrum (parent ion) was consistent with a formula of $Os_4(C_2H_2)(CO)_{14}$. The IR spectrum of this compound has the same CO-stretching pattern observed for **13** and therefore is believed to be $Os_4(\mu\text{-}\eta\text{-}C_2H_2)(CO)_{14}$.

$Os_4(\mu_3\text{-}\eta^2\text{-}C_2Ph_2)(CO)_{13}$ (14) When **13** was stirred in CH_2Cl_2 at room temperature for 2 days cluster **14** was produced in good yield (eq 5.2). The product was

$$Os_4(\mu\text{-}\eta^2\text{-}C_2Ph_2)(CO)_{14} \xrightarrow{25\ ^\circ C} \underset{\mathbf{14}}{Os_4(\mu_3\text{-}\eta^2\text{-}C_2Ph_2)(CO)_{13}} \qquad (5.2)$$

isolated after column chromatography as air-stable red crystals that were characterized by C/H/N analysis, IR, mass (parent ion), ^1H and ^{13}C NMR spectroscopy, and X-ray crystallography.

The structure of **14**[g] has two independent molecules in the unit cell that differ in the orientation of the phenyl rings, but are otherwise identical. A view of both molecules is given in Figure 5.4; selected bond lengths and angles for each molecule are collected in Table 5.2. The structure of **14** consists of an almost flat butterfly or kite arrangement, as found in **13**, but with the alkyne spanning one of the Os_3 triangles. The peripheral OsOs lengths associated with the alkyne in each molecule (range = 2.7392(7) to 2.7740(7) Å) are significantly shorter than the peripheral OsOs lengths that involve Os atoms not directly bound to the C_2Ph_2 (range 2.8665(6) to 2.8947(6) Å). The shorter OsOs bonds can be attributed to the bonding requirements of the bridging C_2Ph_2 ligand. The

[g] Determined by Dr. G. P. A. Yap at the University of Ottawa.

unbridged OsOs bonds are typical for open Os clusters. The hinge OsOs bonds are of intermediate length (2.8204(6) and 2.8007(7) Å).

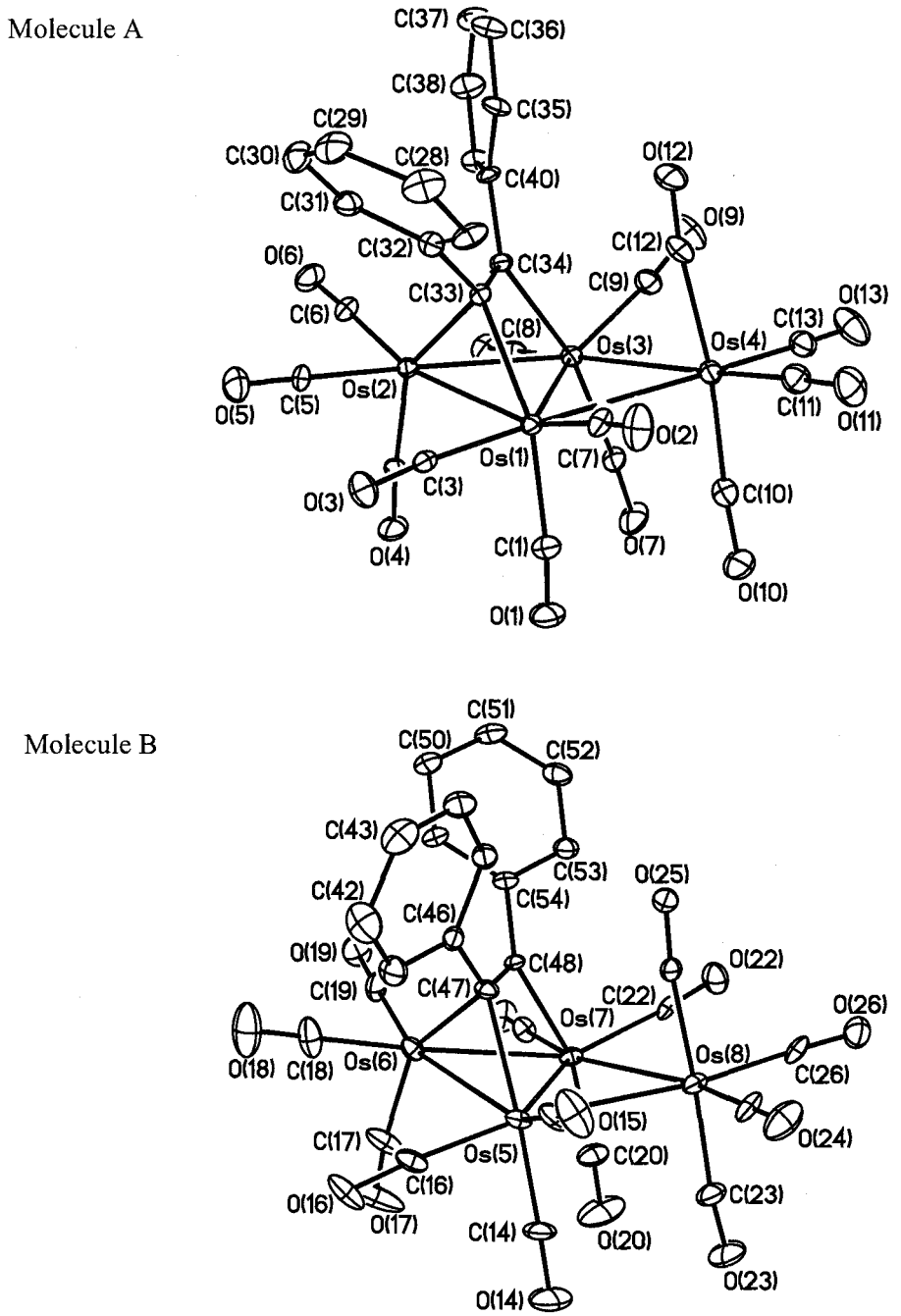

Figure 5.4. Molecular structures of the two independent molecules of $Os_4(\mu_3\text{-}\eta^2\text{-}C_2Ph_2)(CO)_{13}$ (**14**).

Table 5.2. Selected bond lengths (Å) and angles (°) for $Os_4(\mu_3\text{-}\eta^2\text{-}C_2Ph_2)(CO)_{13}$ (**14**).

Bond Lengths			
Molecule **A**		Molecule **B**	
Os(1)-Os(2)	2.7586(6)	Os(5)-Os(6)	2.7392(7)
Os(1)-Os(3)	2.8204(6)	Os(5)-Os(7)	2.8007(7)
Os(1)-Os(4)	2.8665(6)	Os(5)-Os(8)	2.8871(7)
Os(2)-Os(3)	2.7454(6)	Os(6)-Os(7)	2.7740(7)
Os(3)-Os(4)	2.8947(6)	Os(7)-Os(8)	2.8939(7)
Os(1)-C(33)	2.15(1)	Os(5)-C(47)	2.17(1)
Os(2)-C(33)	2.29(1)	Os(6)-C(47)	2.29(1)
Os(2)-C(34)	2.27(1)	Os(6)-C(48)	2.29(1)
Os(3)-C(34)	2.18(1)	Os(7)-C(48)	2.16(1)
C(33)-C(34)	1.42(2)	C(47)-C(48)	1.42(2)
Os-CO *range*	1.89(1)-1.99(1)	Os-CO *range*	1.88(1)-1.98(1)

Bond Angles			
Os(2)-Os(1)-Os(3)	58.94(2)	Os(6)-Os(5)-Os(7)	60.08 (2)
Os(2)-Os(1)-Os(4)	118.26(2)	Os(6)-Os(5)-Os(8)	118.54(2)
Os(3)-Os(1)-Os(4)	61.19(2)	Os(7)-Os(5)-Os(8)	61.14(2)
Os(1)-Os(2)-Os(3)	61.65(2)	Os(5)-Os(6)-Os(7)	61.06(2)
Os(1)-Os(3)-Os(2)	59.41(2)	Os(5)-Os(7)-Os(6)	58.86(2)
Os(1)-Os(3)-Os(4)	60.19(2)	Os(5)-Os(7)-Os(8)	60.90(2)
Os(2)-Os(3)-Os(4)	117.74(2)	Os(6)-Os(7)-Os(8)	117.15(2)
Os(1)-Os(4)-Os(3)	58.62(1)	Os(5)-Os(8)-Os(7)	57.96(2)
Os(3)-Os(1)-C(33)	71.0(3)	Os(7)-Os(5)-C(47)	71.7(3)
Os(1)-Os(3)-C(34)	71.1(3)	Os(5)-Os(7)-C(48)	71.2(3)
Os(1)-C(33)-C(34)	110.4(8)	Os(5)-C(47)-C(48)	107.8(8)
Os(1)-C(33)-Os(2)	76.8(3)	Os(5)-C(47)-Os(6)	75.7(3)
Os(3)-C(34)-C(33)	107.5(8)	Os(7)-C(48)-C(47)	109.3(8)
Os(3)-C(34)-Os(2)	76.1(4)	Os(7)-C(48)-Os(6)	77.0(3)

The 18 electron rule requires that the alkyne fragment donates two electrons to the wingtip Os atom (i.e., Os(2)) and one electron to each hinge Os atom (i.e., Os(1) and Os(3)). The four OsC(alkyne) lengths involving the wingtip Os atoms (Os(2) and Os(6)) are in the range 2.27(1) - 2.29(1) Å and as such are somewhat longer than the other OsC(alkyne) lengths in **14** (range 2.15(1) - 2.18(1) Å). The bonding may be viewed as a dimetallacyclobutene unit but with the C=C double bond acting as a typical alkene ligand

toward the wingtip Os atom. The length of the CC bond (1.42 Å) in the alkyne unit suggests a formal bond order less than two, as observed in similar compounds. The bonding of the alkyne to the Os_3 triangle in **14** is similar to that in compounds such as $Os_3(\mu_3\text{-}\eta^2\text{-}C_2Ph_2)(CO)_{10}$ (**16**),[120c] $Os_5(\mu_3\text{-}\eta\text{-}C_2H_2)(CO)_{17}$[127], $Os_7(\mu_3\text{-}\eta^2\text{-}C_2Me_2)(CO)_{19}$[128] and $Os_3(\mu_3\text{-}\eta^2\text{-}C_2Et_2)(CO)_{10}$[135].

The $^{13}C\{^1H\}$ NMR spectra in the carbonyl region of **14** (^{13}CO-enriched) in CD_2Cl_2/CH_2Cl_2 at -50 and 21 °C are shown in Figure 5.5. The lower temperature

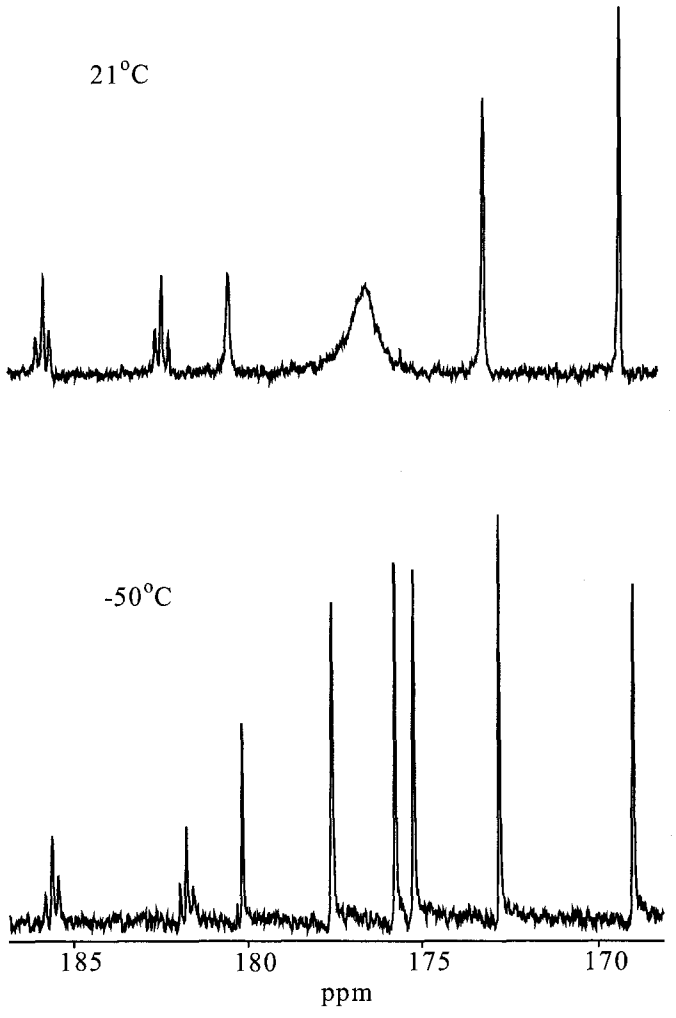

Figure 5.5. VT ^{13}C NMR spectra of CO-enriched $Os_4(\mu_3\text{-}\eta^2\text{-}C_2Ph_2)(CO)_{13}$ (**14**).

spectrum exhibits eight signals in an approximate 1:1:1:2:2:2:2:2 (low to high field). This is consistent with the view that **14** has the same structure in solution as in the solid and that the carbonyls are rigid on the NMR time scale at -50 °C. The two signals at lowest field (i.e., at δ 185.6 and 181.8) that exhibit satellites are therefore readily assigned to the C atoms of the two axial CO ligands on the unbridged wingtip Os atom (i.e., the C atoms labelled (23) and (25) in Figure 5.4). This is because only these peaks would be expected to exhibit observable ^{13}C-^{13}C coupling due to the mutual trans arrangement of these carbonyls. (Recall the complex was ^{13}CO enriched.) The remaining signal of intensity 1 (at δ 180.2) is attributed to the axial carbonyl atom on the bridged wingtip Os atom (i.e., C(17)). The signal at δ 177.6 is assigned to the two C atoms of the axial carbonyls on the hinge Os atoms (i.e., C(14) and C(20)). As stated previously, ^{13}C NMR resonances due to C atoms of axial carbonyls usually appear to lower field than the corresponding signals of equatorial carbonyls.[78] The resonances at δ 175.8 and 175.2 are designated to the C atoms of the equatorial carbonyls on the hinge Os atoms on the basis of their exchange behaviour described below. The remaining resonances at δ 172.8 and 169.0 are attributed to the C atoms of the equatorial carbonyls on the wingtip Os atoms. A more definitive assignment is not possible at this time.

In the spectrum at 21 °C, three of the resonances have coalesced to a broad singlet (Figure 5.5) indicative of exchange between the carbonyls that give rise to the signals in the spectrum at lower temperature. This is believed due to the carbonyl exchange of the hinge $Os(CO)_3$ groupings. Rotation of $Os(CO)_3$ units in condensed Os carbonyl clusters is common. Examples are $Os_6(CO)_{17}(L)$ (L = CO, PPh_3)[80,81] and $Os_7(CO)_{21}$.[50] The hinge Os atoms are seven coordinate whereas the wingtip Os atoms are nominally six

coordinate (if the bond to the C_2Ph_2 is a conventional metal-alkene bond). It is well known that mononuclear six coordinate complexes are usually rigid whereas the corresponding seven coordinate complexes are invariably nonrigid in solution.

Although the reason for the difference in activation barriers to exchange may be based upon electronic considerations, it can be rationalized by using simple steric arguments. It has been shown that the ground state and transition state energies are both important in determining a barrier to rotation of the arene ring in (η^6-arene)$Fe(CO)_2(SiCl_3)$ complexes.[129] In six coordinate complexes the trigonal prismatic transition state has three eclipsing interactions as shown in Chart 5.1. Also of importance

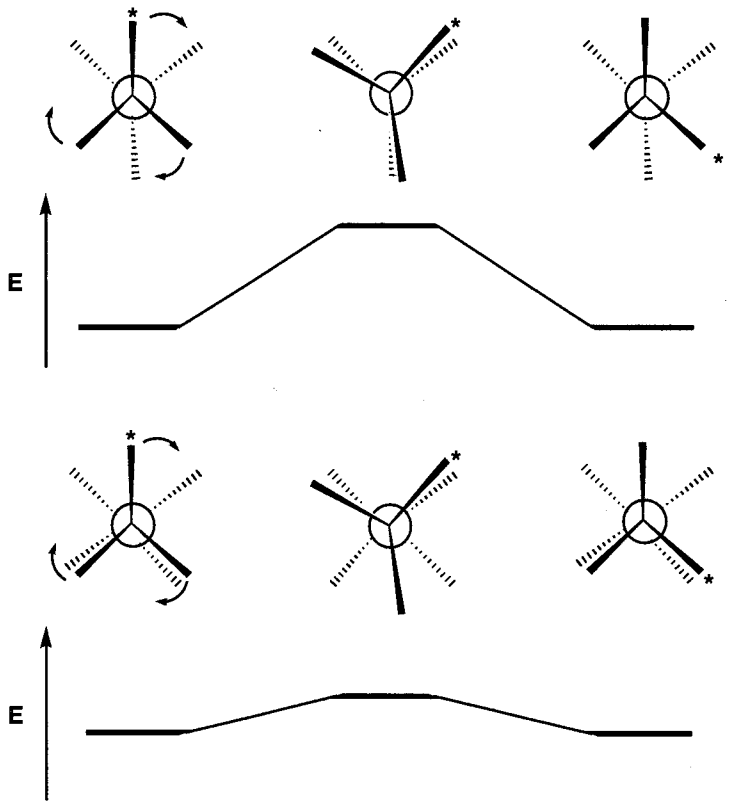

Chart 5.1. Rotation barriers in six and seven coordinate complexes.

is that in the ground state all the substituents are perfectly staggered with their nearest neighbours and hence it is at a low energy. In a seven coordinate complex the transition state to rotation of a trigonal unit only has two close eclipsing interactions and therefore might be expected to be at a lower energy than the transition state energy in the six coordinate case (Chart 5.1). What may not be realized is that in the seven coordinate configuration the ground state is destabilized relative to the six coordinate configuration because in the higher coordination case there are still close interactions in the lowest energy conformation.

It is also apparent in the spectrum at 21 °C that the signals attributed to the wingtip $Os(CO)_3$ group have broadened relative to the signals due to the $Os(CO)_4$ unit. This probably indicates the onset of rotation on the NMR time scale of the $Os(CO)_3$ group and is relevant to the discussion on the rotation of $Os(CO)_3$ units in **15** below. The NMR spectrum of **14** at higher temperatures was not investigated due to its ready decarbonylation as described below.

$Os_4(\mu_4\text{-}\eta^2\text{-}C_2Ph_2)(CO)_{12}$ (15) When the reaction shown in eq 5.2 was carried out at 40 °C, $Os_4(\mu_4\text{-}\eta^2\text{-}C_2Ph_2)(CO)_{12}$ (**15**) was isolated in 90% yield (eq 5.3). The reaction

$$Os_4(\mu_3\text{-}\eta^2\text{-}C_2Ph_2)(CO)_{14} \xrightarrow{40\ ^\circ C} \underset{\mathbf{15}}{Os_4(\mu_4\text{-}\eta^2\text{-}C_2Ph_2)(CO)_{12}} \qquad (5.3)$$

of $Os_4(CO)_{14}$ with C_2Ph_2 was investigated under three different conditions. The results are shown in (Table 5.3). Compound **15** was isolated as bright orange-red crystals that were air stable; they were characterized by C/H/N analysis, IR (Figure 5.6, next page), mass (parent ion), ^1H and ^{13}C NMR spectroscopy, and X-ray crystallography. Compound **15** is thermally stable. Overnight pyrolysis of **15** in C_6F_6 at 230 °C had little effect on the

Table 5.3. Summary of the reaction conditions and percent yields for **13 – 17**.

Ratio[b]	Temp.(°C)	Time	**16**	**15**	**14**	**17**	**13**[a]
1:20	25	1.75 h	<1%	0%	25%	5%	70%
1:1.1	25	2 d	5%	17%	60%	10%	<1%
1:1.1	40	2 d	0%	90%	3%	6%	0%

[a] Corresponds to the elution sequence from column chromatography (**16** first **13** last).
[b] Ratio of $Os_4(CO)_{14}$:C_2Ph_2 used in reaction.

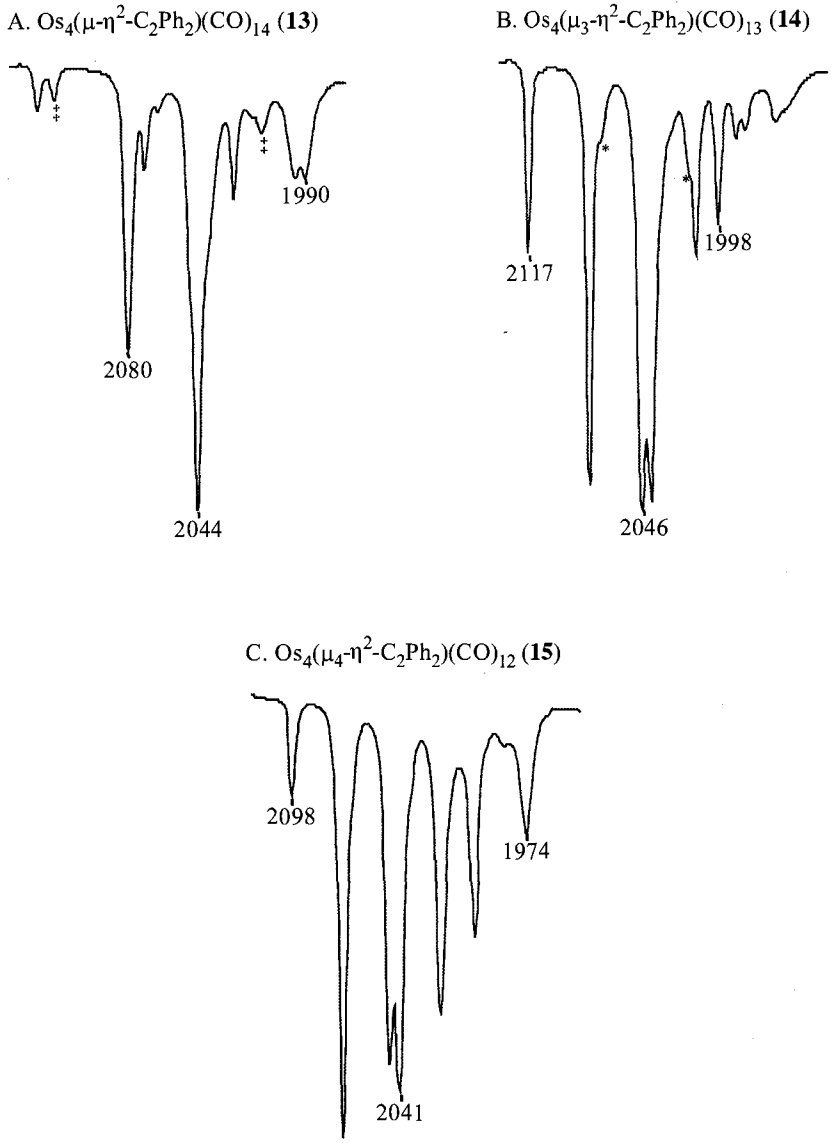

Figure 5.6. IR (hexane) spectra (ν(CO) region) of **13** - **15**. (‡ due to **14**, * due to **15**).

cluster with decomposition to $Os_3(CO)_{12}$ only commencing at 250 °C. Even after 4 days at 250 °C **15** had not completely decomposed.

Although the Ru analogue of **15** has been known since 1977 the Os compound has not been previously reported (as determined by SciFinder Scholar).[130] A view of the structure of **15**[h] is shown in Figure 5.7. The structure is typical of clusters of formula

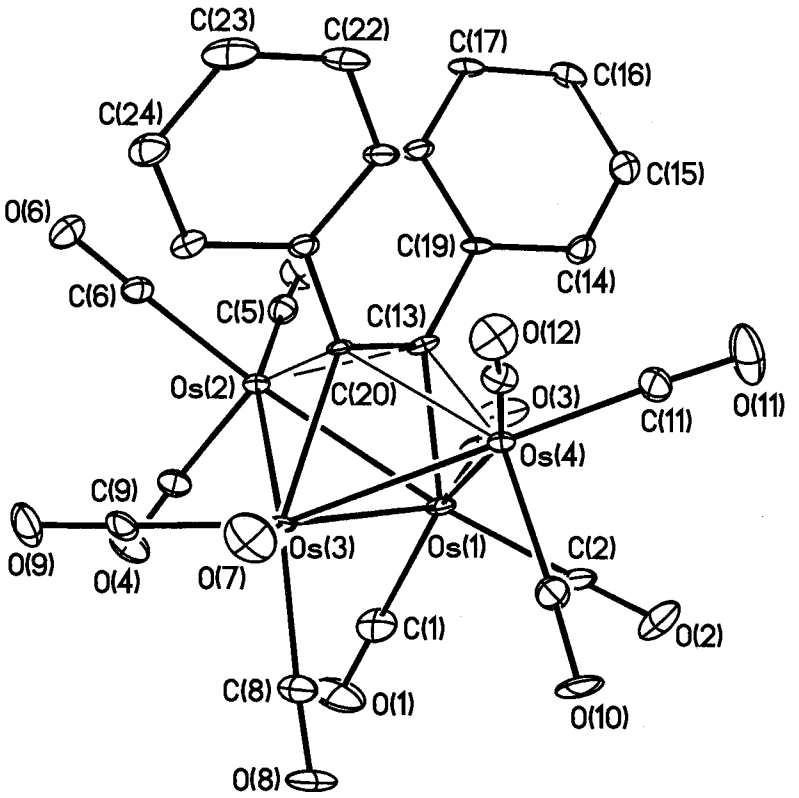

Figure 5.7. Molecular structure of $Os_4(\mu_4\text{-}\eta^2\text{-}C_2Ph_2)(CO)_{12}$ (**15**).

$M_4(\mu_4\text{-}\eta^2\text{-}C_2RR')(CO)_{12}$ (M = Fe, Ru, Os).[119a,130,131] These clusters may be viewed as electron-deficient butterfly clusters with 60 cluster valence electrons, or as *closo*-octahedral clusters with 66 electrons according to PSEPT (discussed in detail in the next

[h] Determined by Dr. G. P. A. Yap at the University of Ottawa.

section). In **15** the peripheral OsOs bonds range in length from 2.7457(5) to 2.7652(5) Å (Table 5.4), lengths that are typical of OsOs lengths in condensed Os clusters. The hinge Os(1)Os(3) bond is longer at 2.8742(5) Å. The OsC lengths of the alkyne unit to the wingtip Os atoms (Os(2) and Os(4)) are slightly longer (2.251(7)- 2.274(8) Å) than the OsC lengths to the hinge Os atoms (2.179(8), 2.201(8) Å). The pattern of the OsOs and OsC lengths closely match those previously found in $Ru_4(\mu_4\text{-}\eta^2\text{-}C_2Ph_2)(CO)_{12}$. The

Table 5.4. Selected bond lengths (Å) and angles (°) for $Os_4(\mu_4\text{-}\eta^2\text{-}C_2Ph_2)(CO)_{12}$ (**15**).

Bond Lengths

Os(1)-Os(2)	2.7515(5)	Os(1)-C(13)	2.179(8)
Os(1)-Os(3)	2.8742(5)	Os(2)-C(13)	2.274(8)
Os(1)-Os(4)	2.7592(5)	Os(2)-C(20)	2.265(7)
Os(2)-Os(3)	2.7652(5)	Os(3)-C(20)	2.201(7)
Os(3)-Os(4)	2.7457(5)	Os(4)-C(13)	2.255(8)
C(13)-C(20)	1.49(1)	Os(4)-C(20)	2.251(7)
Os-CO range	1.912(9)-1.95(1)	C(13)-C(20)	1.49(1)

Bond Angles

Os(2)-Os(1)-Os(3)	58.83(1)	Os(1)-C(13)-C(20)	108.5(5)
Os(2)-Os(1)-Os(4)	91.67(1)	Os(3)-C(20)-C(13)	108.3(5)
Os(3)-Os(1)-Os(4)	58.30(1)		
Os(1)-Os(2)-Os(3)	62.80(1)	Os(4)-Os(1)-C(13)	52.7(2)
Os(1)-Os(3)-Os(2)	58.38(1)	Os(2)-Os(1)-C(13)	53.4(2)
Os(1)-Os(3)-Os(4)	58.76(1)		
Os(2)-Os(3)-Os(4)	91.66(1)	Os(2)-Os(3)-C(20)	52.8(2)
Os(1)-Os(4)-Os(3)	62.95(1)	Os(4)-Os(3)-C(20)	52.7(2)

CC bond length (1.49(1) Å) of the alkyne ligand in **15** is the longest of the three alkyne CC lengths determined in this study. The length is close to that of a CC single bond length and consistent with the donation of 4 electrons from the diphenylacetylene ligand to the Os cluster.[113,131,132]

Carbon-13 NMR spectra in the carbonyl region of **15** (^{13}CO enriched) at different temperatures are shown in Figure 5.8. If the carbonyl groups were rigid each chemically

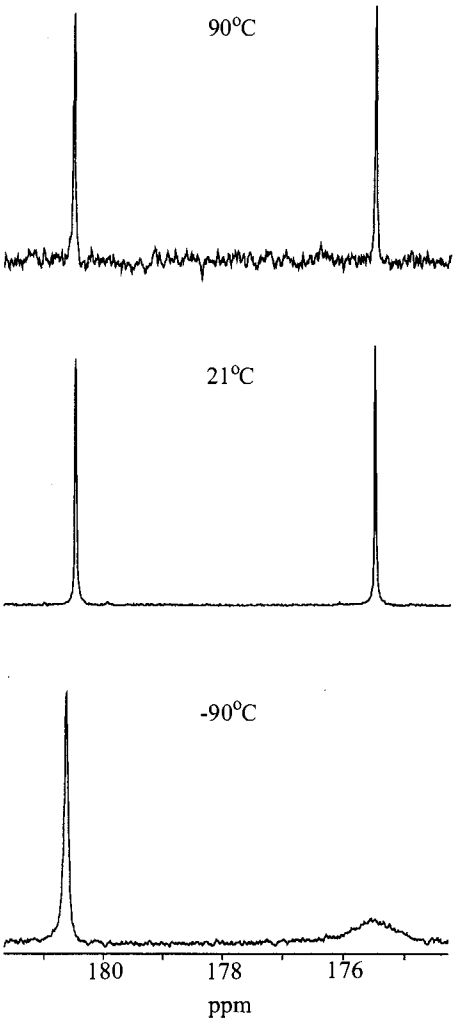

Figure 5.8. VT ^{13}C NMR spectra of CO-enriched $Os_4(\mu_4\text{-}\eta^2\text{-}C_2Ph_2)(CO)_{12}$ (**15**).

distinct $Os(CO)_3$ (i.e., wingtip and hinge moieties) would have a 2:1 pattern for a total of four signals. It is apparent that at 21 and 90 °C there is rapid rotation of the two different types of $Os(CO)_3$ groupings in **15**, but that migration of CO ligands between the wingtip and hinge Os atoms does not occur on the NMR time scale. In the spectrum at -90 °C one of the signals has collapsed almost to the baseline indicative of slowed exchange of one of the pairs of $Os(CO)_3$ units. This was also observed in the variable temperature ^{13}C NMR spectrum of $Ru_4(\mu_4\text{-}\eta^2\text{-}C_2Ph_2)(CO)_{12}$. Given the fluxional behaviour of the

$Os(CO)_3$ units in **14** it is probable that the $Os(CO)_3$ groupings that are undergoing slowed exchange in **15** are the wingtip groupings because these Os atoms are 6 coordinate.

Comparison of the structures of 13, 14 and 15 The unusual susceptibility of $Os_4(CO)_{12}$ to add a 2e ligand under mild conditions has allowed the $Os_4(\mu_x\text{-}\eta^2\text{-}C_2Ph_2)(CO)_n$ (n = 14, x = 2; n = 13, x = 3; n = 12, x = 4) series of clusters. This is the first series where three clusters have been structurally characterized that contain an alkyne ligand and stepwise loss of two carbonyl ligands (Chart 5.2). (For reasons, that

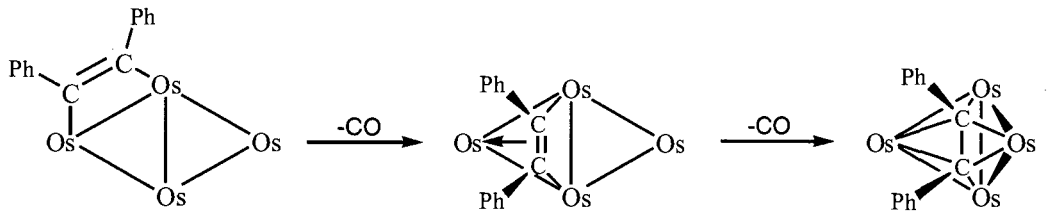

13 **14** **15**

Chart 5.2. Relationship between **13**, **14** and **15**.

will become apparent later, **15** is drawn with one Os_3 triangle of the butterfly in the plane with the remaining Os atom above this plane.) Molecules **13** and **14** are 62 electron systems and have the predicted six metal-metal bonds (and two Os_3 triangles). Both have flattened butterfly (kite) arrangement of metal atoms.

The conversion of **14** to **15** again involves a loss of CO, but according to the 18 electron rule there is not an accompanying increase in the number of electrons donated by the alkyne ligand. This reduces **15** to a 60 electron system and should result in a tetrahedral arrangement of metal atoms, as in $Os_4(CO)_{14}$.[111i] As discussed above, $M_4(\mu_4\text{-}\eta^2\text{-}C_2R_2)(CO)_{12}$ clusters have been known for some time.[133] The bonding in these clusters is best treated by PSEPT where the CPh units are considered part of a closo polyhedron and contribute five electrons to the cluster (the 4 valence electrons from the C

atom and 1 electron from the Ph group). The electron count becomes: No. of e^- = 32 (4Os) + 24 (12CO) + 10 (2CPh) = 66e^-. Each C and Os vertex atom contribute three orbitals to cluster bonding leaving one orbital for C and six orbitals for each Os atom to be filled. The number of e^- to fill external orbitals of vertex atoms is therefore 4 (2C) + 48 (4Os) or 52 e^- that leaves 14 e^- or 7 electron pairs for skeletal cluster bonding. This represents n + 1 cluster bond pairs (n is number of vertex atoms) and PSEPT therefore predicts that **15** will be a closo structure, in this case a regular octahedron (i.e., n = 6). The "sleight of hand" involves the consideration of C_2Ph_2 as two separate CPh units that each contributes 3 cluster electrons (for a total of 6) in the PSEPT treatment. On the other hand, for the 18 electron rule the C_2Ph_2 ligand can contribute a maximum of 4 electrons to the bonding in the cluster. Note the C vertex atoms have square-based pyramidal coordination, that is, they are five coordinate. This geometry is indicative of the unconventional bonding in these closo clusters.

The change in the electron donation of the alkyne ligand in the system is evident from a comparison of the CC bond lengths in the molecules (Table 5.5). In **13** the alkyne ligand acts as a two-electron donor. The CC bond length of 1.32(4) Å is consistent with a

Table 5.5. The CC and OsC bond lengths of the alkyne-Os unit in **13-15**.

Compound	C-C length (Å)	Os-C lengths (Å) (σ)	Os-C lengths (Å) (π)
13	1.32(4)	2.13(3), 2.28(3)	-
14 A	1.42(2)	2.15(1), 2.18(1)	2.27(1), 2.29(1)
14 B	1.42(2)	2.17(1), 2.16(1)	2.29(1), 2.29(1)
15	1.49(1)	2.179(8), 2.201(7)	2.265(7), 2.274(8) 2.251(7), 2.255(8)

CC double bond that makes no contribution to the cluster bonding in **13**. In **14** the alkyne ligand is a four-electron donor and the CC bond length is much longer at 1.42(2) Å. An intermediate in length between a CC double and CC single bond (1.34 and 1.54 Å,

respectively). In **15** the CC bond is still longer at 1.49(1) Å and just slightly shorter than expected for a CC single bond.

Model for surface catalysts Compound **14** (e.g., Chart 5.2) may be taken as a model for C_2Ph_2 bound to a planar metal surface, whereas compound **15**, with its butterfly arrangement of metal atoms, may be taken as a model for an alkyne bound to a step site of a metal surface. Step sites have been proposed as the active sites of metal catalysts.[134] Given that **15** is thermally stable to 230 °C and that the X-ray data (Table 5.5) indicates C_2Ph_2 is tightly bound to the Os_4, it is hard to imagine how this alkyne could be chemically reactive to say hydrogen at moderate temperatures. The same can be said to a lesser extent for the alkyne bound in **14**.

On the other hand, the alkyne is only lightly bound to the Os_4 unit in **13** (Table 5.5). Furthermore, given the ring strain in the dimetallacyclobutene grouping it would be expected to be highly reactive. It is therefore proposed that this unit is a model for the active sites in site-specific surface catalysts. Surface catalysts may be divided into two classes, those that are insensitive to the nature of the metal surface and those that are.[116d] Consider the formation of **13** from $Os_4(CO)_{15}$ that has a planar structure and hence is a model for a metal surface. This is shown in Chart 5.3. Recall that both $Os_4(CO)_{15}$ and $Os_4(CO)_{14}$ have unusual bonding that is not found in higher nuclearity Os clusters.

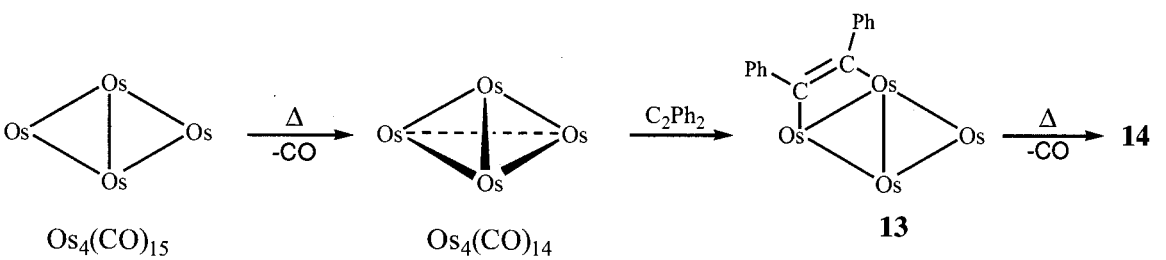

Chart 5.3 Formation of **13** from $Os_4(CO)_{15}$.

We could therefore imagine sites at the corners and some edges of metal surfaces that resemble $Os_4(CO)_{15}$ and $Os_4(CO)_{14}$ that could act as the active sites. This is shown in Chart 5.4; we shall refer to these sites as "PT" sites (planar-tetrahedral sites). Only corners and certain edge sites (e.g., Chart 5.5) would have the metal atom environment required to enable the unique metal atom (shaded atom in Charts 5.4 and 5.5) to hop from

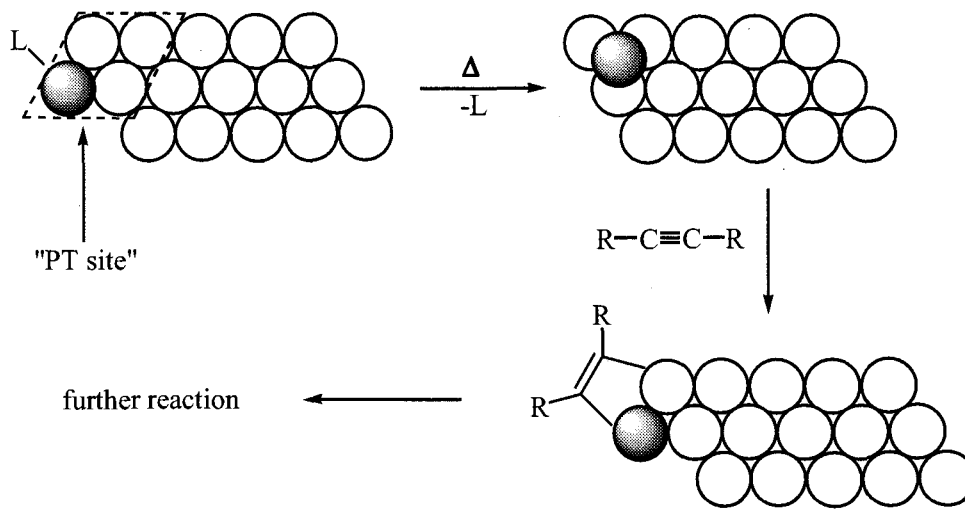

Chart 5.4 Proposed model for site-specific surface catalysts. The corner PT site.

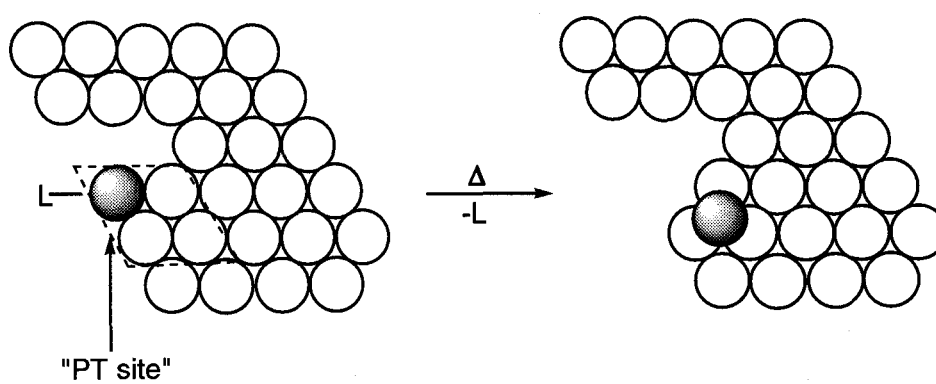

Chart 5.5. Example of an edge PT site.

a site within the plane of metal atoms to the tetrahedral site above the plane and back again. It is assumed that metal atoms below the plane do not coordinate to the unique

atom. In other words, the unique metal atom must not be bound to any other metal atoms except the other three metal atoms comprising the PT site.

It is easy to see why a more finely divided catalyst would be a more active catalyst. This is because there would be more PT sites the greater the surface area of the metal. The same is true for freshly prepared catalysts. This model, however, has several other attractive features that hitherto have been difficult to explain with other models. For some site-specific catalysts there is a lag time before catalysis begins. The other inactive sites on the surface are occupied immediately upon exposure to the organic reactant. This filling of sites is accompanied by surface reorganization that can be slow.[116d] It may be that the PT site only becomes active after the surface reorganization near the surface site has taken place. A ligand must also dissociate from the unique atom of the PT site to allow formation of the active tetrahedral form of the site. The model also explains why only certain metals are active and why bimetallic catalysts can be more active than catalysts composed of the individual metals. As can be seen in Charts 5.4 and 5.5, the active PT site involves two metals that are coordinated to only two (shaded atom) or three other metal atoms, respectively, in the lattice. It would be expected that these atoms would have frontier orbitals somewhat like those in mononuclear complexes. The most effective metals for surface catalysts are often the most effective in homogeneous mononuclear catalysts. This is especially true for rhodium and palladium. These metals are also less likely to undergo oxidation with molecular oxygen. In the model the substrate is bound to just two metal atoms and therefore it will have different susceptibilities to attack depending on if the metals are identical or different. Catalysts are often more effective with oxide promoters. If the layer of atoms below the metal

layer depicted in Charts 5.4 and 5.5 were oxide ions then the formation of the tetrahedral form and its reactivity would be subject to the trans effect of these oxide ions.

Work is planned in Dr Pomeroy's laboratory to investigate the reactivity of **13**, **14** and **15** (and similar clusters) with hydrogen to provide experimental support for the new model.

$Os_3(\mu_3\text{-}\eta^2\text{-}C_2Ph_2)(CO)_{10}$ (16) and $Os_3(\mu\text{-}\eta^2\text{-}C_4Ph_4)(CO)_9$ (17) The synthesis of ^{13}CO-enriched **13** (eq 5.1) also afforded sufficient quantities of $Os_3(\mu_3\text{-}\eta^2\text{-}C_2Ph_2)(CO)_{10}$ (**16**)[7b,120,] and $Os_3(\mu\text{-}\eta^4\text{-}C_4Ph_4)(CO)_9$ (**17**)[7b,122] as ^{13}CO-enriched samples so as to allow for the determination of their $^{13}C\{^1H\}$ NMR spectra in the CO region for the first time.

Variable temperature $^{13}C\{^1H\}$ NMR spectra of **16** are shown in Figure 5.9. The ^{13}C NMR spectrum of **16** in CD_2Cl_2 at -80 °C has six resonances in an approximate 1:1:2:2:2:2 ratio. The ratios are only approximate probably because the C atoms in the Os_3 plane experience nuclear Overhauser enhancement (NOE) due to the decoupled protons of the phenyl protons. Based on the solid state structure (Figure 5.10A, R = Ph), ten resonances would be expected at low temperatures. Some clusters of the type $Os_3(alkyne)(CO)_{10}$, have a bridging CO (Figure 5.10B) and at low temperatures exhibit a NMR pattern similar to that observed for **16**.[135] The ^{13}C NMR pattern of **16** is therefore more consistent with either the bridging configuration (**B**), or one in which the semibridging CO rapidly oscillates between the two Os atoms that are bound to the alkyne via σ bonds, via the symmetrically bridging form. Either way, **16** would have a mirror plane by ^{13}C NMR spectroscopy and hence the more simple pattern of resonances. We prefer the second interpretation. The ^{13}C NMR resonance of this carbonyl is assigned to the signal to lowest field at δ 181.3. From a comparison of the shift to those in $Os_3(\mu_3$-

η^2-C_2R_2)$(CO)_9$(L) (R= Me, Et; L = CO, PR_3) the carbonyl is semibridging. The shifts of symmetrically bridging carbonyls are at much lower field. The IR spectrum of **16** is also consistent with this view as the lowest energy CO stretch is at 1965 cm^{-1}, slightly higher than the normal range of the stretches of bridging carbonyls.

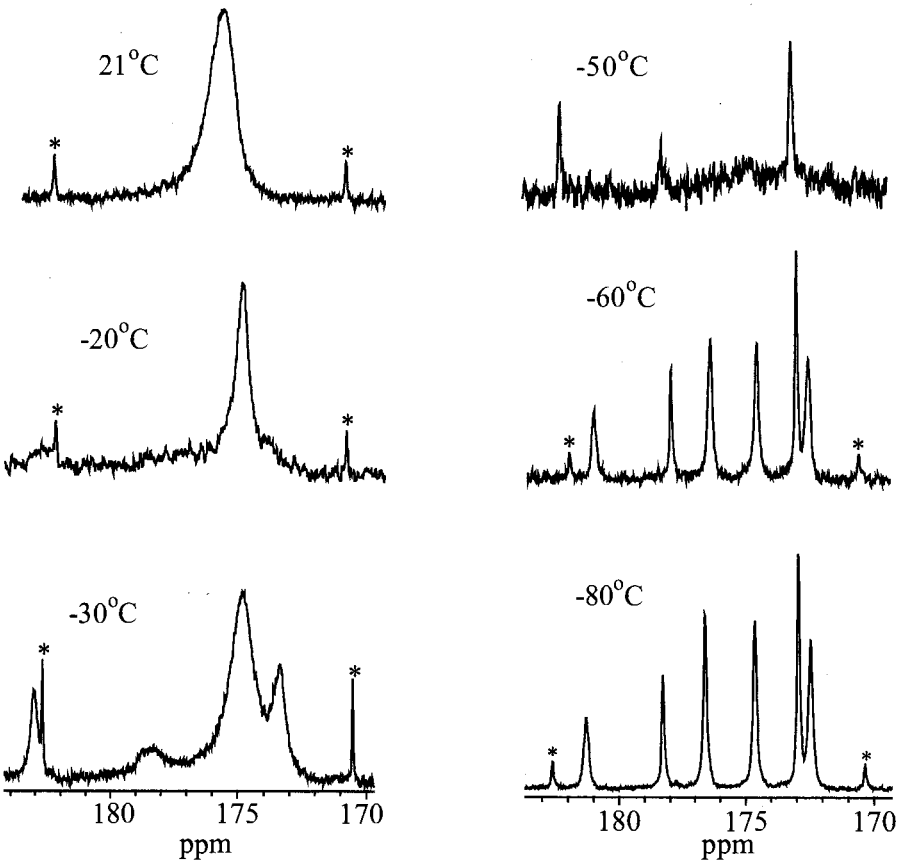

Figure 5.9. The ^{13}C NMR spectra of $Os_3(\mu_3$-η^2-$C_2Ph_2)(CO)_{10}$ (**16**) in CD_2Cl_2/CH_2Cl_2 (* = $Os_3(CO)_{12}$).

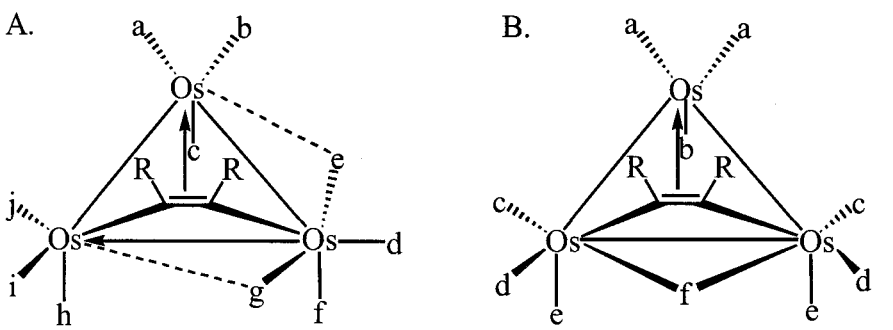

Figure 5.10. (A) Structure of **16**. (B) General structure of Os_3(alkyne)$(CO)_{10}$ clusters.

At -50 °C three of the signals of intensity 2 have collapsed into the baseline to leave signals of intensity 1:1:2, one of which is the peak due to the bridging CO. (The spectrum at -50 °C was on a different sample to that used in the other spectra. It does not contain the impurity of $Os_3(CO)_{12}$ and is of poorer quality than the other spectra.) This type of coalescence has been interpreted for $Os_3(\mu_3\text{-}\eta^2\text{-}C_2R_2)(CO)_{10}$ in terms of the mutual CO exchange caused by rotation of $Os(CO)_3$ units involved in the alkyne bridge (Chart 5.6A: see Scheme 1 ref 135). This is also consistent with the NMR studies of the alkyne derivatives described here in that these Os atoms have seven σ bonds and would therefore be expected to have low barriers to $Os(CO)_3$ rotation. Given this exchange, the other signal of intensity 1 at δ 178.3 in the spectrum at -50 °C is assigned to the carbonyl labeled *b* in Chart 5.10. It is in the typical (lower field) region for an axial carbonyl on Os. It is of less intensity than the bridging carbonyl signal because it is not near the protons of the phenyl groups and hence experiences no NOE. Likewise, the signal of intensity 2 at δ 173.0 is attributed to the carbonyls labeled *a* in Figure 5.10. This signal is in the higher field region where the resonances of equatorial carbonyls appear. The signal is more intense than expected because these carbonyls are close to the phenyl substituents and are subject to NOE.

Above -30 °C all the signals broaden and coalesce to give a broad singlet at 21 °C. As we have seen, CO merry-go-round exchanges in systems with a single bridging carbonyl have low barriers. In this case of **16**, however, the exchange must be accompanied by rotation of the alkyne unit about the Os_3 triangle so that all the Os atoms become equivalent (Chart 5.6B). Essentially the same conclusions have been reached by Rosenberg *et al* in their NMR investigation of the $Os_3(\mu_3\text{-}\eta^2\text{-}C_2R_2)(CO)_9(L)$ clusters.

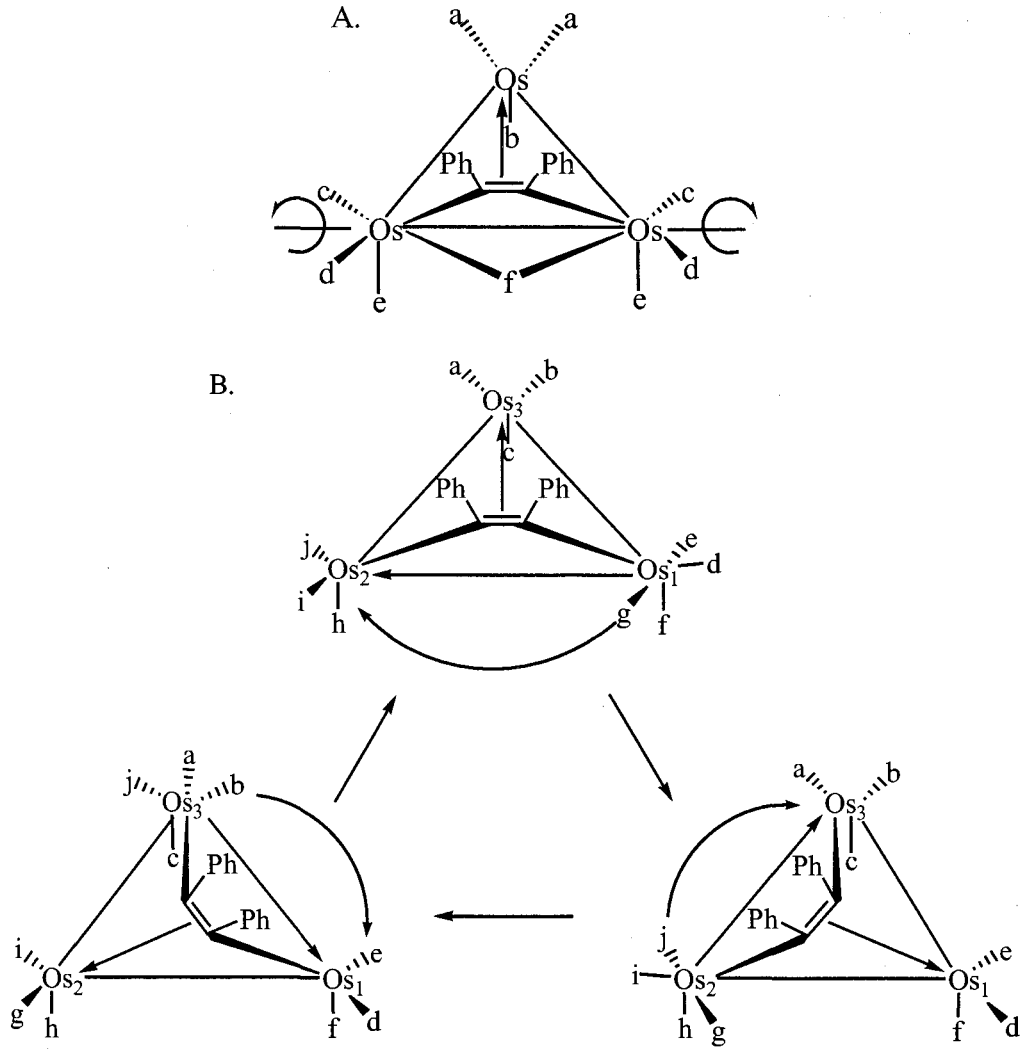

Chart 5.6. (A) Mutual CO exchange on the $Os(CO)_3$ units involved in the alkyne bridge of **16**. (B) Rotation of the alkyne ligand on the Os triangle.

The ^{13}C NMR spectrum of **17** in CD_2Cl_2 at room temperature has six resonances in a 2:2:1:2:1:1 ratio (Figure 5.11). This is consistent with the view that **17** has the same structure in solution as found in the solid state by X-ray crystallography (Figure 5.12). One of the resonances at δ 187.4 and δ 186.8 with intensity 2 is assigned to carbonyls *a*. The resonance due to axial carbonyls appears to lower field than those due to equatorial carbonyls. (Figure 5.11). Based on this argument, the other high field resonance should

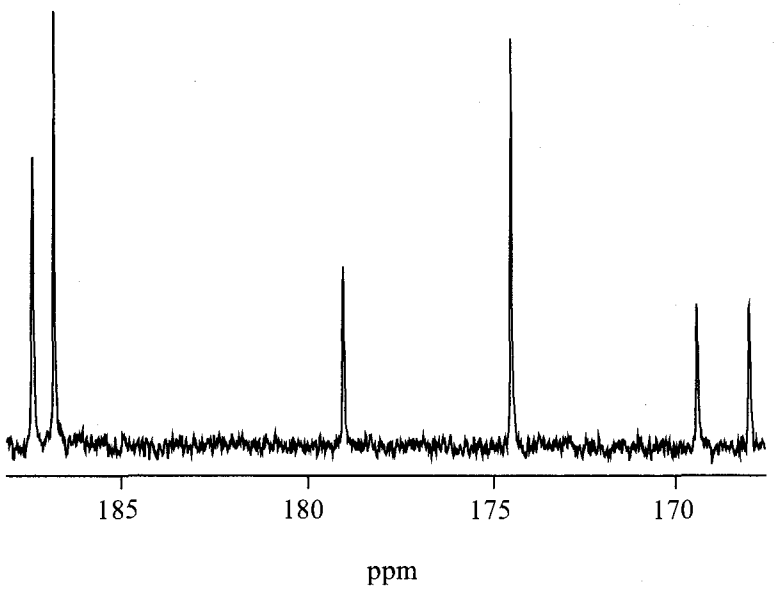

Figure 5.11 The ^{13}C NMR spectrum of $Os_3(\mu\text{-}\eta^4\text{-}C_4Ph_4)(CO)_9$ (**17**).

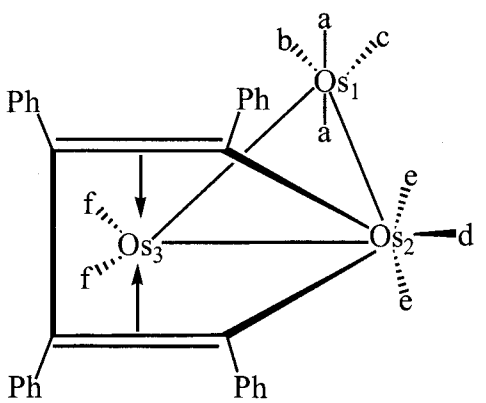

Figure 5.12. Solid-state structure of $Os_3(\mu\text{-}\eta^4\text{-}C_4Ph_4)(CO)_9$ (**17**).

be assigned to carbonyls *e* because they have more axial character than carbonyls *f*, which is assigned to the resonance at δ 174.5. The assignment of these resonances is difficult since ring current effects of the phenyl rings probably influence carbonyl *f*. This could cause a shift in the signal due to these CO ligands. The assignment of the resonances due to carbonyls *e* and *f* could therefore be reversed. Since the carbonyls labelled *b* and *c* are in similar environments compared to carbonyl *d*, the two signals at δ 169.4 and δ 168.0 are assigned to *b* and *c*. This is in the typical region for equatorial

carbonyls of $Os(CO)_4$ units in metal clusters. The remaining resonance with intensity 1 at δ 179.0 is therefore assigned to *d*.

5.3 Experimental section

The general procedure used for the synthesis and analysis has been described in the Experimental Section of Chapter 2. The precursory compound $Os_4(CO)_{14}$ was prepared as reported in Experimental Section of Chapter 2. Carbon-13 NMR spectra were obtained on ^{13}C enriched samples (Chapter 2); unless otherwise stated the solvent employed was CH_2Cl_2/CD_2Cl_2 (4/1) or, infrequently, pure CD_2Cl_2; the operating frequency was 100.6 MHz.

Preparation of $Os_4(\mu\text{-}\eta^2\text{-}C_2Ph_2)(CO)_{14}$ (13) To a solution of $Os_4(CO)_{14}$ (25 mg, 0.021 mmol) in CH_2Cl_2 (25 mL) at room temperature was added an excess of diphenylacetylene, C_2Ph_2 (~60 mg, 0.33 mmol). The solution was stirred for 105 min during which time the solution changed from a brown/red to a deep red. The solvent was removed on the vacuum line and the remaining solid subjected to chromatography on a silica gel column (1.5 x 16 cm). Elution with hexane removed the excess C_2Ph_2. Elution with hexane/CH_2Cl_2 (90/10 by volume) gave the following bands. The first yellow band was a trace amount of the known cluster $Os_3(\mu_3\text{-}\eta^2\text{-}C_2Ph_2)(CO)_{10}$ (**16**). (In some preparations, an orange band of $Os_4(\mu_3\text{-}\eta^2\text{-}C_2Ph_2)(CO)_{13}$ (**15**) was eluted next.) This was followed by a red band that afforded $Os_4(\mu_3\text{-}\eta^2\text{-}C_2Ph_2)(CO)_{13}$ (**14**; ~ 7.1 mg; ~25%), then a purple band of another known cluster, $Os_3(\mu\text{-}\eta^4\text{-}C_4Ph_4)(CO)_9$ (**17**) in <5% yield. (See Table 5.3 for a summary of the percent yields for different reaction conditions.) Finally a deep red band of the desired cluster **13** was obtained in a ~70% yield (~ 28.9 mg). The analytical sample of **13** was obtained (as air-stable, dark red (almost black) needles) by

recrystallization from CH_2Cl_2 and dried overnight under vacuum: IR (hexane) ν(CO) 2126 (w), 2080 (s), 2071 (m), 2065 (vw), 2044 (vs), 2025 (m), 1995 (m), 1989 (m) cm^{-1}; ^1H NMR (CD_2Cl_2) δ 7.15 - 7.10 (m), 7.01 - 6.92 (m), 6.85 - 6.83 (dd); ^{13}C NMR (RT) δ 192.13 (2C), 192.08 (2C), 185.6 (2C), 184.6 (1C), 176.6 (1C), 175.4 (2C), 172.5 (1C), 169.4 (1C), 169.3 (1C), 168.8 (1C), 128.1 (1C, Ph-*C*), 128.0 (2C, Ph-*C*), 126.6 (2C, Ph-*C*); MS (LSIMS) *m/z* 1331.9 (M^+) (Calcd for M^+ = 1332 (100%), 1331 (81.5%)). Anal. Calcd for $C_{28}H_{10}O_{14}Os_4$: C, 25.26; H, 0.76. Found: C, 25.22; H, 0.82.

A sample of **16** as prepared above was purified by further chromatography on a silica gel column: IR (hexane) ν(CO) 2100 (m), 2066 (vs), 2047 (s), 2028 (s), 2011 (s), 1996 (m), 1982 (sh), 1965 (w) cm^{-1} (in close agreement with the literature values[120a]); ^{13}C NMR (RT) δ 175.7 (10C), 129.3 (2C, Ph-*C*), 128.1 (2C, Ph-*C*), 127.4 (1C, Ph-*C*); ^{13}C NMR (-20 °C) δ 183.3 (w/broad, 1C), 174.9 (9C); ^{13}C NMR (-30 °C) δ 183.0 (1C), 178.3 (1C), 174.8 (6C), 173.3 (2C); ^{13}C NMR (-50 °C) δ 182.4 (1C), 178.4 (1C), 174.6 (w/broad), 173.2 (6C); ^{13}C NMR (-60 °C) δ 181.6 (1C), 178.3 (1C), 176.6 (2C), 174.7 (2C), 173.0 (2C), 172.5 (2C); ^{13}C NMR (-80°C) δ 181.3 (1C), 178.3 (1C), 176.6 (2C), 174.7 (2C), 173.0 (2C), 172.5 (2C); MS (LSIMS) *m/z* 1029.9 (M^+) (Calcd for M^+ = 1030 (100%), 1029 (83.3%)).

Similar to the above, a pure sample of **17** was obtained by further chromatography on a silica gel column: IR (hexane) ν(CO) 2113 (s), 2057 (vs), 2043 (vs), 2036 (sh), 2011 (vs), 1999 (m), 1990 (sh), 1974 (m), 1930 (m) cm^{-1} (in agreement with the literature values);[122d] ^{13}C NMR (RT) δ 187.4 (2C), 186.8 (2C), 179.0 (1C), 174.5 (2C), 169.4 (1C), 168.0 (1C), (the following are weak signals due to the phenyl carbons) 131.5, 129.5,

128.9, 127.6, 127.4, 126.9, 126.9, 126.7; MS (LSIMS) *m/z* 1179.9 (M^+) (Calcd for M^+ = 1180 (100%), 1179 (86.1%)).

Preliminary results indicated that the reaction of acetylene with $Os_4(CO)_{14}$ produced a compound similar to **13**. To a Carius tube was added $Os_4(CO)_{14}$ (20 mg, 0.017 mmol) and toluene (10 mL). The solution was degassed by three freeze-pump-thaw cycles. Acetylene was bubbled through the solution for ~60 s to saturate the solution. [***Caution:*** Care must be taken when handling acetylene since it can become spontaneously explosive at pressures greater than about 1 atm.] The mixture was placed overnight in a freezer, which gave a purple precipitate: IR (CH_2Cl_2) ν(CO) 2129 (w), 2081 (s), 2072 (m), 2045 (vs), 2025 (m), 1992 (m), 1981 (m) cm^{-1}; MS (LSIMS) *m/z* 1180.0 (M^+) (Calcd for M^+ = 1180 (100%), 1179 (86.0%)).

Preparation of $Os_4(\mu_3\text{-}\eta^2\text{-}C_2Ph_2)(CO)_{13}$ (14) Cluster **14** was prepared in the same manner used to prepare **13** except only a slight excess of C_2Ph_2 was used (~1:1.1) and the solution was allowed to stir at room temperature for 2 d. Again the initial brown/red solution changed to a red solution. The resulting products were isolated as describe above and the percent yields are summarized in Table 5.3.

The analytical sample of **14** was obtained as air-stable, deep-red crystals by recrystallization from CH_2Cl_2/hexane: IR (hexane) ν(CO) 2117 (m), 2078 (vs), 2046 (vs), 2040 (vs), 2012 (m), 1998 (m), 1987 (w), 1981 (w), 1963 (w), 1956 (w, sh) cm^{-1}; ^1H NMR (CD_2Cl_2) δ 7.15 - 7.07 (m), 6.98 - 6.96 (m); ^{13}C NMR (RT) δ 185.6 (1C, J_{CC} = 38.7 Hz), 182.6 (1C, J_{CC} = 37.2 Hz), 180.5 (1C), 176.5 (6C), 173.2 (1C), 169.3 (1C), 130 (2C, Ph-*C*), 127.8 (2C, Ph-*C*), 127.6 (1C, Ph-*C*); ^{13}C NMR (-50 °C) δ 185.6 (1C), 181.8 (1C), 180.2 (1C), 177.6 (2C), 175.8 (2C), 175.2 (2C), 172.8 (2C), 169.0 (2C); MS (LSIMS) *m/z*

1303.6 (M^+) (Calcd for M^+ = 1304 (100%), 1303 (87.4%)). Anal. Calcd. for $C_{27}H_{10}O_{13}Os_4$: C, 24.85; H, 0.77. Found: C, 25.01; H, 0.98.

Preparation of $Os_4(\mu_4\text{-}\eta^2\text{-}C_2Ph_2)(CO)_{12}$ (15) The same reaction conditions used to produce **14** were employed except the reaction mixture was heated at 40 °C for two d. This resulted in a colour change from brown/red through dark red to orange/red as the initial product, **13**, decarbonylated to **14** and then **15**. The analytical sample of **15** was obtained as air-stable, sparkling red/orange crystals by recrystallization from CH_2Cl_2 (~90%): IR (hexane) ν(CO) 2098 (m), 2071 (vs), 2046 (vs), 2041 (vs), 2019 (s), 2000 (s), 1982 (w), 1971 (m) cm^{-1}; ^1H NMR (CD_2Cl_2) δ 7.21 - 7.17 (m), 7.14 - 7.10 (m); ^{13}C NMR (toluene-d_8, 90°C) δ 180.4 (s, 6C), 175.5 (s, 6C); ^{13}C NMR (RT) δ 180.5 (6C, J_{OsC} (^{187}Os) = 106.9 Hz), 175.5 (6C, J_{OsC} = 117.5 Hz), 132.5 (2C, Ph-*C*), 129.3 (1C, Ph-*C*), 127.2 (2C, Ph-*C*); ^{13}C NMR (-90 °C) δ 180.5 (s, 6C), 175.5 (w/broad); MS (LSIMS) *m/z* 1275.6 (M^+) (Calcd for M^+ = 1276 (100%), 1275 (87.4%)). Anal. Calcd. for $C_{26}H_{10}O_{12}Os_4$: C, 24.45; H, 0.78. Found: C, 24.65; H, 0.88.

(In an alternate procedure 25 mg of **13** or **14** was allowed to stir in hexanes at room temperature for 18 d to give **15** in a ~90% yield.)

Chapter 6. Pyrolysis of binary carbonyl clusters of ruthenium and osmium

6.1 Introduction

High nuclearity transition metal clusters are almost invariably produced from the pyrolysis of lower nuclearity species.[7] In 1975, Eady, Johnson and Lewis reported the first examples of high nuclearity clusters of ruthenium and osmium[8,9] These clusters were produced by the pyrolysis of solid $M_3(CO)_{12}$ (M = Os, Ru) in a sealed Carius tube. In the case of $Ru_3(CO)_{12}$ only $Ru_6(\mu_6\text{-}C)(CO)_{17}$ was produced (eq 6.1). The pyrolysis of $Os_3(CO)_{12}$ however yielded $Os_5(CO)_{16}$, $Os_5(\mu_5\text{-}C)(CO)_{15}$, $Os_6(CO)_{18}$,[i] $Os_7(CO)_{21}$,

$$Ru_3(CO)_{12} \xrightarrow{150\ ^\circ C} \underset{5\%}{Ru_6(\mu_6\text{-}C)(CO)_{17}} \qquad (6.1)$$

$$Os_3(CO)_{12} \xrightarrow{210 - 250\ ^\circ C} \underset{7\text{-}0\%}{Os_5(CO)_{16}} + \underset{0\text{-}5\%}{Os_5(\mu_5\text{-}C)(CO)_{15}} + \underset{60\text{-}80\%\ ^{i}}{Os_6(CO)_{18}} + \underset{10\text{-}20\%}{Os_7(CO)_{21}} + \underset{2\text{-}5\%}{Os_8(CO)_{23}} + \underset{0\text{-}8\%}{Os_8(\mu_6\text{-}C)(CO)_{21}} \qquad (6.2)$$

$Os_8(CO)_{23}$ and $Os_8(\mu_6\text{-}C)(CO)_{21}$ (eq 6.2).[8,136] Today, pyrolysis is still the most common method for the synthesis of osmium carbonyl clusters.[7] For example, it is the only method known to prepare $Os_8(CO)_{23}$ and $[Os_{20}(CO)_{40}]^{2-}$.[8,9,137,] As illustrated by the pyrolysis of solid $Os_3(CO)_{12}$, the method often results in a mixture of products that because of their similar solubility makes them tedious to separate and purify.[104] Furthermore, the yields are often low (e.g., eq 6.2).

---

[i] A maximum yield of 60% was reported when others carried out the reaction for Inorganic Syntheses.

Performing the pyrolysis in solution has the major advantage of being able to monitor the reaction by IR spectroscopy. This allows the reaction conditions to be readily optimized therefore maximizing the production of the desired product.[111b] Solutions can also be purged with nitrogen so as to remove CO and facilitate the condensation of clusters by decarbonylation (e.g., the preparation of $Os_4(CO)_{14}$). Solution pyrolysis can also lead to different products than those obtained by carrying out the reaction in the solid state.[6b]

There is however a problem of finding a suitable solvent in which to carry out the pyrolysis of metal carbonyl clusters.[138] Instead of solely providing a medium for the reaction solvents often react with the metal carbonyl. It is known that common hydrocarbon solvents either act as ligands or are a source of H atoms that attach to the clusters. The pyrolysis of $Ru_3(CO)_{12}$ in any alcohol, ketone or aldehyde yields $Ru_4(\mu\text{-}H)_2(CO)_{13}$ and $Ru_4(\mu\text{-}H)_4(CO)_{12}$ while the same pyrolysis in an arene solution results in $Ru_6(\mu_6\text{-}C)(CO)_{14}(\eta^6\text{-arene})$ (arene = C_6H_5Me, *m*-$C_6H_4Me_2$ or $C_6H_3Me_3$).[139] The clusters $Os_3(CO)_{10}(C_8H_{12})$ and $Os_3(\mu\text{-}H)(CO)_{10}(C_8H_{11})$ are examples of products where the metal carbonyl has reacted with the solvent.[140] Reactions in a chlorinated solvent are also known to produce halogenated metal clusters.

In this study, pyrolysis was carried out in hexafluorobenzene (C_6F_6) to eliminate side reactions of the solvent. Because of the strength of the C-F bonds (488 kJ mol^{-1} vs. 413 kJ mol^{-1} for C-H, and 330 kJ mol^{-1} for C-Cl)[141], it was thought unlikely that the C-F would break and react with the starting material at the temperatures employed. The electron withdrawing properties of fluorine would also prevent C_6F_6 from acting as an η^6-ligand.

The initial aim of the project was to study the pyrolysis of $Os_4(CO)_{14}$ in the hope of obtaining an Os_8 cluster in good yield, by analogy to the pyrolysis of $Os_3(CO)_{12}$ (i.e., eq 6.2). Although this product was not realized, it was found that the C_6F_6 solvent was completely inert towards $Os_4(CO)_{14}$ under the reaction conditions. The pyrolyses of other Ru and Os carbonyls in C_6F_6 were therefore investigated. In this chapter the pyrolysis of $Ru_3(CO)_{12}$, $Ru_2Os(CO)_{12}$, $RuOs_2(CO)_{12}$, $Os_3(CO)_{12}$ and $Os_4(CO)_{14}$ in C_6F_6 are described. This method provides higher yields of known Ru_6 and Os_6 carbonyl clusters, in a more convenient preparation. Previously unreported ^{13}C NMR data for some of these clusters are described. Preliminary results are given that suggest the formation of the new pentanuclear binary carbonyls $Ru_5(CO)_{16}$, $RuOs_4(CO)_{16}$ and $Ru_2Os_3(CO)_{16}$. Also reported is the synthesis of a form of RuC, and the pyrolysis of $Os_6(CO)_{18}$ with C_{60} and $Os_4(\mu\text{-}H)_2(CO)_{12}$.

6.2 Results and Discussion

$Ru_6(\mu_6\text{-}C)(CO)_{17}$ (18) The pyrolysis of $Ru_3(CO)_{12}$ in C_6F_6 in a sealed, evacuated and flame-dried Carius tube at 150 °C for 18 hours afforded the known cluster $Ru_6(\mu_6\text{-}C)(CO)_{17}$ (**18**; eq 6.3). There was no evidence of reactions with the C_6F_6 solvent. The

$$Ru_3(CO)_{12} \xrightarrow{150\ ^\circ C} \underset{\mathbf{18}}{Ru_6(\mu_6\text{-}C)(CO)_{17}} \qquad (6.3)$$

compound was purified by column chromatography and recrystallized from CH_2Cl_2 to give red-brown, air-stable crystals in 84% yield. The product was identified by IR spectroscopy: the CO stretching frequencies were in excellent agreement with the values reported in the literature. Variable temperature ^{13}C NMR data for **18** are reported for the first time in a separate section of this chapter.

The yield of **18** by the method reported here represents a ~14% improvement over that obtained by Johnson *et al.* from the reaction of $Ru_3(CO)_{12}$ and ethylene (~30 atm) at 150 °C.[142] (The duration of the reaction was not reported.) Pyrolysis of $Ru_3(CO)_{12}$ in *n*-butyl ether, benzene, or toluene at 150 °C produced **18** in only ~5% yield.[103,138]

RuC (19) Pyrolysis of $Ru_3(CO)_{12}$ in C_6F_6 for 4 days at 200 °C gave a Ru mirror that covered the surface of the Carius tube along with a dark grey compound with a metallic lustre that appeared homogeneous. The C/H/N analysis of the grey product was consistent with RuC (**19**) (eq 6.4). (The grey compound produced after one day at 200 °C

$$Ru_3(CO)_{12} \xrightarrow{200\ °C} \underset{\mathbf{19}}{RuC} \qquad (6.4)$$

analyzed as $RuC_{1.5}$ by C/H/N analysis.) Compound **19** was isolated by removing the solvent and washing the remaining solid with CH_2Cl_2 and drying the sample on the vacuum line. The C/H/N analysis of **19** gave 10.14% C (calculated for RuC = 10.60%) and a trace amount of H (probably due to adsorbed water). It was initially assumed that the product was the result of the complete removal of carbonyl ligands from $Ru_6(\mu_6\text{-}C)(CO)_{17}$ to give Ru_6C, but such a compound would have a C analysis of 1.94%. There are two sources of carbon in this reaction. The interstitial C in the $Ru_6(\mu_6\text{-}C)$ unit can remain in the Ru lattice and further CO ligands can be converted to carbide atoms by the process shown in eq 6.5.

$$Ru(CO)_2 \longrightarrow RuC + CO_2 \qquad (6.5)$$

The most common composition for metal carbides is MC (1:1 ratio) but cases with a 2:1 ratio (M_2C) as well as with a nonstoichiometric composition MC_x (x = 0.5-0.97) are known.[143,144] Ruthenium carbide, RuC, is a known material.[145] (A review by

Storms briefly mentioned that it has not been determined whether RuC is stabilized by oxygen.[146])

The mass spectrum **19** was not useful as might have been expected. The IR of the compound as a KBr disk is shown in Figure 6.1. The spectrum contains two bands at 2066 and 1999 cm^{-1} which suggest that the compound still contains carbonyl ligands.

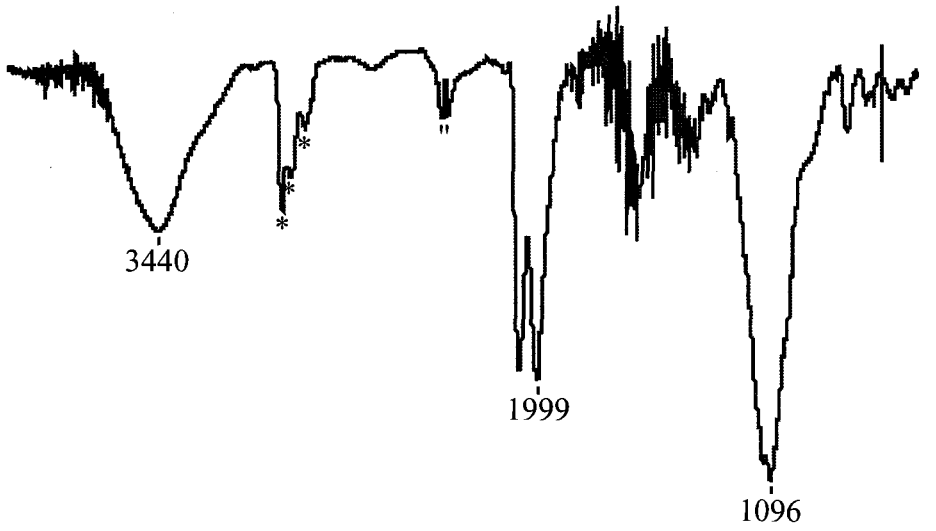

Figure 6.1. IR (KBr) spectrum of **19**. (* due to CH_2Cl_2, " due to CO_2)

(The stretches are not due to $Ru_3(CO)_{12}$.) Although the CO stretches of **19** overlap those found in the IR (KBr) spectrum of **18** (ν(CO) KBr: 2066 (vs), 2047 (vs) cm^{-1}) the mass spectrum of **19** suggests that it does not contain any **18**. The spectrum also contains stretches at 1126 (w) and 1096 (s) cm^{-1}, which occur in the same region as the stretches observed in the solid state IR spectrum of WC (1220 and 1067 cm^{-1} for the hexagonal phase; 1144 cm^{-1} for the cubic phase).[147] These stretches are not consistent with the IR (KBr) spectrum of SiO_2 (mentioned later).[148]

X-ray powder diffraction (XRD) and energy dispersive X-ray (EDX) analyses of **19** were performed, as well as the surface of **19** was probed by a scanning electron

microscopy (SEM). The quality of the X-ray powder diffraction of **19**, shown in Figure 6.2 suggested that the sample was mainly amorphous. A comparison of the data from the XRD of **19** with the values previously reported for RuC showed no correlation of the peaks. This was not unexpected since the original sample of RuC (which has a hexagonal phase like WC) was produced by mixing C and Ru at 2600 °C while **19** was produced at

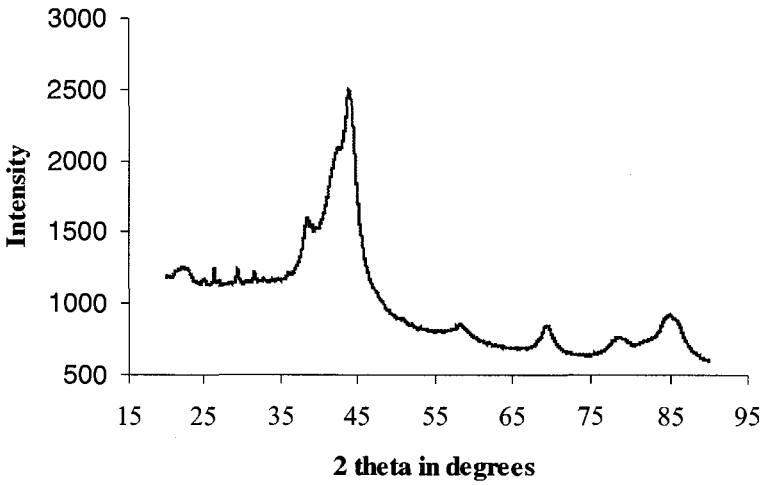

Figure 6.2. XRD spectrum of **19**.

200 °C. Phase changes commonly occur with variation of the temperature. A >2000 °C difference may have produced a different form of RuC. The XRD of **19** was found to be consistent with signals seen in the XRD of Ru metal, as shown in Table 6.1.[149]

Table 6.1. X-ray powder diffraction (XRD) pattern of **19** and Ru metal.

19		**Ru metal**	
2 theta	Intensity[a]	2 theta	Intensity
85.5	190	84.4	108
		83.6	148
78.7	90	78.1	136
69.5	130	68.2	142
58.3	90	57.9	127
44.0	1000	43.5	1000
42.7	500	42.2	244
38.5	270	37.8	258

Table cont'd

34.9	weak
31.6	weak
29.4	weak
26.9	weak
26.1	weak
25.8	weak

[a]Intensity values are only a rough approximate. Signals are broad.

The surface of the powdered sample of **19** was examined by SEM prior to its analysis by EDX (Figure 6.3). The examination of the surface revealed three distinct

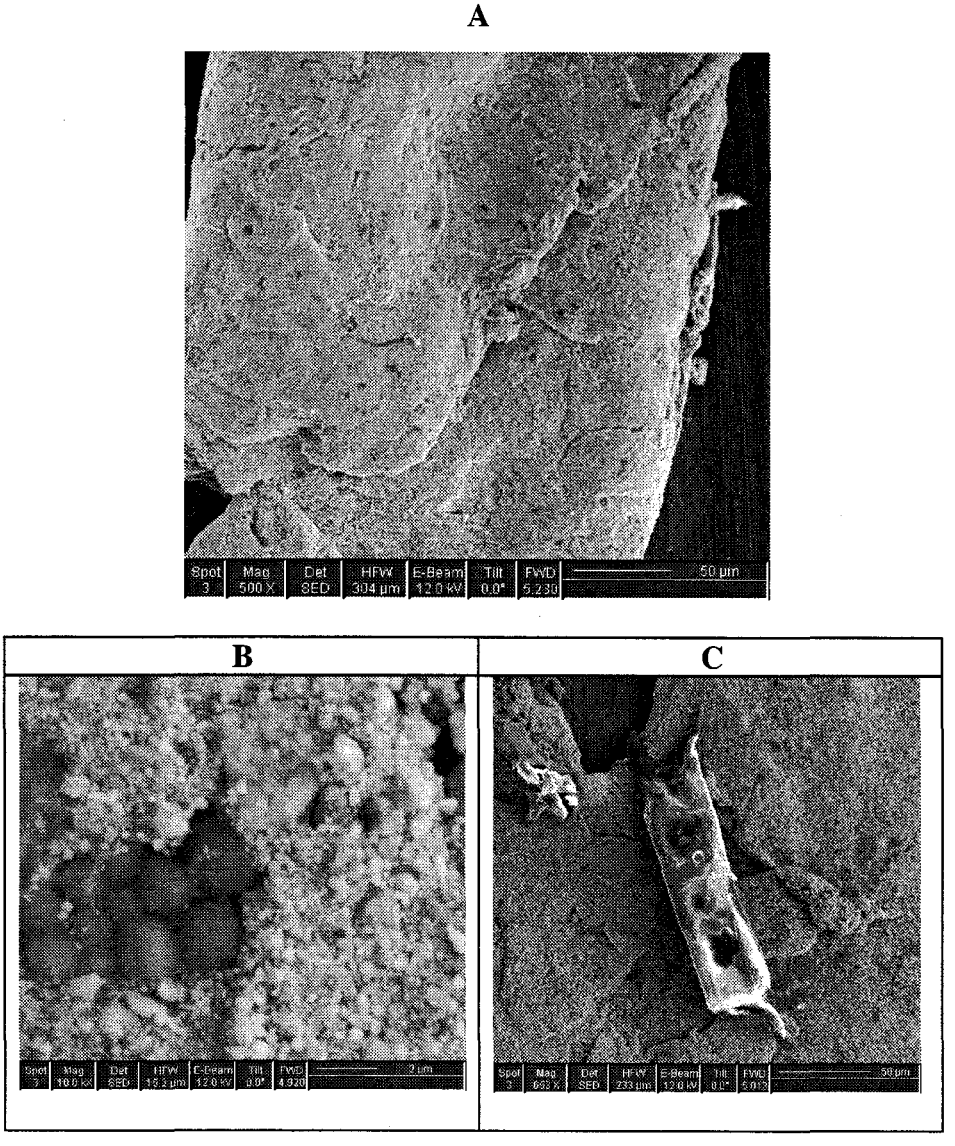

Figure 6.3. SEM of **19**. (A) Bulk material. (B) Granular composition of **19** and the spheres of SiO_2. (C) Carbon rich rectangular compound on surface of **19**.

areas. Over approximately 90% of the powder consisted of the granular surface shown in Figure 6.3 A, with few random pockets containing spheres and a limited amount of areas containing rectangular structures (Figure 6.3 B/C). The EDX analysis of the spheres contained within the pockets surprisingly revealed them to be SiO_2 (Table 6.2 A). Presumably, the reaction conditions resulted in some attack of the reaction vessel. The analysis of the rectangular regions also did not support the RuC formulation for **19**. These few regions were found to consist mainly of C with amounts of Ru, O, F and Si (Table 6.2 B).

Table 6.2. Summary of EDX data for minor materials of **19**. (A) spheres; (B) rectangular plates.

A			**B**		
Element	Weight %	Atomic %	Element	Weight %	Atomic %
C	2.46	4.30	C	37.72	66.29
O	43.33	56.90	O	15.15	20.01
F	3.99	4.41	F	2.46	2.73
Si	44.34	33.17	Si	3.02	2.27
Ru	5.89	1.22	Ru	41.64	8.70

The EDX data of the bulk material revealed the presence of C, O, F, Si and Ru. The source of the elements is probably as follows. The Si found in the sample is due to SiO_2; F is presumable due to trace amount of solvent (C_6F_6) or more reactive impurities in the solvent. The sources of oxygen are air, SiO_2 and CO; with C due to CO (and $Ru_6(C)$), and C_6F_6. Analysis of the results from four separate locations (Table 6.3) showed that not all the C present could be assigned to CO and C_6F_6. Once the percent of C due to these other sources were removed the ratio of Ru to C (from the atomic %) could be determined. The ratio ranged from 1:0.87 to 1:0.58 (average ratio 1:0.67). As seen in Table 6.3, the value of the weight % of C obtained were close to the value found by C/H/N analysis (For run A: 10.21 %C (EDX) versus 10.14 %C (C/H/N)).

Table 6.3. Summary of EDX data for bulk **19**.

	A			**B**	
Element	Weight %	Atomic %	Element	Weight %	Atomic %
C	10.21	41.14	C	9.80	40.36
O	3.88	11.75	O	4.34	13.41
F	1.41	3.59	F	1.24	3.24
Si	2.39	4.12	Si	1.25	2.20
Ru	82.12	39.37	Ru	83.36	40.79
	C			**D**	
Element	Weight %	Atomic %	Element	Weight %	Atomic %
C	8.50	37.89	C	7.54	35.09
O	3.50	11.70	O	2.90	10.12
F	1.05	2.95	F	1.22	3.58
Si	1.04	1.99	Si	1.66	3.31
Ru	85.91	45.48	Ru	86.68	47.91

The nature of **19** still remains to be determined. From the various data it may be the sodium chloride form of RuC rather than the tungsten carbide lattice of the known RuC. In an MC compound with a sodium chloride lattice the metal atoms adopt a cubic closepacked array and all the octahedral interstices are occupied with C atoms. In **19** some oxygen atoms have replaced the C atoms in the interstices.

This material is not the metallic Ru reported by Johnson, Lewis and Eady to be the sole product from the pyrolysis of $Ru_3(CO)_{12}$ at temperatures greater than 180 °C.[8]

$Ru_5(CO)_{16}$ (20) The pyrolysis of $Ru_3(CO)_{12}$ in perfluorodecalin (*cis/trans* mixture) at 125 °C for 10 hours (or at 110 °C in $C_6H_4Cl_2$) with an N_2 purge afforded an unknown product in a low yield which appears to be the previously unknown binary carbonyl of ruthenium, $Ru_5(CO)_{16}$ (**20**) (eq 6.6). (At 125 °C the yield of **20** appeared to

$$Ru_3(CO)_{12} \xrightarrow{125\ ^\circ C} \underset{\mathbf{20}}{Ru_5(CO)_{16}} + \underset{\mathbf{18}}{Ru_6(\mu\text{-}C)(CO)_{17}} \qquad (6.6)$$

be greater.) The identity of the compound was based on its IR spectrum and the variable temperature ^{13}C NMR spectrum that resembled that of $Os_5(CO)_{16}$ (see below). All

attempts to obtain crystals of **20** and to isolate a pure sample by column chromatography proved to be unsuccessful. It appeared **20** decomposed in air to $Ru_3(CO)_{12}$ and other unidentifiable decomposition products. One crystallization attempt of **20** from hexane did result in a small amount of a black precipitate, the IR spectrum of which indicated it to be an almost pure sample of **20** (~ 5 mg, ~ 3%) (Figure 6.4).

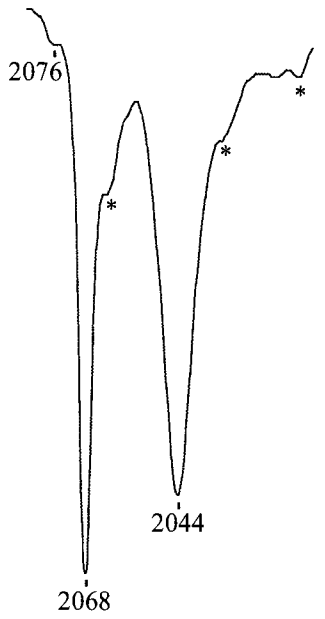

Figure 6.4. IR spectrum of $Ru_5(CO)_{16}$ (* due to $Ru_3(CO)_{12}$).

Results showed that **20** was also produced when a solution of $Ru_3(CO)_{12}$ and octane (in a quartz Carius tube) was irradiated with ultraviolet light with the solution purged with N_2. The production of **20** appeared to be concentration dependent and it was never produced in large amounts.

The identity of **20** is mainly based on its IR spectrum. It is known that the $Ru_{3-x}Os_x(CO)_{12}$ (x = 0-3) clusters have similar IR patterns (Table 6.4A).[150] As can be seen there is a steady shift to higher wavelengths in the IR spectrum as Ru atoms in

$Ru_3(CO)_{12}$ are replaced by Os atoms. When the IR spectra of $Os_5(CO)_{16}$, $Ru_2Os_3(CO)_{16}$ and $RuOs_4(CO)_{16}$ are compared to that of **20** (Table 6.4B) it is noticed that they all have the same pattern with a shift in the peak values as observed for the trimetallic clusters. This suggests that **20** has the same structure as $Os_5(CO)_{16}$ which has a trigonal bipyramidal metal skeleton (Chart 6.3 later).[54]

Table 6.4. Carbonyl stretching frequencies (cm^{-1}) for (A) $Ru_xOs_{3-x}(CO)_{12}$ (x = 0-3) and (B) $Ru_xOs_{5-x}(CO)_{12}$ (x = 0 - 2, 5). (The solvent is hexane.)

A

$Ru_3(CO)_{12}$	$RuOs_2(CO)_{12}$	$Ru_2Os(CO)_{12}$	$Os_3(CO)_{12}$
2061 vs	2063 vs	2066 vs	2069 vs
2031 s	2033 vs	2035 vs	2036 vs
2012 m	2019 sh/ 2014 m	2018 sh/ 2014 m	2016 m
-	2007 m	2004 m	2004 m

B

$Ru_5(CO)_{16}$	$Ru_2Os_3(CO)_{16}/RuOs_4(CO)_{16}$	$Os_5(CO)_{16}$
2078 w	2080 w	-
2068 vs	2066 vs	2066 vs
2044 vs	2046 s	2051 s/ 2043 sh
-	-	1 996 w

Without careful monitoring of the pyrolysis of $Ru_3(CO)_{12}$ by IR spectroscopy it would be easy to miss **20** since its IR peaks closely match some of the IR peaks of $Ru_6(\mu_6\text{-}C)(CO)_{17}$ (Table 6.5). This is an illustration of the advantage of solution pyrolysis versus the solid state reaction.

Table 6.5. The CO-stretching frequencies (cm^{-1}) for $Ru_5(CO)_{16}$ and $Ru_6(\mu_6\text{-}C)(CO)_{17}$ in hexane.

$Ru_5(CO)_{16}$	$Ru_6(\mu_6\text{-}C)(CO)_{17}$
2078 w	-
2068 vs	2066 vs
2044 vs	2047 vs
-	2003 w
-	1995 w

$Os_6(CO)_{18}$ (21) A solution of $Os_3(CO)_{12}$ in C_6F_6 was heated at 175 °C in an evacuated Carius tube for 26 days. The solution was degassed daily with three freeze-

pump-thaw cycles. The reaction mixture was then evaporated on the vacuum line and CH_2Cl_2 was added. This mixture (including the solid) was filtered through silica gel to remove **21** from an insoluble dark grey material (**22**, discussed below) that had also formed. The collected solution was evaporated on the vacuum line to give the known $Os_6(CO)_{18}$ in 68% yield (eq 6.7).[j] The product was pure by IR spectroscopy. The

$$Os_3(CO)_{12} \xrightarrow{175\ ^\circ C} \underset{\mathbf{21}}{Os_6(CO)_{18}} + \mathbf{22} \qquad (6.7)$$

compound can be obtained as air-stable, dark-brown crystals by crystallization from CH_2Cl_2/hexane. The product was characterized by IR, mass (parent ion) and ^{13}C NMR spectroscopy. The IR spectrum was in agreement with the reported values.

Compared to the literature methods this is a far more convenient procedure to prepare $Os_6(CO)_{18}$. The reported preparations either have multiple reaction steps (starting from $Os_3(CO)_{12}$) or an isolation step that requires weeks to complete.[8,104,136] At 68% the yield is a slight improvement over the highest reported values that have been independently checked.[8,104,136]

As mentioned in the Introduction (eq 6.2), pyrolysis of $Os_3(CO)_{12}$ in the solid state produces not only **21** but also $Os_5(CO)_{16}$, $Os_5(\mu_5\text{-}C)(CO)_{15}$, $Os_7(CO)_{21}$, $Os_8(CO)_{23}$ and $Os_8(\mu_6\text{-}C)(CO)_{21}$ that required careful chromatography techniques to separate.[8,136] The present method is carried out at a lower temperature and yields **21** as the only identifiable product.

---

[j] Ms. C. Wilcox at Simon Fraser University contributed to the optimization of the reaction conditions.

The stable cluster $Os_3(CO)_9(\mu_3:\eta^2:\eta^2:\eta^2\text{-}C_6H_6)$ provides hints to the reaction mechanism of the formation of **21** in C_6F_6. This arene cluster has the benzene ring symmetrically bonded over the open face of an $Os_3(CO)_9$ unit (Figure 6.5).[151] Reaction (eq 6.7) may proceed via an initial formation of $Os_3(CO)_9(\mu_3:\eta^2:\eta^2:\eta^2\text{-}C_6F_6)$ where the C_6F_6 unit is only weakly coordinated to the $Os_3(CO)_9$ unit. When two $Os_3(CO)_9(C_6F_6)$ intermediates interact the C_6F_6 rings are displaced and the two $Os_3(CO)_9$ units condense to form **21**. This mechanism explains why only **21** is formed in the reaction.

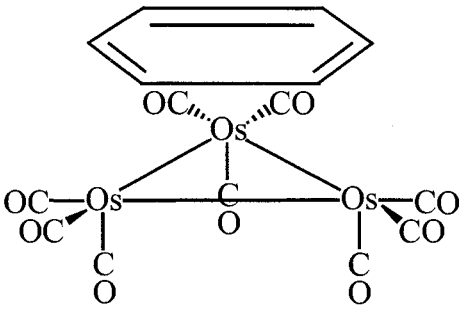

Figure 6.5. Molecular structure of $Os_3(CO)_9(\mu_3:\eta^2:\eta^2:\eta^2\text{-}C_6H_6)$.

The insoluble (**22**) material, which accompanied the production of **21**, consisted of a homogenous dark grey powder with a metallic lustre, similar to **19**. The C/H/N analysis of **22** (5.78 % C) is consistent with a formula of OsC, which is a known compound. As for **19**, **22** was also examined by mass and IR spectroscopy (Figure 6.6), X-ray powder diffraction (XRD), energy dispersive X-ray (EDX) analysis, as well the surface was probed by a scanning electron microscope (SEM). Because of the insolubility of **22** the mass spectrum did not prove useful. The poor quality of the XRD spectrum suggested that the sample did not contain any crystalline material. The IR spectrum (KBr disk) contained stretches due to carbonyl ligands and signals at 1091 cm^{-1} and 1080 cm^{-1} which are similar to the bands found in **19** and WC. These bands are not due to SiO_2 (mentioned later).

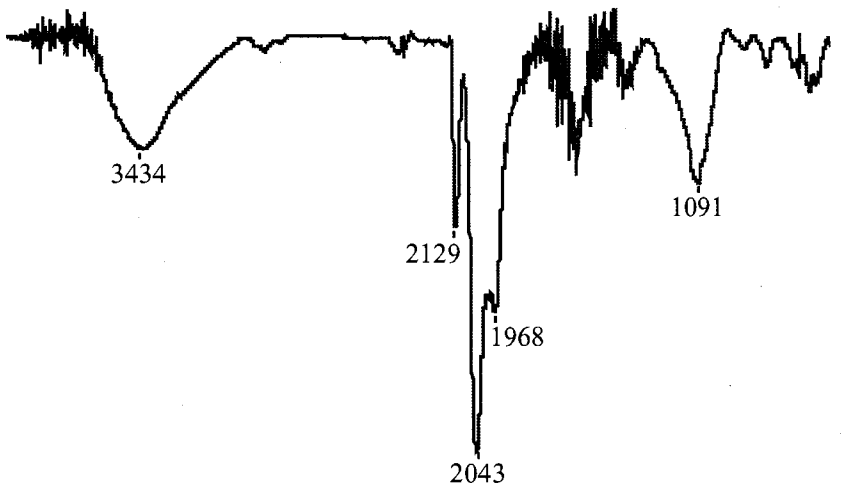

Figure 6.6. IR (KBr) spectrum of **22**.

Examination of the surface of the **22** showed a granular material (Figure 6.7) with a few cube-like structures, which were shown by EDX analysis to be SiO_2. The EDX analysis of three separate regions of the bulk material showed that **22** consists mainly of

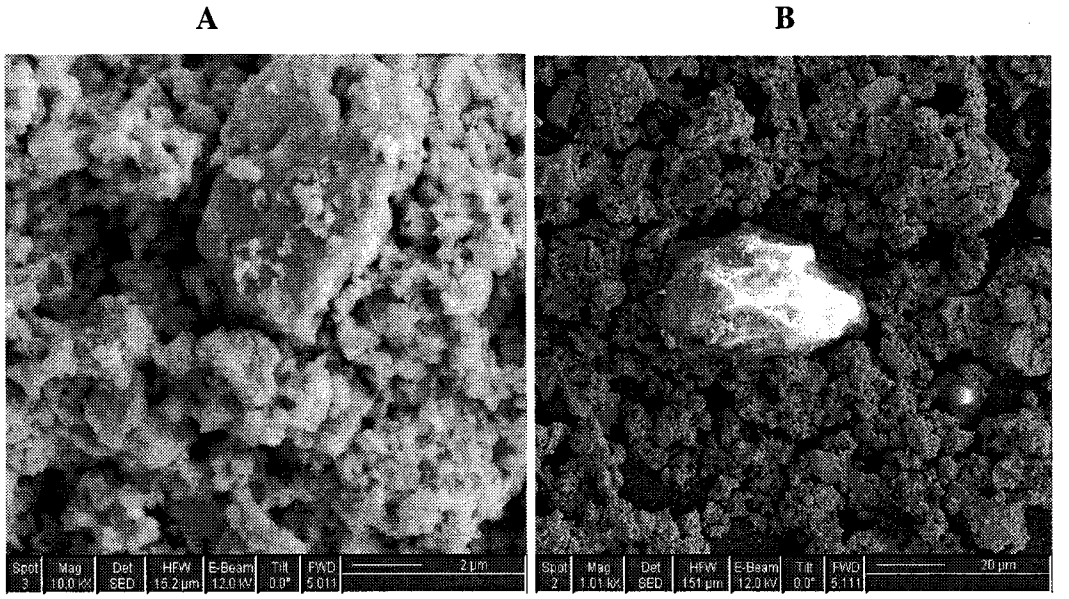

Figure 6.7. SEM of **22**. (A) Bulk material. (B) SiO_2 on the bulk material.

Os with smaller amounts of C and O in an approximate 1:1 ratio, which implied the presence of carbonyl ligands (Table 6.6). The nature of **22** remains unclear though the presence of CO ligands does imply the possibility of an unknown carbonyl cluster. All that can be said with certainty about **22** is it is not pure Os.

Table 6.6. Summary of C/O/Os values from the EDX analysis of **22**.

	A			**B**	
Element	Weight %	Atomic %	Element	Weight %	Atomic %
C	1.7	17.9	C	4.21	28.19
O	1.8	13.9	O	5.19	26.09
Os	94.1	62.9	Os	85.66	36.23

	C	
Element	Weight %	Atomic %
C	1.6	17.0
O	1.1	8.6
Os	94.33	63.7

$RuOs_2(CO)_{12}$ (23) and $[Ru(CO)_4]_n$ (24) Unpublished work by the Pomeroy group has found that the reaction of $Ru(CO)_5$ and $Os(CO)_5$ in hexane for 4 hours, under the exclusion of light, affords the known $Ru_2Os(CO)_{12}$ (**25**) as yellow/orange air-stable crystals in >95% yield (eq 6.8).[k] The cluster was characterized by C/H/N analysis, IR,

$$Os(CO)_5 + Ru(CO)_5 \xrightarrow{RT} \underset{\mathbf{25}}{Ru_2Os(CO)_{12}} \qquad (6.8)$$

mass (parent ion) and VT ^{13}C NMR spectroscopy. This improved method of synthesis of **25** allowed for its pyrolysis to be investigated.

The pyrolysis of $Ru_2Os(CO)_{12}$ (**25**) in C_6F_6 at 140 °C for 4 hours afforded the known $RuOs_2(CO)_{12}$ and an insoluble material that may be $[Ru(CO)_4]_n$ (**24**, eq 6.9).

---

[k] The samples for analysis were prepared by Ms. J. Logan at Simon Fraser University (SFU). The initial work into eq 6.8 was done by Dr. A. Becalska at SFU. Mr. J. Loo (SFU) also contributed to the investigation of this cluster.

$$2\ Ru_2Os(CO)_{12} \xrightarrow{140\ ^\circ C} \underset{\mathbf{23}}{RuOs_2(CO)_{12}} + (3/n)\underset{\mathbf{24}}{[Ru(CO)_4]_n} \qquad (6.9)$$

Isolation of **23** was achieved by decanting the reaction solution from **24**. The solution was then evaporated on the vacuum line and the remaining solid recrystallized from CH_2Cl_2 to give air-stable, orange crystals of **23** in 35% yield. The compound appeared pure by IR spectroscopy and did not contain bands due to $Os_3(CO)_{12}$ (see below). Isolation of the **23** allowed for its characterization by IR spectroscopy, mass spectroscopy (parent ion) and variable temperature ^{13}C NMR spectroscopy. The sample of ^{13}CO-enriched **23** used for the NMR study showed that in this case that it did contain some $Os_3(CO)_{12}$. This is due to the difficulty of monitoring reactions by IR spectroscopy of compounds that contain both ^{12}CO and ^{13}CO ligands.

Previous methods used to obtain **23** would also give **25** along with $Os_3(CO)_{12}$, and $Ru_3(CO)_{12}$ in a statistical distribution. The separation of these products is exceedingly tedious. The procedures reported here (eq 6.8, 6.9) are much more convenient and for the first time represent separate routes to **23** and **25**. The yields for these reactions are substantially improved over the synthesis reported in the literature.[150]

Compound **24** remained after the reaction solvent was removed. It was washed with CH_2Cl_2 to remove any soluble metal carbonyls and dried on the vacuum line. The compound is insoluble in common organic solvents. The mass spectrum of **24** exhibited an envelope of peaks of highest mass centered at 853.6 that corresponds to $Ru_4(CO)_{16}$. Given the instability of $Os_4(CO)_{16}$ it is almost certain that **24** is not $Ru_4(CO)_{16}$.[30] It may be that **24** is $[Ru(CO)_4]_n$ an insoluble polymer that has only been partially characterized.[152,153] Fragmentation of the polymer would then account for the

$[Ru(CO)_4]_4^+$ ion in the mass spectrum. The structure of $[Ru(CO)_4]_n$ as determined by X-ray powder diffraction is shown diagrammatically in Figure 6.8. [153]

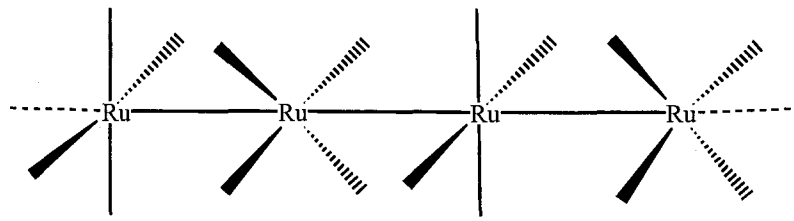

Figure 6.8. Part of the chain structure of the $[Ru(CO)_4]_n$.

The concentration of the reactant (**25**) was found to be critical in the production of **23** and **24**. It was found that below a certain concentration the reaction did not proceed. For example 20 mg of **25** in 15 mL of C_6F_6 showed no sign of producing **23**/**24**, but the reaction proceeded when the solvent was reduced to 10 mL. This suggests a bimolecular mechanism in which two **25** molecules combine to produce an $Ru_4Os_2(CO)_x$ ($x < 24$) intermediate which then decomposes into **23** and leaving an $Ru_3(CO)_x$ fragment that combines in the presence of CO to give **24** rather than $Ru_3(CO)_{12}$. Neither $Ru_3(CO)_{12}$ nor $Ru_6(\mu_6\text{-}C)(CO)_{17}$ were observed in this reaction.

To explain how **24** results from the photolysis of $Ru_3(CO)_{12}$ Hastings and Baird suggested a mechanism in which diradical $Ru_3(CO)_{12}$ units are first produced which couple to give **24**. This mechanism is not without controversy.

$Ru_2Os_3(CO)_{16}$ (26) and $RuOs_4(CO)_{16}$ (27) The pyrolysis of $Ru_2Os(CO)_{12}$ (**25**) in C_6F_6 was repeated but with an extended time of 20 hours. The solution was heated at 140 °C for two 10 hour periods, with degassing of the solution by three freeze-pump-thaw cycles every 2 hours (eq 6.10). The products were an inseparable mixture of

$$Ru_2Os(CO)_{12} \xrightarrow{140\ ^\circ C} \underset{\mathbf{26}}{Ru_2Os_3(CO)_{16}} + \underset{\mathbf{27}}{RuOs_4(CO)_{16}} + Os_5(CO)_{16} \qquad (6.10)$$

$Ru_2Os_3(CO)_{16}$ (**26**) and $RuOs_4(CO)_{16}$ (**27**), plus a trace amount of $Os_5(CO)_{16}$. Also formed in the reaction was an insoluble black solid that may have been **24**. The mixture of **26** and **27** eluted together as an orange/brown band on column chromatography. The separation of similar mixed metal clusters is often difficult. Further separation was therefore set aside and the mixture was analyzed.

The mass spectrum of the mixture contained two intense sets of peaks centred at 1222 and 1312 attributed to the parent ions of **26** and **27** (Figure 6.9). As seen in Figure 6.9 there is a weak set of signals at 1400 due to $Os_5(CO)_{16}$.

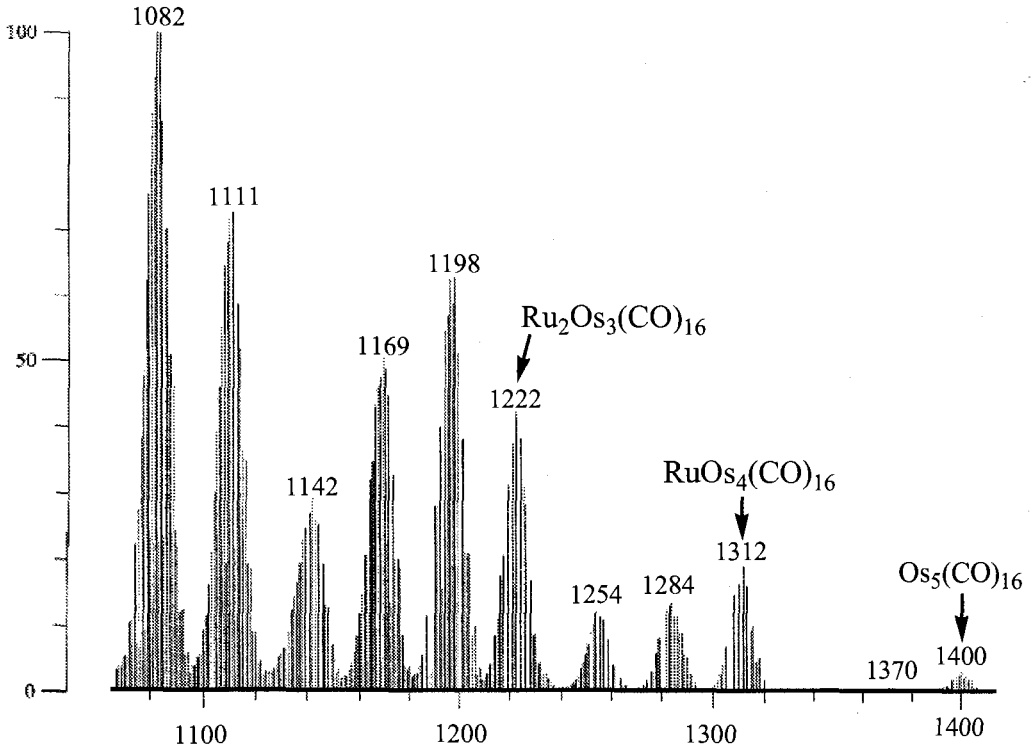

Figure 6.9. Mass spectrum of **26/27**.

As discussed above clusters with the same metal skeletal shapes (and similar ligands) often have similar IR patterns. This can be used to propose structures of new products such as **26** and **27**. As shown earlier in Table 6.4b the IR pattern of **26/27** (Figure 6.10) is similar to the IR spectrum of $Os_5(CO)_{16}$ which suggests that they all have

the same structure as $Os_5(CO)_{16}$, namely a trigonal bipyramidal metal skeleton. (See Chart 6.3 (later) for the structure of $Os_5(CO)_{16}$.) There are a number of isomers possible especially for $Ru_2Os_3(CO)_{12}$.

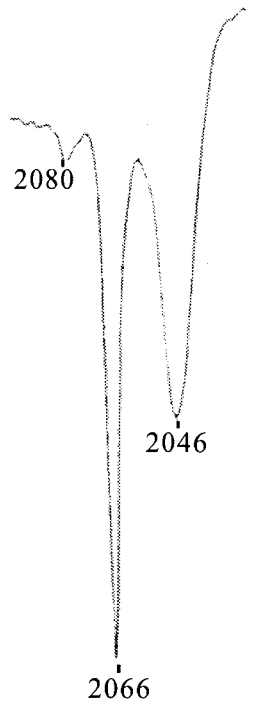

Figure 6.10. IR spectrum (ν(CO) region) of the mixture of **26/27** (in hexane).

The reaction (i.e., eq 6.10) also had concentration dependence. The variety of products suggests it has a complex mechanism. It is known that $Os_5(CO)_{16}$ results from the pyrolysis of $Os_5(CO)_{19}$ via $Os_5(CO)_{18}$ at temperatures greater then 70 °C. This suggests that initially $RuOs_4(CO)_{19}$ and $Ru_2Os_3(CO)_{19}$ are produced which lose a CO to give $RuOs_4(CO)_{18}$ and $Ru_2Os_3(CO)_{18}$ and finally the products **26** and **27**.

New preparation of $Os(CO)_5$ The parent carbonyl cluster of osmium is $Os_3(CO)_{12}$ (air stable yellow crystals) that can be produced in a small (200 mL) high pressure autoclave (small bomb) in essentially quantitative yield from OsO_4 in methanol at 150 °C and 80 atm of CO. When this reaction is carried out in hexane at 175 °C it is

accompanied by a small amount of $Os(CO)_5$ (15 - 20%). The usual preparation of $Os(CO)_5$ requires specialized equipment, namely, a booster pump, heater, rocker and a high pressure reaction vessel to handle the high temperatures ~300 °C and high pressures (200 atm) required.[90] Under these conditions OsO_4 is converted into $Os_3(CO)_{12}$ and $Os(CO)_5$; the latter in a ~60 % yield. It would therefore be convenient to convert $Os_3(CO)_{12}$ into $Os(CO)_5$ under less demanding conditions.

It was known that $Os_3(CO)_{12}$ can be converted into $Os_3(CO)_{10}(\mu\text{-}Cl)_2$ in almost quantitative yield.[154] In this work it was shown that the overnight reaction of $Os_3(CO)_{10}(\mu\text{-}Cl)_2$ with an excess of Zn powder and CO (80 atm) in hexane at 175 °C (in a small bomb) produces $Os(CO)_5$ in ~33% yield after collection by distillation (eq 6.11).

$$Os_3(CO)_{10}(Cl)_2 + CO \xrightarrow[Zn]{175\ ^\circ C} Os_3(CO)_{12} + Os(CO)_5 + \text{trace products} \qquad (6.11)$$

(The absorptivity of $Os(CO)_5$ was experimentally determined (see Experimental section). This allowed for the calculation of the percent yield.) The solution of $Os(CO)_5$ contained a trace amount of $Os(CO)_4(H)_2$,[112] which has been observed in other high pressure procedures to give $Os(CO)_5$. It has been suggested that it results from the reaction of $Os(CO)_5$ with the solvent.[90] In our preparation $Os(CO)_4(H)_2$ probably arises from reaction of $Os(CO)_5$ with the hydrogen present in the technical grade carbon monoxide that was employed. The remaining solid consisted of Zn, $Os_3(CO)_{12}$ and trace amounts of chlorinated products that were recycled. Without the addition of Zn a large amount of $Os_2(CO)_8(Cl)_2$ resulted from the reaction instead of $Os_3(CO)_{12}$ and although not investigated in detail it may be a better preparation of $Os_2(CO)_8(Cl)_2$ than those in the literature.[155]

Improved Preparation of $Os_4(CO)_{15}$ and $Os_4(CO)_{14}$ The previous preparation of $Os_4(CO)_{15}$ (by Pomeroy and coworkers) involved the conversion of $Os_3(CO)_{12}$ to $Os_3(\mu\text{-}H)_2(CO)_{10}$ then to $Os_3(CO)_{10}(COE)_2$ (COE = cyclooctene) and finally reaction of the COE derivative with $Os(CO)_5$. During this study an improved synthesis of $Os_4(CO)_{15}$ (and $Os_4(CO)_{14}$) was developed from $Os_3(CO)_{10}(CH_3CN)_2$ which is readily made from $Os_3(CO)_{12}$.[91] An excess amount of $Os(CO)_5$ was added to a solution of $Os_3(CO)_{10}(CH_3CN)_2$ (eq 6.12) which was allowed to stir at room temperature for 4 hours

$$Os_3(CO)_{10}(CH_3CN)_2 + Os(CO)_5 \xrightarrow{21\ ^\circ C} Os_4(CO)_{15} \qquad (6.12)$$

and stored at -29 °C overnight to precipitate $Os_4(CO)_{15}$. The solution was decanted away from the solid which was washed twice with hexane to give the desired product $Os_4(CO)_{15}$ in approximately 55% yield. The IR spectrum (ν(CO) region) of $Os_4(CO)_{15}$ matched that previously reported.[29,36]

To a round-bottom flask topped with a water-cooled condenser was added toluene and $Os_4(CO)_{15}$. This solution was heated for 3.5 hours at 90 °C while a strong stream of nitrogen gas was bubbled through it (eq 6.13). The solution was reduced in volume and

$$Os_4(CO)_{15} \xrightarrow{90\ ^\circ C} Os_4(CO)_{14} \qquad (6.13)$$

placed overnight at -29 °C producing the air-stable, brown crystals of $Os_4(CO)_{14}$ (86% yield). The IR spectrum of $Os_4(CO)_{14}$ matched that in the literature.[31]

Although the yield is slightly lower than the reported value it was found that this method more consistently produces a high yield of a pure samples of $Os_4(CO)_{14}$ through a more convenient procedure.[29,31,36]

$Os_4(\mu\text{-}H)(\mu\text{-}OH)(CO)_{13}$ (28) and $Os_5(CO)_x$ (x = 16 (29), 19 (30)) The pyrolysis of $Os_4(CO)_{14}$ (with or without C_6F_6) at 125 °C for 24 hours produced $Os_3(CO)_{12}$ and

$Os_5(CO)_{16}$ (**29**) in an approximate 1:1 ratio (~ 50% yield for both) as well as trace amounts of $Os_6(CO)_{18}$ and $Os_4(\mu\text{-H})(\mu\text{-OH})(CO)_{13}$ (**28**) as isolated by chromatography (eq. 6.14). An alternative method to make **28** in good yield and its complete

$$Os_4(CO)_{14} \xrightarrow{125^{\circ}C} Os_3(CO)_{12} + \underset{\mathbf{29}}{Os_5(CO)_{16}} + \underset{\text{trace}}{Os_6(CO)_{18}} + \underset{\mathbf{28}\ (\text{trace})}{Os_4(\mu\text{-H})(\mu\text{-OH})(\mu\text{-CO})(CO)_{12}} \qquad (6.14)$$

characterization are presented in Chapter 7. The 1:1 ratio of $Os_3(CO)_{12}$ to **29** was determined by a ^{13}C NMR spectrum of the product mixture (^{13}CO-enriched) after completion of the reaction .

The 1:1 ratio suggests that the reaction may proceed through a bimolecular mechanism in which $Os_4(CO)_{14}$ couples to give an $Os_8(CO)_n$ intermediate that decomposes into $Os_3(CO)_{12}$ and **29**. The ~50% yield for **29** is not an improvement over other reported preparations though the overall procedure is simpler.[54,156] After separation by column chromatography **29** was recrystallized from CH_2Cl_2 to give air-stable, pink/red crystals. These were investigated by IR and variable temperature ^{13}C NMR spectroscopy.

The failure to produce an octanuclear binary carbonyl of Os from the pyrolysis of $Os_4(CO)_{14}$ suggests that Os_8 binary carbonyls may be thermodynamically unstable with respect to Os_3 and Os_5 carbonyl clusters. The binary carbonyl $Os_8(CO)_{23}$ has been claimed as isolated from the pyrolysis of $Os_3(CO)_{12}$ in the solid state (eq 6.2).[8] The evidence for $Os_8(CO)_{23}$ is however weak. No crystal structure has been reported and its formula is claimed on the basis of mass spectral evidence (*circa* 1975) on alleged M^{2+} ions. Such ions are rarely if ever produced from neutral species by electrospray ionization (EI) techniques. Other work from the Pomeroy laboratory has shown that

$Os_4(\mu\text{-}H)_2(CO)_{13}$ is produced in the pyrolysis reaction and has a similar infrared spectrum and elution properties as $Os_8(CO)_{23}$.

A preliminary investigation showed that ultraviolet radiation (through quartz) of $Os_4(CO)_{14}$ in C_6F_6 afforded $Os_3(CO)_{12}$, $Os_5(CO)_{19}$ and a trace amount **28**, after chromatography (eq 6.15). The yields of the products were not determined but it

$$Os_4(CO)_{14} \xrightarrow{h\nu} Os_3(CO)_{12} + Os_5(CO)_{19} + \underset{\mathbf{28}}{Os_4(\mu\text{-}H)(\mu\text{-}OH)(\mu\text{-}CO)(CO)_{12}} \qquad (6.15)$$

appeared that the yield of $Os_5(CO)_{19}$ was not an improvement over the literature procedures.[44] Note that the UV method differs from the pyrolysis in that it produces **30** rather then **29**. Note there must be other products formed so that there is a mass balance with the carbonyl ligands.

$Os_4(\mu_4\text{-}C)_2(CO)_{12}$ or $Os_4(\mu_4\text{-}C_2)(CO)_{12}$ (31) As previously discussed the pyrolysis of $Ru_3(CO)_{12}$ gives $Ru_6(\mu_6\text{-}C)(CO)_{17}$ whereas pyrolysis of $Os_3(CO)_{12}$ yields $Os_6(CO)_{18}$. The osmium analogue of $Ru_6(\mu_6\text{-}C)(CO)_{17}$ has been prepared in low yield from the reaction of $Os_3(CO)_{12}$ with Na at 140 °C.[104] In an attempt to prepare $Os_6(\mu_6\text{-}C)(CO)_{17}$, $Os_3(CO)_{12}$ was pyrolyzed with graphite in C_6F_6. The reaction did not produce the desired product, but $Os_6(CO)_{18}$ along with a small amount of $Os_4(\mu\text{-}H)_4(CO)_{12}$ [157] which probably resulted from water in the graphite. To investigate the reaction of $Os_6(CO)_{18}$ with graphite as a method to prepare $Os_6(\mu_6\text{-}C)(CO)_{17}$ the reaction mixture was further pyrolyzed which resulted in a trace amount of an unknown compound (**31**). Further reactions showed that the replacement of graphite with C_{60} also gave **31**. The pyrolysis of $Os_6(CO)_{18}$, $Os_4(\mu\text{-}H)_4(CO)_{12}$ and C_{60} (or dry activated C) in a sealed, evacuated Carius tube at 230 °C for 5 days gave brown crystals after chromatography in a

<6% yield (eq 6.16). The reaction of any two of the three reactants under the same conditions failed to give this product.

$$Os_6(CO)_{18} + Os_4(\mu\text{-}H)_4(CO)_{12} + C_{60} \xrightarrow{230\ ^\circ C} \mathbf{31} \qquad (6.16)$$

The product is tentatively identified as $Os_4(\mu_4\text{-}C)_2(CO)_{12}$ or $Os_4(\mu_4\text{-}C_2)(CO)_{12}$ based on its mass and IR spectrum. The calculated isotope pattern for the molecular ion peak of **31** was in agreement with the observed pattern (M^+ = 1121.1) (Figure 6.11). The IR spectrum in the CO region is shown in Figure 6.12. The simplicity of the spectrum indicates that **31** must be symmetric. Two clusters related to that proposed for **31** are

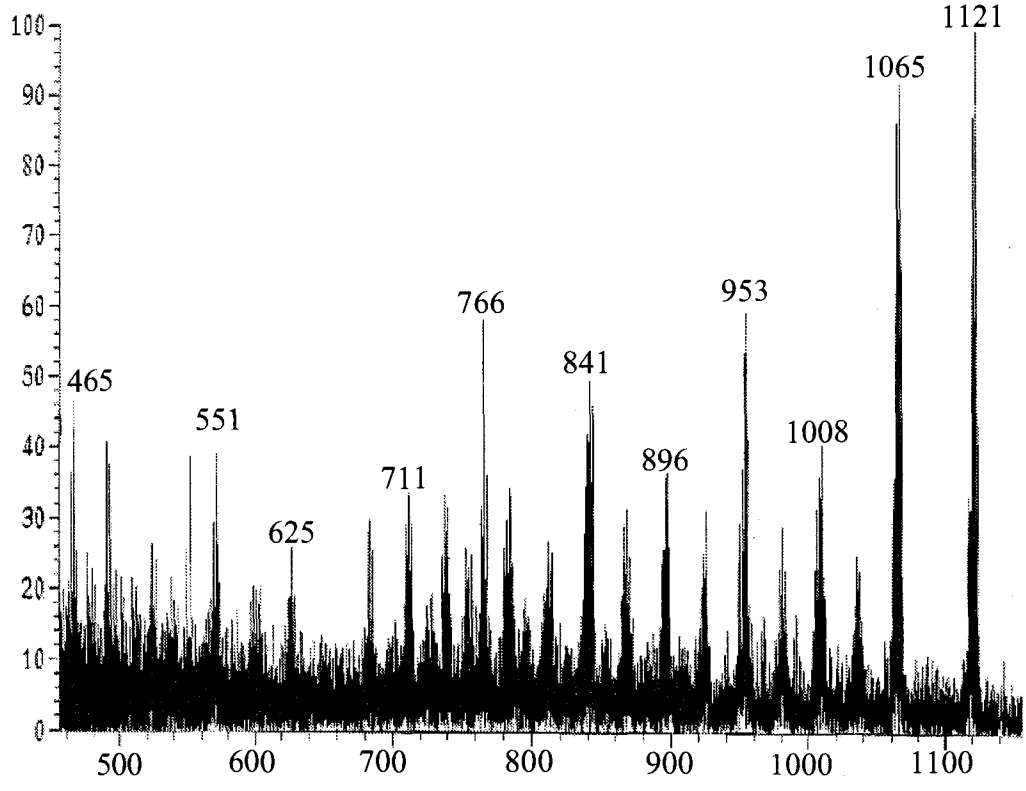

Figure 6.11. Mass spectrum of **31**.

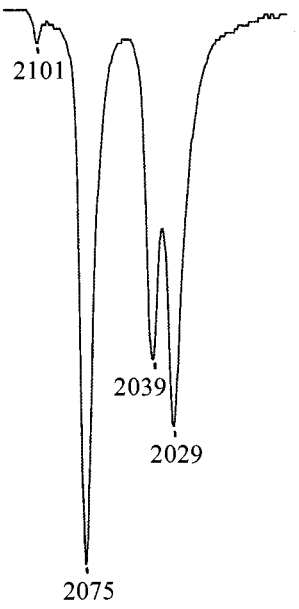

Figure 6.12. IR spectrum (hexane; ν(CO) region) of **31**.

$M_4(\mu_4\text{-}E)_2(CO)_{12}$ with M = Ru, Os and E = Bi that have the structures shown in Figure 6.13. The different structures are both symmetric and consequently they have simple IR spectra.[158] A comparison of their IR data with that of **31** failed to provide a hint as to which structure it adopts. The replacement of Bi with C can cause a change in the IR pattern (Table 6.7). Furthermore in $Ru_4(CO)_{11}(\mu_4\text{-}L)_2$ (L = S, Te) both clusters adopt a square arrangement of Ru atoms but the IR spectra are different.

It has been suggested that $Os_4(\mu_4\text{-}Bi)_2(CO)_{12}$ adopts the butterfly arrangement of transition metal atoms in preference to the square arrangement found in $Ru_4(\mu_4\text{-}Bi)_2(CO)_{12}$ because the butterfly configuration reduces the number of metal-ligand bonds while increasing the number of metal-metal bonds.[159] The same metal atom arrangement (butterfly) is present in $M_4(\mu_4\text{-}C_2H_2)(CO)_{12}$ (M = Ru, Os), which have a similar formula to **31**.[131,160] The IR data confirms that **31** is not $Os_4(\mu_4\text{-}C_2H_2)(CO)_{12}$. This would suggest

that **31** could also have a butterfly arrangement of the Os atoms, though there are other examples of clusters with the $M_4(\mu_4\text{-}E)_2$ (M = Ru, E = S, Se, Te) unit that have the square M_4 arrangement.[159,161] Both structures seem possible for **31** (Figure 6.14).

The "bare" C atoms proposed in Figure 6.14. have been seen in other clusters, such as, $Fe_5(\mu_4\text{-}C)(CO)_{15}$ and $Ru_5(\mu_4\text{-}C)(CO)_{15}$.[162] These can be thought of as having the same structure as shown on the left in Figure 6.14 except one C has been replaced by a $M(CO)_3$ unit. The cluster **31** would be the first to contain an $M_4(\mu_4\text{-}C)_2$ unit.

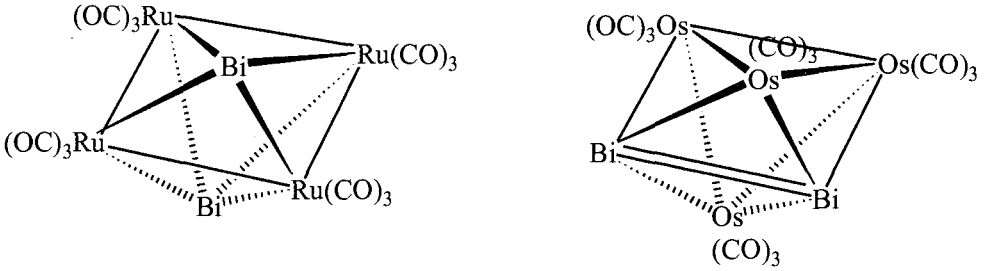

Figure 6.13. Structures of $M_4(\mu_4\text{-}Bi)_2(CO)_{12}$ (M= Ru, Os).

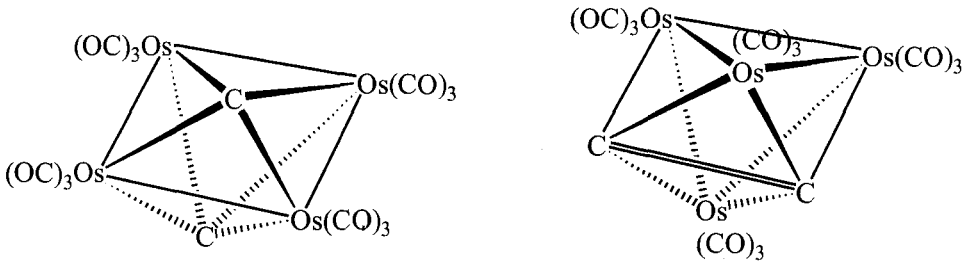

Figure 6.14. Possible structures for $Os_4(\mu_4\text{-}C)_2(CO)_{12}$. There may or may not be a C-C bond in structure on the right.

Table 6.7. Comparison of the IR spectrum (ν(CO) region; in hexane) of **31** with those of some $M_4(\mu_4\text{-}X)_2(CO)_{12}$ clusters (cm^{-1}).

31	$Os_4(\mu_4\text{-}C_2H_2)(CO)_{12}$	$Os_4(\mu_4\text{-}Bi)_2(CO)_{12}$	$Ru_4(\mu_4\text{-}Bi)_2(CO)_{12}$
2101 w	2102 w	2053 w	-
2075 vs	2075 vs	2033 vs	2045 vs
2039 s	2049 s	2017 vs	2002 m
2029 vs	2039 s	1981 m	-
	2018 m		
	2004 m		
	1973 w		

6.3 Variable temperature ^{13}C NMR studies of the pyrolysis products

Introduction The clusters $M_3(CO)_{12}$ (M = Fe, Ru, Os) and their derivatives have been important in developing models to explain the mechanism of carbonyl exchange in transition metal clusters. The subject is far from being understood and debate continues over the most plausible mechanisms even for the parent $M_3(CO)_{12}$ compounds.[102,163] Five different mechanisms have been postulated in order to explain the CO exchange in $Fe_3(\mu\text{-}CO)_2(CO)_{10}$. The most popular mechanisms are the Fe_3 rotation in a fixed CO shell model of Johnson, and the axial-equatorial merry-go-round CO exchange mechanism (Chart 6.1) proposed by Cotton in 1966.[163c] Work by Li and Jug has shown that the Cotton proposal to be the most probable mechanism for carbonyl exchange, but the controversy continues.[164]

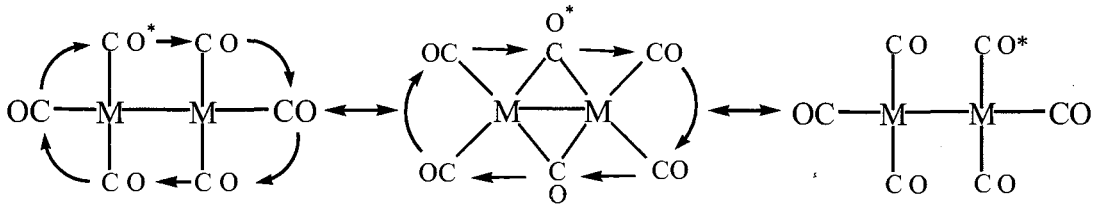

Chart 6.1. Axial-equatorial merry-go-round exchange of carbonyl ligands across an M-M bond (M = Fe, Ru, Os).

Because carbonyl exchange often occurs on the NMR timescale (~10^2 to 10^5 s^{-1}) variable temperature ^{13}C NMR studies of metal carbonyls offer a means to probe the fluxional processes by NMR line broadening techniques.[163a] (The CO exchange in $Fe_3(CO)_{12}$ is however still too fast on the NMR timescale even at -150 °C.[163c]) Although the ^{13}C NMR spectra of $M_3(CO)_{12}$ and their derivatives have been extensively investigated, the examination of the mixed metal clusters ($M_2M'(CO)_{12}$; M, M'= Fe, Ru, Os; M ≠ M') has been limited. NMR studies of $Ru_2Os(CO)_{12}$ and $RuOs_2(CO)_{12}$ would help to understand the exchange processes that occur in the homonuclear metal carbonyls

because having different metals lower the symmetry of the compound and hence provides more information of the mechanism of exchange.

In this section the variable temperature ^{13}C NMR spectroscopy studies of two mixed metal clusters $Ru_2Os(CO)_{12}$ and $RuOs_2(CO)_{12}$ are presented that are consistent with the axial-equatorial merry-go-round mechanism of CO exchange. Within the merry-go-round exchange mechanism proposed for these two clusters an explanation will be presented to explain why the rates of carbonyl exchange over the different metal-metal (M-M′) bonds are not the same.

The ^{13}C NMR spectra and mode of carbonyl exchange for some higher nuclearity metal carbonyls will also be presented. The unusual ^{13}C NMR resonance of the carbide atom in $Ru_6(\mu_6\text{-}C)(CO)_{17}$ is reported for the first time.

6.3 Variable Temperature ^{13}C NMR Studies

$Ru_6(\mu_6\text{-}C)(CO)_{17}$ (18) The room temperature ^{13}C NMR spectrum of **18** (Figure 6.15) in $CDCl_3$ contains a single sharp signal at δ 197.5 consistent with a rapid carbonyl exchange over the Ru_6 frame, as previously suggested by Dyson.[103] This resonance remains sharp at -25 °C ($CD_2Cl_2/CHFCl_2$) but begins to broaden at -55 °C. At -95 °C the singlet is split into two broad resonances (δ 200.1, 191.7). The spectrum at -125 °C contains two sharp signals in the carbonyl region in an ~11:6 ratio (δ 199.9, 191.2) plus a weak singlet at δ 453.7. The spectra are shown in Figure 6.15.

The 11:6 ratio indicates that exchange of carbonyls over the whole cluster has ceased at -125 °C. The sharp signal at δ 199.9 with an integration of 11 is assigned to the 11 CO ligands attached to the four Ru atoms in the equatorial plane which are still undergoing rapid exchange (Figure 6.15). Clusters with a bridging CO generally undergo

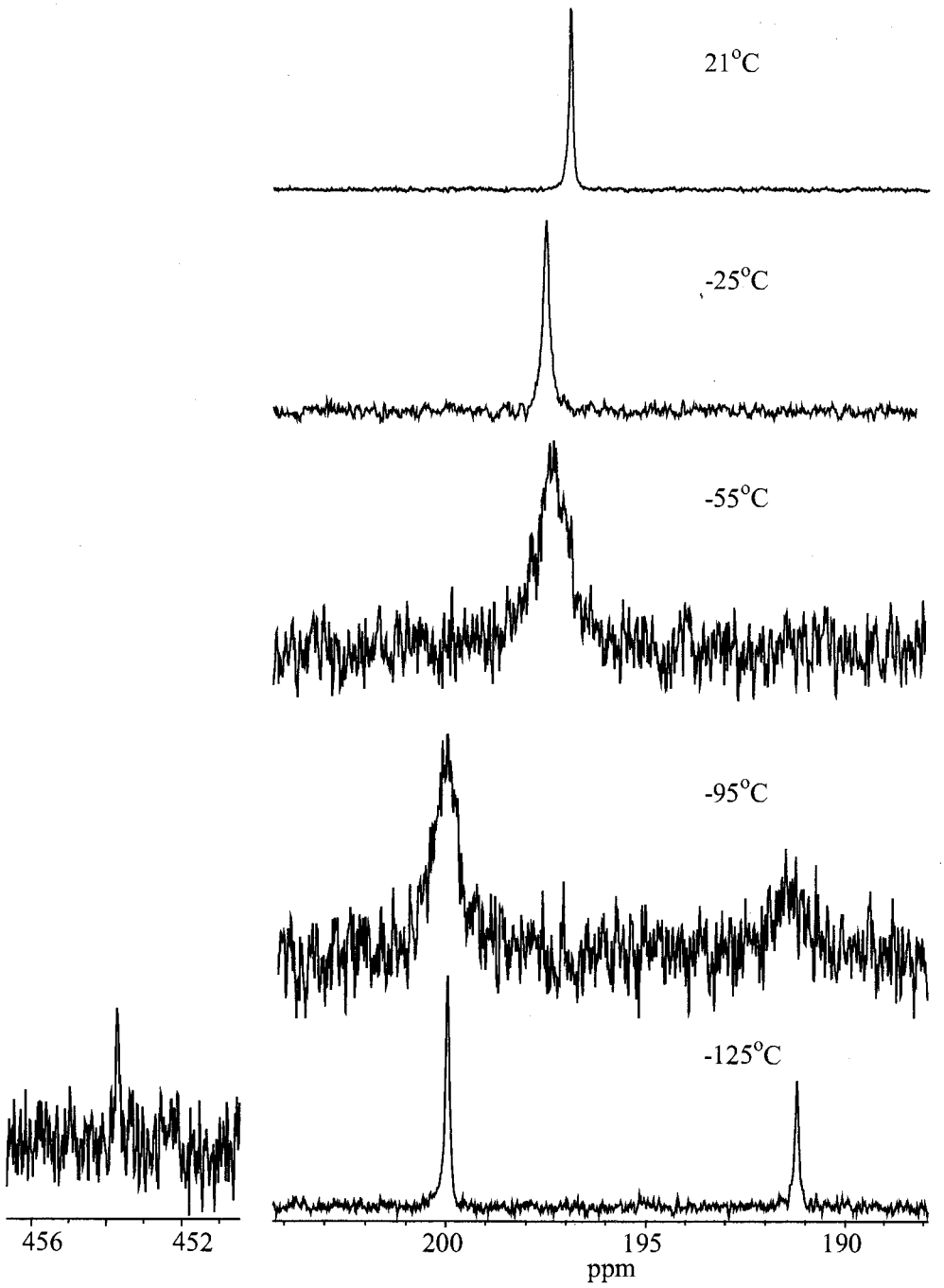

Figure 6.15. VT ^{13}C NMR spectra of $Ru_6(\mu_6\text{-}C)(CO)_{17}$.

a rapid merry-go-round exchange (Chart 6.1) in the plane containing the bridging CO.[77] The bridging CO in the equatorial plane lowers the overall symmetry of **18**. The exchange of carbonyls has to be over all 4 Ru atoms in the plane and not localized at

individual Ru atoms otherwise more resonances would be observed. Furthermore, the carbonyls above and below the equatorial plan must exchange with the carbonyls in the equatorial plane including the bridging CO in order to produce a singlet for the carbonyls bound to Ru atoms in the equatorial plane.

A mechanism for the exchange in this plane is as follows. As CO(*a*) (Chart 6.2) moves towards Ru(2) (the exchange could proceed towards Ru(1) with equal probability) it breaks its bond to Ru(1), the other two CO ligands on Ru(2) (CO's *b* and *c*) shift towards Ru(3). This causes a repulsive interaction between the two axial CO's (*b* and *c*)

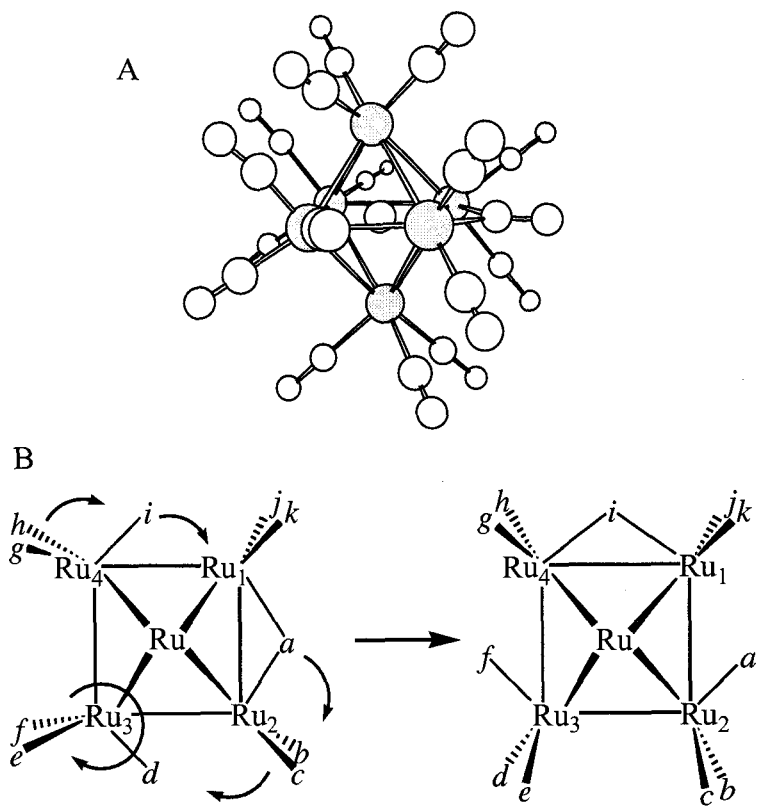

Chart 6.2. (A) Structure of $Ru_6(\mu_6\text{-}C)(CO)_{17}$ (**18**). (B). Mode of CO exchange for carbonyls attached to the equatorial Ru atoms in **18**.

on Ru(2) and the CO on Ru(3) labelled *d*. To reduce this interaction the carbonyls on Ru_3 twist clockwise (counter clockwise is equally possible but not shown) which converts the position of CO(*d*) from an equatorial into an axial position and CO(*f*) from an axial to an

equatorial site. The carbonyl labelled *e* retains its equatorial position but shifts from being almost trans to the Ru(3)-Ru(4) bond to almost cis. The new position of CO(*f*), again through repulsive interactions, will shift the CO's on Ru(4) towards Ru(1). The carbonyl labelled *i* is shifted towards Ru(1) is now able to bridge the Ru(1)-Ru(4) bond completing one quarter of the cycle of exchange. For every quarter turn of the cycle a pair of carbonyls exchanges their axial and equatorial positions while a CO transfers from one Ru to another. The net effect of these two motions is a complete scrambling of CO over the $Ru_4(CO)_{11}$ unit.

The ^{13}C resonances of bridging CO ligands in rigid molecules are usually separated from the resonances of terminal CO ligands in the same molecule by at least 20 ppm (~2000 Hz at an operating frequency of 100.6 MHz).[78] In order to coalesce two NMR signals separated by $\Delta\nu$ to a sharp peak an exchange rate of $\pi(\Delta\nu)^2$ is required.[31,78] This indicates that the carbonyls in the equatorial plane are exchanging at a rate greater than ~1.3×10^7 s^{-1} at -125 °C. If it is assumed that the rate doubles for every 10 °C rise in temperature this would result in a rate of exchange of ~4.3×10^{11} s^{-1} at 25 °C. This corresponds to exchange near the IR timescale (~10^{13} s^{-1}) and is enough to cause line broadening of CO stretches.[165] This has been proposed for $Os_4(CO)_{14}$ and $Fe_3(CO)_{12}$.[31] Group theory predicts **18** (of C_{2v} symmetry) should exhibit 13 IR-active CO stretches, but only four bands are observed. The IR spectrum of $Os_4(CO)_{14}$ and $Fe_3(CO)_{12}$ are remarkably similar and similar to that of **18** (Figure 6.16).[31,166] (The low temperature IR spectra of $Os_4(CO)_{14}$ and **18** are currently under investigation.)[1]

---

[1] Collaboration with Dr. A. Bengali Department of Chemistry, Dickinson College, Carlisle, PA.

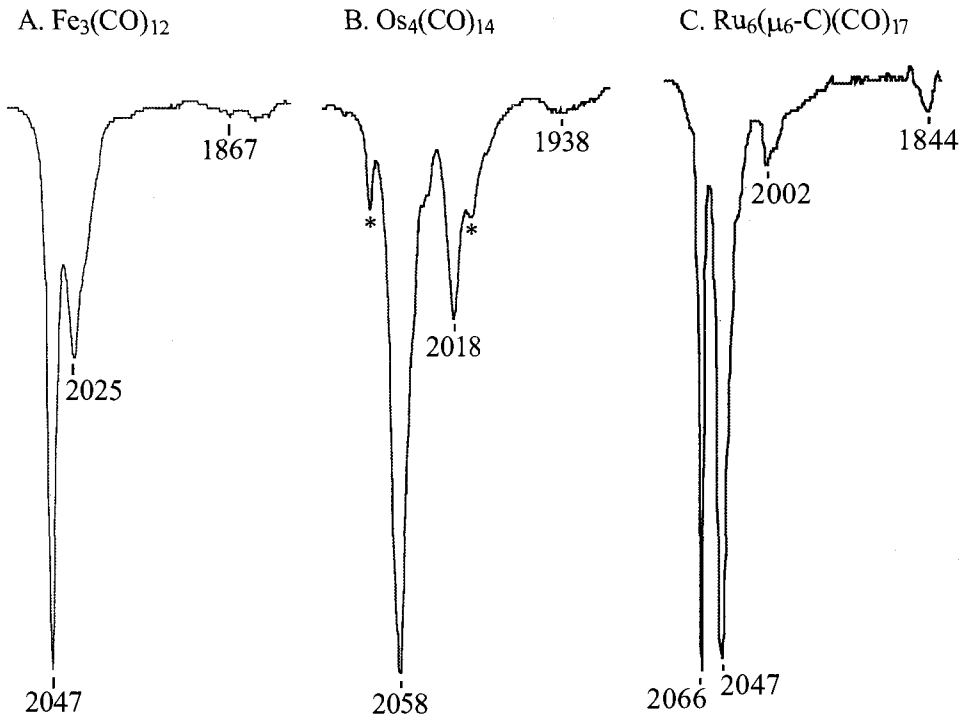

Figure 6.16. IR (hexane) spectra (ν(CO) region) of (A) $Fe_3(CO)_{12}$, (B) $Os_4(CO)_{14}$, (C) $Ru_6(\mu_6\text{-}C)(CO)_{17}$. (* = impurity)

It may be that coupled to the merry go round exchange is the mutual exchange of the CO's on the individual equatorial $Ru(CO)_3$ units that do not contain the bridging CO, but there is no way to ascertain this. This type of exchange (with low activation barriers) is found for $Os(CO)_3$ units in the condensed Os clusters (eg., $Os_6(CO)_{17}(L)$ (L = CO,[80] PPh_3 [81]) and $Os_7(CO)_{21}$[50]).

he signal of intensity 6 at δ 191.2 is assigned to the carbonyls bound to the apical Ru atoms. Because the carbonyls in the equatorial plane are undergoing rapid exchange on the NMR time scale the carbonyls of the apical $Ru(CO)_3$ groups are chemically equivalent. Nothing can be said about the possible rotation of the carbonyls in the individual $Ru(CO)_3$ units. As mentioned previously, this is common for condensed Os

clusters. It has been shown that the capping $Os(CO)_2(CNBu^t)$ group in $Os_7(CO)_{20}(CNBu^t)$ rapidly rotates in solution.[167]

A weak singlet at δ 453.7 in the ^{13}C NMR spectrum of **18** is assigned to the interstitial carbide. This is in the region found for the resonances of other carbide C atoms in an octahedral environment of molecular transition metal clusters.[168] Molecules with a carbon atom in such an octahedral hole have given ^{13}C NMR signals in the range of 425-475 ppm, whereas a carbon atom in a trigonal prismatic interstice has a resonance in the range 250-300 ppm. The carbide C atom found in these clusters has an atomic radius that is less than the covalent radius of carbon (0.77 Å). The radius of the interstitial C in **18** is approximately 0.60 Å which is close to the average atom radius for carbides found in octahedral clusters. Mason has pointed out that the degree of radius contraction depends on the geometric shape it resides in. As the size of the cavity changes, it affects the degree of overlap between the orbitals of the C atom and of the metal atoms. This in turn changes the amount of shielding the carbide C experiences and hence its resonance position.

Although the nature of the bonding of the carbide to the metal cage would be more accurately described by molecular orbital arguments, Heaton *et al.* have rationalized the bonding based on hybridization. Their results are summarised below. Based on ^{13}C NMR studies of other transition metal clusters with interstitial carbides Heaton *et al.* concluded that a C atom in an octahedral cavity must be sp hybridized. This hybridization was suggested since it maximizes the overlap of the orbitals on C with the orbitals associated with the metal atoms.[169] The *sp* orbital on C is oriented towards the apical Ru atoms leaving two *p* orbitals to point towards the four Ru atoms in the Ru_4 unit.

$Ru_5(CO)_{16}$ (20) The ^{13}C NMR spectrum in CD_2Cl_2/CH_2Cl_2 (at -90 °C) of the products produced by the pyrolysis of $Ru_3(CO)_{12}$ in 1,2-dichlorobenzene revealed signals belonging to $Ru_6(\mu_6\text{-}C)(CO)_{17}$ (**18**), $Ru_3(CO)_{12}$ as well as two signals assigned to **20** in an approximate 10:6 ratio (Figure 6.17). (The signal to noise ratio prevents an accurate measurement of signal intensities.) The two sharp singlets assigned to **20** coalesced into a broad signal at ~ 195.0 ppm as the temperature was raised to 21 °C (Figure 6.17). The signal pattern of **20** at -90 °C and the coalescence of the peaks at higher temperature are similar to the ^{13}C NMR spectrum of $Os_5(CO)_{16}$ (Chart 6.3 later). This supports the idea that **20** has the same trigonal bipyramidal metal skeleton as $Os_5(CO)_{16}$.[54]

The ^{13}C NMR spectra of **20** at various temperatures can be explained if it is assumed to adopt a trigonal bipyramidal structure. The approximate 10:6 ratio of the signals attributable to **20** at -90 °C indicates that the CO exchange over the whole structure has ceased (Figure 6.17). The sharp signal at δ 188.8 corresponds to the 6 CO's of the two apical $Ru(CO)_3$ units. The remaining 10 CO ligands attached to the equatorial Ru atoms are undergoing an exchange to give the signal at δ 197.7 of intensity ~10. At room temperature exchange of carbonyls over the whole structure occurs. (A more detailed explanation of the ^{13}C NMR of $Os_5(CO)_{16}$ is given below.)

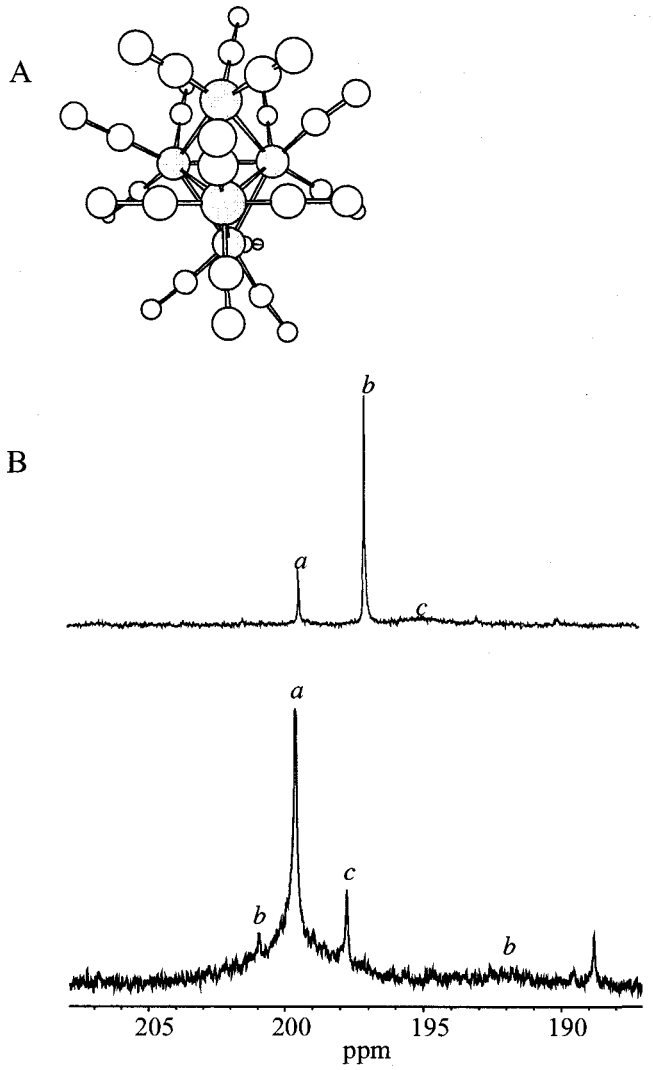

Figure 6.17. (A) Proposed structure of $Ru_5(CO)_{16}$. (B) The ^{13}C NMR spectra of products from eq 6.6 (a = $Ru_3(CO)_{12}$, b = $Ru_6(\mu_6\text{-}C)(CO)_{17}$, c = $Ru_5(CO)_{16}$)

$Os_6(CO)_{18}$ (21) The ^{13}C NMR spectrum of ^{13}CO-enriched **21** at 21 °C consists of two broad peaks and one sharp resonance in an approximate 1:1:1 ratio (Figure 6.18). This spectrum is consistent with the ^{13}C NMR spectra reported by Eady *et al.*[80] The paper shows spectra of **21** at various temperatures ranging from -123 to 100 °C, but not a spectrum at ambient temperature. The structure of **21** (Figure 6.18) may be described as either a bicapped tetrahedron or a capped trigonal prism. As explained by Eady *et al.*, **21**

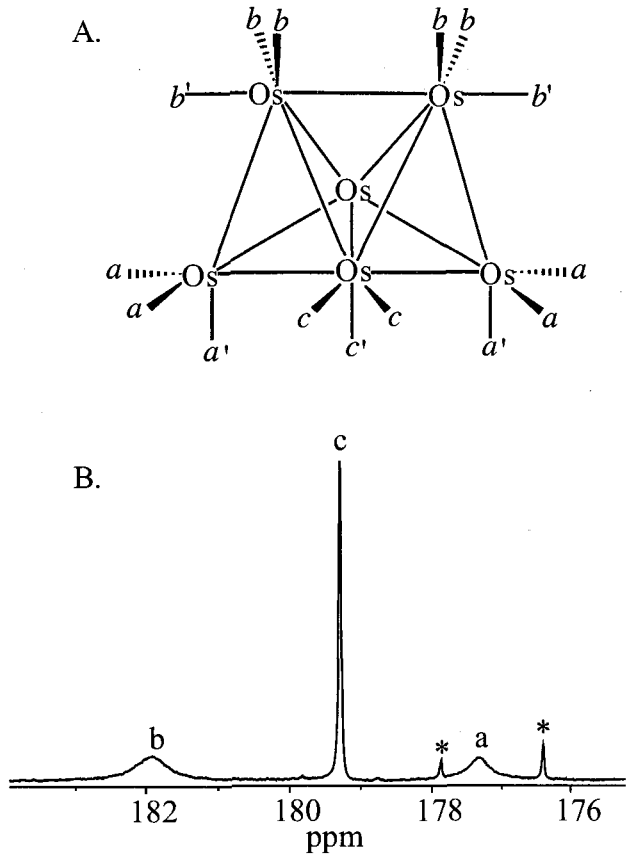

Figure 6.18. (A) Structure of $Os_6(CO)_{18}$ (**21**) (CO groups on rear hinge Os atom omitted). (B) The ^{13}C NMR spectrum of **21** (a = a', b = b', c = c' at 21°C). (* impurities)

has three chemically different $Os(CO)_3$ groups (*a*, *b* and *c* in Figure 6.18) that undergo apparent rotation at different rates. In **21** there is no exchange of CO ligands between Os atoms, only exchange of carbonyls on the individual Os centers (a = a', b = b', c = c' in Figure 6.18)). The higher the coordination number of the Os atom the faster the $Os(CO)_3$ rotation.[80] (This also occurs in $Os_4(\mu_3\text{-}\eta^2\text{-}C_2Ph_2)(CO)_{13}$ as described in Chapter 5)

The broad resonance at δ 181.9 corresponds to the three CO ligands on Os(*b*) while the sharp resonance at δ 179.3 is assigned to the carbonyls on Os(*c*) (Figure 6.18). The remaining broad signal at δ 177.3 is assigned to the carbonyls bonded to Os(*a*). The hinge Os atoms (labelled *c*) are formally 8 coordinate and the carbonyl attached to these

Os atoms undergo rapid exchange on the NMR time scale and hence gives rise to a sharp ^{13}C NMR resonance for these carbonyls. The osmium atoms labelled *a* and *b* are seven and six coordinate respectively and undergo exchange that is intermediate on the NMR timescale. This results in broad signals for these carbonyls at room temperature. At higher temperatures the exchange becomes fast and the signals become sharp.[80] For a full explanation of the fluxional process occurring in **21** see reference 80.

$Os_5(CO)_{16}$ (29) The ^{13}C NMR spectrum of **(29)** in CD_2Cl_2 at room temperature shows a singlet at δ 176.0, which indicates rapid carbonyl exchange over the Os_5 frame. At -90 °C the spectrum contains two resonances (at δ 176.1 and δ 175.8) with an approximate intensity ratio of 10:6 which is consistent with the solid state structure of **29** (Figure 6.19). The signal at δ 176.1 was assigned to the 10 CO's found in the equatorial region of the structure. Rapid exchange of these carbonyls was expected since the plane contains two carbonyls with bridging character (C_a in Chart 6.3). As discussed previously, clusters with a bridging carbonyl generally undergo a rapid merry-go-round exchange in the plane containing this CO.[77] Coupled to the merry-go-round motion is the mutual CO exchange on the individual equatorial Os atoms that renders all of the carbonyls attached to them equivalent. It is known that 7 or 8 coordinate Os atoms are invariably nonrigid in solution.

The signal at δ 175.8 is assigned to the 6 CO ligands bound to the two apical $Os(CO)_3$ units (Figure 6.19). In the solid state structure these apical carbonyls are not equivalent due to their relation to the unique $Os(CO)_4$ unit found in the equatorial plane. As with **18** equivalence is brought about by carbonyl exchange in the equatorial plane. It

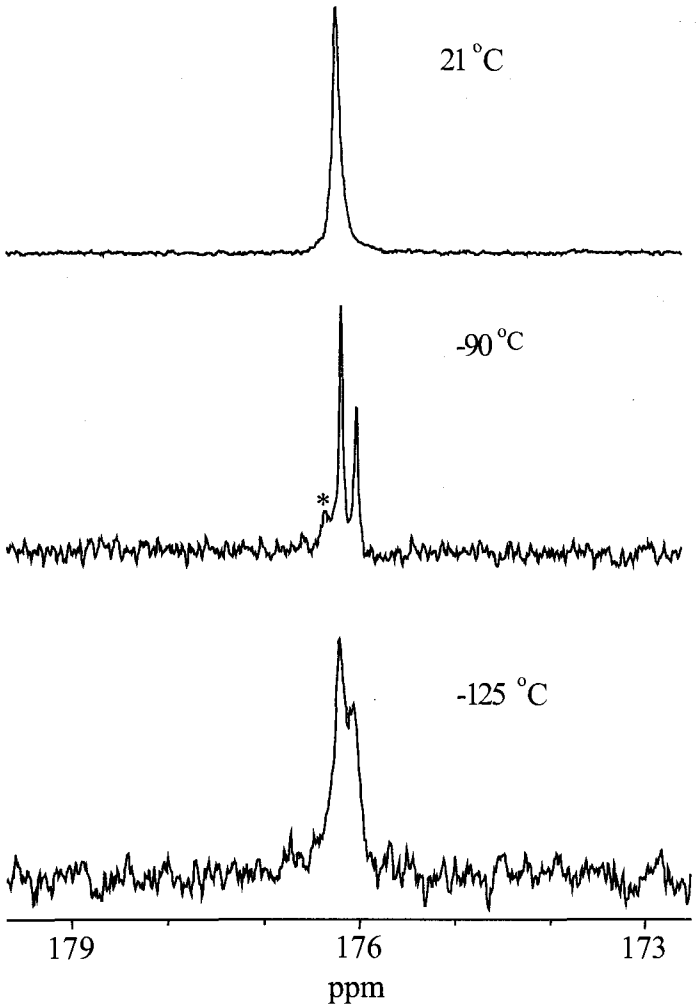

Figure 6.19. VT ^{13}C NMR spectra of $Os_5(CO)_{16}$. (It is uncertain if the peak marked with an asterisk (*) is genuine or an artifact produced by the spectrometer.)

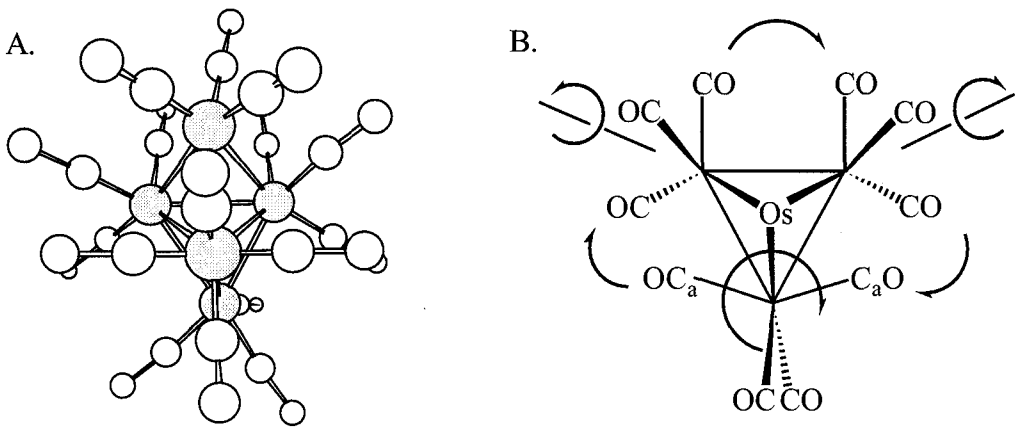

Chart 6.3. Structure of $Os_5(CO)_{16}$ and proposed carbonyl exchanges in the molecule.

could be accompanied by mutual exchange of CO ligands on the individual apical $Os(CO)_3$ units. The apical Os atoms are 6 coordinate and therefore the carbonyls attached to them may be stationary at -90 °C. This might be ascertained by studying the ^{13}C NMR spectrum of the apical isomer of $Os_5(CO)_{15}(PMe_3)$ at low temperature. The ^{13}C NMR spectrum of **29** at -125 °C in $CD_2Cl_2/CHFCl_2$ also has two resonances (at δ 176.2, 176.1) though the signals have broadened indicating that at least one of the exchange processes occurring at -90 °C had started to slow down.

$Ru_2Os(CO)_{12}$ (25). The ^{13}C NMR spectrum of ^{13}CO-enriched **25** in CH_2Cl_2/CD_2Cl_2 at 0 °C consisted of a singlet at δ 199.4 (Figure 6.20). In a brief note Koridze and coworkers also reported a singlet for the ^{13}C NMR spectrum of **25** at room temperature (no solvent was given).[170] The singlet was still sharp at -40 °C, which

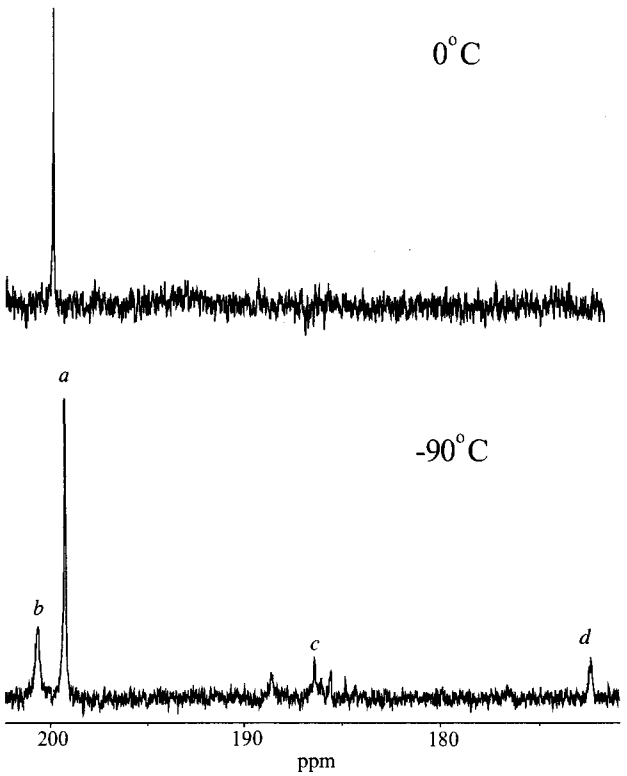

Figure 6.20. The ^{13}C NMR spectra of $Ru_2Os(CO)_{12}$ at 0 °C and -90 °C. (Other weaker signals are assumed to be due to impurities.)

indicates the carbonyls are still rapidly exchanging over all the metal atoms at this temperature. The ^{13}C NMR spectrum of **25** in CD_2Cl_2 at -90 °C showed four signals with the approximate intensity ratio 2:6:2:2. (The solubility of **25** at this temperature resulted in the lowered quality of the spectrum.) Mechanisms that are consistent with these observations are as follows. At room temperature and -40 °C (not shown) a merry-go-round CO exchange over both the RuOs and RuRu bonds occur, scrambling all the carbonyls to give the singlet. Rapid rotation of the Ru_2Os triangle in a rigid cage of 12 carbonyls would also achieve the same result. The spectrum at -90 °C is consistent with slowed exchange for the axial-equatorial merry-go-round CO exchange over the Ru-Os bond. It is not consistent with slowed rotation of the metal triangle within the carbonyl polyhedron. The broadness of the signals at this temperature suggests that the exchange over the Ru-Os bond has not completely stopped. The signal at δ 199.2 with an intensity of 6 is assigned to the 6 CO ligands undergoing the merry-go-round exchange across the Ru-Ru bond (carbonyls *a* in Chart 6.4).[m] This leaves a CO on each Ru atom (CO ligands labelled *b* in Chart 6.4) that are no longer undergoing exchange. These two equivalent carbonyls give rise to the low field resonance at δ 200.6 which has an intensity of 2 as expected. (Resonances of carbonyls bound to Ru occur further downfield than those on Os.[78]) Because resonances of axial carbonyls on Os clusters appear at a lower field than those of equatorial carbonyls, the signal at δ 186.4 is assigned to the two axial carbonyls

[m] The structure of **25** shown in Chart 6.4 is based on the unpublished crystal structure by J. Logan and R. K. Pomeroy at Simon Fraser University, and G. P. A. Yap at the University of Ottawa.

on Os. The resonance at δ 172.4 is therefore attributed to the two equivalent equatorial CO groups on Os (carbonyls *c* and *d* in Chart 6.4).[78]

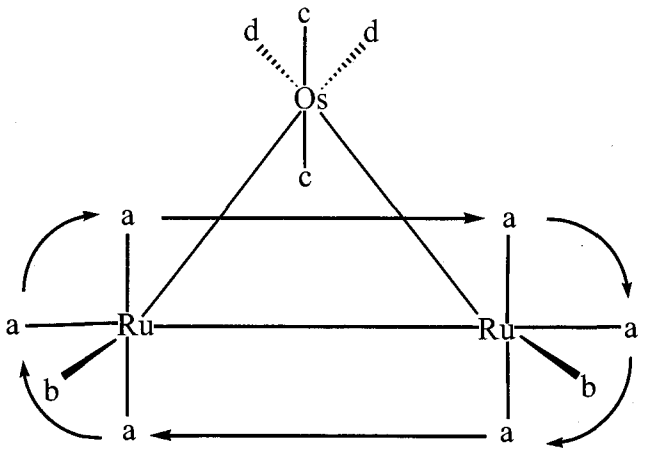

Chart 6.4. Mode of carbonyl exchange in $Ru_2Os(CO)_{12}$ at -90 °C.

As mentioned previously, the results presented here are not in agreement with Johnson's cluster rotation in CO shells.[163a] If cluster rotation inside the rigid carbonyl shell stopped one would expect decoalescence to a 4:2:2:2:2 pattern.[163b] The first three signals are due to three types of carbonyls on the Ru atoms and the remaining signals are due to the axial and equatorial CO's on Os. It is noted here that axial-equatorial merry-go-round CO exchanges are clearly indicated in $Os_3(CO)_{11}[P(OMe)_3]$ [57] and (in unpublished studies in the Pomeroy laboratory) other $Os_3(CO)_{11}PR_3$ clusters.

$RuOs_2(CO)_{12}$ (23) The ^{13}C NMR spectrum of ^{13}CO-enriched **23** at room temperature exhibits two signals with an approximate intensity ratio of 10:2 (Figure 6.21). This observation is consistent with the view that axial-equatorial merry-go-round CO exchange takes place and that the barrier to exchange over an OsOs bond is greater than that across a RuOs bond (Chart 6.1).[164,171] As can be seen from Chart 6.5, merry-go-round exchanges across the RuOs metal bonds equilibrates ten of the carbonyls (labelled

a and *b*) to give rise to the broad signal at δ 186.8. At -50 °C this signal has collapsed into the baseline, which indicates the exchange is slowing on the NMR time scale. The

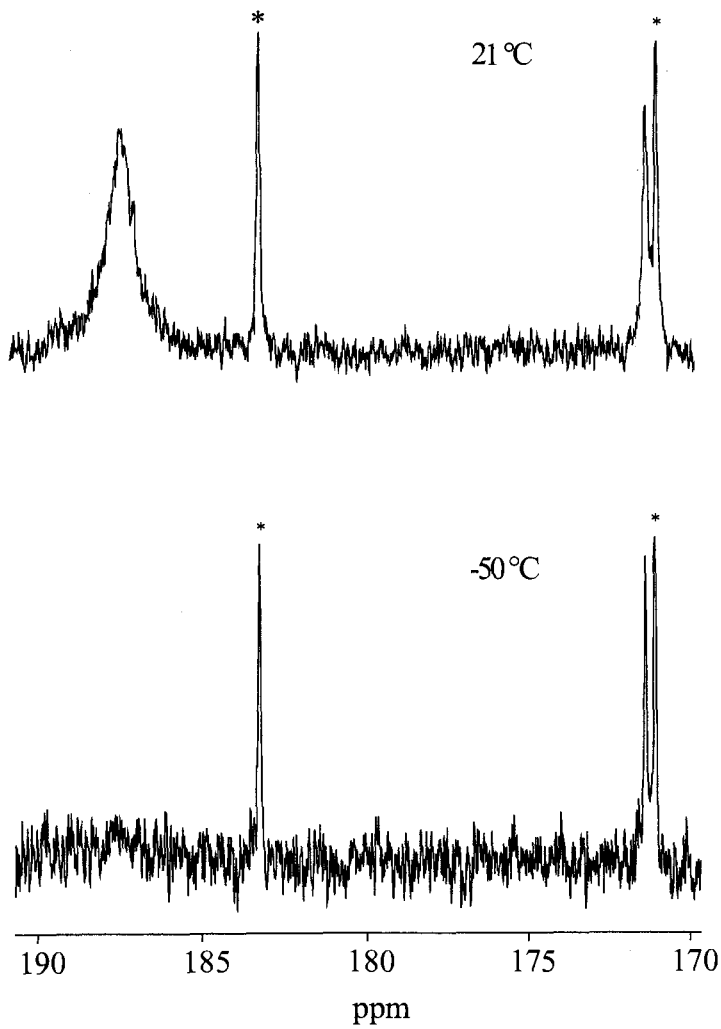

Figure 6.21. The ^{13}C NMR spectra of $RuOs_2(CO)_{12}$ at 21 °C and -50 °C (* = $Os_3(CO)_{12}$).

merry-go-round exchange over the Ru-Os bonds excludes one equatorial CO (carbonyls *c* in Chart 6.5) on each Os atom. These two carbonyls do not undergo exchange and therefore give rise to the sharp signal at δ 171.0 at room temperature. This is the region

at which the resonances of equatorial carbonyls occur.[57] At -50 °C the signal remains sharp at δ 171.3 as expected.

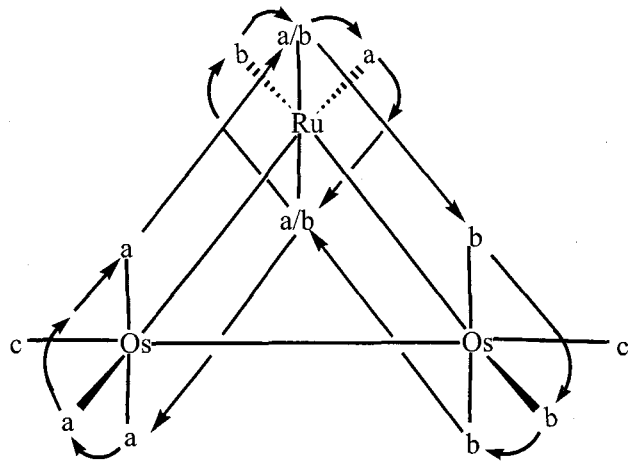

Chart 6.5. Mode of carbonyl exchange in $RuOs_2(CO)_{12}$ at -55 °C.

Koridze *et al.* has examined the ^{13}C NMR spectrum of **23** at higher temperature. They reported that at 70 °C the two signals seen at room temperature coalesced into the baseline. As the temperature was raised to 105 °C a broad signal at δ 183.9 was obtained which sharpened, as the temperature was increased to 145 °C. (The solvent used was not reported and the spectrum below room temperature was also not investigated.) The insolubility of **23** below -50 °C prevented its study by ^{13}C NMR spectroscopy at lower temperatures. The spectrum at lower temperature is predicted to contain a 4:2:2:2:2 resonance pattern, as would be predicted by both the merry-go-round and cluster rotation in a CO shell mechanisms for CO exchange.[163b] (see section above)

Merry-go-round exchange. The energy barrier for CO transfer across a metal-metal (M-M) bond (M = Fe, Ru, Os) via an axial-equatorial merry-go-round exchange (Chart 6.1 above)[57] increases as the principal quantum number of the metals involved in the M-M bond increases.[164,171] The CO exchange over an Fe-Fe bond (a 3d metal) has a

lower barrier than across an Os-Os bond (5d metal).[164,171] The ^{13}C NMR spectrum of $Fe_3(CO)_{12}$ indicates that the carbonyls are still exchanging rapidly at -150 °C. On the other hand, a temperature above +50 °C is required for the exchange on $Os_3(CO)_{12}$ to be observable and a temperature of ~100 °C is required for coalescence of the signals due to the axial and equatorial carbonyls.[163b,g] This difference can be explained through an extension of arguments used by Hunstock *et al.* and Braga *et al.* to explain why $Fe_3(CO)_{12}$ contains bridging carbonyl ligands while $M_3(CO)_{12}$ (M = Ru, Os) does not.[171a,b] The difference to the energy barrier to CO exchange via the merry-go-round mechanism is due to the degree of orbital repulsion experienced between the two metal centers when the CO is in a bridging mode.[164,171] When carbonyls exchange in an axial-equatorial merry-go-round manner (Chart 6.1) two initially terminal carbonyls form bridges in the intermediate. In order for a carbonyl ligand to bridge two atoms the π^* orbital on the CO (which is part of the back donation element of the M-CO bond) must interact with orbitals on both metals. For this overlap to occur the orbitals on the metal centers must be of opposite phases, but this anti-bonding arrangement of the metal orbitals is repulsive (Figure 6.22). The degree of repulsion increases going from 3d to 5d metals. Because the axial-equatorial merry-go-round mechanism includes bridging carbonyls, as the repulsive interaction increases so will the barrier to CO exchange.[164,171] In a mixed metal system such as **25** and **23** the M-M bond that contains the metal with the largest principal quantum number will have the largest barrier to an axial-equatorial merry-go-round CO exchange. The fluxional process across this M-M bond will be the first to cease as the temperature is lowered.[164,171] This is clearly illustrated in the low temperature ^{13}C NMR spectra of **25** and **23** presented above.

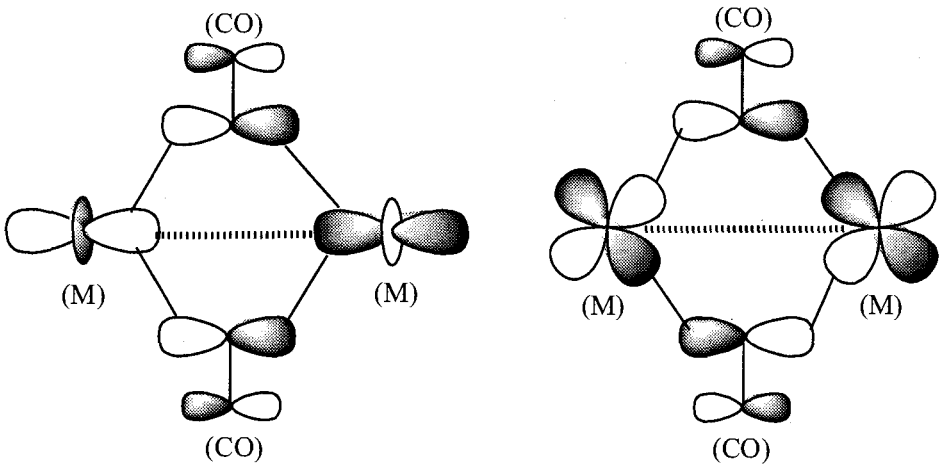

Figure 6.22. Overlap of the d orbital on M (M= Fe, Ru, Os) with the in-phase and out-of-phase combinations of the π^* orbital of CO.

6.4 Experimental Section

The general procedure used for the synthesis and analysis has been described in the Experimental Section of Chapter 2. The EDX and SEM studies were obtained on a FEI Dual Beam Field Emission SEM with focused Ion Beam at Simon Fraser University. The XRD data was obtained on a Ragaku X-ray diffraction spectrometer at Simon Fraser University. In this section the preparations of $Os(CO)_4(H)_2$,[112] $Os_3(CO)_{12}$,[91] $Os_3(CO)_{10}(\mu\text{-}Cl)_2$, $Os_4(\mu\text{-}H)_4(CO)_{12}$,[109] $Os_3(CO)_{10}(CH_3CN)_2$,[91] $Ru(CO)_5$[90] and $Ru_3(CO)_{12}$ were carried out by literature procedures. The ^{13}CO-enriched Ru compounds were synthesized from ^{13}CO-enriched $Ru_3(CO)_{12}$ (~ 35% ^{13}C); ^{13}CO-enriched $Os_6(CO)_{18}$ was synthesized from ^{13}CO-enriched $Os_3(CO)_{12}$ (~ 35% ^{13}C).[57,150] The ^{13}CO-enriched sample of $RuOs_2(CO)_{12}$ was synthesized from ^{13}CO-enriched $Ru_2Os(CO)_{12}$. This was produced by employing the method used to enrich $Os_3(CO)_{12}$ except 2 atm of ^{13}CO was used and the solution was heated at 115 °C for 24 hours.

The use of $Os(CO)_5$ as a tool for the stepwise increase in the nuclearity of osmium clusters is well documented.[7,8,104,111b,136b] For example, $Os(CO)_5$ is required for most of the starting material used to produce the compounds presented in this thesis. The concentration of $Os(CO)_5$ is generally not accurately known (a result of how it is made) and therefore an excess of $Os(CO)_5$ is usually used in reactions. As part of this study the molar absorptivity (extinction coefficient) (ε) of $Os(CO)_5$ was determined. By use of Beer's Law, the concentration of $Os(CO)_5$ can now be calculated once the absorbance is determined by IR spectroscopy.[172]

Molar absorptivity (extinction coefficient) (ε) of $Os(CO)_5$ **[Warning:** Given the known toxicity of $Fe(CO)_5$, $Os(CO)_5$ should be handled with extreme caution.] A sample of the volatile $Os(CO)_5$ in hexane was vacuum transferred from a round bottom flask to a Schlenk tube, in order to obtain pure $Os(CO)_5$ in hexane. A volumetric pipette was used to transfer a 10 mL aliquot of this sample to a flame-dried Carius tube. The tube was cooled to -196 °C and degassed with three freeze-pump-thaw cycles. The vessel was sealed under vacuum and heated overnight at 120 °C which resulted in the complete conversion of $Os(CO)_5$ to $Os_3(CO)_{12}$ and CO. Upon completion of the reaction the solution was vacuum transferred to a Schlenk tube and the IR spectrum examined to verify the absence of $Os(CO)_5$. The remaining $Os_3(CO)_{12}$ was collected, dried on the vacuum line and weighed. This weight was used to calculated the initial concentration (c) of $Os(CO)_5$ in solution.

Another aliquot of the purified solution of $Os(CO)_5$ in hexane was used to determine the absorbance (A) of $Os(CO)_5$. By use of Beer's Law ($(A = cl\varepsilon)$ (l = path length, which was set at 0.1 cm)) the molar absorptivity was calculated. The above

procedure was then repeated with a new sample of $Os(CO)_5$. The mean molar absorptivity from the two runs are: For ν(CO) 2035 cm^{-1}, ε = 440 $M^{-1}cm^{-1}$ (433, 447); ν(CO) 1993 cm^{-1}, ε = 597 $M^{-1}cm^{-1}$ (601, 593). (The values in brackets are the values from the two determinations.)

Improved Preparation of $Ru_6(\mu_6\text{-}C)(CO)_{17}$ (18) and preparation of a ruthenium carbide RuC (19) To a flame-dried Carius tube was added $Ru_3(CO)_{12}$ (25 mg, 0.039 mmol) and C_6F_6 (15 mL). The solution was degassed with three freeze-pump-thaw cycles and the vessel sealed under vacuum. The reaction mixture was heated overnight at 150 °C for 18 h during which time the solution changed from orange to dark brown with a metallic mirror coating the wall of the Carius tube in contact with the solution. The solution was evaporated to dryness and the resulting solid was subject to chromatography on a silica gel column (1 x 10 cm). Elution with hexane gave the desired product, **18**. Analytically pure sample was obtained by recrystallization in CH_2Cl_2 (21 mg, 84%). IR (hexane) ν(CO) 2066 (vs), 2047 (vs), 2002 (vw), 1844 (vw) cm^{-1}; ^{13}C NMR (CD_2Cl_2/CH_2Cl_2, RT) δ 196.9 (17C); ^{13}C NMR ($CD_2Cl_2/CHFCl_2$, -25 °C) δ 197.4 (17 C); ^{13}C NMR ($CD_2Cl_2/CHFCl_2$, -55 °C) δ 197.3 (broad, 17C); ^{13}C NMR ($CD_2Cl_2/CHFCl_2$, -95 °C) δ 200.1 (broad, 11C), 191.7 (broad, 6C); ^{13}C NMR ($CD_2Cl_2/CHFCl_2$, -125 °C) δ 453.7 (1C), 199.9 (11C), 191.2 (6C).

In another reaction, $Ru_3(CO)_{12}$ (50 mg, 0.078 mmol) and C_6F_6 (50 mL) was added to a flame-dried Carius tube. The solution was degassed with three freeze-pump-thaw cycles and the vessel sealed under vacuum. The reaction mixture was heated for 4 d at 200 °C (and degassed daily) during which time the solution changed from an orange through a dark brown to a pale brown colour. The Carius tube once again had a metallic

mirror, with the solution containing an insoluble homogenous dark grey solid. The solution was decanted and the solid collected. It was washed with CH_2Cl_2 (2 x 10 mL) and dried on the vacuum line resulting in a ruthenium carbide (**19**) with a Ru to C ratio corresponding to RuC (23 mg, 86%). IR (KBr) 2066 (s), 1999 (s); 1126 (s, broad), 1096 (s, broad) cm^{-1}; Anal. Calcd for **19**: C, 10.60; H, 0.00. Found: C, 10.14; H, 0.00; EDX (see Table 6.2/6.3 in Results and Discussion section.)

Preparation of $Ru_5(CO)_{16}$ (20) To a 250 mL round-bottom flask capped with a water cooled condenser was added $Ru_3(CO)_{12}$ (200 mg, 0.313 mmol) and $C_{10}F_{18}$ (50 mL, *cis/trans* mixture of perfluorodecalin) While this mixture was heated at 125 °C a steady stream of N_2 was bubbled through the solutions. After 10 h at these conditions the original orange solution had turned black and was decanted from a black decomposition product that had formed. The solution was evacuated to dryness and the remaining solid was recrystallized from hexane to give a black precipitate of **20** (~ 5 mg, ~3%). IR (hexane) ν(CO) 2076 (w), 2068 (vs), 2044 (vs) cm^{-1}.

In another preparation similar conditions were employed except ^{13}C labelled $Ru_3(CO)_{12}$ (30 mg, 0.047 mmol) and $C_6H_4Cl_2$ (1,2-dichlorobenzene) (20 mL) were added to the round-bottom flask, which was heated at 110 °C for 10 h. Upon completion of the reaction the solution was decanted from the decomposition material and evaporated. The remaining solid was immediately analyzed by ^{13}C NMR spectroscopy. The spectra showed a mixture of $Ru_3(CO)_{12}$, $Ru_6(\mu_6\text{-}C)(CO)_{17}$ (**18**) and **20**: ^{13}C NMR (CD_2Cl_2, RT) δ ~ 199.4 ($Ru_3(CO)_{12}$), 197.0 (**18**), ~195.0 (v. broad); ^{13}C NMR (CD_2Cl_2, -90 °C) δ 197.7 (~10 C), 188.8 (~ 6 C); δ 200.9, 192.6: (**18**); δ 199.6: $Ru_3(CO)_{12}$.

Due to the unstable nature of this cluster all further attempts to fully characterize and isolate a pure sample of **20** were unsuccessful.

Improved preparation of $Os_6(CO)_{18}$ (21) and preparation of 22 A large (500 mL) flame-dried Carius tube with dry $Os_3(CO)_{12}$ (500 mg, 0.552 mmol) and dry C_6F_6 (50 mL) was heated at 175 °C for 26 d. (At higher temperature the reaction proceed more rapidly though the yield suffers.) The solution was degassed twice daily, during which time the initial yellow solution turned black and an insoluble homogenous dark grey material (with a metallic lustre) was produced. The solvent was then removed on the vacuum line. In order to redissolve **21**, CH_2Cl_2 was added to the solid and this mixture was passed through silica gel isolating a grey material (**22**). The collected solution was evaporated to dryness on the vacuum line to produce a clean sample of **21** (308 mg, 68 %). (The compound was pure by its IR spectrum and was used in other syntheses without further purification.) Crystallization can be accomplished by dissolving **21** in a minimum amount of CH_2Cl_2 with an equal amount of hexane and placing it in the freezer (at -29 °C). This produces dark brown crystals of **21**. IR (hexane) ν(CO) 2100 (w), 2076 (vs), 2063 (vs), 2039 (s) 2031 (m); ^{13}C NMR (CD_2Cl_2, RT) δ 181.9 (broad, 6 C), 179.3 (6 C), 177.3 (broad, 6 C); MS (LSIMS) *m/z* 1645.4 (M^+) (calcd for M^+ = 1645 (93.2 %), 1646 (100%)).

The grey material (**22**) that was isolated in the filtration step was collected and washed with CH_2Cl_2 (3 x 10 mL) and dried on the vacuum line. IR (KBr) 2129 (m), 2043 (vs), 1992 (w), 1989 (w), 1968 (w), 1964 (w); 1091 (m, broad), 1080 (m, broad) cm^{-1}; Anal. Calcd. for OsC: C, 5.94. Found C, 5.78. For the EDX results see Table 6.6 in the Results and Discussion section.

Improved preparation of $RuOs_2(CO)_{12}$ (23) and preparation of $[Ru(CO)_4]_n$ (24) To a flame-dried Carius tube was added $Ru_2Os(CO)_{12}$ (**25**) (20 mg, 0.027 mmol) and C_6F_6 (10 mL). The tube was cooled to -196 °C and the solution degassed with three freeze-pump-thaw cycles and the vessel sealed under vacuum. The reaction mixture was heated for 4 h at 140 °C during which time the initial yellow/orange solution turned brown with a black solid (**24**) deposited on the Carius tube at the reflux ring. In another attempt the same conditions were employed except 15 mL of C_6F_6 was used. After 2.5 h there was no reaction by IR spectroscopy. When ~5 mL of solvent was removed on the vacuum line and the solution heated again the reaction occurred as described above. After the completion of the reaction the solution was transferred to a Schlenk tube and evaporated on the vacuum line. The resulting solid was recrystallized from CH_2Cl_2 to give **23** (4 mg, 35%) as spectroscopically-pure air-stable orange crystals: (The compound was identified as **23** by IR,[22] mass and ^{13}C NMR spectroscopy at room temperature.) IR (hexane) ν(CO) 2066 (vs), 2035 (vs), 2018 (sh), 2014 (m), 2004 (m) cm^{-1}; ^{13}C NMR (CD_2Cl_2, RT) δ 186.8 (broad, 10 C), 171.0 (2 C); ^{13}C NMR (CD_2Cl_2, -50 °C) δ 171.3 (2 C); MS (LSIMS) *m/z* 817.6 (M^+) (calcd for M^+ = 818 (100%), 817 (90%)).

The black solid which deposited on the wall of the Carius tube was washed with CH_2Cl_2 (2 x 10 mL) and dried on the vacuum line to give **24**: MS (LSIMS) *m/z* 853.6 (M^+) (calcd for $Ru_4(CO)_{16}$ = 854 (100%), 853 (96%)).

New preparation of $Ru_2Os(CO)_{12}$ (25)[n] To a solution of $Ru(CO)_5$ (~0.2 mmol) in hexane (6 mL) was added $Os(CO)_5$ (0.2 mmol) in hexane (10 mL) and the resulting

[n] First carried out by Dr. A. Becalska at S.F.U.

solution stirred at room temperature for 4 h, with the exclusion of light. The solution was then evaporated to dryness and the resulting solid recrystallized from toluene. The analytical sample of **25** was obtained in a greater than 95% yield as air-stable, yellow/orange crystals: (The compound was identified as **25** by IR, C/H/N analysis, X-ray structure and mass spectroscopy.[o]) IR (hexane) ν(CO) 2063 (vs), 2033 (vs), 2019 (sh), 2014 (m), 2007 (m) cm^{-1}; ^{13}C NMR (CD_2Cl_2, 0 °C) δ 199.4; ^{13}C NMR (CD_2Cl_2, -90 °C) δ 200.6 (6C), 199.2 (2C), 186.4 (2C), 172.4 (2C); MS (LSIMS) *m/z* 728.6 (M^+) (calcd for M^+ = 729 (100%), 728 (90.6%)); Anal. Calcd for $C_{12}O_{12}OsRu_2$: C, 19.78. Found: C, 19.89.

Preparations of $Ru_2Os_3(CO)_{16}$ (26) and $RuOs_4(CO)_{16}$ (27) To a flame-dried Carius tube was added $Ru_2Os(CO)_{12}$ (20 mg, 0.027 mmol) and C_6F_6 (10 mL). The tube was cooled to -196 °C and the solution degassed with three freeze-pump-thaw cycles and the vessel sealed under vacuum. The reaction mixture was heated for two 10-h periods at 140 °C during which time the initial yellow/orange solution turned brown with a black deposited on the side of the Carius tube at the reflux ring (assumed to be **24**). Every 2 h the solution was degassed with three freeze-pump-thaw cycles and the vessel sealed under vacuum and heated. After completion of the reaction the solution was transferred to a Schlenk tube and the solvent removed on the vacuum line. The resulting solid was subjected to chromatography on a silica gel column (1.5 x 14 cm). Elution with hexane (100%) gave an orange/brown band which contained a mixture of the desired products (~2 mg) as well as a trace amount of $Os_5(CO)_{16}$.[44] (The IR and mass spectra given are

---

[o] The mass spectrum, C/H/N and X-ray structure samples were prepared by Ms. J. Logan at Simon Fraser University.

from a mixture of the products) IR (hexanes) ν(CO) 2080 (w), 2066 (vs), 2046 (s, broad) cm^{-1}; MS (LSIMS) **26** *m/z* 1222 (M^+) (calcd for $Ru_2Os_3(CO)_{16}$ = 1222 (100%), 1221 (95.3%)), MS (LSIMS) **27** *m/z* 1312 (M^+) (calcd for $RuOs_4(CO)_{16}$ = 1310 (100%), 1312 (98.9%)).

New preparation of $Os(CO)_5$ To a high pressure metal bomb (200 mL) with a glass liner was added hexane (50 mL), $Os_3(CO)_{10}(\mu\text{-}Cl)_2$ (466 mg, 0.506 mmol) and an excess of previously flame dried zinc powder. Three times the autoclave (bomb) was pressurized to 500 psi of CO and vented, to remove air. The reaction vessel was then pressurized to 1150 psi and heated overnight at 180 °C. At this time the reaction was allowed to return to room temperature before the bomb was vented. The solution was transferred to a round bottom flask and the $Os(CO)_5$ product was vacuum distilled into a trap cooled to -196 °C. From the absorbance of an accurately diluted sample the yield of the $Os(CO)_5$ was 33%. The purity of the $Os(CO)_5$ solution was determined by IR spectroscopy: IR (hexane) ν(CO) 2035 (s), 1993 (s) cm^{-1}.[90] There was a trace of $Os(CO)_4(H)_2$: IR (hexanes) ν(CO) Os: 2067 (m), 2056 (s), 2050 (vs) cm^{-1}.[112] The remaining solid was found to consist of $Os_3(CO)_{12}$, a trace amount of chlorinated products[154,155] and zinc/$ZnCl_2$. Without the addition of Zn to the reaction a large amount of $Os_2(CO)_8(Cl)_2$ was produced.

Improved preparation of $Os_4(CO)_{14}$ To a solution of $Os_3(CO)_{10}(CH_3CN)_2$ (prepared from 200 mg, 0.214 mmol of $Os_3(CO)_{12}$) in CH_2Cl_2 (20 mL) was added an excess of $Os(CO)_5$ in hexane. The resulting solution was stirred at room temperature for 4 h, then stored at -29 °C overnight to precipitate $Os_4(CO)_{15}$. The mother solution was decanted and the remaining dark red-green solid was washed with two 15 mL portions of

hexane and then dried to give pure $Os_4(CO)_{15}$ (140 mg, 55%): IR (hexane) ν(CO): 2086 (s), 2073.5 (m), 2045 (vs), 2023 (m), 2002 (sh), 1939 (m, br) cm^{-1}.[29,36] To a round-bottom flask (250 mL) equipped with a water-cooled reflux condenser was added $Os_4(CO)_{15}$ (90 mg, 0.076 mmol) in toluene (40 mL). The solution was heated to 90 °C and nitrogen bubbled through it for 3.5 h. The solution was transferred to a Schlenk tube and the volume of toluene was reduced to ~ 30 mL and stored overnight at -29 °C to yield crystals of $Os_4(CO)_{14}$. The solution was removed from the crystals that were washed with hexane (2 x 15 mL) and dried to give pure $Os_4(CO)_{14}$ (76 mg, 86%) as brown crystals that are air stable: IR (hexane) ν(CO): 2058 (s, br), 2018 (m, br) 1938 (vw, br) cm^{-1}.[31]

Preparation of $Os_4(\mu\text{-}H)(\mu\text{-}OH)(CO)_{13}.H_2O$ (28) and $Os_5(CO)_x$ (x = 16 (29), 19 (30)) A flame-dried Carius tube with solid $Os_4(CO)_{14}$ (25 mg, 0.022 mmol) was heated at 125 °C for 24 hours. An IR spectrum of the solid in hexane showed the products to be $Os_3(CO)_{12}$ and $Os_5(CO)_{16}$ (**29**) (in a 1:1 ratio) as well as a trace amount of **28** and $Os_6(CO)_{18}$. The same products were isolated when the pyrolysis was carried out in 10 mL of C_6F_6. Upon completion of the reaction, the mixture was subject to chromatography on a silica gel column (1.5 x 16 cm). Elution with hexane gave $Os_3(CO)_{12}$ (~5 mg, ~50%), $Os_5(CO)_{16}$ (~8 mg, ~50 %) and $Os_6(CO)_{18}$ (trace). Subsequent elution with hexane/CH_2Cl_2 (10:90) gave product **28** in a trace amount. The analytical sample of $Os_5(CO)_{16}$ was obtained as air-stable, pink/red crystals by recrystallization from CH_2Cl_2: ^{13}C NMR (CD_2Cl_2, RT) δ 176.0; ^{13}C NMR (CD_2Cl_2, -90 °C) δ 176.1 (10C), 175.8 (6C); ^{13}C NMR ($CD_2Cl_2/CHFCl_2$, -125 °C) δ 176.2, 176.1.

In another preparation $Os_4(CO)_{14}$ (10 mg, 0.0087 mmol) and C_6F_6 (10 mL) was added to a flame-dried quartz Carius tube. The solution was degassed with three freeze-pump-thaw cycles and the vessel sealed under vacuum. It was subjected to ultraviolet irradiation overnight (200 W Hanovia lamp; ~3cm between source and edge of reaction vessel). The solvent was removed on the vacuum line and the remaining solid was subjected to chromatography on a silica gel column (1.5 x 16 cm). Elution with hexane gave $Os_3(CO)_{12}$ and $Os_5(CO)_{19}$ (not in a 1:1 ratio). Subsequent elution with hexane/CH_2Cl_2 (10:90) gave **28** as a trace amount. (The amount of product obtained was not determined although the yields were low.)

Preparation of $Os_4(\mu_4\text{-}C)_2(CO)_{12}$ (31) To a flame-dried Carius tube was added $Os_6(CO)_{12}$ (25 mg, 0.039 mmol), $Os_4(\mu\text{-}H)_4(CO)_{12}$ (5 mg, 0.005 mmol), C_{60} (buckminster-fullerene) (1mg, 0.001 mmol) (or ~20 mg of flame-dried, activated graphite) and C_6F_6 (15 mL). This mixture was heated for 5 d at 230 °C. The solution was degassed daily with three freeze-pump-thaw cycles and the vessel sealed under vacuum. There were no obvious changes from the initial black solution except the development of an insoluble back coating on the side of the Carius tube. Upon completion of the reaction the solution was evaporated to dryness and the resulting solid was subjected to chromatography on a silica gel column (1 x 10 cm). The column was initially flushed with hexane to remove unreacted $Os_6(CO)_{18}$ and $Os_4(\mu\text{-}H)_4(CO)_{12}$. Elution with hexane/$CH_2Cl_2$ (90:10) gave a peach coloured band. This was collected and the solution evaporated to dryness. The remaining solid was washed with two 10 mL portions of hexane and dried on the vacuum line to give a pure sample of **31** (< 1mg, < 6%). Small black crystals were obtained by recrystallization from toluene: IR (hexane)

ν(CO) 2101 (w), 2075 (vs), 2039 (s), 2029 (vs) cm^{-1}; MS (LSIMS) *m/z* 1121.0 (M^+) (calcd for M^+ = 1122 (100%), 1121 (85.7%)).

Chapter 7. $Os_4(\mu\text{-}H)(\mu\text{-}OH)(\mu\text{-}CO)(CO)_{12}$ and $Os_4(\mu\text{-}H)(\mu\text{-}OD)(\mu\text{-}CO)(CO)_{12}$

7.1. Introduction

In the study of the pyrolysis (and photolysis) of $Os_4(CO)_{14}$ (Chapter 6) trace amounts of a compound were isolated that were tentatively identified as $Os_4(H_2O)(CO)_{13}$ by mass spectrum. No doubt this complex arose from the reaction of $Os_4(CO)_{14}$ with adventitious water in the reaction vessel (e.g., from water adsorbed on the walls of the reaction vessel). Deliberately adding water to the pyrolysis reaction did not however increase the yield of this product.

In this chapter a rational synthesis and characterization of $Os_4(\mu\text{-}H)(\mu\text{-}OH)(\mu\text{-}CO)(CO)_{12}$ (**28**) is reported. The solid state structure of **28** as the hydrate (i.e., **28.H_2O**) is a rare example of a structure with a water molecule interacting with a carbonyl ligand through hydrogen bonding. The first example of hydrogen bonding between a molecule of water of crystallization and a terminal carbonyl ligand was reported in 1992.[173] A search of the Cambridge Structural Database (CSD) revealed only 25 examples of crystalline hydrates with a water molecule bound to carbonyl ligands of transition metals.[173,174] These examples contain a total of 49 interactions of which 25 involve H_2O and a bridging CO. Of the reported examples, none studied the effect of substitution of H_2O with D_2O.

During the investigation of the partially deuterated analogue of **28** (i.e. $Os_4(\mu\text{-}H)(\mu\text{-}OD)(\mu\text{-}CO)(CO)_{12}$; **32**) it was noticed that the bridging CO stretch in the solid state IR spectrum of **32** was much weaker than that in **28**. This prompted a determination of the crystal structure of **32** that revealed it did not contain D_2O of crystallization. This

chapter reports the details of this study. It appears to be the first study of a hydrated metal carbonyl complex examined in both the H and D forms (from literature searches of the CSD and by SciFinder Scholar).

7.2. Results and Discussion

$Os_4(\mu\text{-}H)(\mu\text{-}OH)(\mu\text{-}CO)(CO)_{12}$ (28) Dropwise addition of Me_3NO (in CH_2Cl_2) to $Os_4(CO)_{14}$ in CH_2Cl_2 at room temperature over 5.25 hours afforded the new cluster $Os_4(\mu\text{-}H)(\mu\text{-}OH)(\mu\text{-}CO)(CO)_{12}$ (**28**) in a 40% yield after column chromatography (eq 7.1). Although the Me_3NO was sublimed before use it is believed that it still contained

$$Os_4(CO)_{14} + Me_3NO \xrightarrow{H_2O} \underset{\mathbf{28}}{Os_4(\mu\text{-}H)(\mu\text{-}OH)(\mu\text{-}CO)(CO)_{12}} \qquad (7.1)$$

some water of crystallization and this is the source of the H_2O in the product. The compound was isolated as air-stable, yellow crystals by crystallization from CH_2Cl_2. It was characterized by IR spectroscopy (Figure 7.1), mass spectroscopy (parent ion), C/H/N analysis, ^1H and ^{13}C NMR spectroscopy and X-ray crystallography (as the hydrate, **$28.H_2O$**). The elemental analysis was determined on a sample that had been dried overnight on the vacuum line and analyzed as the unhydrated form.

The molecular structure of **28** (Figure 7.2)[p] has a butterfly arrangement of Os atoms with the O atom of the OH group bridging the wingtip atoms. This type of structure is found in $Os_4(\mu\text{-}H)_3(\mu\text{-}X)(CO)_{12}$ (X = OH, OPO_3H_2, NO),[175] $Os_4(\mu\text{-}H)_3(\mu\text{-}I)(CO)_{12}$[176] and $[Os_4(\mu\text{-}H)_4(\mu\text{-}OH)(CO)_{12}]^+$.[177] The Os...Os vector of the Os(μ-OH)Os in **28** is calculated to be 3.44 Å which is clearly nonbonding. The OsOs lengths of **$28.H_2O$**

---

[p] Determined by Dr. G. P. A. Yap at the University of Ottawa.

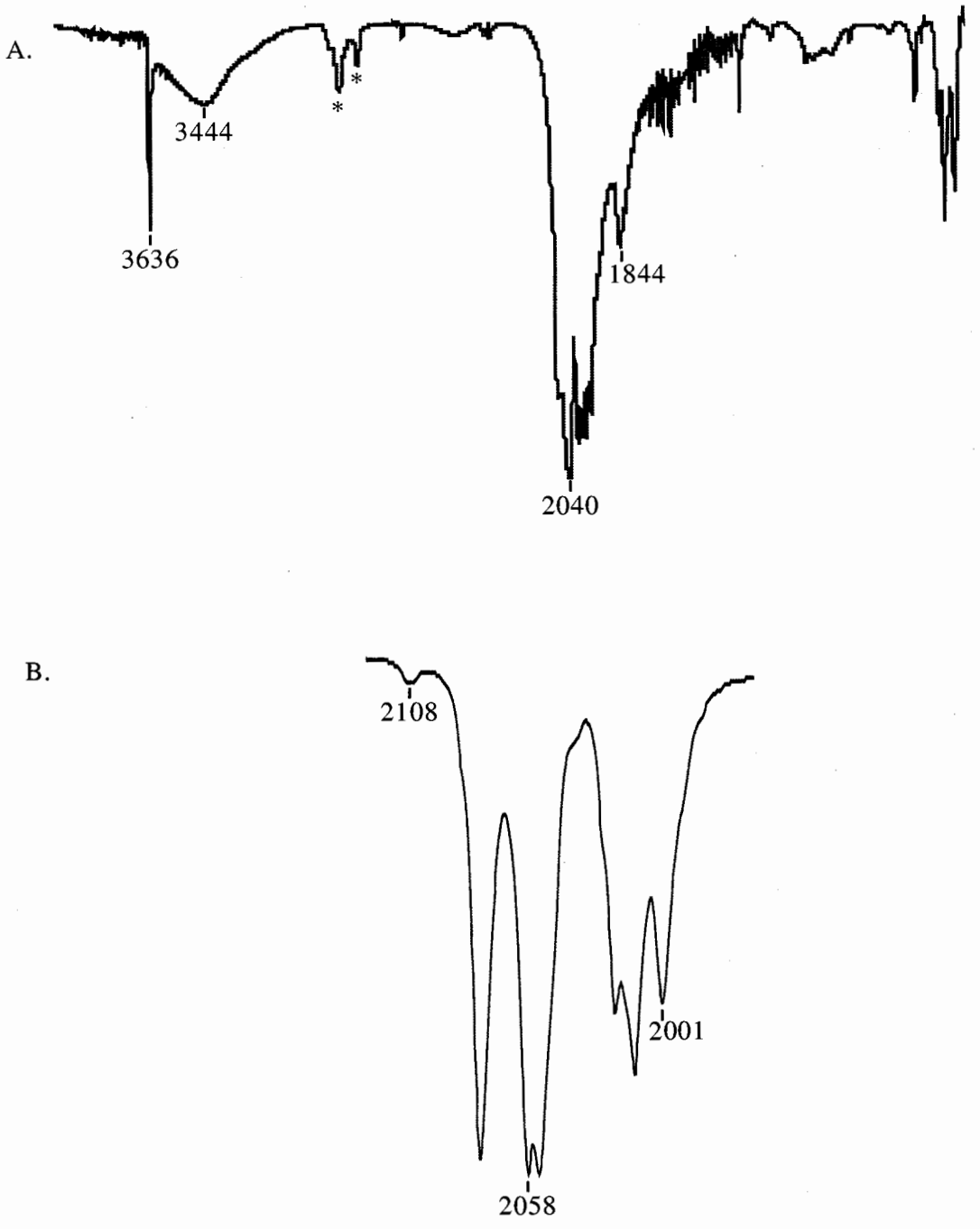

Figure 7.1. (A) IR spectrum (KBr disk) of $Os_4(\mu\text{-}H)(\mu\text{-}OH)(\mu\text{-}CO)(CO)_{12}$ (**28**). (B) IR spectrum (hexane; ν(CO) region) of **28**. (No CO stretches below 1800 cm^{-1}).

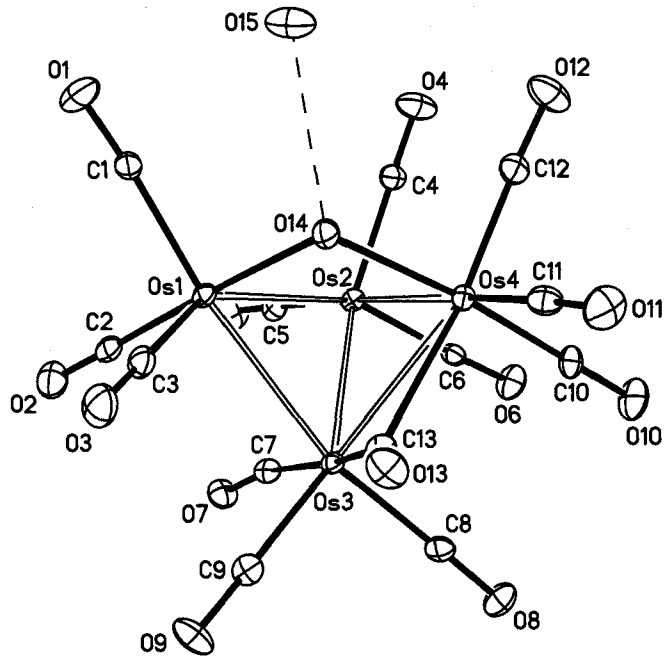

Figure 7.2. The molecular structure of $Os_4(\mu\text{-H})(\mu\text{-OH})(\mu\text{-CO})(CO)_{12}.H_2O$ (**28.H_2O**). The O15 is from the H_2O of crystallization; the H ligand bridges the Os(1)Os(2) bond.

Table 7.1. Bond lengths (Å) and angles (°) for $Os_4(\mu\text{-H})(\mu\text{-OH})(\mu\text{-CO})(CO)_{12}.H_2O$ (**28.H_2O**) and $Os_4(\mu\text{-H})(\mu\text{-OD})(\mu\text{-CO})(CO)_{12}$ (**32**).

Bond Lengths

28.H_2O		**32**	
Os(1)-Os(2)	2.9701(5)	Os(1)-Os(2)	2.9482(8)
Os(1)-Os(3)	2.8343(5)	Os(1)-Os(3)	2.8309(8)
Os(2)-Os(3)	2.8170(4)	Os(2)-Os(3)	2.8188(8)
Os(2)-Os(4)	2.8466(4)	Os(2)-Os(4)	2.8547(8)
Os(3)-Os(4)	2.8569(4)	Os(3)-Os(4)	2.8288(7)
Os(3)-C(13)	1.963(8)	Os(3)-C(13)	1.99(1)
Os(4)-C(13)	2.472(7)	Os(4)-C(13)	2.37(1)
C(13)-O(13)	1.152(9)	C(13)-O(13)	1.18(2)
Os-$CO_{term.}$	1.864 9) - 1.959(8)	Os-$CO_{term.}$	1.86(1) - 1.94(2)
$(C\text{-}O)_{term.}$	1.124(9) - 1.15(1)	$(C\text{-}O)_{term.}$	1.11(2) - 1.17(2)
Os(1)-O(14)	2.123(5)	Os(1)-O(14)	2.122(9)
Os(4)-O(14)	2.132(5)	Os(4)-O(14)	2.11(1)
Os(1)-H[a]	1.75[a]	Os(1)-H	1.80[a]
Os(2)-H	1.76[a]	Os(2)-H	1.85[a]
O(14)-O(15)	2.669(8)		

Table cont'd

[a] Determined with the XHYDEX program

Bond Angles

28.H_2O		**32**	
Os(2)-Os(1)-Os(3)	58.01(1)	Os(2)-Os(1)-Os(3)	58.34(2)
Os(1)-Os(2)-Os(3)	58.58(1)	Os(1)-Os(2)-Os(3)	58.75(2)
Os(1)-Os(2)-Os(4)	72.42(1)	Os(1)-Os(2)-Os(4)	72.52(2)
Os(3)-Os(2)-Os(4)	60.58(1)	Os(3)-Os(2)-Os(4)	59.81(2)
Os(1)-Os(3)-Os(2)	63.41(1)	Os(1)-Os(3)-Os(2)	62.91(2)
Os(1)-Os(3)-Os(4)	74.31(1)	Os(1)-Os(3)-Os(4)	74.68(2)
Os(2)-Os(3)-Os(4)	60.22(1)	Os(2)-Os(3)-Os(4)	60.72(2)
Os(2)-Os(4)-Os(3)	59.20(1)	Os(2)-Os(4)-Os(3)	59.47(2)
Os(3)-Os(4)-C(13)	42.5(2)	Os(3)-Os(4)-C(13)	43.9(3)
Os(4)-Os(3)-C(13)	58.2(2)	Os(4)-Os(3)-C(13)	55.7(4)
Os(3)-C(13)-Os(4)	79.3(2)	Os(3)-C(13)-Os(4)	80.4(5)
Os(1)-O(14)-Os(4)	107.8(2)	Os(1)-O(14)-Os(4)	108.4(4)

range from 2.8170(4) - 2.8569(4) Å (Table 7.1) if the long OsOs bond of the Os(μ-H)Os unit (i.e., Os(1)Os(2) = 2.9701(5) Å) is excluded. The average OsOs length of the short OsOs bonds in **28** is 2.839 Å, which is close to 2.877 Å the average OsOs length in $Os_3(CO)_{12}$.[64] As mentioned previously, OsOs bond distances are usually shorter in more condensed Os clusters than in $Os_3(CO)_{12}$.

Placement of the H ligand across the Os(1)Os(2) bond gave a site energy of 2.4 by the XHYDEX program. This value is in the range of 0.2-10.6 that was previously found for bridging hydride ligands. The lowest site energy for a terminal position (18.7 kcal mol^{-1}) was outside the range (2.2-7.5) previously determined for terminal metal hydride site energies (Table 7.2). The Os(1)Os(2) vector at 2.9701(5) Å is by far the longest OsOs distance in the molecule and is entirely consistent with view that this bond is the one that is H-bridged. The distance may be compared with 2.985 Å the average OsOs lengths for the Os(μ-H)Os units in the structures of $Os_4(\mu\text{-}H)_3(\mu\text{-}I)(CO)_{12}$ (by neutron diffraction) and $Os_4(\mu\text{-}H)_3(\mu\text{-}X)(CO)_{12}$ (X = OH, OPO_3H_2, NO). The other OsOs lengths in these molecules are, like those in **28**, considerably shorter and in the range 2.830(2) – 2.876(1) Å.

Table 7.2. Site energies (kcal mol^{-1}) for the terminal and bridging hydride positions in $Os_4(\mu\text{-}H)(\mu\text{-}OH)(\mu\text{-}CO)(CO)_{12}.H_2O$ (**28.H_2O**) and $Os_4(\mu\text{-}H)(\mu\text{-}OD)(\mu\text{-}CO)(CO)_{12}$ (**32**).

Bridging Positions			
28.H_2O		**32**	
Os(1)-Os(2)	**2.4**	Os(1)-Os(2)	**2.2**
Os(1)-Os(3)	14.9	Os(1)-Os(3)	14.4
Os(1)-Os(4)	16.3	Os(1)-Os(4)	14.1
Os(2)-Os(3)	15.3	Os(2)-Os(3)	16.6
Os(2)-Os(4)	13.8	Os(2)-Os(4)	16.3
Os(3)-Os(4)	24.4	Os(3)-Os(4)	27.6
Terminal Positions			
Os(1)	21.3	Os(1)	18.7
Os(2)	20.8	Os(2)	22.2
Os(3)	66.7	Os(3)	61.8
Os(4)	75.3	Os(4)	83.6

The structure of **28.H_2O** also contains a rare example of a semi-bridging carbonyl (CO(13)) in an Os carbonyl cluster. It bridges the Os(3)Os(4) bond (Os(3)C(13) = 1.963 (8) Å; Os(4)C(13) = 2.472 (7) Å). These OsC distances are similar to those to the asymmetric bridging CO in $Os_5(CO)_{18}$ and $[\eta^5\text{-}C_5Me_5]Os_4(\mu\text{-}H)(CO)_{11}$.[44,178]

The H_2O molecule in **28** bridges three cluster molecules through hydrogen bonding interactions with the hydroxyl ligands on two adjacent clusters and the bridging CO on a third (Figure 7.3). The O(14)O(15) bond length was found to be 2.669(8) Å. The other two hydrogen bond interactions were not determined. The water molecule does not H-bond to any terminal carbonyls. There is an increase in the metal-to-CO π back-donation on going from a terminal to bridging carbonyl as evidenced by their respective CO stretching frequencies. In other words, there is more electron density on the O atom of a bridging CO and this probably results in a preference for H-bonding to the O atom of a bridging CO.[179]

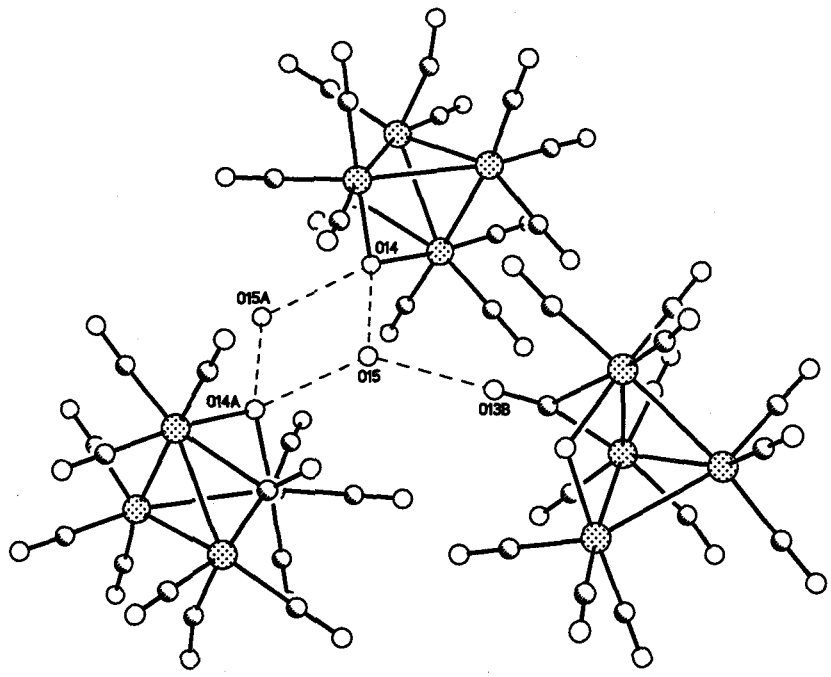

Figure 7.3. Hydrogen bonding interactions in **28.H_2O**.

The ^1H NMR spectrum of **28** contains singlets at δ -2.8 and -13.8 that are assigned to the OH and Os(μ-H)Os protons, respectively (Figure 7.4). These resonances are in the normal range for such groupings.[180] After exposure to D_2O the resonance at δ -2.8 disappeared consistent with the signal as being due to the proton of the OH ligand.

The $^{13}C\{^1H\}$ NMR spectrum of **28** at -50 °C showed six signals with an approximate intensity ratio of 7:1:1:1:1:2, which is consistent with solid-state molecular structure after allowing for the CO exchange described below (Figure 7.5). The signal of intensity 7 is assigned to the carbonyls labelled *a* (Chart 7.1) that are undergoing exchange in the Os(2)Os(3)Os(4) plane that also contains the bridging carbonyl. As discussed previously in this thesis, clusters with a bridging CO generally undergo a rapid merry-go-round exchange in the plane containing this CO.[77] The signals at δ 175.4 (J_{CH}

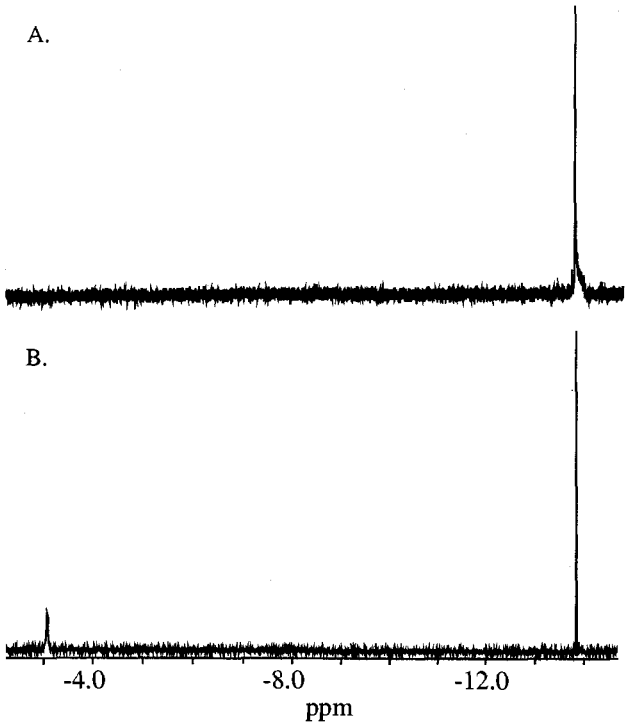

Figure 7.4. ^{1}H NMR spectrum of (A) $Os_4(\mu\text{-H})(\mu\text{-OD})(\mu\text{-CO})(CO)_{12}$ (**32**) and (B) $Os_4(\mu\text{-H})(\mu\text{-OH})(\mu\text{-CO})(CO)_{12}$ (**28**).

= 12.2 Hz) and 173.1 (J_{CH} = 11.4 Hz) both with intensity 1 showed coupling to the bridging H atom. This allowed for the assignment of these resonances as due to the carbonyls labelled *b* and *e*. The highest field resonance at δ 170.6 with intensity 2 is believed to be the result of the overlap of two signals. One signal is assigned to *d* while the other resonance is due to one of *c*, *f* or *g*. (An explanation for the assignment of *d* is given in the next paragraph.) The final two resonances at δ 178.2 and 175.4 both with intensity 1 are assigned to two of *c*, *f* or *g*. As the temperature of the sample was raised to room temperature changes occurred in the spectrum indicative of two further exchange mechanisms taking place. At room temperature (Figure 7.5) the spectrum showed a similar pattern to the spectrum obtained at -50 °C except the intensity ratio had changed to 7:1:1:1:1:1 (from 7:1:1:1:1:2) and the lowest field signal had become broader

indicating that exchange on the NMR time scale of the carbonyls labelled *a* with another carbonyl (or carbonyls) had commenced.

The highest field signal at δ 170.6 became sharper but reduced in intensity from 2 to 1. Because all the other signals in the spectrum remained sharp this indicated that the carbonyls labelled *a* were now exchanging with one of the signals originally at δ 170.6. When a signal of intensity 1 coalesces with a signal of intensity 7 due to exchange the

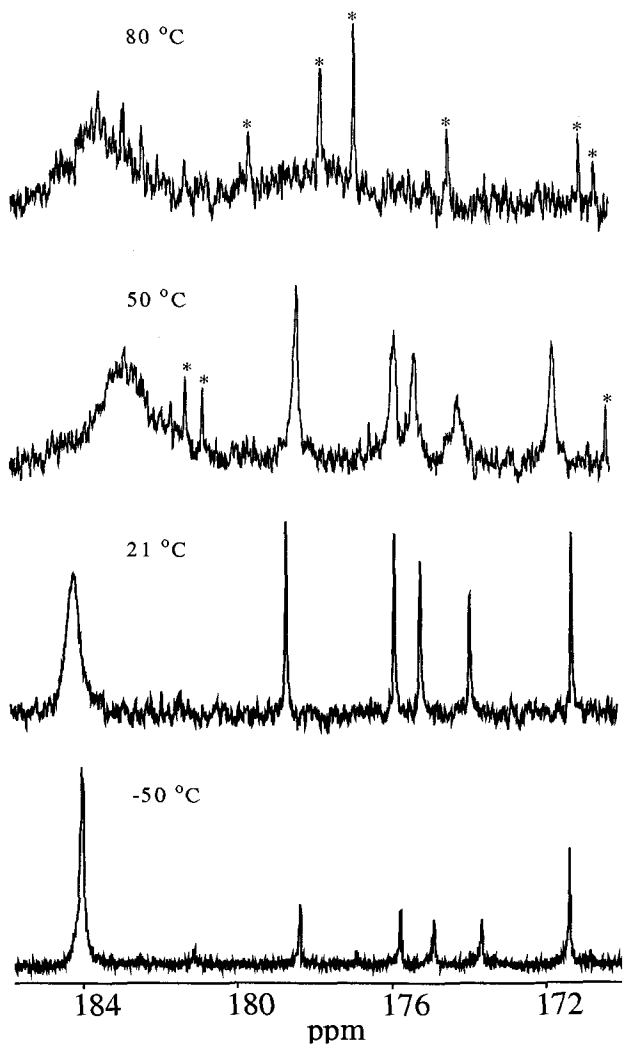

Figure 7.5. Variable temperature $^{13}C\{^{1}H\}$ NMR spectra of $Os_4(\mu\text{-}H)(\mu\text{-}OH)(\mu\text{-}CO)(CO)_{12}$. (* = decomposition products)

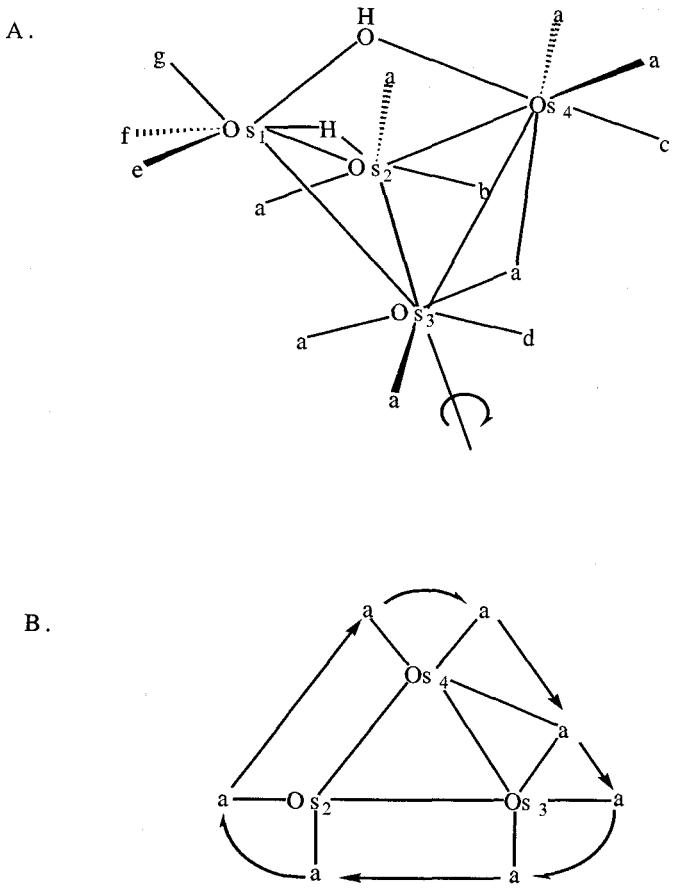

Chart 7.1. Labelling in the ^{13}C NMR spectrum of $Os_4(\mu\text{-}H)(\mu\text{-}OH)(\mu\text{-}CO)(CO)_{12}$. (A) Carbonyl exchange at Os(3). (B) Merry-go-round CO exchange about the Os(2)Os(3)Os(4) triangle of $Os_4(\mu\text{-}H)(\mu\text{-}OH)(\mu\text{-}CO)(CO)_{12}$.

weaker signal disappears into the baseline more rapidly than the stronger signal (i.e., it is a weighted average phenomenon). The resonances assigned to *e* and *b* remained sharp at room temperature indicating that the carbonyls that give rise to these signals are not undergoing exchange. Because the carbonyls on Os(1) can only undergo a mutual exchange and *e* is stationary, the carbonyls labelled *f* and *g* also do not exchange. This is expected since the carbonyls attached to an Os atom with a bridging ligand (other than CO) do not normally undergo mutual CO exchange.[181] Although two carbonyls on Os(4) participate in the merry-go-round exchange of the carbonyls labelled *a*, because of the bridging OH group a mutual exchange of the carbonyls on Os(4) does not occur. As a

result, the carbonyl labelled *c* is not involved in any exchange mechanism at this temperature. Therefore the only CO ligand available to exchange with the carbonyls *a* is that labelled *d*. This occurs through a mutual exchange of the carbonyls on Os(3) that exchange *d* and *a*. Because the bridging CO is only a semi-bridging it does not prevent the exchange on Os(3).

At 50 °C all the signals in the ^{13}C NMR spectrum had broadened, and at 80 °C they had essentially collapsed into the baseline (Figure 7.5). The sharp signals in the latter spectrum are attributed to decomposition products that may be due to reaction of **28** with the solvent (toluene-d_8) at this temperature. Other mechanisms of CO exchange are therefore taking place at elevated temperatures so that all the carbonyls are undergoing some form of exchange. This may involve mutual exchange of the carbonyls of the $Os(CO)_3$ groupings.

$Os_4(\mu\text{-}H)(\mu\text{-}OD)(\mu\text{-}CO)(CO)_{12}$ (32) In the ^1H NMR study described above it was noticed that the solid-state IR spectrum of $Os_4(\mu\text{-}H)(\mu\text{-}OD)(\mu\text{-}CO)(CO)_{12}$ (**32**) was significantly different to that of **28**, and this prompted a fuller investigation of **32**. The partially deuterated sample of **28** (i.e., **32**) was prepared as follows. A powdered sample of **28** was placed under vacuum for one day. It was then dissolved in dry CH_2Cl_2 and an excess of D_2O added to the solution, which was then stirred for 5 days under an N_2 atmosphere (eq 7.2). The CH_2Cl_2 solution was pipetted from D_2O and placed in another

$$\underset{\textbf{28}}{Os_4(\mu\text{-}H)(\mu\text{-}OH)(\mu\text{-}CO)(CO)_{12}} \xrightarrow{D_2O} \underset{\textbf{32}}{Os_4(\mu\text{-}H)(\mu\text{-}OD)(\mu\text{-}CO)(CO)_{12}} \qquad (7.2)$$

Schlenk tube where the solvent was removed on the vacuum line. The resulting solid was recrystallized from wet (D_2O) CH_2Cl_2 to give air-stable, yellow crystals of $Os_4(\mu\text{-}$

H)(μ-OD)(μ-CO)$(CO)_{12}$ (**32**) that were characterized by IR spectroscopy (discussed later), ^{1}H NMR spectroscopy and X-ray crystallography.

As expected, the molecular structure[q] of **32** (Figure 7.6) has essentially the same

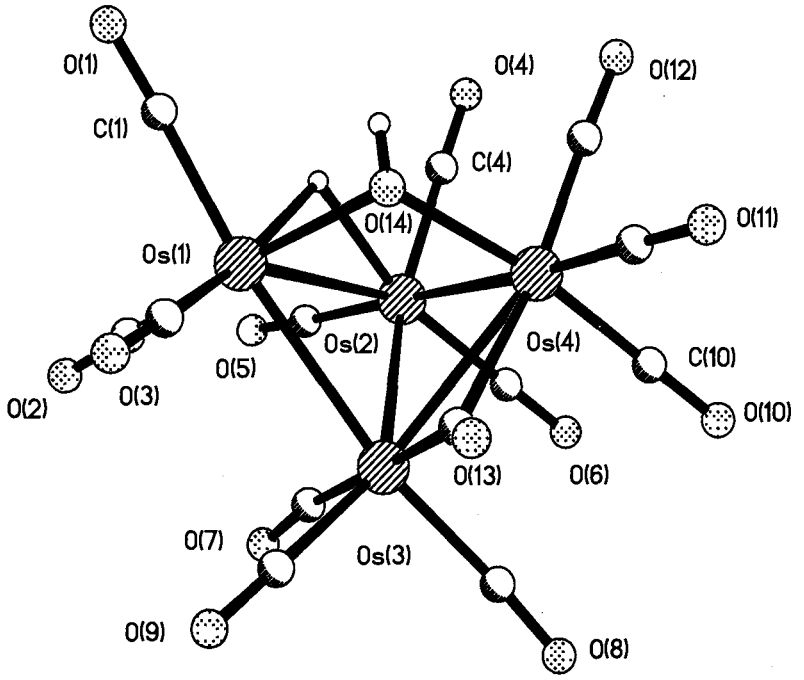

Figure 7.6. The molecular structure of Os_4(μ-H)(μ-OD)(μ-CO)$(CO)_{12}$ (**32**).

structure as **28**. The remarkable feature of the structure, however, is that **32** does not contain a molecule of D_2O of crystallization. The discussion of this finding is left until a later section. Selected bond length and angle data for **32** are presented in Table 7.1 (i.e., along with those of **28**). Likewise, site energies for the H ligand in **32** are given in Table 7.2. The bond lengths of **32** range from 2.8188 (8) - 2.9482 (8) Å (Table 7.1). Excluding

---

[q] Determined by Dr. M. Jennings (University of Western Ontario).

the longest OsOs bond of the Os(μ-H)Os grouping the average of the Os-Os bond lengths is 2.833 Å which is similar to the average OsOs length in **28**.

Interconversion of 28.H_2O and 32 The reversibility of eq 7.2 was examined by the addition of H_2O to **32** in solution. A sample of **32** was dissolved in CH_2Cl_2 to which a few drops of H_2O was added (eq. 7.3). The solution was stirred for one day before the

$$\underset{\mathbf{32}}{Os_4(\mu\text{-}H)(\mu\text{-}OD)(\mu\text{-}CO)(CO)_{12}} \xrightarrow{H_2O} \underset{\mathbf{28.H_2O}}{Os_4(\mu\text{-}H)(\mu\text{-}OH)(\mu\text{-}CO)(CO)_{12}.H_2O} \qquad (7.3)$$

solvent was removed on the vacuum line. The remaining solid as a KBr disk was examined by IR spectroscopy. The IR spectrum (discussed below) was consistent with that of **28.H_2O**, thus indicating that conversion of **32** back to **28.H_2O** had occurred. A sample of **28.H_2O** was also dissolved in dry CH_2Cl_2 that contained equal amounts of H_2O and D_2O ('DHO') and allowed to stir for one day (eq 7.4). The solvent was then

$$\underset{\mathbf{28.H_2O}}{Os_4(\mu\text{-}H)(\mu\text{-}OH)(\mu\text{-}CO)(CO)_{12}.H_2O} \xrightarrow{\text{'DHO'}} \underset{\mathbf{32}}{Os_4(\mu\text{-}H)(\mu\text{-}OD)(\mu\text{-}CO)(CO)_{12}} \qquad (7.4)$$

removed on the vacuum line and the solid investigated by IR spectroscopy as a KBr disk. The IR spectrum showed the product was **32**, that is, the exposure of **28** to H_2O/D_2O gives the form that does not contain water in the solid state lattice.

The effect of D_2O, H_2O or a 1:1 mixture of both on the conversion of **28.H_2O** into **32** (and vice versa) is summarized in eq 7.5. The addition of D_2O or H_2O/D_2O (1/1)

$$\underset{\mathbf{28.H_2O}}{Os_4(\mu\text{-}H)(\mu\text{-}OH)(\mu\text{-}CO)(CO)_{12}.H_2O} \underset{H_2O}{\overset{D_2O \text{ or 'DHO'}}{\rightleftharpoons}} \underset{\mathbf{32}}{Os_4(\mu\text{-}H)(\mu\text{-}OD)(\mu\text{-}CO)(CO)_{12}} \qquad (7.5)$$

to **28.H_2O** promotes the conversion to **32** while the addition of H_2O to **32** produces **28.H_2O**.

Comparison of the IR (KBr) spectra of $28.H_2O$ and 32 Although the metal skeletal arrangements of **$28.H_2O$** and **32** are the same, **$28.H_2O$** contains H_2O in the crystalline lattice which is hydrogen bonded to the semi-bridging CO and bridging OH unit. The deuterated sample does not contain water in the crystalline lattice. All attempts to produce a "dry" crystal of **$28.H_2O$** failed while recrystallization of **32** in a solvent spiked with D_2O failed to produce a "wet" sample. The removal of water from the lattice changed the space group of the sample from C2/c (for **$28.H_2O$**) to P2(1)/n (for **32**). Furthermore, **32** is more dense as calculated from the X-ray data: **$28.H_2O$**: 3.72 Mg m^{-3}; **32**: 3.82 Mg m^{-3}.

The bond lengths and angles found in the two structures are similar (Figure 7.2/7.6) with average OsOs lengths of 2.865 Å in **$28.H_2O$** and 2.856 Å in **32** (Table 7.1). An examination of the Os-C bond lengths of the bridging carbonyl in **$28.H_2O$** and **32** showed that the bridging CO in **32** is somewhat more symmetric (i.e. less terminal character) than the bridging CO in **$28.H_2O$**. In **28** the OsC lengths to the bridging carbonyl are 1.963(8) and 2.472(7) Å, whereas in **32** the corresponding lengths are 1.99(1) and 2.37(1) Å.

The IR (KBr) spectra of **$28.H_2O$** and **32** are of particular interest (Figure 7.7). The spectrum of **$28.H_2O$** contains terminal ν(CO) stretches in the region 2083-1958 cm^{-1}. It also has a band of medium intensity due to the semi-bridging CO at about 1844 cm^{-1}. The terminal ν(CO) stretches are also present in the corresponding spectrum of **32,** but the peak due to the semi-bridging CO is extremely weak so as to be hardly observable (Figure 7.7). There was not an extra band in the spectrum (ν(CO) region) of **32** that might be attributed to the bridging carbonyl. Terminal carbonyl ligands bound to

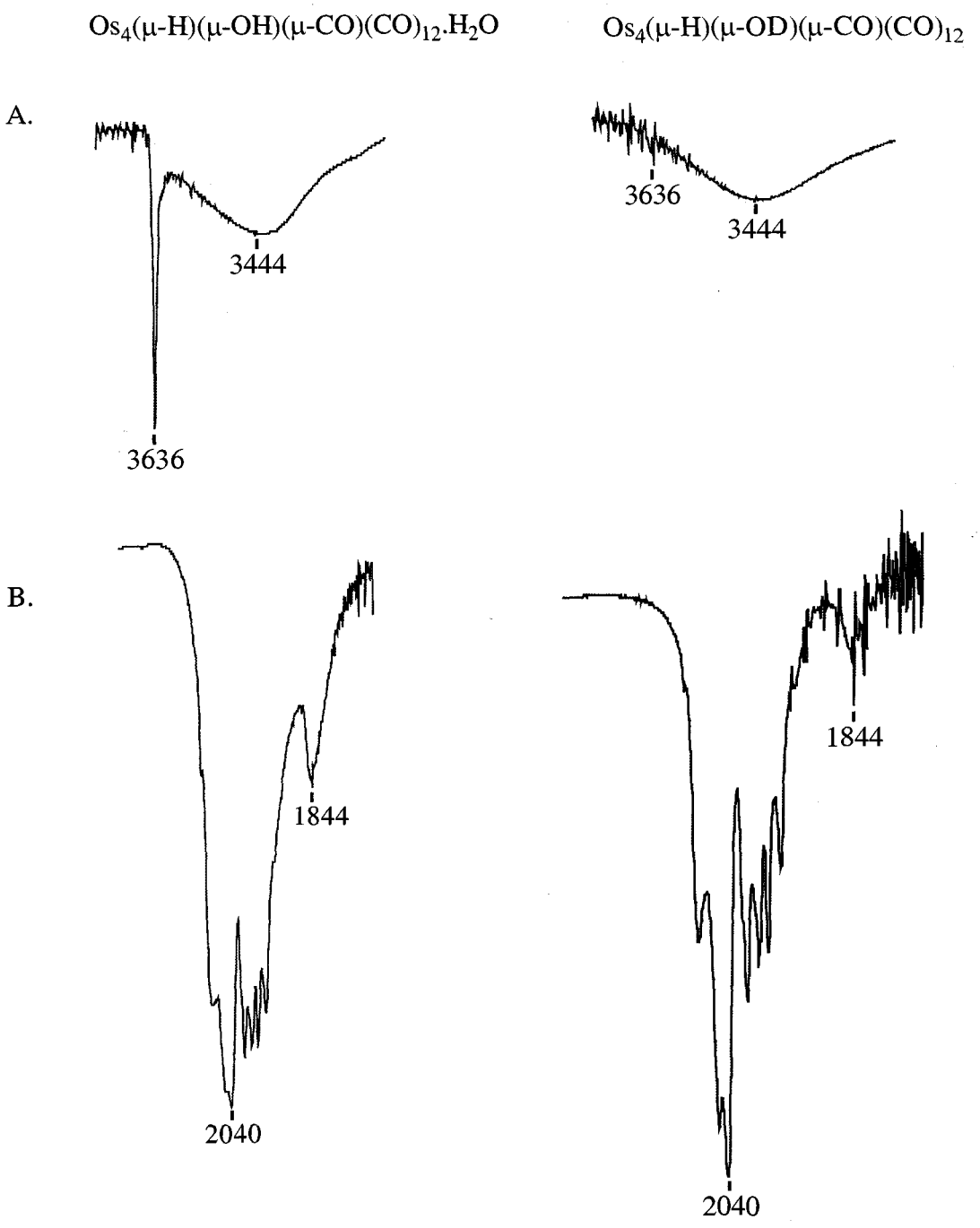

Figure 7.7. IR (KBr) spectra of $Os_4(\mu\text{-}H)(\mu\text{-}OH)(\mu\text{-}CO)(CO)_{12}.H_2O$ (**28.H_2O**) and $Os_4(\mu\text{-}H)(\mu\text{-}OD)(\mu\text{-}CO)(CO)_{12}$ (**32**). (A) The ν(OH) region. (B) The ν(CO) region.

transition metals have CO stretching frequencies usually in the 1900-2150 cm^{-1} region, while bridging carbonyl stretches appear in the region of 1750-1850 cm^{-1}.[182] The ν(CO) stretch of a semi-bridging CO ligand can appear in either the terminal or bridging region (depending on the degree of terminal and bridging character). It is difficult to predict whether the CO stretch in **32** should be at a higher or lower frequency than that in **28.H_2O** as there are several factors to consider, such as, the amount of bridging character of the carbonyls (i.e., occupancy of the π^* MOs on the carbonyl) and the effect of the hydrogen bonding interaction on the CO bond strength. Although the bond length of the semi-bridging CO in **32** at 1.18(2) Å is longer than that in **28.H_2O** (1.152(9) Å) the difference is not statistically significant.

The IR spectrum of $Os_4(\mu\text{-H})(\mu\text{-OH})(\mu\text{-CO})(CO)_{12}$ (in hexane) does not contain stretching frequencies in the bridging carbonyl region (Figure 7.1). There is also no signal in the ^{13}C NMR spectrum that can be assigned to this carbonyl as it is undergoing rapid exchange with other (terminal) CO ligands. It may be that, as proposed for $Ru_6(\mu_6\text{-C})(\mu\text{-CO})(CO)_{16}$, the exchange is taking place on the IR time scale at ambient temperature for **28** and the CO stretch of the semi-bridging carbonyl is broadened into the baseline.

There is another difference between the IR (KBr) spectrum of **28.H_2O** and **32**. The spectrum of **28.H_2O** contains a sharp ν(OH) band at 3636 cm^{-1}, but it is not observed in the spectrum of **32** (Figure 7.7). If the ν(OH) stretch in the IR spectrum of **28.H_2O** is due to the bridging OH group a shift to a lower wavenumber would be observed in the IR spectrum of the deuterated sample (which contains a bridging OD unit).[174h] Because of isotopic substitution a ν(OD) stretch should appear around 2570 cm^{-1}. Since the band did

not shift but disappeared the ν(OH) stretch must have been due to the water of crystallization in **28.H_2O**. The disappearance of the ν(OH) band in **32** is consistent with the crystal structure that has no H_2O in the lattice. As this study was tangential to the main theme of the thesis the system was not investigated further. A low temperature IR investigation of **28** would be worthwhile.

Comparison of the structures of 28.H_2O and 32

Introduction

Before comparing the two structures a brief summary of what is known about the deuterium isotope effect on hydrogen bonding is presented. The H/D isotope effect in solid state structures is generally small with minor variations that do not normally result in a change of the molecular shape or the space group of the structures. There are however some exceptions. In the crystal structures of the H- and D- forms of oxalic acid and potassium dihydrogen phosphate the orientation of the water molecule of crystallization differs.[183] The principles governing these changes are not clear although Ichikawa noted that these structural changes have some similarities to the pressure effect on crystalline systems.[183]

The effect of H/D substitution on hydrogen bonding interactions in molecules is complicated. Studies of organic compounds have shown that the effect of D substitution on the strength of the H-bond depends on the system.[184,185] In water the H-bonds are stronger in the deuterated system, but the reverse is true for $(C_6H_5OH)_2$.[184,185] When certain molecules (for example NH_3, H_2CO, $SrCl_2$ and $BaCl_2$) are hydrated with HDO a random distribution of D/H is not seen, rather there is a preference for D to be located in certain environments.[184,186] The rules governing the changes in the bond strength are not

fully understood, making it difficult to rationalize the effect of H versus D on systems containing H-bonds.

Vinogradov and Linnell have suggested that the isotope effect on hydrogen bonding in solids depends on the X/Y distance of the X...H...Y system.[187] When the X/Y distance is greater than 2.7 Å there is shortening and strengthening of the H-bond upon deuterium substitution, but when the X/Y distance is less than 2.7 Å the H-bond becomes longer and weaker. When the X/Y is close to 2.7 Å the two effects cancel and there is no isotope effect on the H-bond.

Discussion

The difficulty in understanding the **28.H_2O/32** system is that it is unique and consequently it cannot be compared to other systems. Most osmium carbonyl compounds have soft ligands with atoms (e.g., P and S) that do not engage in hydrogen bonding. It has only recently become apparent that Os carbonyl clusters with hard ligands are stable, unlike their first and second row transition metal analogues. An example of this is $[Os(\mu_3\text{-}O)(CO)_3]_4$ first reported in 1972[188] but currently under investigation by Pomeroy and co-workers.

With this in mind a proposed explanation of the system is presented. Unlike most metal carbonyls **28.H_2O** contains two ligands that can form strong H-bond interactions with water. First, **28.H_2O** has a semi-bridging CO, which is able to produce stronger H-bonds than terminal carbonyls. The OH ligand also forms strong H-bonds. The stability that the H-bonds provide to the **28.H_2O** is enough for the hydrated form to be favoured. Although the effect on the H-bond strength in the H and D samples depends on the system, in **32** it appears that the D-bonding is weaker and hence D_2O is not incorporated

into the structure. In other words, the deuterium bonding in **32** is weaker than the hydrogen bonding in **28.H_2O**, and is not sufficient to bind the D_2O in the lattice in **32**. The hydrogen form appears to be on the cusp of favouring the hydrated system (O(14)-O(15) 2.669(8) Å) since the small change in the H-bond strength of the deuterated sample is enough to cause loss of D_2O (or DHO) in the sample.

7.3 Experimental

The general procedure used for the synthesis and analysis has been described in the Experimental Section of Chapter 2. The trimethylamine oxide was purified by the overnight sublimation of $Me_3NO.2H_2O$ at 70 °C under vacuum. At the time it was believed the Me_3NO was anhydrous, but it probably was not and this was the source of the water in **28.H_2O**.

Preparation of $Os_4(\mu\text{-}H)(\mu\text{-}OH)(\mu\text{-}CO)(CO)_{12}.H_2O$ (28.H_2O) A Schlenk tube with $Os_4(CO)_{14}$ (20 mg, $1.7x10^{-3}$ mmol) in CH_2Cl_2 (15 mL) was stirred at room temperature while 0.26 mL of a 0.0405 M solution of Me_3NO in CH_2Cl_2 was added drop wise over the course of 5.25 hours, during which time the original brown/red solution darkened slightly. (Slow addition of the Me_3NO solution is necessary to minimize the formation of decomposition products.) The solution was then evaporated to dryness on the vacuum line and the remaining solid chromatographed on a silica gel column (1.5 x 16 cm). The side products ($Os_3(CO)_{12}$, $Os_4(\mu\text{-}H)_2(CO)_{13}$) were first removed by an elution with hexane/CH_2Cl_2 (50:50). Elution with hexane/CH_2Cl_2 (10:90) gave a yellow band that contained the desired product **28.H_2O** (10 mg, 40 %).

The analytical sample of **28.H_2O** was obtained as air-stable, yellow crystals by recrystallization from CH_2Cl_2: IR (hexane) ν(CO) 2108 (w), 2078 (vs), 2058 (vs), 2053

(vs), 2021 (m), 2013 (s), 2001 (m) cm^{-1}; IR (KBr) ν(OH) 3636 (m, sharp), ~3460 (w, vbr) cm^{-1}, ν(CO) 2083 (sh, w), 2053 (sh), 2040 (s), 2009 (s), 1991 (s), 1977 (s), 1958 (s), 1844 (br, m) (semi-bridging CO) cm^{-1}. (The IR (KBr) spectrum of **32** was the same as that for **28.H_2O** except that the peak at 3636 (m) was missing and the peak at 1844 had decreased in intensity from medium to very weak.); ^1H NMR (CD_2Cl_2) δ -2.8 (s), -13.8 (s); (Addition of D_2O to the NMR solution caused the disappearance of the peak at δ -2.8 (s)) $^{13}C/^{13}C\{^1H\}$ NMR (CD_2Cl_2, -50 °C) δ 184.3 (7C), 178.2 (1C), 175.4 (1C), 174.4 (1C, J_{CH} = 12.2 Hz) 173.1 (1C, J_{CH} = 11.4 Hz), 170.6 (2C); $^{13}C\{^1H\}$ NMR (toluene-d_8, RT) δ 184.1 (7C), 178.6 (1C), 175.8 (1C), 175.2 (1C), 173.9 (1C), 171.2 (2C); $^{13}C\{^1H\}$ NMR (toluene-d_8, 50 °C) δ 183.4 (7C, broad), 178.5 (1C), 175.7 (1C), 175.1 (1C), 173.9 (1C), 171.1 (1C); $^{13}C\{^1H\}$ NMR (toluene-d_8, 80 °C) δ 182.0 (weak, broad), 176.5 (weak, broad); MS (LSIMS) *m/z* 1143.7 (M^+) (Calcd for M^+ = 1144 (100%)). Anal. Calcd for $C_{13}H_2O_{14}Os_4$: C, 13.65; H, 0.18. Found: C, 13.66; H, 0.20.

As reported in Chapter 6, **28** was produced in a trace amounts from the pyrolysis or photolysis of $Os_4(CO)_{14}$.

Preparation of $Os_4(\mu\text{-}H)(\mu\text{-}OD)(\mu\text{-}CO)(CO)_{12}$ (32) A sample of powdered **28** (25 mg, 0.022 mmol) in a Schlenk tube was placed on the vacuum line for one day before being dissolved in thoroughly dried CH_2Cl_2 (~15 mL) (dried with P_2O_5). To this solution was added D_2O (~5 mL) and it was allowed to stir under a N_2 atmosphere for 5 d. The CH_2Cl_2 solution was transferred by pipette to another Schlenk tube (leaving behind the D_2O) and the collected solution evaporated on the vacuum line. The resulting solid was recrystallized from dry CH_2Cl_2 that had been exposed to D_2O producing air-stable, yellow crystals of **32** in essentially quantitative yield.

A sample of **32** was also obtained by dissolving **28** (5 mg, $4x10^{-3}$ mmol) in dry CH_2Cl_2 (8 mL) to which was added equal amounts (1 mL) of H_2O and D_2O. The solution was allowed to stir for one d. The sample was dried on the vacuum line to afford **32** as indicated by its IR (KBr) spectrum.

References

1. Shriver, D.; Atkins, P. *Inorganic Chemistry 3rd ed.*; W. H. Freeman and Company: New York, 1999, p. 572.

2. Dewar, J.; Jones, H. O. *Proc. R. Soc. (London)*, **1907**, *A79*, 66.

3. *The Chemistry of Metal Cluster Complexes*; Shirver, D. F.; Kaesz, H. D.; Adams, R. D., Eds.; VCH: New York, 1990.

4. (a) *Metal Cluster in Chemistry*; Braustein, P.; Oro, L.; Raithby, P. R., Eds.; Wiley-VCH: Weinheim, Germany, 1999. (b) Elschenbroich, C.; Salzer, A. *Organometallics A Concise Introduction*; VCH: New York, 1989. (c) *Metal Clusters*; Moskovits, M., Ed.; Wiley: New York, 1986. (d) Cotton, F. A.; Wilkinson, G. *Advanced Inorganic Chemistry* 5th ed.; Wiley: New York, 1989. (e) *Transition Metal Clusters*; Johnson, B. F. G., Ed.; Wiley: New York, 1980. (f) Mingos, D. M. P.; Wales, D. J. *Introduction to Cluster Chemistry*; Prentice Hall: Englewood Cliff, New Jersey, 1990.

5. *Comprehensive Organometallic Chemistry II*; Wilkinson, G.; Stone, F. G. A.; Abel, E. W., Eds.; Pergamon: New York, 1995, Vol. 7, Ch. 15.

6. (a) Vahrenkamp, H. *Adv. Organomet. Chem.* **1983**, *22*, 169. (b) Vargas, M. D.; Nicholls, J. N. *Advances in Inorganic Chemistry and Radiochemistry*; Emelēus, H. J.; Sharpe, A. G., Eds.; Academic: New York, 1986, Vol. 30, (c) Roberts, D. A.;Geoffroy, G. L.; *Comprehensive Organometallic Chemistry*; Wilkinson, G.; Stone, F. G. A.; Abel, E. W., Eds.; Pergamon: Oxford, 1982: Ch. 40.

7. (a) Ditzel, E. J.; Johnson, B. F. G.; Lewis, J.; Raithby, P. R.; Taylor, M .J. *J. Chem. Soc. Dalton Trans.*, **1985**, 555. (b) Deeming, A. J. *Advances in Organometallic Chemistry*; Stone, F. G. A; West. R, Eds.; Academic: New York, 1986, Vol. 26.

8. Eady, C. R.; Johnson, B. F. G.; Lewis, J. *J. Chem. Soc., Dalton Trans.* **1975**, 2606.

9. Jackson, P. F.; Johnson, B. F. G.; Lewis, J. *J. Chem. Soc., Chem. Commun.* **1980**, 224.

10. Wong, J. S. Y.; Lin, Z.Y.; Wong, W. T. *Organometallics* **2003**, *22*, 4798.

11. (a) *Comprehensive Organometallic Chemistry*; Wilkinson, G.; Stone, F. G. A.; Abel, E. W., Eds.; Pergamon: Oxford 1982. (b) *Comprehensive Organometallic Chemistry II*; Wilkinson, G.; Stone, F. G. A.; Abel, E. E., Eds.; Pergamon: Oxford, 1995.

12. Sánchez-Cabrera, G.; Zuno-Cruz, F. J.; Rosales-Hoz, M. J.; Bakhmutov, V. I. *J. Organomet. Chem.* **2002**, *660*, 153.

13. Davis, H. B.; Einstein, F. W. B.; Johnston, V. J.; Pomeroy, R. K. *J. Am. Chem. Soc.* **1988**, *110*, 4451.

14. Lawson, R. J.; Shapley, J. R. *J. Am. Chem. Soc.* **1976**, *98*, 7433.

15. Adams, R. D.; Babin, J. E.; Mathur, P.; Natarajan, K.; Wang, J. G. *Inorg. Chem.* **1989**, *28*, 1440.

16. Cabeza, J. A.; del Rio, I.; Riera, V.; Suarez, M.; Garcia-Granda, S. *Organometallics* **2004**, *23*, 1107.

17. Jääskeläinen, S.; Haukka, M.; Riihimäki, H.; Pursiainen, J. T.; Pakkanen, T. A. *J. Organomet. Chem.* **2004**, *689*, 1064.

18. Bruce, M. I.; Zaitseva, N. N.; Skelton, B. W.; White, A. H. *J. Chem. Soc., Dalton Trans.* **2002**, 3879.

19. Adams, R. D.; Captain, B.; Smith, M. D. *J. Cluster Sci.* **2004**, *15*, 139.

20. Zhang, W.; Zhu, B.; Hu, B.; Zhang, Y.; Zhao, Q.; Yin, Y.; Sun, J. *J. Organomet. Chem.* **2004**, *689*, 714.

21. Ebner, A.; Wachter, J.; Zabel, M. *J. Cluster Sci.* **2004**, *15*, 163.

22. Zhang, L.; Zhu, B.; Xiao, N.; Xu, Q.; Tsumori, N.; Sun, J.; Yin, Y.; Chen. J. *Organometallics* **2003**, *22*, 4369.

23. Sánchez-Nieves, J.; Sterenberg, B. T.; Udachin, K. A.; Carty, A. J. *J. Cluster Sci.* **2004**, *15*, 151.

24. Plečnik, C. E.; Liu, S.; Chen, X.; Meyers, E. A.; Shore, S. G. *J. Am. Chem. Soc.* **2004**, *126*, 204.

25. Tachikawa, M.; Shapley, J. R. *J. Organomet. Chem.* **1977**, *124*, C19.

26. Johnson, B. F. G.; Lewis, J.; Pippard, D. A. *J. Chem. Soc., Dalton Trans.* **1981**, 407.

27. (a) Johnson, B. F. G.; Khattar, R.; Lewis, J.; McPartlin, M.; Morris, J.; Powell, G. L. *J. Chem. Soc., Chem. Commun.* **1986**, 507. (b) Churchill, M. R.; Hollander, F. J.; Shapley, J. R.; Foose, D. S. *J. Chem. Soc., Chem. Commun.* **1978**, 534. (c) Couture, C.; Farrar, D. H. *J. Chem. Soc., Dalton Trans.* **1986**, 1395. (d) Freeman, M. J.; Miles, A. D.; Murray, M; Orpen, A. G.; Stone, F. G. A. *Polyhedron*, **1984**, *3*, 1093.

28. Wilcox, C. T.; Jennings, M. C.; Pomeroy, R. K. *J. Cluster Sci.* **2004**, *15*, 107.

29. Johnston, V. J.; Einstein, F. W. B.; Pomeroy, R. K. *J. Am. Chem. Soc.* **1987**, *109*, 7220.

30. Johnston, V. J.; Einstein, F. W. B.; Pomeroy, R. K. *J. Am. Chem. Soc.* **1987**, *109*, 8111.

31. Johnston, V. J.; Einstein, F. W. B.; Pomeroy, R. K. *Organometallics* **1988**, *7*, 1867.

32. Evans, D. G.; Mingos, D. M. P. *Organometallics* **1983**, *2*, 435.

33. Mingos, D. M. P. *Inorg. Chem.*, **1982**, *21*, 464.

34. Martin, L. R.; Einstein, F. W. B.; Pomeroy, R. K. *Organometallics* **1988**, *7*, 294.

35. Churchill, M. R.; Hollander, F. J. *Inorg. Chem.* **1977**, *16*, 2493.

36. Einstein, F. W. B.; Johnston, V. J.; Ma, A. K.; Pomeroy, R. K. *Can. J. Chem.* **1995**, *73*, 1223.

37. Lu, C-Y.; Einstein, F. W. B.; Johnston, V. J.; Pomeroy, R. K. *Inorg. Chem.* **1989**, *28*, 4212.

38. (a) Churchill, M. R.; DeBoer, B. G.; Rotella, F. J. *Inorg. Chem.* **1976**, *15*, 1843. (b) Bau, R.; Teller, R. G.; Kirtley, S. W.; Koetzle, T. F. *Acc. Chem. Res.* **1979**, *12*, 176. (c) Elliot, D. J.; Vittal, J. J.; Puddephatt, R. J.; Holah, D. G. *Inorg. Chem.* **1992**, *31*, 1247.

39. Adams, R. D.; Selegue, J. P in *Comprehensive Organometallic Chemistry*; Wilkinson, G.; Stone, F. G. A.; Abel, E. W., Eds.; Pergamon: Oxford, 1982, Vol. 4, p. 967.

40. Einstein, F. W. B.; Pomeroy, R. K.; Rushman, P.; Willis, A. C. *J. Chem. Soc. Chem. Commun.* **1983**, 854.

41. Davis, H. B.; Einstein, F. W. B.; Glavina, P. G.; Jones, T.; Pomeroy, R. K.; Rushman, P. *Organometallics* **1988**, *8*, 1030.

42. Einstein, F. W. B.; Johnston, V. J.; Ma, A. K.; Pomeroy. R. K. *Organometallics* **1990**, *9*, 52.

43. Jiang, F.; Male, J. L.; Biradha, K. ;Leong, W. K.; Pomeroy, R. K.; Zaworotko, M. J. *Organometallics* **1998**, *17*, 5810.

44. Wang, W.; Einstein, F. W. B.; Pomeroy, R. K. *J. Chem. Soc., Chem. Commun.* **1992**, 1737.

45. Wang, W.; Batchelor, R. J.; Einstein, F. W. B.; Lu, C. Y.; Pomeroy, R. K. *Organometallics* **1993**, *12*, 3598.

46. Wang, W.; Einstein, F. W. B.; Pomeroy, R. K. *Organometallics* **1994**, *13*, 1114.

47. Goudsmit, R. J.; Johnson, B. F. G.; Lewis, J.; Raithby, P. R.; Whitmire, K. H. *J. Chem. Soc., Chem. Commun.* **1982**, 640.

48. Martin, L. R.; Einstein, F. W. B.; Pomeroy, R. K. *J. Am. Chem. Soc.* **1986**, *108*, 338.

49. Martin, L. R.; Einstein, F. W. B.; Pomeroy, R. K. *Inorg. Chem.* **1988**, *27*, 2986.

50. Eady, C. R.; Johnson, B. F. G.; Lewis, J.; Mason, R.; Hitchcock, P. B.; Thomas, K. M. *J. Chem. Soc., Chem. Commun.* **1977**, 385.

51. Ditzel, E. J.; Holden, H. D.; Johnson, B. F. G.; Lewis, J.; Saunders, A.; Taylor, M. J. *J. Chem. Soc., Chem. Commun.* **1982**, 1373.

52. Farrar, D. H.; Johnson, B. F. G.; Lewis, J.; Nicholls, J. N.; Raithby, P. R.; Rosales, M. J. *J. Chem. Soc., Chem. Commun.* **1981**, 273.

53. Coughlin, D.; Lewis, J.; Moss, J. R.; Edwards, A. J.; McPartlin, M. *J. Organomet. Chem.* **1993**, *444*, C53.

54. Eady, C. R.; Johnson, B. F. G.; Lewis, J.; Reichert, B. E.; Sheldrick, G. M. *J. Chem. Soc., Chem. Commun.* **1976**, 271.

55. (a) Knight, J.; Mays, M. J. *J. Chem. Soc., Chem. Commun.* **1971**, 62. (b) Knight, J.; Mays, M. J. *J. Chem. Soc., Dalton Trans.* **1972**, 1022.

56. Einstein, F. W. B.; Johnston, V. J.; Pomeroy, R. K. *Organometallics* **1990**, *9*, 2754.

57. Alex, R. F.; Pomeroy, R. K. *Organometallics* **1987**, *6*, 2437.

58. Churchill, M. R.; Hollander, F. J. *Inorg. Chem.* **1978**, *17*, 3546.

59. (a) Churchill, M. R.; Hollander, F. J.; Lashewycz, R. A.; Pearson, G. A.; Shapley, J. R. *J. Am. Chem. Soc.* **1981,** *103*, 2430. (b) Churchill, M. R.; Hollander, F. J. *Inorg. Chem.* **1981**, *20*, 4124.

60. Dhawan, R.; Jiang, F.; Yap, G. P. A.; Pomeroy, R. K. *J. Cluster Sci.* **2003**, *14*, 9.

61. Adams, C. J.; Bruce, M. I.; Skelton, B. W.; White, A. H. *J. Organomet. Chem.* **1996**, *513*, 255.

62. Galsworthy, J. R.; Housecroft, C. E.; Edwards, A. J.; Raithby, P. R. *J. Chem. Soc., Dalton Trans.* **1995**, 2935.

63. Ang, H. G.; Koh, L. L.; Ang, S. G.; Ng, S. Y.;Yang, G. Y. *J. Chem. Soc., Dalton Trans.* **1996**, 4083.

64. Churchill, M. R.; DeBoer, B. G. *Inorg. Chem.* **1977**, *16*, 878.

65. Mealli, C.; Proserpio, D. M. *J. Am. Chem. Soc.* **1990**, *112*, 5484.

66. Churchill, M. R. *Transition Metal Hydrides*; Bau, R. Ed.; Adv. Chem. Ser. (ACS) **1978**, *167*, 36.

67. Orpen, A. G. *J. Chem. Soc., Dalton Trans.* **1980**, 2509. See: http://xray.chm.bris.ac.uk:8000/software/xhydex/index.html.

68. (a) Brown, S. S. D.; Salter, I. D.; Dent, A. J.; Kitchen, G. F. M.; Orpen, A. G.; Bates, P. A.; Hursthouse, M. B. *J. Chem. Soc., Dalton Trans.* **1989**, 1227. (b) Martin, A.; Orpen, A. G.; *J. Am. Chem. Soc.* **1996**, *118*, 1464.

69. Biradha, K., Hansen, V. M.; Leong, W. K.; Pomeroy, R. K.; Zaworotko, M. J. *J. Clust. Sci.* **2000**, *11*, 285.

70. Schmidt, S. P.; Basolo, F.; Jensen, C. M.; Trogler, W. C. *J. Am. Chem. Soc.* **1986**, *108*, 1894.

71. Cifuentes, M. P.; Humphrey, M. G. *Comprehensive Organometallic Chemistry II*; Wilkinson, G., Stone, F. G. A., Abel, E. W., Eds.; Pergamon: Oxford, 1995, Vol. 7. p. 907.

72. Mason, R.; Thomas, K. M.; Mingos, D. M. P. *J. Am. Chem. Soc.* **1973**, *95*, 3802.

73. Ang, H. G.; Koh, L. L.; Yang, G. Y. *J. Chem. Soc., Chem. Commun.* **1996**, 1075.

74. Muna, R. A. A.; Lewis, J.; Raithby, P. R. *J. Organomet. Chem.* **1997**, *530*, 247.

75. Buntem, R.; Gallagher, J. F.; Lewis, J.; Raithby, P. R.; Rennie, M. A.; Shields, G. P. *J. Chem. Soc., Dalton Trans.* **2000**, 4279.

76. Demartin, F.; Manassero, M.; Sansoni, M.; Garlaschelli, L.; Raimondi, C.; Martinengo, S.; Canziani, F. *J. Chem. Soc., Chem. Commun.* **1981**, 528.

77. For example: (a) Bodensieck, U.; Stoeckli-Evans, H.; Süss-Fink, G. *J. Organomet. Chem.* **1992**, *433*, 149. (b) Field, J. S.; Haines, R. J.; Smit, D. N. *J. Chem. Soc., Dalton Trans.* **1988**, 1315.

78. Mann, B.E.; Taylor, B. F. *^{13}C NMR Data for Organometallic Compounds*; Academic: New York, 1981.

79. Gansow, O. A.; Burke, A. R. *J. Chem. Soc., Chem. Commun.* **1972**, 456.

80. Eady, C. R.; Jackson, W. G.; Johnson, B. F. G.; Lewis, J.; Matheson, T. W. *J. Chem. Soc., Chem. Commun.* **1975**, 958.

81. Johnson, B. F. G.; Lewis, J.; Pearsall, M.; Scott, L. G. *J. Organomet. Chem.* **1991**, *413*, 337.

82. Shapley, J. R.; Pearson, G. A.; Tachikawa, M.; Schmidt, G. E.; Churchill, M. R.; Hollander, F. J. *J. Am. Chem. Soc.* **1977**, *99*, 8064.

83. Wang. W.; Batchelor, R. J.; Davis, H. B.; Einstein, F. W. B.; Pomeroy, R. K. *Inorg. Chem.* **1992**, *31*, 5150.

84. Harris, R. K. *Nuclear Magnetic Resonance Spectroscopy: A Physicochemical View.* Longman: Essex, 1986, p.135.

85. Connor, J. A. *Metal Clusters in Catalysis*; Gates, B. C., Guczi, L., Knözinger, H. Eds. Elsevier: Amsterdam, 1986, p. 33.

86. Canal, J. P.; Yap, G. P. A.; Pomeroy, R. K. *Organometallics* **2003**, *22*, 3439.

87. Dyson, P. J.; McIndoe, J. S. *Transition Metal Carbonyl Cluster Chemistry*; Gordon and Breach: Amsterdam, 2000.

88. Atwood, J. D.; Brown, T. L. *J. Am. Chem. Soc.* **1975**, *97*, 3380.

89. Urbanic, M. A.; Shapley, J. R. *Inorganic Synthesis, Vol. 28.*; Angelici, R. J. Ed. Wiley: New York, **1990**, p. 165.

90. Rushman, P.; van Buuren, G. N.; Shiralian, M.; Pomeroy, R. K. *Organometallics* **1983**, *2*, 693.

91. Nicholls, J. N.; Vargas, M. D. *Inorganic Synthesis, Vol. 28.*; Angelici, R. J. Ed. Wiley: New York, **1990**, p. 232.

92. Johnson, B. F. G.; Bott, A. W.; Hugh-Jones, D.; Rodger, A. *Polyhedron* **1990**, *9*, 1769.

93. (a) Tolman, C. A. *J. Am. Chem. Soc.* **1970**, *92*, 2953. (b) Rahman, M. M.; Liu, H. Y.; Prock, A.; Giering, W. P. *Organometallics* **1987**, *6*, 650. (c) McAuliffe, C. A.; Levason, W. *Phosphine, Arsine and Stibine Complexes of the Transition Elements*; Elsevier: New York, 1979.

94. Giordano. R.; Sappa, E.; Tiripicchio. A.; Camellini. M. T.; Mays, M. J.; Brown, M. P. *Polyhedron* **1989**, *8*, 1855.

95. Wang, W.; Einstein, F. W. B.; Pomeroy, R. K. *Organometallics* **1993**, *12*, 3079.

96. Eady, C. R.; Johnson, B. F. G.; Lewis, J. *J. Organomet. Chem.* **1973**, *57*, C84.

97. (a) *Transition Metal Hydrides*; Muetterties, E. L., Ed.; Marcel Dekker: New York, 1971, p. 119. (b) Jenkins, J. M.; Shaw, B. L. *J. Chem. Soc. A* **1966**, 1407.

98. Wang, W. Ph.D. Thesis, Simon Fraser University, 1994.

99. Adams, R. D.; Selegue, J. P. *Comprehensive Organometallic Chemistry*; Wilkinson, G.; Stone, F. G. A.; Abel, E. W., Eds.; Oxford: Pergamon, 1982; Vol. 4, p. 967.

100. Crabtree, R. H.; Lavin, M. *Inorg. Chem.* **1986**, *25*, 805.

101. (a) Jiang, F.; Jenkins, H. A.; Biradha, K.; Davis, H. B.; Pomeroy, R. K.; Zaworotko, M. J. *Organometallics* **2000**, *19*, 5049. (b) Hansen, V. M.; Ma, A. K.; Biradha, K.; Pomeroy, R. K.; Zaworotko, M. J. *Organometallics* **1998**, *17*, 5267. (c) Randall, L. H.; Cherkas, A. A.; Carty, A. J. *Organometallics* **1989**, *8*, 568.

102. Cotton, F. A.; Wilkinson, G.; Murillo, C. A.; Bochmann, M. *Advanced Inorganic Chemistry* 6^{th} *ed.*; Wiley: New York, 1999.

103. Dyson, P. J. *Advances in Organometallic Chemistry*; West, R.; Hill, A. F.; Stone, F. G. A., Eds.; Academic: New York, 1999, Vol. 43, p. 43.

104. Hayward, C. T.; Shapley, J. R. *Inorg. Chem.* **1982**, *21*, 3816.

105. Byers, B. H.; Brown, T. L. *J. Am. Chem. Soc.* **1977**, *99*, 2527.

106. Goudsmit, R. J.; Jeffery, J. G.; Johnson, B. F. G.; Lewis, J.; McQueen, R. C. S.; Sanders, A. J.; Liu, J. C. *J. Chem. Soc., Chem. Commun.* **1986**, 24.

107. McPartlin, M.; Eady, C. R.; Johnson, B. F. G.; Lewis, J. *J. Chem. Soc., Chem. Commun.* **1976**, 883.

108. (a) Guy, J. J; Sheldrick, G. M. *Acta. Cryst.* **1978**, *B34*, 1725. (b) Leong, W. K.; Einstein, F. W. B.; Pomeroy, R. K. *Acta. Cryst.* **1996**, *C34*, 1607.

109. Eady, C. R.; Johnson, B. F. G.; Lewis, J. *J. Chem. Soc., Dalton Trans.* **1977**, 838.

110. Krause, J. A.; Siriwardane, U.; Salupo, T. A.; Wermer, J. R.; Knoeppel, D. W.; Shore, S. G. *J. Organomet. Chem.* **1993**, *454*, 263.

111. (References taken from Sànchez-Nieves, J.; Sterenberg, B. T.; Udachin, K. A.; Carty, A. J. *Can. J. Chem.* **2004**, in press.) (a) Sappa, E.; Tiripicchio, A.; Carty, A. J.; Toogood, G. E. *Prog. Inorg. Chem.* **1978**, *35*, 437. (b) Corrigan, J. F.; Doherty, S.; Taylor, N. J.; Carty, A. J. *J. Am. Chem. Soc.* **1994**, *116*, 9799. (c) Tunik, S. P.; Krym, V. R.; Stanova, G. L.; Nikolskii, A. B.; Podkorytov, I. S.; Ooi, S.; Yamasaki, M.; Shiro, M. *J. Organomet. Chem.* **1994**, *481*, 83. (d) Schamer, C. K.; Harris, S.; Sabat, M.; Voss, E. J.; Shriver, D. F. *Inorg. Chem.* **1995**, *34*, 5017. (e) Ferrand, V.; Süss-Fink, G.; Neels, A.; Stoeckli-Evans, H. *J. Chem. Soc., Dalton Trans.* **1998**, 3825. (f) Ang, H. G.; Ang, S. G.; Du, S. *J. Chem. Soc., Dalton Trans.* **1999**, 2963. (g) Haak, S.; Neels, H.; Stoeckli-Evans, H.; Süss-Fink, G.; Thomas, C. M.; *J. Chem. Soc., Chem. Commun.* **1999**, 1959. (h) Ferrand, V.; Süss-Fink, G.; Neels, A.; Stoeckli-Evans, H. *Eur. J. Inorg. Chem.* **1999**, 853. (i) Notaras, E. G. A.; Lucas, N. T.; Blitz, J. P.; Humphrey, M. G. *J. Organomet. Chem.* **2001**, *631*, 143. (j) Choualeb, A.; Braunstein, J.R.; Bouaoud, S. E.; Welter, R. *Organometallics* **2003**, *22*, 4405. (k) Li, Y.; Wong, W. T. *J. Chem. Soc., Dalton Trans.* **2003**, 398.

112. L'Eplattenier, L; Calderazzo, F. *Inorg. Chem.* **1967**, *6*, 2092.

113. a) Raithby, P. R.; Rosales, M. J. *Advances in Inorganic Chemistry and Radiochemistry*; Emeléus, H. J.; Sharpe, A. G., Eds.; Academic: New York, 1985; Vol. 29, p. 169. (b) Busetti, V.; Granozzi, G.; Alme, S.; Gobetto, R.; Osella, D. *Organometallics*, **1984**, *3*, 1510. (c) Sappa, E.; Tiripicchio, A.; Camellini, M. T. *J. Chem. Soc., Dalton Trans.* **1978**, 419. (d) Sappa, E.; Tiripicchio, A.; Braunstein, P. *Chem. Rev.* **1983**, *83*, 203. (e) Low, P. J.; Bruce, M. I. *Advances in Organometallic Chemistry*; West, R.; Hill, A. F.; Stone, F. G. A., Eds.; Academic: New York, 2001; Vol. 48, p. 71.

114. (a) Deng, M.; Leong, W. K. *Organometallics* **2002**, *21*, 1221. (b) Chen, G.; Deng, M.; Lee, C. K.; Leong, W. K. *Organometallics* **2002**, *21*, 1227.

115. *Catalysis by Di- and Polynuclear Metal Cluster Complexes* Adams, R. A.; Cotton, F. A., Eds.; Wiley-VCH: New York, 1998.

116. (a) Muetterties, E. L.; Rhodin, T. N.; Band, E.; Brucker, C. F.; Pretzer, W. R. *Chem. Rev.* **1979**, *79*, 91. (b) Ulan, J. G.; Maier, W. F.; Smith, D. A. *J. Org. Chem.* **1987**, *52*, 3132. (c) Morrison, S. R. *The Chemical Physics of Surfaces 2nd ed.*; Plenum: New York, 1990. (d) Somorjai, G. A. *Introduction to Surface Chemistry and Catalyst*; Wiley: New York, 1994.

117. Deabate, S.; Giordano, R.; Sappa, E. *J. Cluster Sci.* **1997**, *8*, 407.

118. Examples: (a) Gallop, M. A.; Johnson, B. F. G.; Khattar, R.; Lewis, J.; Raithby, P. R. *J. Organomet. Chem.* **1990**, *386*, 121. (b) Akita, M.; Moro-oka, Y. *Bull. Chem. Soc. Jpn.* **1995**, *68*, 420. (c) Ellis, D.; Farrugia, L. J. *J. Cluster Sci.* **2001**, *12*, 243. (d) Adams, R. D.; Qu, B.; Smith, M. D. *Organometallics* **2002**, *21*, 4847. (e) Takao, T.; Takemori, T.; Moriya, M.; Suzuki, H. *Organometallics* **2002**, *21*, 5190. (f) Zuno-Cruz, F. J.; Carrasco, A. L.; Rosales-Hoz, M. J. *Polyhedron* **2002**, *21*, 1105. (g) Lin, Q.; Leong, W. K.; Gao, J. *J. Organomet. Chem.* **2004**, *689*, 25.

119. Examples: (a) Bantel, H.; Hansert, B.; Powell, A. K.; Tasi, M.; Vahrenkamp, H. *Angew. Chem. Int. Ed.* **1989**, *28*, 1059. (b) Park, J. T.; Shapley, J. R. *J. Am. Chem. Soc.* **1983**, *105*, 6182. (c) Dickson, R. S. *Polyhedron* **1991**, *10*, 1995. (d) Adams, H.; Guio, L. V. J.; Morris, M. J.; Wildgoose, F. A. *J. Organomet. Chem.* **2002**, *659*, 142. (e) Zhu, B.; Zhang, W.; Zhao, Q.; Bian, Z.; Hu, B.; Zhang, Y.; Yin, Y.; Sun, J. *J. Organomet. Chem.* **2002**, *650*, 181. (f) Lucas, N. T.; Notaras, E. G. A.; Petrie, S.; Stranger, R.; Humphrey, M. G. *Organometallics* **2003**, *22*, 708. (g) Lucas, N. T.; Notaras, E. G. A.; Cifuentes, M. P.; Humphrey, M. G. *Organometallics* **2003**, *22*, 284. (h) Choualeb, A.; Rosé, J.; Braunstein, P.; Welter, R. *Organometallics* **2003**, *22*, 2688.

120. (a) Tachikawa, M.; Shapley, J. R.; Pierpont, C. G. *J. Am. Chem. Soc.* **1975**, *97*, 7172. (b) Poë, A. J.; Sampson, C. N.; Smith, R. T. *J. Am. Chem. Soc.* **1986**, *108*, 5459. (c) Peirpoint, C. G. *Inorg. Chem.* **1977**, *16*, 636.

121. (a) Clauss, A. D.; Shapley, J. R.; Wilson, S. R. *J. Am. Chem. Soc.* **1981**, *103*, 7387. (b) Jackson, W. G.; Johnson, B. F. G.; Kelland, J. W.; Lewis, J.; Schorpp, K. T. *J. Organomet. Chem.* **1975**, *87*, C27.

122. (a) Poë, A. J.; Moreno, C. *Organometallics* **1999**, *18*, 5518. (b) Poë, A. J.; Farrar, D. H.; Ramachandran, R.; Moreno, C. *Inorg. Chem. Acta.* **1998**, *274*, 82. (c) Ferraris, G.; Gervasio, G. *J. Chem. Soc., Dalton Trans.* **1974**, 1813. (d) Gambino, O; Vaglio, G. A; Ferrari, R. P.; Cetini, G. *J. Organomet. Chem.* **1971**, *30*, 381.

123. Burke, M. R.; Takats, J. *J. Organomet. Chem.* **1986**, *302*, C25.

124. Anderson, O. P.; Bender, B. R.; Norton, J. R. *Organometallics* **1991**, *10*, 3145.

125. Heveldt, P. F.; Johson, B. F. G.; Lewis, J.; Raithby, P. R.; Sheldrick, G. M. *J. Chem. Soc., Chem. Commun.* **1978**, 340.

126. (a) Hoffman, D. M.; Hoffman, R. *J. Chem. Soc., Dalton Trans.* **1982**, 1471. (b) Gagné, M. R.; Takats, J. *Organometallics* **1988**, *7*, 561. (c) Krebs, A.; Jacobsen-Bauer, A.; Haupt, E.; Veith, M.; Huch, V. *Angew. Chem.* **1989**, *101*, 640. (d) Cherkas, A. A.; Hadj-Bagheri, N.; Carty, A. J.; Sappa, E.; Pellinghelli, M. A; Tiripicchio, A. *Organometallics* **1990**, *9*, 1887. (e) Mirza, H. A.; Vittal, J. J.; Puddephatt, R. J. *Organometallics* **1994**, 13, 3063. (f) Casey, C. P.; Boese, W. T.;

Carino, R. S.; Ford, P. C. *Organometallics* **1996**, 15, 2189. (g) Casey, C. P.; Carino, R. S.; Sakaba, H.; Hayashi, R. K. *Organometallics* **1996**, 15, 2640. (h) Mirza, H. A.; Vittal, J. J.; Puddephatt, R. J. *J. Coord. Chem.* **1996**, *37*, 131. (i) Casey, C. P.; Carino, R. S.; Hayashi, R. K.; Schladetzky, K. D. *J. Am. Chem. Soc.* **1996**, *118*, 1617. (j) Comstock, M. C.; Shapley, J. R. *Organometallics* **1997**, *16*, 4816. (k) Doherty, S.; Waugh, M.; Scanlan, T. H.; Elsegood, M. R. J.; William, C. *Organometallics* **1999**, 18, 679.

127. Johnson, B. F. G.; Lewis, J.; Raithby, P. R.; Rosales, M. J. *J. Chem. Soc., Dalton Trans.* **1983**, 2645.

128. Braga, D.; Grepioni, F.; Johnson, B. F. G.; Lewis, J.; Lunniss, J. A. *J. Chem. Soc., Dalton Trans.* **1992**, 1101.

129. Hansen, V. M.; Batchelor, R. J.; Einstein, F. W. B.; Male, J. L.; Pomeroy, R. K. *Organometallics* **1997**, *16*, 4875.

130. Johnson, B. F. G; Lewis, J.; Reichert, B. E.; Schorpp, K. T.; Scheldrick, G. M. *J. Chem. Soc., Dalton Trans.* **1977**, 1417.

131. Jackson, R.; Johnson, B. F. G; Lewis, J.; Raithby, P. R.; Sankey, S. W. *J. Organomet. Chem.* **1980**, *193*, C1.

132. Solomons, T. W. G. *Organic Chemistry* 5^{Th} *ed.*; Wiley: New York, 1992, p. 493.

133. Pomeroy, R. K. *Comprehensive Organometallic Chemistry II*; Wilkinson, G.; Stone, F. G. A., Abel, E. W., Eds.; Pergamon: Oxford, 1995; Vol. 7, p. 835.

134. Somorjai, G. A. *J. Phys. Chem. B* **2002**, *106*, 9201.

135. Rosenberg, E.; Bracker-Novak, J.; Gellert, R. W.; Aime, S.; Gobetto, R.; Osella, D. *J. Organomet. Chem.* **1989**, *365*, 163.

136. Nicholls, J. N.; Vargas, M. D. *Inorganic Synthesis*; Kaesz, H. D. Ed.; Wiley-Interscience: New York, **1989**, Vol. 26, p. 295.

137. Amoroso, A. J.; Gade, L. H.; Johnson, B. F. G.; Lewis, J.; Raithby, P. R.; Wong, W. *Agnew. Chem. Int. Ed. Engl.* **1991**, *30*, 107.

138. Eady, C. R.; Johnson, B. F. G.; Lewis, J. *J. Organomet. Chem.* **1972**, *37*, C39.

139. Johnson, B. F. G.; Johnston, R. D.; Lewis, J. *J. Chem. Soc. (A)* **1968**, 2865.

140. Canal, J. P.; Pomeroy, R. K. to be published.

141. Radel, S. R.; Navidi, M. H.; *Chemistry*; West: New York, 1990; p. 363.

142. Johnson, B. F. G.; Lewis, J.; Sankey, S. W.; Wong, K.; McPartlin, M.; Nelson, W. J. H. *J. Organomet. Chem.* **1980**, *191*, C3.

143. Paine, R. T. *Inorganometallic Chemistry*; Fehlner, T. P., Ed.; Plenum: New York, 1992, p. 359.

144. Kempter, C. P. *J. Chem. Phys.* **1964**, 1515.

145. Kempter, C.P.; Nadler, M. R. *J. Chem. Phys.* **1960**, 1580.

146. Storm, E. K. *Inorganic Reactions and Methods. Vol. 12B*; Zuckerman, J. J.; Hagen, A. P., Eds.; VCH: New York, 1991, p. 318.

147. Hoffmann, P.; Galindo, H.; Zambrano, G.; Rincón, C.; Prieto, P. *Materials Characterization* **2003**, *50*, 255.

148. *The Sadtler Standard Spectra*, Sadtler Research Laboratories: Philadelphia, 1975, 41214P

149. Urashima, Y.; Wakabayashi, T.; Masaki, T.; Teresaki, Y. *Mineralogical Journal* **1974**, *7*, 438.

150. Battiston, G. A.; Bor, G.; Dietler, U. K.; Kettle, S. F. A.; Rossetti, R.; Sbrignadello, G.; Stanghellini, P. L. *Inorg. Chem.* **1980**, *19*, 1961.

151. Gallop, M. A.; Gomez-Sal, M. P.; Housecroft, C. E.; Johnson, B. F. G.; Lewis, J; Owen, S. M.; Raithby, P. R.; Wright, A. H. *J. Am. Soc.* **1992**, *114*, 2502.

152. Hastings, W. R.; Baird, M. C. *Inorg. Chem.* **1986**, *25*, 2913.

153. Masciocchi, N.; Moret, M.; Cairati, P., Ragaini, F., Sironi, A. *J. Chem. Soc., Dalton Trans.* **1993**, 471.

154. Sanati, H. K.; Becalska, A.; Ma, A. K.; Pomeroy, R. K. *J. Chem. Soc., Chem. Commun.* **1990**, 197.

155. Moss, J. R.; Graham, W. A. G. *J. Chem. Soc., Dalton Trans.* **1977**, 89.

156. Drake, S. R.; Johnson, B. F. G.; Lewis, J. *J. Chem. Soc., Chem. Commun.* **1988**, 1033.

157. Knox, S. A. R.; Koepke, J. W.; Andrews, M. A.; Kaesz, H. D. *J. Am. Chem. Soc.* **1975**, *97*, 3942.

158. Ang, H. G.; Hay, C. M.; Johnson, B. F. G.; Lewis, J.; Raithby, P. R.; Whitton, A. J. *J. Organomet. Chem.* **1987**, *330*, C5.

159. Hay, C. M.; Johnson, B. F. G.; Lewis, J.; Raithby, P. R.; Whitton, A. J. *J. Chem. Soc., Dalton Trans.* **1988**, 2091.

160. Bruce, M. I.; Skelton, B. W.; White, A. H.; Zaitseva, N. N. *J. Chem. Soc., Dalton Trans.* **1999**, 1445.

161. (a) Pradeep, M; Thimmappa, B. H. S.; Rheingold, A. L. *Inorg. Chem.* **1990**, *29*, 4658. (b) Adams, R. D.; Babin, J. E.; Tasi, M. *Inorg. Chem.* **1986**, *25*, 4514. (c) Layer, T. M.; Lewis, J.; Martin, A.; Raithby, P. R.; Wong, W. *J. Chem. Soc., Dalton Trans.* **1992**, 3411.

162. (a) Braye, E. H.; Dahl, L. F.; Hübel, W.; Wampler, D. L. *J. Am. Chem. Soc.* **1962**, *84*, 4633. (b) Eady, C. R.; Johnson, B. F. G.; Lewis, J.; Matheson, T. *J. Organomet. Chem.* **1973,** *57*, C82.

163. (a) Johnson, B. F. G.; Roberts, Y. V. *Polyhedron*, **1993**, *12*, 977. (b) Farrugia, L. J.; Senior, A. M.; Braga, D.; Grepioni, F.; Orpen, A. G.; Crossley, J. G. *J. Chem. Soc., Dalton Trans.* **1996**, 631. (c) Mann, B. E. *J. Chem. Soc., Dalton Trans.* **1997**, 1457. (d) Johnson, B. F. G.; Roberts, Y. V.; Parisini, E. *J. Chem. Soc., Dalton. Trans.* **1992**, 2573. (e) Johnson, B. F. G. *J. Chem. Soc., Dalton. Trans.* 1997, 1473. (f) Johnson, B. F. G.; Tay, S. *Inorg. Chim. Acta* 2002, 332, 201. (g) Forster, A.; Johnson, B. F. G.; Lewis, J. J.; Matheson, T. W.; Robinson, B. H.; Jackson, G. *J. Chem. Soc., Chem. Commun.* **1974**, 1042.

164. (a) Li, J; Jug, K. *Inorg. Chim. Acta* **1992**, *196*, 89. (b) Johnson, B. F. G. *J. Chem. Soc., Dalton. Trans.* **1997**, 1473.

165. Huheey, J. E. *Inorganic Chemistry: Principles of structure and reactivity*; Harper & Row: New York, 1972, p. 498.

166. Braterman, P.S. *Metal Carbonyl Spectra*; Academic: NewYork, 1975, p. 226.

167. Bruce, M. I.; Matisons, J. G.; Wallis, R. C.; Patrick, J. M.; Skelton, B. W.; White, A. H. *J. Chem. Soc., Dalton Trans.* **1983**, 2365.

168. Mason, J. *J. Am. Chem. Soc.* **1991**, *113*, 6056.

169. Heaton, B. T.; Iggo, J. A.; Longoni, G.; Mulley, S. *J. Chem. Soc., Dalton Trans.* **1995**, 1985.

170. Koridze, A. A.; Kizas, O. A., Astakhova, N. M.; Petrovskii, P.V. *Seriya Khimicheskaya* **1981**, *5*, 1181.

171. (a) Hunstock, E.; Calhorda, M. J.; Hirva, P.; Pakkanen, T. A. *Organometallics*, **2000**, *19*, 4624. (b) Braga, D.; Grepioni, F.; Byrne, J. J.; Calhorda, M. J. *J. Chem. Soc., Dalton Trans.* **1995**, 3287. (c) Evans, D. G. *J. Chem. Soc., Chem. Commun.* **1983**, 675.

172. Skoog, D. A.; West, D. M.; Holler, F. J. in *Analytical Chemistry An Introduction* 6th ed.; Harcourt Brace: Philadelphia, 1994, p. 404.

173. Braga, D.; Grepioni, F. *Acc. Chem. Res.* **1997,** *30*, 81.

174. Some examples of crystalline hydrates interacting with carbonyl ligands: (a) Chan, S.; Wong, W. *J. Chem. Trans., Dalton Trans.* **1995**, 3987. (b) Greene, P. T.; Bryan, R. T. *Inorg. Chem.* **1969**, *8*, 1464. (c) Albano, V.; Chini, P.; Scatturin, V. *J. Chem. Soc., Chem. Commun.* **1968**, *3*, 163. (d) Ablano, V. P.; Bellon, P. L.; Chini, P.; Scatturin, V. *J. Organomet. Chem.* **1969**, *16*, 461. (e) Albano, V. P.; Chini, P.; Scatturin, V. *J. Organomet. Chem.*, **1968**, *15*, 423. (f) Bhaduri, S.; Sharma, K.; Jones, P. G.; Erdbrügger, C. F. *J. Organomet. Chem.*, **1987**, *326*, C46. (g) Carriedo, G. A.; Riera, V.; Sanchez, M. G.; Jeannin, Y.; Philoche-Levisalles, M. *J. Organomet. Chem.*, **1989**, *361*, 197. (h) Kubas, G. J.; Burns, C. J.; Khalsa, G. R. K.;Van Der Sluys, L. S.; Kiss, G.; Hoff, C. D. *Organometallics* **1992**, *11*, 3390.

175. Johnson, B. F. G.; Lewis, J.; Nelson, W. J. H.; Puga, J.; Henrick, K.; McPartlin, M. *J. Chem. Soc., Dalton Trans.* **1983**, 1203.

176. Johnson, B. F. G.; Lewis, J.; Raithby, P. R.; Sheldrick, G. M.; Wong, K.; McPartlin, M. *J. Chem. Soc., Dalton Trans.* **1978**, 673.

177. Johnson, B. F. G.; Lewis, J.; Raithby, P. R.; Zuccaro, C. *J. Chem. Soc., Dalton Trans.* **1980**, 716.

178. Wang, W.; Davis, H. B.; Einstein, F. W. B.; Pomeroy, R. K. *Organometallics* **1994**, *13*, 5113.

179. Brammer, L. *Crystal Design: Structure and Function;* Desiraju, G. R., Ed.; Wiley: San Francisco, 2003: Vol. 7, p. 14.

180. Deeming. A. J.; Manning, P. J.; Rothwell, I. P.; Hursthouse, M. B.; Walker, N. P. C. *J. Chem. Soc., Dalton Trans.* **1984**, 2039.

181. Bryan, E. G.; Forster, A.; Johnson, B. F. G.; Lewis, J.; Matheson, T. W. *J. Chem. Soc., Dalton Trans.* **1978**, 196.

182. Cotton, F. A.; Wilkinson, G. *Advanced Inorganic Chemistry: A Comprehensive Text. 3rd Ed.*; Interscience, New York, 1972, p. 692.

183. Ichikawa, I. *Pol. J. Chem.* **1998**, *72*, 230.

184. Scheiner, S. *Hydrogen Bonding: A Theoretical Perspective*; Oxford University: New York, 1997, p. 119.

185. Joesten, M. D.; Schaad, L. J. *Hydrogen Bonding*; Marcel Dekker: New York, 1974, p. 183.

186. Lutz, H. D.; Möller, H. *J. Mol. Struct.* **1993**, *295*, 147.

187. Vinogradov, S. N.; Linnell, R. H. *Hydrogen Bonding*; Van Nostrand Reinhold, New York, 1971, p. 124.

188. Bright, D. *Chem. Commun.* **1970**, *18*, 1169.